# Untersuchung lichtinduzierter Dynamiken in konjugierten Terpyridinen und deren Koordinationsverbindungen

Dissertation

zur Erlangung des akademischen Grades
*doctor rerum naturalium (Dr. rer. nat.)*


seit 1558

vorgelegt dem Rat der Chemisch-Geowissenschaftlichen Fakultät
der Friedrich-Schiller-Universität Jena

von Diplomchemiker Ronald Siebert
geboren am 29.09.1983 in Gera

Gutachter:

1. Prof. Dr. Jürgen Popp

2. Prof. Dr. Ulrich S. Schubert

3. Prof. Dr. Wolfgang Kiefer

Tag der öffentlichen Verteidigung: 21.12.2012

Alles in der Natur demonstriert mir: Du hast Zeit. Nichts geht zu Ende, nur die Formen wechseln. Ich aber bilde mir ein, nur die Form, in der ich jetzt existiere, sei gültig, und das Leben höre auf, wenn ich die Form wechsele.

Erwin Strittmatter

# Inhaltsverzeichnis

# Abbildungsverzeichnis

# Abkürzungsverzeichnis

| | |
|---|---|
| AFM | Atomic Force Microscopy (Rasterkraftmikroskopie) |
| $cm^{-1}$ | Wellenzahlen, 1 $cm^{-1}$ entspricht 0,0001240 eV |
| DFT | Density Functional Theory (Dichtefunktionaltheorie) |
| DP | Degree of Polymerization (Polymerisationsgrad eines Makromoleküls) |
| dppz | Dipyrido[3,2-a:2‘,3‘-c]phenazin |
| eV | Elektronenvolt, 1eV entspricht 8065,54 $cm^{-1}$ |
| fs | Femtosekunde, 1 fs entspricht $10^{-15}$ Sekunden |
| IC | Internal Conversion; strahlungsloser Übergang zwischen zwei Zuständen gleicher Multiplizität |
| ISC | Intersystem Crossing; strahlungsloser Übergang zwischen zwei Zuständen unterschiedlicher Multiplizität |
| IVR | Intramolecular Vibrational Energy Redistribution, Umverteilung von Energie zwischen verschiedenen Schwingungsmoden innerhalb eines elektronischen Zustands |
| $k_B$ | Boltzmann-Konstante; $k_B$ = 1,3806455 $10^{-23}$ J/K |
| MALDI | Matrix Assisted Laser Desorption Ionisation (Matrix-unterstützte Laser-Desorption/Ionisation) |
| MEH-PPV | Poly[2-methoxy-5-(2‘-ethylhexyloxy)-p-phenylen-vinylen] |
| $^1$MLCT | Singlet Metal-to-Ligand Charge-Transfer (Singulett Metall-zu-Ligand Ladungstransfer-Zustand) |
| $^3$MLCT | Triplet Metal-to-Ligand Charge-Transfer (Triplett Metall-zu-Ligand Ladungstransfer-Zustand) |
| $\mu$s | Mikrosekunde, 1 $\mu$s entspricht $10^{-6}$ Sekunden |
| ms | Millisekunde, 1 ms entspricht $10^{-3}$ Sekunden |
| NIR | nahes Infrarot, entspricht dem Wellenlängenbereich zwischen ca. 800 und 3000 nm |
| nm | Nanometer, 1 nm entspricht $10^{-9}$ Metern |
| ns | Nanosekunde, 1 ns entspricht $10^{-9}$ Sekunden |
| PBI | Perylenbisimid |
| PMA | Polymethacrylat |
| PMMA | Polymethylmethacrylat |
| PPV | Poly(p-phenylen-vinylen) |
| PS | Polystyrol |
| ps | Pikosekunde, 1 ps entspricht $10^{-12}$ Sekunden |

| | |
|---|---|
| $S_0$ | elektronischer Singulettgrundzustand |
| $S_1$ | erster elektronisch angeregter Singulettzustand |
| SEC | Size Exclusion Chromatography (Größenausschlusschromatographie) |
| $\tau$ | Zeitkonstante eines Prozesses |
| $T_1$ | erster elektronisch angeregter Triplettzustand |
| TCSPC | Time Correlated Single Photon Counting (zeitkorrelierte Einzelphotonenzählung) |
| TDDFT | Time Dependent Density Functional Theory (zeitabhängige Dichtefunktionaltheorie) |
| TOF | Time of Flight (Flugzeitanalyse) |

# 1 Einleitung

Ein zentraler Aspekt der Umwandlung von Licht in elektrische Energie in organischen Halbleitern ist die Dissoziation eines Exzitons in freie Ladungsträger. Während in herkömmlichen, anorganischen Siliziumsolarzellen dieser Prozess bei entsprechender Dotierung freiwillig und instantan abläuft, ist in den klassischen organischen Halbleitermaterialien eine zusätzliche Triebkraft nötig.[3] Unter Laboratoriumsbedingungen kann dies einfach durch das Anlegen eines äußeren elektrischen Feldes erfolgen, was jedoch im Falle einer breiten Anwendung unter reellen Bedingungen unzweckmäßig ist. Eine etablierte Strategie zur Überwindung dieses Nachteils ist die Mischung des Polymers mit starken Elektronenakzeptoren zu sogenannten „Blends".[4, 5] Als Elektronenakzeptoren werden in der Regel Fullerenderivate verwendet, da ihre Redoxeigenschaften durch Modifikation der Leitstruktur einstellbar sind und diese Systeme bis zu sechs Elektronen aufnehmen können.[6] Befindet sich in einem solchen „Blend" ein Exziton in direkter Nachbarschaft zu einem Fulleren, so kann es durch Elektronentransfer über die Phasengrenze hinweg relativ einfach zur Bildung freier Ladungsträger kommen.

So einfach dieser Ansatz konzeptionell ist, so ist es doch schwierig, einen hinreichend großen Wirkungsgrad zu erzielen, um mit handelsüblichen Siliziumsolarzellen konkurieren zu können. Die zentrale Schwäche dieses Ansatzes offenbart sich bei der Betrachtung des „Blends" auf einer mikroskopischen Skala. Bedingt durch die unterschiedlichen physikalischen Eigenschaften, kommt es zur Entmischung des Polymers und des Fullerens. Ein im Inneren eines Polymerclusters erzeugtes Exziton muss nun bis zu einer Grenzfläche diffundieren, bis es dort in freie Ladungsträger dissoziieren kann. Das Diffusionsvermögen eines Exzitons hängt dabei sowohl von der Strukturierung der Polymerphase auf molekularer Ebene, als auch von der Lebensdauer des Exzitons ab, da sich eine definierte Anordnung der Polymermoleküle positiv auf die Effizienz von intramolekularem Energietransfer auswirkt.[5, 7] Hier stellt Förster-Resonanz-Energietransfer (FRET) den dominanten Energietransferprozess dar, wobei es sich um eine Wechselwirkung der Übergangsdipolmomente zweier Chromophore handelt. Dadurch kann es zu einem strahlungslosen Energietransfer über Distanzen von einigen wenigen Nanometern kommen.[8] Durch eine sukzessive Abfolge solcher Prozesse in einem polymeren Multichromophorsystem können theoretisch auch Distanzen im zwei- bis dreistelligen nm-Bereich überbrückt werden, was jedoch meist an der mangelnden Ordnung in solchen Systemen scheitert. Durch Tempern des Polymerfilms können große geordnete, quasi zweidimensional periodische Bereiche erzeugt werden,[9, 10] was die Diffusionslänge der Exzitonen erhöht. Dagegen hat der Chemiker auf die Exzitonenlebensdauer nur einen geringen Einfluss. Diese liegt für die meisten relevanten Chromophore im Bereich weniger Nanosekunden.[11]

Eine Möglichkeit Exzitonen mit langer Lebensdauer und somit großer Diffusionslänge zu erzeugen, ist die Verwendung von Materialien, bei denen es zu einer schnellen und effektiven Bildung von Triplettzuständen kommt.[4, 12] Die einfachsten Vertreter dieser Substanzklasse, die im Kontext von Polymersolarzellen intensiv untersucht wurden, stellen Polythiophenderivate dar. In diesen Polymeren kommt es aufgrund des inneren Schweratomeffektes zur Bildung von Triplettexzitonen mit Quantenausbeuten von ca. 30 %.[13] Weitaus höhere Quantenausbeuten für diesen gewünschten Effekt zeigen Metallopolymere, die in ihrem Rückgrat schwere Übergangsmetalle wie Platin enthalten.[14, 15] Wurden diese speziellen Polymere in Solarzellen integriert, konnten trotz schlechter Überlappung des Absorptions- mit dem Sonnenspektrum teilweise beachtliche Wirkungsgrade gemessen werden. Dies kann wiederum auf die lange Lebensdauer der Triplettexzitonen und die damit verbundene große Diffusionslänge zurückgeführt werden.

Unter Berücksichtigung dieser Rahmenbedingungen wird deutlich, dass im Bezug auf ihre Diffusionslänge Triplettexzitonen den Singulettexzitonen überlegen sind, woraus sich unter anderem das hohe Interesse an polymeren Halbleitern mit hoher Intersystem-Crossing (ISC)-Rate ableitet. Der wohl einfachste und auch zielführendste Weg ist die Konstruktion linearer Aggregate, in denen sowohl Chromophore mit hohem Absorptionsquerschnitt, als auch Schwermetalle, die für ein effizientes ISC sorgen, enthalten sind. All diese Aspekte können durch die Verwendung *bis*-terpyridinbasierter Koordinationspolymere abgedeckt werden.[16, 17, 18, 19, 20] So bieten diese zum einen die Möglichkeit, ein beliebiges Chromophor als zentrale Einheit zwischen die beiden Terpyridineinheiten einzubauen,[1, 21, 22] woraus sich die Möglichkeit ableitet, Koordinationspolymere mit beliebigen Absorptionseigenschaften aus *bis*-Terpyridinen zu generieren.[1, 23] Dadurch kann bei statistischem Einbau verschiedener *bis*-Terpyridine ein signifikanter Teil des Sonnenspektrums abgedeckt werden. Darüber hinaus bieten diese Systeme die Option, lineare Aggregate oder auch Koordinationspolymere zu erzeugen. Das kann durch die Komplexierung von Metallen, die eine oktaedrische Koordinationsgeometrie bevorzugen, erreicht werden. Allgemein weisen derartige Koordinationspolymere einen niedrigen Polymerisationsgrad (DP) und eine annähernd lineare Konformation auf.[17, 23, 24] Im Falle der Verwendung von Eisen- und vor allem Ruthenium- und Osmiumkationen ist es möglich, Koordinationspolymere mit hohen ISC-Raten und einem Gradienten für Triplett-Energietransfer zwischen verschiedenen MLCT-Zuständen zu synthetisieren.[25, 26, 27]

Neben all diesen positiven Eigenschaften, die in der Klasse *bis*-terpyridinbasierter Koordinationspolymere zu erwarten sind, hängt die Eignung solcher Materialien für eine Anwendung in der Photovoltaik letztendlich davon ab, ob und mit welcher Effizienz es zur Bildung freier Ladungsträger kommt. Für die bereits eingehend untersuchten Vertreter der halbleitenden Polymere aus der Familie der PPV Derivate konnte diese Frage in den letzten 20 Jahren durch zeit- und spektral aufgelöste Techniken geklärt werden.[4, 5, 11] Trotz der teilweise hohen strukturellen Ähnlichkeit dieser Systeme mit einer Reihe konjugierter *bis*-Terpyridine, können diese Ergebnisse jedoch nicht a priori auf die Substanzklasse der hier untersuchten Koordinationspolymere übertragen werden. Das liegt vor allem an der konsequenten und systematischen Segmentierung des Polymers, sowie an der Anwesenheit von Übergangsmetallionen, die die

angeregte Zustandsdynamik signifikant beeinflussen. Aus diesen Gründen erwächst die Notwendigkeit einer systematischen Charakterisierung dieser relativ neuen Substanzklasse. Hier bietet sich, bedingt durch den Bau der untersuchten Koordinationspolymre, eine schrittweise Untersuchung einzelner, schrittweise größer werdender Bausteine der Polymere an, was eine detailierte und systematische Zuordnung der photoinduzierten Prozesse ermöglicht. Dabei muss festgehalten werden, dass auch die kleinen Bauelemente an sich eine sehr interessante Photophysik aufweisen, die über die schlichte Absorption und Emission eines Photons hinausgeht. Bereits an diesen Vorstufen können mitunter Prozesse identifiziert werden, die auch im Koordinationspolymer ablaufen und einen signifikanten Beitrag zu dessen angeregter Zustandsdynamik haben.

# 2 Ziele der Arbeit

Mit Hinblick auf das hohe Potential, welches in den Übergangsmetallkoordinationspolymeren konjugierter Terpyridine liegt, ist es das Ziel dieser Arbeit, derartige Systeme grundlegend spektroskpisch zu charakterisieren. Da Multichromophorsysteme, wie sie beispielsweise Koordinationspolymere darstellen, intrinsisch eine sehr komplexe Photophysik ausfweisen, wird der Ansatz gewählt, sie schrittweise aufzubauen und die jeweiligen Zwischenstufen zu charakterisieren. Der Schwerpunkt liegt dabei klar auf der spektral- und zeitaufgelösten Analyse verschiedener Zerfallskanäle eines angeregten Molekülensembles und einer exakten Identifizierung der photoinduzierten molekularen Prozesse, wie etwa Geometrieänderungen, Ladungs- oder Energietransfer.

Um diese Strategie umzusetzen, wurde in enger Zusammenarbeit mit der Arbeitsgruppe von Prof. Dr. Ulrich S. Schubert eine Auswahl von konjugierten Terpyridinen und die sich daraus ableitenden mono- di- und polynuklearen Koordinationsverbindungen in dieser Reihenfolge untersucht. Diese Herangehensweise bietet die Möglichkeit auftretende Effekte direkt strukturellen Variationen, wie dem Einführen eines Metallkations oder der Modifikation des konjugierten Systems zuzuordnen. Des Weiteren ist man so in der Lage auftretende Prozesse in relativ großen, supramolekularen Gebilden durch Analogiebeziehungen zu ihren kleineren Bausteinen exakt zuzuordnen.

Die wesentlichen spektroskopischen Techniken, die neben stationären Absorptions- und Emissionsexperimenten zur Lösung dieser Aufgabe verwendet wurden, sind die fs-zeitaufgelöste transiente Absorptionsspektroskopie, die ps-zeitaufgelöste Emissionsspektroskopie mittels Schmierbildkamera und zeitkorrelierter Einzelphotonenzählung (TCSPC) sowie die Resonanz-Raman-Spektroskopie. Durch systemeatische Variation definierter Umgebungsparameter, wie der Polarität, der Viskosität und der Temperatur, konnte der Informationsgehalt der genannten Experimente noch weiter erhöht werden.

# 3 Angeregte Zustandsdynamiken in konjugierten Terpyridinen

Teile dieses Kapitels wurden in den folgenden Artikeln publiziert:

[**RS1**] R. Siebert, D. Akimov, M. Schmitt, A. Winter, U. S. Schubert, B. Dietzek and J. Popp, Spectroscopic Investigation of the Ultrafast Photoinduced Dynamics in $\pi$-Conjugated Terpyridines, *ChemPhysChem*, **2009**, *10*, 910-919.

[**RS2**] R. Siebert, A. Winter, U. S. Schubert, B. Dietzek and J. Popp, Excited-State Planarization as Free Barrierless Motion in a $\pi$-Conjugated Terpyridine, *Journal of Physical Chemistry C*, **2010**, *114*, 6841-6848.

## 3.1 Definition eines konjugierten Terpyridins

Im Kontext der vorliegenden Arbeit werden solche Verbindungen als konjugierte Terpyridine bezeichnet, bei denen das Terpyridin in 4‘-Position mit einem konjugationsfähigen Rest, beispielsweise einem Farbstoffmolekül, verknüpft ist. Darüber hinaus muss eine signifikante Konjugation zwischen beiden Systemen vorliegen, was für die hier untersuchten Systeme bereits durch Presselt *et al.* gezeigt werden konnte.[28, 29] Aufgrund der relativ allgemeinen Definition und der enormen strukturellen Vielfalt möglicher Substituenten stellen die konjugierten Terpyridine eine sehr große Substanzklasse dar. Dies wirft die Frage auf, ob es Korrelationen zwischen dem Auftreten bestimmter Strukturelemente und den spektroskopischen Eigenschaften konjugierter Terpyridine sowie den sich daraus ableitenden Koordinationsverbindungen gibt. Um sich dieser Fragestellung systematisch zu nähern, ist es zunächst unerlässlich die Familie konjugierter Terpyridine in kleinere Gruppen einzuteilen, die sich durch ein bestimmtes, gemeinsames Strukturelement auszeichnen. Am einfachsten ist dabei die Unterteilung nach der Art der Verknüpfung zwischen dem Terpyridin selbst und dem konjugationsfähigen Substituenten, da sich diese direkt auf die Konjugation zwischen beiden Resten auswirkt. Obwohl auch hier eine große strukturelle Vielfalt möglich ist, wurden bisher nur wenige Strategien zur Verknüpfung beider Elemente verfolgt. Am häufigsten sind dabei 4‘-arylsubstituierte konjugierte Terpyridine, die über eine modifizierte Kröhnke-Reaktion hergestellt werden können,[30] und 4‘-ethinylsubstituierte Terpyridine, welche über Kreuzkupplungsreaktionen zugänglich sind.[31] Im ersten Fall erfolgt die Verknüpfung beider Fragmente in der Regel über einen Phenylring, welcher in vielen Fällen mit einer weiteren Ethinylgruppe substituiert ist. Alle im Rahmen der vorliegenden Arbeit spektroskopisch untersuchten Terpyridine und Metallkomplexe leiten sich

von diesem Strukturmotiv ab, da es einfach synthetisiert und modifiziert werden kann, wie aus Abbildung 3.1 hervorgeht.[1, 2] Das bestimmende Merkmal dieses Typs ist die sterische Hinderung der Protonen in 3‘- und 5‘-Position des Terpyridins und des benachbarten Phenylrings. Dadurch bedingt ist eine Verdrillung beider Gruppen von ca. 30 bis 35° relativ zueinander. Das setzt die Konjugation zwischen ihnen herab, unterbricht diese aber nicht.[28, 32] Beim Zweiten, ebenfalls weit verbreiteten Typ eines konjugierten Terpyridins, erfolgt die Verknüpfung beider Fragmente über eine Ethinyleinheit.[33, 34] Dieser Weg führt zu wesentlich geringeren sterischen Wechselwirkungen und einer deutlich höheren, jedoch nicht uneingeschränkten Konjugation beider Reste.

Neben diesen beiden Ansätzen existieren noch weitere Verküpfungsmöglichkeiten, zum Beispiel über Ether- oder Amidstrukturen.[35, 36, 37] Der Einfluss dieser Verküpfungsmöglichkeiten auf die Konjugation und somit auf die spektroskopischen Eigenschaften, ist jedoch nur unzureichend bis garnicht untersucht. Die Kenntnisse über Struktur-Eigenschaftsbeziehungen sind bei den 4‘-Phenylterpyridinen jedoch am tiefgründigsten. Deshalb bilden spektroskopische Untersuchungen an konjugierten Terpyridinen dieses Typs und den sich daraus ableitenden Koordinationsverbindungen den Kern der vorliegenden Arbeit.

## 3.2 Grundlegende spektroskopische Eigenschaften konjugierter Terpyridine

Die grundlegenden spektroskopischen Eigenschaften konjugierter Terpyridine, das heißt die Lage und Intensität der Banden im Absorptions- und Emissionsspektrum, die Emissionsquantenausbeute sowie die Emissionslebensdauer werden im Wesentlichen von dem in 4‘-Position gebundenen Chromophor bestimmt. Durch die Wahl dieses Chromophors lassen sich Absorptions- und Emissionsspektrum des Moleküls relativ frei im sichtbaren Spektralbereich einstellen. Ein klassisches Absorptionsspektrum eines konjugierten Terpyridins besteht unter anderem aus terpyridinzentrierten Übergängen, die den ultravioletten Spektralbereich dominieren. Dagegen tragen chromophorbasierte Übergänge in der Regel im sichtbaren Spektralbereich zum Absorptionsspektrum bei. Trotz der Konjugation beider Teilfragmente ist eine derartige diskrete Zuordnung der Beiträge zum Absorptionsspektrum möglich, da im elektronischen Grundzustand beide Molekülfragmente um ca. 30 bis 35° gegeneinander verdreht sind und somit die konjugation deutlich herabgesetzt ist.

Ist ein Farbstoff in 4‘-Position gebunden, so wird auch das Emissionsspektrum des Gesamtsystems von dessen elektronischer Struktur dominiert. Somit ist es möglich, maßgeschneiderte Bausteine supramolekularer Systeme auf der Basis konjugierter Terpyridine herzustellen, deren Absorptions- und Emissionseigenschaften in Abhängigkeit des verwendeten Chromophors fast beliebig variiert werden können.[1, 22] Der erste Schritt dieser Arbeit beschäftigt sich somit mit der zeit- und spektral aufgelösten Untersuchung der angeregten Zustandsdynamik in einer

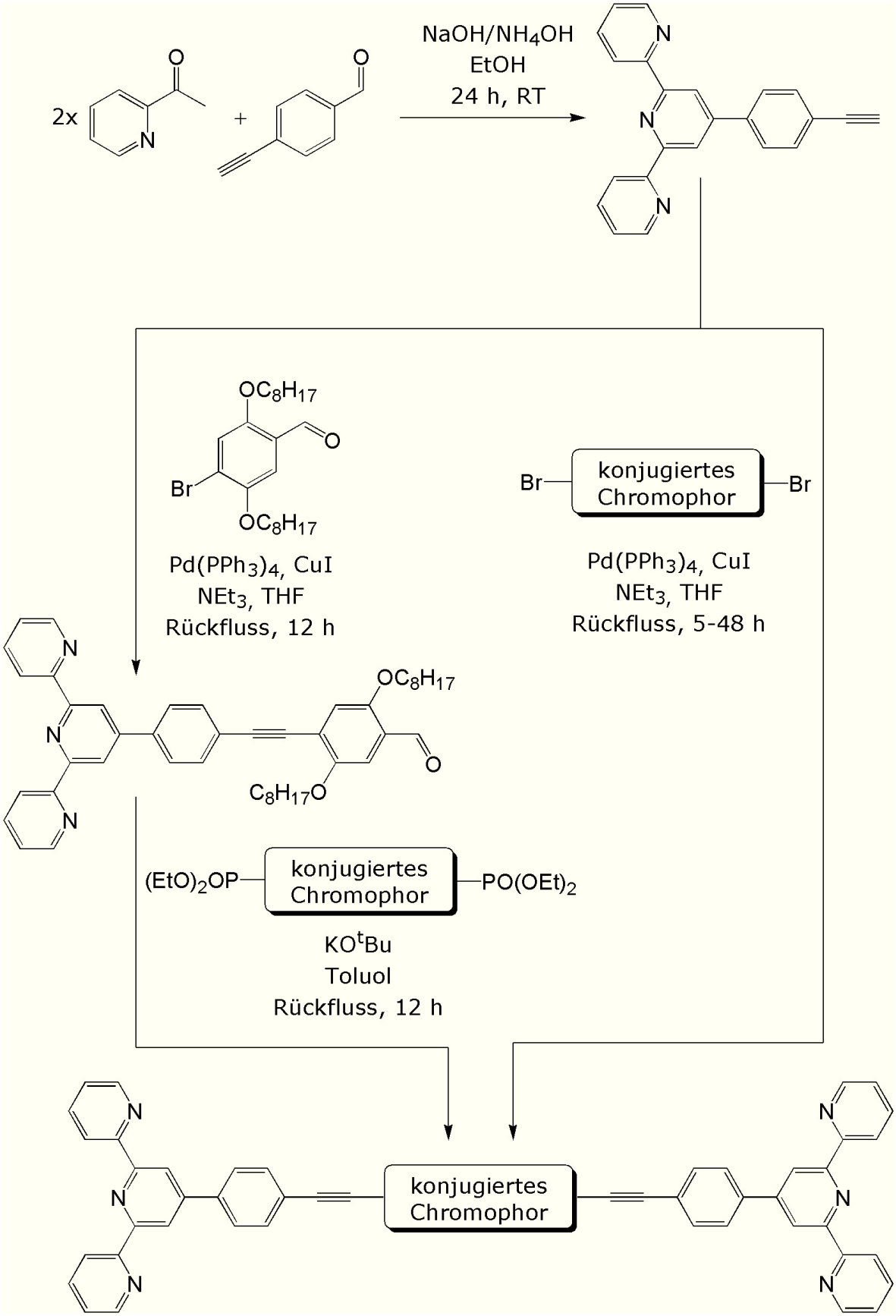


**Abbildung 3.1:** Schematische Darstellung der Synthese eines vom Strukturmotiv des 4-Arylterpyridins abgeleiteten konjugierten *bis*-Terpyridins.[1, 2]

Reihe von Terpyridinen, deren in 4‘-Position gebundenens Chromophor systematische Variationen aufweist. Dadurch soll zum einen der Einfluss systematischer struktureller Variationen auf die photoinduzierten Dynamiken näher untersucht werden. Zum anderen sollen durch diese Untersuchungen die Eignung der gewählten Terpyridinliganden zum Aufbau photoaktiver Koordinationspolymere sicher gestellt werden. Die Strukturen, sowie das Absorptions- und Emissionsspektrum zweier dieser Vertreter sind in Abbildung 3.2 graphisch dargestellt. Dabei zeigt sich die direkte Abhängigkeit der spektroskopischen Eigenschaften von strukturellen Parametern dadurch, dass eine Vergrößerung des in 4‘-Position verknüpften Chromophors zu einer bathochromen Verschiebung der Spektren führt.

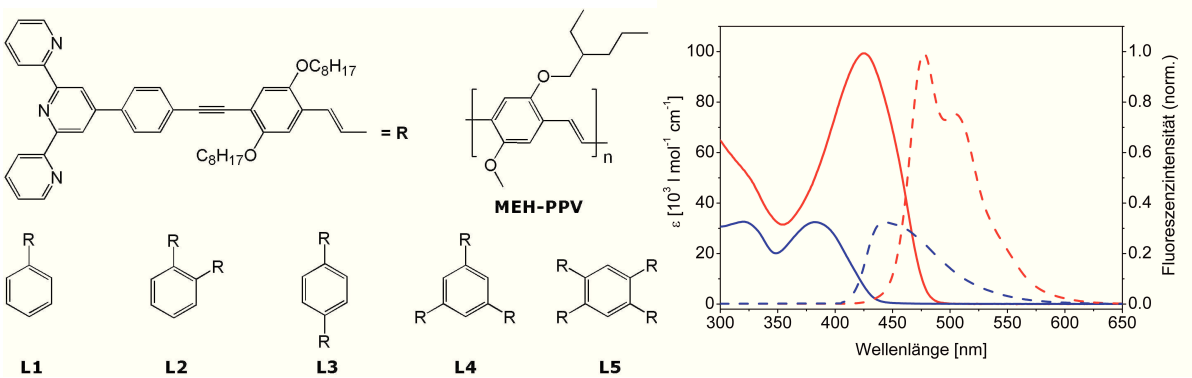


**Abbildung 3.2:** Schematische Darstellung der Strukturen der in diesem Abschnitt diskutierten konjugierten Terpyridine und dem strukturell verwandeten Polymer MEH-PPV, zusammen mit dem Absorptions- und Emissionsspektrum der linearen Vertreter **L1** (blau) und **L3.** (rot)

Bei der Untersuchung der lichtinduzierten angeregten Zustandsdynamiken in konjugierten Terpyridinen sind Absorption und Emission eines Photons nur Anfang und Ende eines möglichen Relaxationspfades. Mit Hinblick auf die potentielle Anwendung solcher Systeme stellen stationäre spektroskopische Methoden eine unvollständige Charakterisierung dar, da eine Vielzahl relevanter Prozesse auf einer Zeitskala weniger Femto- bis einiger Mikrosekunden abläuft. Es ist somit von fundamentalem Interesse zu wissen, welche Konkurenzprozesse außerdem ablaufen, auf welchen Zeitskalen sie stattfinden und was mit der, durch Absorption eines Photons, eingetragenen Energie entlang möglicher Reaktionskoordinaten passiert. Durch zeitaufgelöste spektroskopische Methoden wie transiente Absorptionsspektroskopie und Schmierbildkameramessungen, konnte für die konjugierten Terpyridine, die das charakteristische Strukturmerkmal der PPV-Derivate tragen und darüber hinaus noch verschiedene Verzweigungsmuster aufweisen, der Relaxationspfad qualitativ und quantitativ nachgezeichnet werden.

Die Absorptionsspektren der hier untersuchten Terpyridinderivate spiegeln exakt das oben dargelegte Verhalten wieder. Dementsprechend zeigen die Derivate mit der größten Konjugationslänge im Chromophor die langwelligsten Absorptionsbanden um 425 nm, während die Absorption des Terpyridins mit der kürzesten Konjugationslänge bei 380 nm liegt (siehe Abbildung 3.2). Die verzweigten Systeme, die durch Substitution mehrerer Terpyridinsubstituenten an einem zentralen Phenylring erhalten werden, zeigen keine so eindeutigen Korrelationen

im Absorptionsspektrum. Hier scheint die sterische Wechselwirkung der einzelnen Substituenten am zentralen Phenylring eine deutliche Abweichung von der planaren Geometrie zu bewirken, was eine Verringerung oder gar den Bruch der Konjugation im Chromophor selbst zur Folge hat. Ein ähnliches Verhalten ist von den klassischen konjugierten Polymeren bekannt. Hier kommt es ebenfalls zur Segmentierung des Poly(p-phenylen-vinylen)s durch sterischen Bruch der Konjugation entlang des Polymerrückgrates in sogenannte spektroskopische Einheiten.[38]

Bedingt durch das verwendete Chromophor sind auch die Emissionsspektren der konjugierten Terpyridine relativ ähnlich zu denen klassischer PPV-Derivate. Das bedeutet, dass für alle Systeme eine intensive Fluoreszenz mit mehr oder weniger stark ausgeprägter vibronischer Feinstruktur beobachtet werden kann. Jedoch muss festgehalten werden, dass die Emissionsquantenausbeuten sowie die Emissionlebensdauern deutlich höher sind als bei klassischen PPV Derivaten.[2]

Durch zeitaufgelöste transiente Absorptionsspektroskopie im Femtosekundenbereich war es möglich, den Relaxationspfad der verschiedenen Terpyridine zwischen Anregung und Emission näher zu untersuchen. Dabei ist festzuhalten, dass alle untersuchten und in Abbildung 3.2 gezeigten Systeme eine vergleichbare angeregte Zustandsdynamik mit ähnlichen spektralen Signaturen auf einer ähnlichen Zeitskala aufweisen. Im Detail bedeutet das, dass in allen Fällen Signale mit negativer Amplitude den kurzwelligen Spektralbereich der transienten Absorptionsspektren dominieren. Dagegen können im langwelligen Spektralbereich intensive, positive Signale gemessen werden (siehe Abbildung 3.3). Diese Form der transienten Absorptionsspektren im Bereich zwischen ca. 500 und 700 nm ist auf die Überlagerung von stimulierter Emission und angeregter Zustandsabsorption zurückzuführen. Die Zuordnung dieser Prozesse erfolgt durch das Vorzeichen des Signals, da sowohl die stimulierte Emission als auch die Grundzustandsbleichung stets Signale mit negativer Amplitude liefern. Positive Signale in den transienten Absorptionsspektren können stets der Absorption angeregter Zustände zugeordnet werden. Demzufolge ist das starke positive Signal im langwelligen Bereich Absorptionsprozessen aus dem ersten angeregten Zustand in höher angeregte Zustände zuzuordnen. Das negative Signal im kurzwelligen Bereich kann dagegen zweifelsfrei stimulierten Emissionsprozessen aus dem angeregten $S_1$ Zustand in den Grundzustand zugeschrieben werden. Eine eindeutige Abgrenzung zur Grundzustandsbleichung erfolgt hier aufgrund der spektralen Lage des Signals (die Grundzustandsbleichung erscheint blau verschoben) und der beobachteten Feinstruktur, die denen der Emissionsspektren gleicht (Abbildung 3.3).

Da sowohl stimulierte Emission als auch angeregte Zustandsabsorption, die zu den experimentellen transienten Spektren beitragen, von dem selben angeregten Zustand ausgehen, enthalten sie prinzipiell dieselbe Information über den Zerfall dieses Zustands. Dieser erfolgt in allen untersuchten Terpyridinen multiexponentiell, beschrieben durch die Zeitkonstanten $\tau_1$ = 1,4 - 4 ps; $\tau_2$ = 20 - 45 ps und $\tau_3 \approx$ 1 ns. Die ersten beiden Zeitkonstanten können Prozessen zugeordnet werden, durch die das angeregte Molekül in ein globales Energieminimum des $S_1$ relaxiert, da beide Prozesse zum Ansteigen der stimulierten Emission führen und

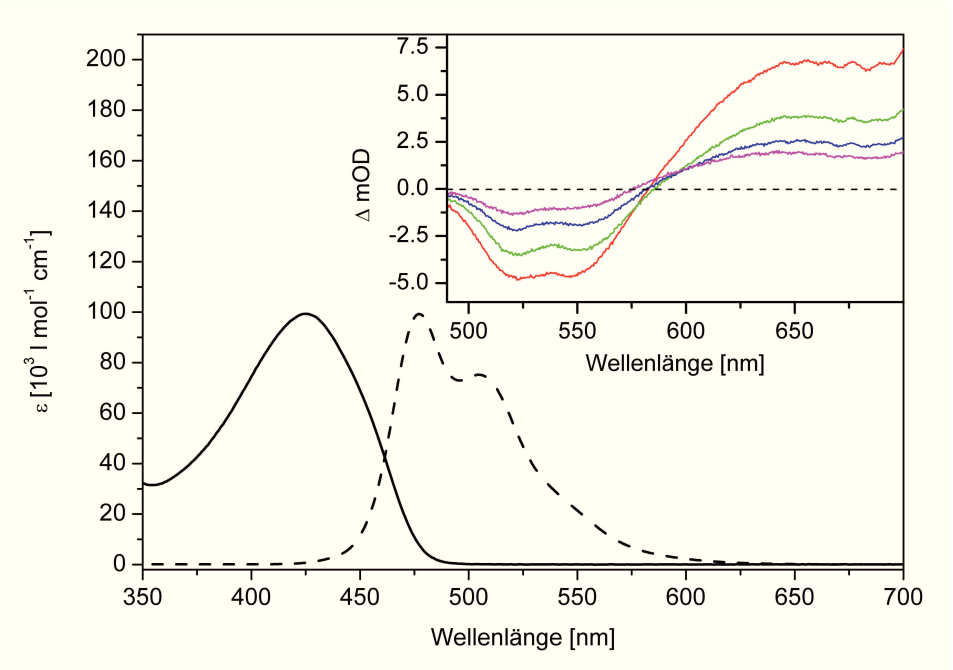


**Abbildung 3.3:** Gegenüberstellung der stationären Absorptions- und Emissionsspektren von **L3** (schwarz) mit den transienten Absorptionsspektren; 5 ps (rot), 500 ps (grün), 1 ns (blau) und 1,5 ns (magenta) nach Anregung bei 400 nm.

von einer dynamischen Rotverschiebung des Emissionssignals begleitet sind. Der erste Prozess wird in Übereinstimmung mit der Literatur Energiedissipations- und Solvatisierungsprozessen zugeschrieben.[39, 40] Bei dem zweiten Prozess ($\tau_2$), handelt es sich um die dynamische Planarisierung des konjugierten Terpyridins, welches im Grundzustand um ca. 30 - 35° verdrillt ist. Ein derartiger Prozess ist in ausgedehnten konjugierten Systemen mit Abweichungen von einer idealen, planaren Geometrie und entsprechenden sterischen Spannungen zu erwarten. Eine solche merkliche Strukturänderung wird dadurch begünstigt, dass die im $S_1$ herabgesetzte Bindungsordnung im Chromophor zu größeren Bindungslängen führt, was die sterischen Spannungen im Molekül minimiert. Nach Einnahme der sterisch entspannten angeregten Zustandsgeometrie erfolgt die Rückkehr angeregter Moleküle in den Grundzustand. Dieser Prozess erfolgt auf einer Zeitskala von ca. 1 ns, was durch Schmierbildkameramessungen belegt wird.

## 3.3 Detaillierte Untersuchung lichtinduzierter Prozesse in konjugierten Terpyridinen

Nachdem durch stationäre und zeitaufgelöste Experimente ein erstes, grobes Bild der angeregten Zustandsdynamik in den hier untersuchten konjugierten Terpyridinen gezeichnet werden konnte, ist eine eindeutige Zuordnung der auftretenden Prozesse unabdingbar. Eine zentrale Fragestellung ist dabei die Zuordnung der Komponente $\tau_2$ zu einer Planarisierung im $S_1$-Zustand. Alternativ besteht die Möglichkeit, dass es sich bei diesem Prozess um die Ausbildung eines Ladungstransferzustandes handelt.[41] Eine eindeutige Antwort konnte in diesem Fall durch zeitaufgelöste transiente Absorptionsspektroskopie anhand des strukturell einfachsten konjugierten Terpyridins unter variierenden Umgebungsparametern gegeben werden. Während sich kein Einfluss der Polarität des Lösungsmittels auf die angeregte Zustandsdynamik des Moleküls feststellen ließ, zeigte dagegen die Erhöhung der Viskosität einen deutlichen Effekt. Es ist aus einer Vielzahl von Studien an Molekülen unterschiedlicher Ausdehnung bekannt, dass eine Reorganisation der Molekülgeometrie im angeregten Zustand von einer deutlichen Lösungsmittelabhängigkeit begleitet wird.[42, 43, 44, 45] Ein solches Verhalten konnte z.B. bei Isomerisierungsreaktionen an Cyaninfarbstoffen direkt einer Änderung der Geometrie des angeregten Zustands zugeschrieben werden. Auch im Fall von arylsubstituierten Mono- und Bipyridinen ist eine Planarisierung innerhalb der angeregten Zustandsgeometrie belegt. Für die hier untersuchten 4‘-Phenylterpyridine konnte durch systematische Studien ebenfalls eine Korrelation zwischen dem Torsionswinkel und den spektroskopischen Eigenschaften gefunden werden. Dabei wurde die Struktur des Terpyridins und somit auch der Winkel zwischen der Terpyridinsphäre und dem sich anschließenden Phenylring konsequent variiert. Auf diesen Vorkenntnissen aufbauend, stellt die im Rahmen dieser Arbeit gefundene lineare Abhängigkeit einer Zeitkonstante die erste direkte Beobachtung der Planarisierung in einem 4‘-Phenylterpyridin in Echtzeit dar. Die gefundene Viskositätsabhängigkeit deutet des Weiteren auf einen barrierefreien Prozess hin.

Diese experimentellen Befunde bestätigen, dass in den hier untersuchten konjugierten Terpyridinen ein signifikanter Unterschied zwischen Grundzustands- und angeregte Zustandsgeometrie besteht. Weiterhin ist durch den hohen Energieunterschied von ca. 2,5 - 2,9 eV, gemäß dem „Energy Gap Law“ nach Engelman und Jortner nur eine geringe Franck-Condon Überlappung zwischen den Schwingungswellenfunktionen beider Zustände zu erwarten, was als Erklärung für die hohen Quantenausbeuten von 53 - 98% angenommen werden kann.[46] Dieser Effekt scheint auch durch den starken Geometrieunterschied zwischen Grund- und angeregtem Zustand nicht kompensiert zu werden, was durch temperaturabhängige Lebensdauermessungen bestätigt werden kann. Diese ergaben eine Aktivierungsenergie für den strahlungslosen Relaxationspfad von ca. 0,34 eV. Durch die hier beschriebenen experimentellen Arbeiten kann somit bestätigt werden, dass es sich bei den untersuchten konjugierten Terpyridinen um geeignete Bausteine für die angestrebten Koordinationspolymere handelt. Das liegt zum einen an ihrem hohen Absorptionsquerschnitt als auch an der Stabilität der angeregten Zustände, die sich aus einer Planarisierung im angeregten Zustand ableitet.

# 4 Angeregte Zustandsdynamiken in mononuklearen Komplexen konjugierter Terpyridine

Teile dieses Kapitels wurden in den folgenden Artikeln publiziert:

[**RS3**] R. Siebert, A. Winter, B. Dietzek, U. S. Schubert and J. Popp, Dual Emission from Highly Conjugated 2,2‘:6‘:2“-Terpyridine Complexes - A Potential Route to White Emitters, *Macromolecular Rapid Communications*, **2010**, *31*, 883-888

[**RS4**] R. Siebert, A. Winter, U. S. Schubert, B. Dietzek and J. Popp, The Molecular Mechanism of Dual Emission in Terpyridine Transition Metal Complexes - Ultrafast Investigation of Photoinduced Dynamics, *Physical Chemistry Chemical Physics*, **2011**, *13*, 1606-1617

[**RS6**] R. Siebert, F. Schlütter, A. Winter, M. Presselt, H. Görls, U. S. Schubert, B. Dietzek and J. Popp, Ruthenium(II)-*bis*(4‘-(4-ethinylphenyl)-2,2‘:6‘,2“-terpyridine) - A Versatile Synthon in Supramolecular Chemistry. Synthesis and Characterization. *Central European Journal of Chemistry*, **2011**, *9*, online

Auf dem Weg zu photoaktiven Koordinationspolymeren, basierend auf konjugierten Terpyridinen, ist der nächste konsequente Schritt die Untersuchung der entsprechenden Übergangsmetallkomplexe der Metalle der 6. Nebengruppe. Dieser Schritt ist der direkten Untersuchung von Koordinationspolymeren vorzuziehen, da hierdurch der unmittelbare Einfluss der Komplexierung auf die nun bekannte angeregte Zustandsdynamik der Liganden untersucht werden kann. Intramolekulare Prozesse, wie z.B. Energietransfer zwischen zwei Metallzentren, die in den Koordinationspolymeren zu erwarten wären und zu wesentlich komplexeren Dynamiken führen würden, können auf dieser Stufe ausgeschlossen werden. Der Fokus liegt hier auf der Rekonstruktion des Relaxationspfades angeregter Moleküle nach Lichtabsorption. Das beinhaltet sowohl die Charakterisierung des Franck-Condon-Punktes, als auch der Prozesse, die zu Bildung und Zerfall eines relaxierten angeregten Zustandsensembles führen.

## 4.1 Grundlegende spektroskopische Eigenschaften der Übergangsmetallkomplexe der 6. Nebengruppe

Ein Charakteristikum der Übergangsmetallkomplexe der 6. Nebengruppe ist das Auftreten einer Reihe von elektronischen Übergängen, in die die d-Orbitale der Metallatome involviert

sind: Das sind zum einen symmetrieverbotene, intensitätsschwache Übergänge zwischen den im oktaedrischen Ligandenfeld in $e_g$ und $t_{2g}$ Zustände aufgespaltenen d-Orbitalen und zum anderen Metall-zu-Ligand-Ladungstransferzustände. Bei diesen Übergängen handelt es sich um die Anregung eines d-Elektrons aus den voll besetzten $t_{2g}$ Zuständen in ein $\pi^*$-Orbital des Liganden. Sofern sich bei diesen Übergängen die Multiplizität des Systems nicht ändert, handelt es sich um sogenannte $S_0 \rightarrow {}^1$MLCT-Übergänge.[47, 48] Diese spinerlaubten Übergänge weisen teilweise hohe Extinktionskoeffizienten bis zu 40.000 l/mol cm auf. Werden schwere Metallatome wie Osmium koordiniert, wird das strenge Spinverbot durch den inneren Schweratomeffekt gelockert und es können auch $S_0 \rightarrow {}^3$MLCT Übergänge beobachtet werden. Durch das Wegfallen der Spinpaarungsenergie liegen die $^3$MLCT-Zustände energetisch tiefer als die $^1$MLCT-Zustände. Das zeigt sich unter anderem in typischer Weise anhand von ca. 0,14-0,26 eV bathochrom verschobenen Absorptionsbanden.

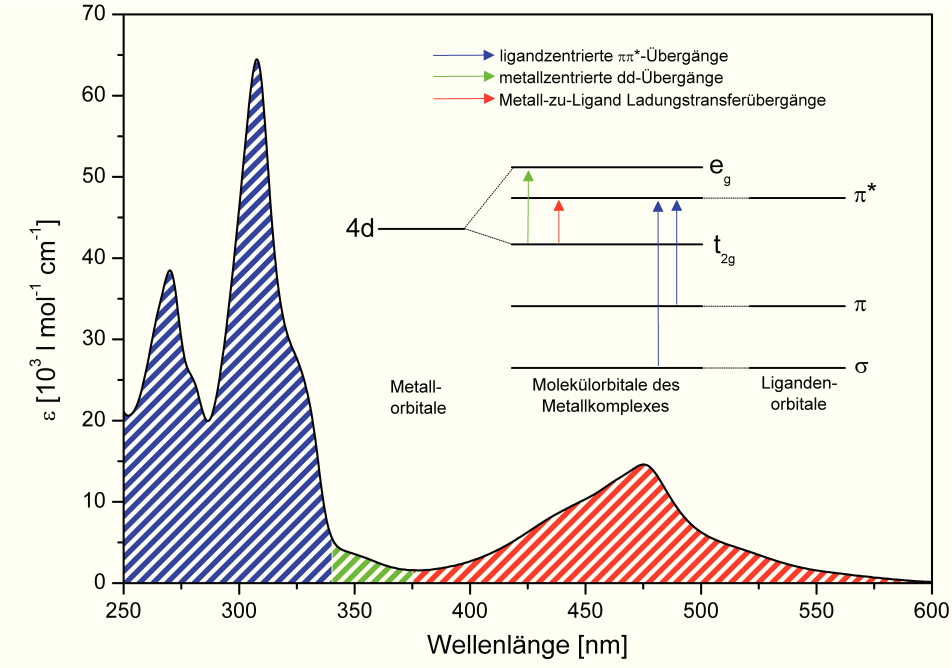


**Abbildung 4.1:** Schematische Darstellung der Energieniveaus im einfachsten oktaedrischen Ruthenium(II)-Terpyridinkomplex (**M1** siehe Abbildung 4.2) zusammen mit den zu beobachtenden optischen Übergängen. Die Farbkodierung ordnet dabei einzelnen elektronischen Übergängen direkt eine Bande oder Bandenfolge im Absorptionsspektrum des Komplexes zu.

Das Absorptionsspektrum eines Terpyridinkomplexes setzt sich letztendlich aus den ligandzentrierten $\pi\pi^*$-Übergängen und den metallzentrierten dd- und MLCT-Übergängen zusammen. Im Allgemeinen stellen die MLCT-Zustände die angeregten Zustände mit der niedrigsten Energie dar. Das wird z.B. auch anhand von Abbildung 4.1 deutlich, in der die elektronischen Übergänge in **M1** dargestellt sind. Das dort enthaltene Jablonski Diagram ordnet dabei die spektralen Beiträge den verschiedenen, im vorangegangenen Text beschriebenen, Übergängen zwischen den Molekülorbitalen des Metallkomplexes zu. Hier stellen die MLCT-Übergänge die Absorptionsbanden mit der niedrigsten Energie dar, weshalb sie in der Regel als eine Art „Trichter“ für die in das System eingetragene Lichtenergie wirken. So kann generell bei allen

drei Metallen der 6. Nebengruppe ein sehr effektiver Energietransfer zwischen den ligandzentrierten $\pi\pi^*$- und den $^1$MLCT-Zuständen beobachtet werden, der zur teilweisen oder gar völligen Löschung der Fluoreszenz aus den ligandzentrierten $\pi\pi^*$-Zuständen führt. Bei allen drei Metallen kommt es des Weiteren im angeregten Zustand zu einem ultraschnellen und effizienten ISC vom $^1$MLCT in den $^3$MLCT.[49, 50] Aus diesem Zustand kann im Fall von Ruthenium und Osmium auch Phosphoreszenz beobachtet werden, die im Vergleich mit den entsprechenden Bipyridinkomplexen jedoch sehr schwach und kurzlebig ist. Aufgrund der energetisch ungünstigen Lage des $^3$MLCT-Zustands, relativ zu den angeregten dd-Zuständen, kommt es in den entsprechenden Eisenkomplexen zu einer sehr schnellen und effizienten Entvölkerung dieser Zustände.[51, 52, 53] Aus diesem Grund kann z.B. in Eisen(II)-Terpyridinkomplexen keine Phosphoreszenz beobachtet werden.

## 4.2 Charakterisierung des Franck-Condon-Punktes, Stabilisierung und Delokalisierung des $^1$MLCT

Ein besonders bei Übergangsmetallkomplexen von 4'-Phenylterpyridinen viel diskutierter Effekt ist die Delokalisierung des initial angeregten $^1$MLCT-Zustandes über den in 4'-Position des Terpyridins substituierten Phenylring und weitere daran gebundene konjugationsfähige Reste.[54, 55] Das es zu einer solchen Delokalisierung kommt, geht unter anderem aus der systematischen Rotverschiebung der $^1$MLCT Absorptionsbande mit zunehmender Größe des substituierten konjugierten Chromophors hervor, da es mit einer zunehmenden Stabilisierung, d.h. energetischen Absenkung, des $^1$MLCT-Zustands einher geht. Allerdings stagniert diese Verschiebung bei ca. 500 nm, was dafür spricht, dass das Ausmaß der Delokalisierung des initial bevölkerten $^1$MLCT nicht beliebig eingestellt werden kann. Vielmehr scheint sie sich nur auf die Terpyridineinheit selbst und das unmittelbar daran gebundene Strukturelement zu beschränken.[56]

Um zu klären, wie weit die Delokalisierung voranschreitet, bietet es sich an, die vibronische Feinstruktur der $^1$MLCT Absorptionsbanden näher zu analysieren. Sie enthält alle an den elektronischen Übergang gekoppelten Schwingungsmoden, die sich bestimmten Strukturmerkmalen des Moleküls zuordnen lassen. Dadurch kann die räumliche Lokalisierung des angeregten Zustands im Molekül abgeschätzt werden, sofern es sich bei den Banden der Schwingungsfeinstruktur um diskrete „Markerbanden" für bestimmte molekulare Strukturelemente handelt. Dieser Ansatz scheitert jedoch im Allgemeinen an homogenen und inhomogenen Linienverbreiterungsprozessen, die bei Raumtemperatur in kondensierten Phasen die vibronische Feinstruktur verschmieren. Eine starke Abkühlung der Proben kann hier helfen, jedoch ist eine eindeutige Identifizierung der an den elektronischen Übergang gekoppelten Moden erst bei sehr tiefen Temperaturen um 5 K möglich.[57] Durch Resonanz-Raman-Spektroskopie, die denselben Informationsgehalt wie ein Absorptionsspektrum trägt, konnte jedoch zweifelsfrei die Lokalisierung sowie der Grad der Delokalisierung des initial bevölkersten $^1$MLCT in einer Reihe von Ruthenium(II)-Polypyridinkomplexen bestimmt werden.[58, 59, 60] Dies soll anhand

der drei in Abbildung 4.2 gezeigten Ruthenium(II)-Terpyridinkomplexe **M1**,**M2** und **M4**, die sich durch den Substituenten in 4‘-Position unterscheiden, aufgezeigt werden. Dabei befindet sich an dieser Position der Terpyridinliganden ein sukzessive größer werdendes konjugiertes System aus Aromaten, Doppel- und Dreifachbindungen. Alle diese Strukturmerkmale haben charakteristische, intensive Raman-Banden in definierten Bereichen des Spektrums. Über das Auftreten dieser spezifischen Banden in den Resonanz-Raman-Spektren der Komplexe kann festgestellt werden, ob eine Delokalisierung des initial bevölkerten $^1$MLCT-Zustands über diese Strukturelemente erfolgt.

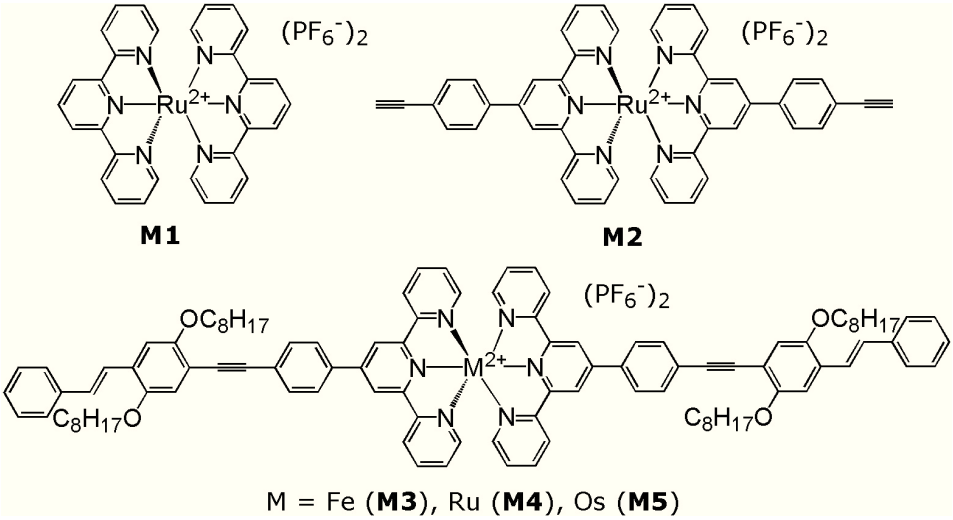


**Abbildung 4.2:** Strukturen der Ruthenium(II)-Terpyridinkomplexe, deren angeregte Zustandsdynamik in diesem Kapitel diskutiert wird.

Beim Vergleich der Spektren, die in Resonanz mit den $^1$MLCT-Übergängen gemessen wurden, wird deutlich, dass die Komplexe mit konjugierten Substituenten ein nahezu identisches Resonanz-Raman-Spektrum zeigen. Unterschiede zwischen den Spektren von **M2** und **M4** bestehen lediglich in der Intensität der Banden. Die zu beobachtende Resonanzverstärkung von Banden, die zweifelsfrei dem in 4‘-Position substituierten Phenylring zuzuordnen sind,[28] beweisen zusammen mit dem Fehlen der symmetrischen Valenzschwingung der Ethinyleneinheit, dass der initial bevölkerte $^1$MLCT-Zustand auf dem Terpyridin selbst und dem direkt mit ihm verbundenen Phenylring lokalisiert ist. Eine weitere Vergrößerung des konjugierten Systems über die 4‘-Position hinaus führt zu keiner erhöhten Delokalisierung des Zustandes, sondern lediglich zu einer erhöhten Konjugation zwischen dem Terpyridin und dem sich direkt anschließenden Phenylring. Dadurch lässt sich das Auftreten identischer Moden in den Komplexen **M2** und **M4** sowie die erhöhte Intensität dieser im Falle von **M4** erklären. Das Resonz-Raman-Spektrum von **M1** hingegen, welcher keinen konjugierten Substituent in 4‘-Position trägt, hat eine völlig andere Gestalt als die Spektren von **M2** und **M4**. Dies ist auf einen, lediglich auf dem Terpyridinliganden selbst lokalisierten, $^1$MLCT-Zustand zurückzuführen.[61]

## 4.3 Rekonstruktion des Relaxationspfades in konjugierten Terpyridinkomplexen der 6. Nebengruppe

Nach Aufklärung der Lokalisierung des initial angeregten $^1$MLCT-Zustands stellt sich die Frage nach der Topologie des angeregten Zustands und dem Verlauf der photoinduzierten Dynamik. Nähert man sich dieser Fragestellung durch stationäre Absorptions- und Emissionsspektroskopie anhand der in Abbildung 4.2 gezeigten Übergangsmetallkomplexe **M3** - **M5**, so fällt auf, dass je nach gewählter Anregungswellenlänge unterschiedliche Emissionsspektren gemessen werden können. Während bei Anregung der $^1$MLCT Absorption im Falle von **M4** und **M5** lediglich Phosphoreszenz mit ausgeprägtem MLCT Charakter zu sehen ist, kann nach Anregung der ligandzentrierten Übergänge zusätzlich noch Fluoreszenz beobachtet werden. Dieser Sachverhalt, der im Allgemeinen als duale Lumineszenz bezeichnet wird, ist auf eine Verzweigung des Relaxationspfades nahe des Franck-Condon-Punktes des $S_0 \rightarrow S_1$-Übergangs zurückzuführen. Beide Zerfallskanäle sind dabei voneinander unabhängig und führen jeweils zur Bevölkerung eines emittierenden angeregten Zustands. Um diesen verzweigten Relaxationspfad näher zu untersuchen, wurden vergleichende Experimente bei unterschiedlichen Anregungswellenlängen im Bereich ligandzentrierter $\pi\pi^*$-Übergänge oder $^1$MLCT-Übergänge durchzuführt. Die transiente Absorptionsspektroskopie stellt hierfür eine geeignete Methode dar, da es die hohe Zeitauflösung ermöglicht, sehr schnelle Prozesse zwischen der Bevölkerung des Franck-Condon-Punktes und dem energetisch tiefsten $^3$MLCT-Zustand zu beobachten.

Mit Hilfe dieser Technik konnte gezeigt werden, dass sowohl die photoinduzierte Dynamik als auch die spektrale Charakteristik der transienten Absorptionsspektren für **M4** und **M5** keine Abhängigkeit von der Anregungswellenlänge aufweisen. Es konnte weiterhin gezeigt werden, dass im Falle der Anregung ligandzentrierter Übergänge eine Auftrennung des angeregten Ensembles in zwei parallele Populationen aus einem „heißen“ Zustand nahe dem Franck-Condon-Punkt heraus erfolgt. Dieser Prozess geschieht auf einer Zeitskala schneller als 100 fs und entzieht sich damit der direkten Beobachtung. Aus vergleichenden Messungen der Fluoreszenzquantenausbeuten der ligandzentrierten Emission konnte darüber hinaus die Effizienz dieser internen Konversion aus dem „heißen“ $S_1$ in einen „heißen“ $^1$MLCT-Zustand abgeschätzt werden. Diese ist für **M4** und **M5** größer als 99 Prozent und im Fall von **M3** ca. 98 Prozent. Demzufolge bleibt bei **M3** ein messbarer Anteil der angeregten Moleküle im $S_1$ und liefert im transienten Absorptionsspektrum die typischen Beiträge der angeregten Zustandsabsorption des angeregten Liganden. In Bereichen, in denen die metallzentrierten Zustände nur einen geringen Absorptionsquerschnitt aufweisen, können diese Beiträge gemessen werden. Im Fall von **M3** führen sie zu leichten Abhängigkeiten der transienten Absorptionsspektren von der Anregungswellenlänge.

In allen drei untersuchten Komplexen kommt es somit je nach Anregungswellenlänge zu einer fast quantitativen Population des $^1$MLCT-Zustands. Aus diesem erfolgt anschließend, ebenfalls auf einer Zeitskala kleiner 100 fs, ein sehr schnelles ISC in den $^3$MLCT.[49] Die hohe Geschwindigkeit dieses spinverbotenen Prozesses leitet sich aus dem inneren Schweratomeffekt

der Metallkationen ab. Alle sich anschließenden Prozesse laufen nun auf einer Zeitskala von wenigen Pikosekunden bis mehreren Nanosekunden ab und können somit unter den experimentellen Gegebenheiten aufgelöst werden.

Die Prozesse, die zur „Abkühlung“ des „heißen“ $^3$MLCT führen, zeigen in allen drei Komplexen ein biexponentielles Verhalten, das durch $\tau_1$ = 2 - 6 und $\tau_2$ = 20 - 25 ps gekennzeichnet ist. Während es sich bei dem 2 - 6 ps Prozess um Energiedissipations- und Solvatisierungsprozesse handelt,[39, 40] kann der langsamere Prozess, analog dem freien Terpyridin, der dynamischen Planarisierung des Liganden im elektronisch angeregten Zustand zugeordnet werden. Dieser Prozess wirkt sich auch auf die Lage des $^3$MLCT aus, da durch die Planarisierung die Konjugation im Liganden zunimmt und es durch Delokalisierung zu einer effektiven Stabilisierung des $^3$MLCT kommt.[28, 29, 55, 62, 63] Aus dem bevölkerten energetisch tiefsten angeregten Zustand existieren diverse Desaktivierungskanäle für das angeregte Ensemble. Diese entziehen sich der direkten Beobachtung durch fs-zeitaufgelöste transiente Absorption, können aber durch temperaturabhängige Emissionsexperimente hinsichtlich ihrer Kopplung mit dem phosphoreszierenden $^3$MLCT untersucht werden.

Legt man das etablierte Modell der strahlenden und nicht-strahlenden Zerfallskanäle in Ruthenium(II)-Polypyridin Verbindungen zugrunde, existieren drei verschiedene Desaktivierungsmöglichkeiten für ein angeregtes $^3$MLCT Ensemble, die in Abbildung 4.3 schematisch angedeutet sind:[64, 65, 66]

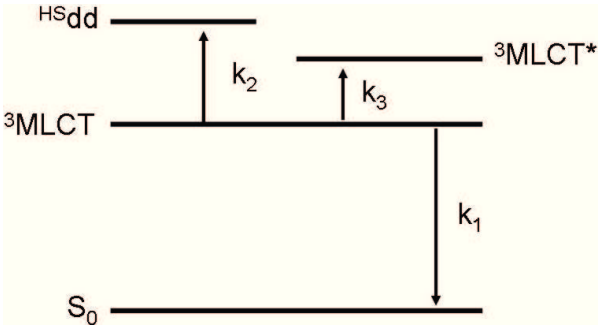


**Abbildung 4.3:** Übersichtsdarstellung strahlender ($k_1$) und nicht strahlender Zerfallskanäle ($k_2$ und $k_3$) in einem angeregten Ruthenium(II)-Terpyridinkomplex, dargestellt in einem qualitativen Jablonski Termschema.

- strahlende Desaktivierung des $^3$MLCT (Phosphoreszenz, $k_1$),
- nicht strahlende Kopplung des $^3$MLCT mit den energetisch höher liegenden $^{HS}$dd-Zuständen ($k_2$) und
- nicht strahlende Kopplung des $^3$MLCT mit einem energetisch höher liegenden $^3$MLCT*-Zustand ($k_3$).

Da die beiden letzten Prozesse Kopplungen zu energetisch höher liegenden Zuständen darstellen, benötigen sie eine Aktivierungsenergie und lassen sich somit durch Absenken der Temperatur sukzessive ausfrieren. Die damit einhergehende Blockierung dieser Zerfallskanäle führt zur Zunahme der Phosphoreszenzlebensdauer mit fallender Temperatur. Durch Anpassung einer, dem Modell von Svante Arrhenius folgenden, Exponentialgleichung ist es darüber hinaus möglich, die Aktivierungsenergien für diese Prozesse zu bestimmen (siehe Gleichung 4.1). Hier sind $k_1$ die radiative Konstante und $k_2$ - $k_3$ die Ratenkonstanten bei uendlich hoher Temperatur für die an der Entvölkerung des angeregten Zustands beteiligten und in Abbildung 4.3 schematisch dargestellten Prozesse. Die Parameter $\Delta E_2$ und $\Delta E_3$ sind die Aktivierungsenergien für

die Prozesse, die thermisch aktiviert verlaufen, $\tau$ die experimentell bestimmte Phosphoreszenzlebensdauer und $T$ die thermodynamische Temperatur. Die beim Anpassen von Gleichung 4.1 an die experimentellen Daten erhaltenen Resultate stimmen gut mit Werten ähnlicher Verbindungen überein.[66, 56] Besonders die hohe Aktivierungsenergie von ca. 3200 $cm^{-1}$ (1700 $cm^{-1}$ für **M1**[66]) für die strahlungslose Kopplung zwischen dem $^3$MLCT und den $^{HS}$dd-Zuständen spricht für eine effektive Stabilisierung des $^3$MLCT, was auf die angeregte Zustandsplanarisierung und damit einhergehende zunehmende Delokalisierung des $^3$MLCT zurückgeführt werden kann.

$$\tau(T) = \frac{1}{k_r + \Sigma k_{nr}(T)} = \frac{1}{k_1 + k_2 \exp\left(\frac{-\Delta E_2}{k_B T}\right) + k_3 \exp\left(\frac{-\Delta E_3}{k_B T}\right)} \tag{4.1}$$

Abschließend ist festzustellen, dass die verwendeten konjugierten Terpyridine einen positiven Effekt auf die photophysikalischen Eigenschaften ihrer Übergangsmetallkomplexe haben. Das manifestiert sich zum einen in einer Lokalisierung des initial bevölkerten $^1$MLCT auf dem Terpyridinfragment und dem sich direkt anschließenden Phenylring. Diese erhöhte Delokalisierung des $^1$MLCT führt zu einer deutlichen batho- und hyperchromen Verschiebung der Absorptionsbanden, relativ zu Ruthenium(II)-*bis*-Terpyridin (**M1**). Weiterhin führt eine angeregte Zustandsplanarisierung im $^3$MLCT zu einer weiteren energetischen Absenkung und Stabilisierung, was eine Verstärkung dieses Effekts mit sich bringt. Diese energetische Absenkung schlägt sich in erhöhten Aktivierungsenergien für strahlungslose Desaktivierungsprozesse und längeren Phosphoreszenzlebensdauern als bei Ruthenium(II)-*bis*-Terpyridin nieder.

Es muss festgehalten werden, dass diese Effekte durch den direkt in 4‘-Position des Terpyridinliganden gebundenen Phenylring hervorgerufen werden. Ein mittelbarer Einfluss des restlichen Chromophors ist hier nicht ersichtlich. Ob dies auch für Terpyridinliganden mit noch größeren konjugierten Systemen zutrifft, wie sie beispielsweise in Koordinationspolymeren zu finden sind, soll im folgenden Kapitel näher untersucht werden.

# 5 Angeregte Zustandsdynamiken in dinuklearen Komplexen konjugierter Terpyridine

Teile dieses Kapitels wurden in den folgenden Artikeln publiziert:

[**RS5**] R. Siebert, C. Hunger, J. Guthmuller, F. Schlütter, A. Winter, U. S. Schubert, L. Gonzàlez, B. Dietzek and J. Popp, Direct Observation of Temperature Dependent Excited-State Equilibrium in Dinuclear Ruthenium Terpyridine Complexes Bearing Electron-Poor Bridging Ligands, *Journal of Physical Chemistry C*, **2011**, *115*, 12677-12688

Bisher wurden konjugierte Terpyridinliganden und deren mononukleare Übergangsmetallkomplexe der 6. Nebengruppe untersucht. Aus diesen Experimenten ist bekannt, wie der Relaxationspfad in diesen Molekülen nach erfolgter Photoanregung verläuft. Diese Erkenntnisse stellen eine Grundvoraussetzung dar, um die angeregten Zustandsdynamiken in den entsprechenden Koordinationspolymeren zu verstehen Daraus erübrigt sich jedoch nicht die detaillierte Untersuchung dieser. Um sich der Untersuchung photoaktiver Koordinationspolymere einen weiteren, systematischen Schritt zu nähern, werden in diesem Abschnitt die experimentellen Ergebnisse dinukleaer *bis*-Terpyridinkomplexe diskutiert. Bei den hier zusammenfassend dargestellten Arbeiten wurde besonderes Augenmerk auf den Einfluss der elektronischen Struktur des Brückenliganden auf die angeregte Zustandsdynamik der dinuklearen Komplexe gelegt. Die dabei untersuchten Koordinationsverbindungen sind in Abbildung 5.1 graphisch dargestellt. Der wesentliche Unterschied zwischen den in Kapitel 4 untersuchten Verbindungen und den hier untersuchten dinuklearen Komplexen besteht in der Verwendung von *bis*-Terpyridinen mit einem ausgedehnteren konjugierten Chromophor.

## 5.1 Grundlegende spektroskopische Eigenschaften dinuklearer Übergangsmetallkomplexe der 6. Nebengruppe

Die grundlegenden spektroskopischen Eigenschaften dinuklearer Übergangsmetallkomplexe unterscheiden sich nicht wesentlich von denen ihrer mononuklearen Homologen, solange beide Metallzentren hinreichend räumlich und damit auch elektronisch separiert sind. Dies trifft auf die hier untersuchten Verbindungen zu, da sie im Bereich der $S_0 \rightarrow {}^1$MLCT-Übergänge

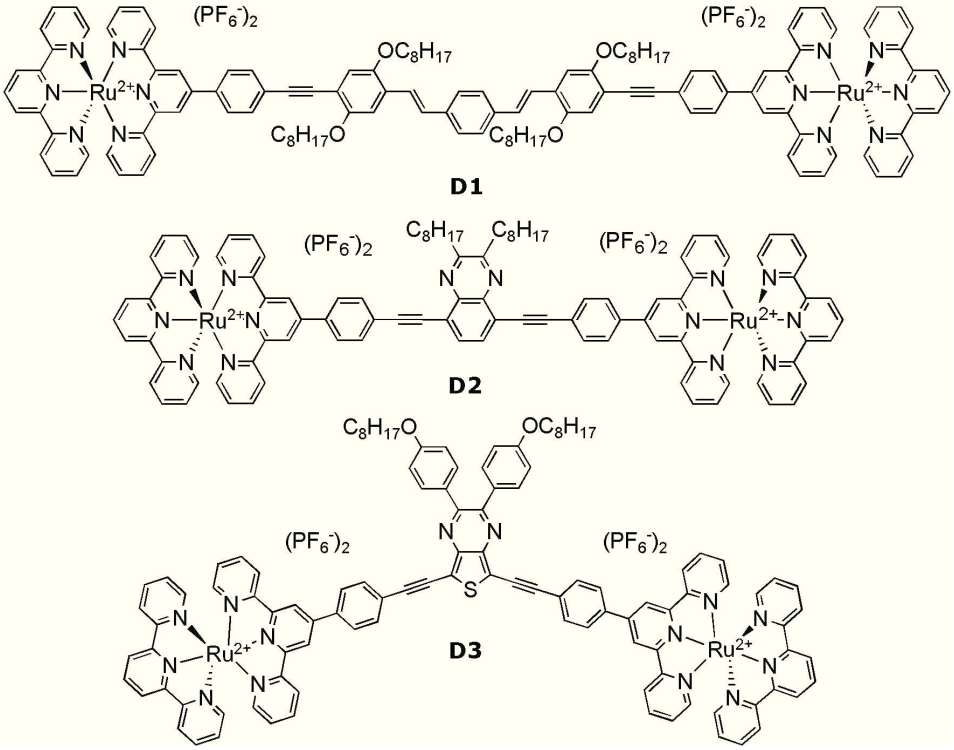


**Abbildung 5.1:** Strukturen der dinuklearen Ruthenium(II)-*bis*-Terpyridinkomplexe, deren angeregte Zustandsdynamik in diesem Kapitel diskutiert wird.

eine ähnliche spektrale Charakteristik wie die im Kapitel 4 beschriebenen mononuklearen Verbindungen aufweisen. Auch hier kommt es durch Delokalisierung und Stabilisierung der Ladungstransferzustände zu intensiven Absorptionsbanden um ca. 500 nm und einer schwachen Raumtemperaturphosphoreszenz um ca. 650 nm. Diese wird mit abnehmender Temperatur intensiver, was einen generellen Trend innerhalb der Terpyridinkomplexe von Ruthenium und Osmium darstellt. Ein wesentlicher Unterschied zwischen den hier untersuchten mono- und dinuklearen Komplexen besteht jedoch darin, das Letztere eine wesentlich längere Phosphoreszenzlebensdauer von ca. 150 - 250 ns im Vergleich zu ca. 36 ns im Fall der mononuklearen Komplexe aufweisen. Eine mögliche Erklärung dieses Phänomens ist ein Gleichgewicht im angeregten Zustand, welches sich durch Triplett-Energietransfer zwischen dem $^3$MLCT und dem ligandzentrierten $^3\pi\pi^*$ ($T_1$) ausbildet.[54, 55] Die Lebensdauer des angeregten Ensembles kann in diesem Falle als das mit Hilfe der Besetzungszahlen gewichtete Mittel der Lebensdauern des $^3$MLCT und des $^3\pi\pi^*$ ($T_1$) ausgedrückt werden.[67, 68] Derartige Prozesse wurden bereits für Ruthenium(II)-Koordinationsverbindungen beobachtet, die mit aromatischen Chromophoren wie Naphtalen, Anthracen und Pyren substituiert sind.[26, 69, 70, 71, 72, 73]

## 5.2 Gleichgewicht zwischen $^3$MLCT und $^3\pi\pi^*$ ($T_1$) in angeregten dinuklearen Rutheniumkomplexen

Ein Gleichgewicht zwischen zwei angeregten Zuständen sollte, wie bei thermodynamischen Gleichgewichten üblich, eine deutliche Temperaturabhängigkeit aufweisen. Demzufolge stellen temperaturabhängige spektroskopische Experimente die Methode der Wahl dar, um derartige Gleichgewichte zu untersuchen. Da sich der vermutete Gleichgewichtsprozess direkt auf die Bevölkerung und die Lebensdauer des energetisch tiefsten $^3$MLCT auswirkt, bietet es sich wie bei den mononuklearen Komplexen an, temperaturabhängige Emissionsexperimente durchzuführen. Dabei konnte für **D2** und **D3** nach anfänglicher Zunahme der Phosphoreszenzlebensdauer mit weiter abnehmender Temperatur ein plötzlicher Rückgang der Lebensdauer gemessen werden. Ein derartiges Verhalten wurde so bisher ausschließlich für Ruthenium(II)-dppz Komplexe beobachtet und dort ebenfalls auf einen Gleichgewichtsprozess im angeregten Zustand zurückgeführt.[67] Der experimentelle Befund kann so gedeutet werden, dass nach ISC aus dem $^1$MLCT in den $^3$MLCT sowie nach Energiedissipationsprozessen und angeregter Zustandsplanarisierung ein Teil des angeregten Ensembles durch Triplett-Energietransfer in den energetisch tiefer liegenden $^3\pi\pi^*$ relaxiert (siehe Abbildung 5.2). Dieser Prozess ist nicht quantitativ und benötigt, genau wie der analoge Prozess in umgekehrter Richtung, eine gewisse Aktivierungsenergie. Mit abnehmender Temperatur fehlt diese Aktivierungsenergie jedoch im System und die Gleichgewichtseinstellung wird zunehmend gehemmt und letztlich verhindert. Das führt in einem bestimmten Temperaturbereich zu einer zeitweiligen Abnahme der Lebensdauer, während sie global, durch das Ausfrieren anderer Zerfallskanäle, ansteigt. Die Überlagerung dieses Gleichgewichtsprozesses mit diesen, bereits von den mononuklearen Metallkomplexen bekannten, temperaturabhängigen Zerfallskanälen führt hier zu einer sehr komplexen Temperaturabhängigkeit. Diese kann nicht ohne weiteres durch eine simple, dem Modell von Svante Arrhenius folgende, Exponentialgleichung beschrieben werden. Um dennoch quantitative Informationen aus experimentellen Ergebnissen zu ziehen, wurden je nach Temperaturbereich zwei unterschiedliche Gleichungen verwendet. Oberhalb von 250 K spielt nur der Gleichgewichtsprozess zwischen $^3$MLCT und $^3\pi\pi^*$ eine Rolle, was zu einer stark verlängerten Lebensdauer führt. Das Emissionsverhalten unterhalb von 250 K kann in guter Näherung lediglich durch die Kopplung des $^3$MLCT zu den $^3$MLCT* und $^{HS}$dd-Zuständen erklärt werden. Diese beiden Grenzfälle werden jeweils durch Gleichung 5.1 bzw. 5.2 beschrieben. Dabei sind $k_1$ die radiative Konstante und $k_2$ bis $k_5$ die Geschwindigkeitskonstanten der einzelnen Zerfallskanäle des angeregten Ensembles bei unendlich hoher Temperatur. $k_6$ ist die Geschwindigkeitskonstante für den nicht strahlenden Zerfall des liganszentrierten $^3\pi\pi^*$, welcher jedoch so langsam abläuft das er in den Gleichungen 5.1 und 5.2 nicht berücksichtigt wird. $\Delta E_2$ bis $\Delta E_5$ sind die Aktivierungsenergien für die Prozesse, die thermisch aktiviert verlaufen. $\tau$ ist die experimentell bestimmte Phosphoreszenzlebensdauer und $T$ die thermodynamische Temperatur.

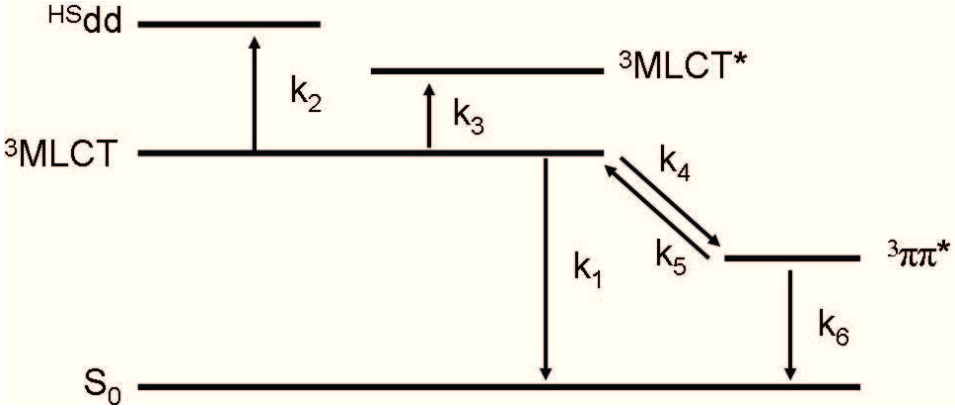


**Abbildung 5.2:** Übersichtsdarstellung strahlender und nicht strahlender Zerfallskanäle in einem angeregten dinuklearen Ruthenium(II)-*bis*-Terpyridinkomplex in einem qualitativen Jablonski Termschema

$$\tau(T < 250K) = \frac{1}{k_1 + k_2 \exp\left(\frac{-\Delta E_2}{k_B T}\right) + k_3 \exp\left(\frac{-\Delta E_3}{k_B T}\right)} \tag{5.1}$$

$$\tau(T > 250K) = \frac{1}{k_1 + k_4 \exp\left(\frac{-\Delta E_4}{k_B T}\right) + k_5 \exp\left(\frac{-\Delta E_5}{k_B T}\right)} \tag{5.2}$$

Im Falle der Komplexe **D2** und **D3** (siehe Abbildung 5.1) kann der Effekt einer Gleichgewichtseinstellung im angeregten Zustand quantitativ beschrieben werden. Die experimentellen Befunde stehen darüber hinaus in sehr guter Übereinstimmung mit Berechnungen der energetischen Lage der beteiligten angeregten Zustände, die mittels TDDFT Rechnungen in der Arbeitsgruppe von Prof. González durchgeführt wurden. Dies erlaubt eine eindeutige Zuordnung der koexistierenden Zustände bezüglich ihrer Multiplizität, Lokalisierung und energetischen Lage. Dadurch werden die teils etablierten Annahmen über den Charakter der am Gleichgewicht beteiligten angeregten Zustände untermauert.

Das temperaturabhängige Emissionsverhalten von **D1** kann mit Gleichung 5.1 und 5.2 nicht angepasst werden. Dies ist auch unter Verwendung des einfacheren Modells, das nur Kopplungen zu den $^3$MLCT*- und $^{HS}$dd-Zuständen berücksichtigt (siehe Gleichung 4.1), nicht möglich. Die Ursache dafür ist wahrscheinlich, dass auch hier ein Gleichgewichtsprozess zwischen zwei angeregten Zuständen eine Rolle spielt, der sich jedoch nicht so eindeutig in den temperaturabhängigen Messungen äußert. Das liegt möglicherweise an der individuellen und zu **D2** und **D3** verschiedenen relativen Lage der angeregten Zustände. Ein Ansatzpunkt zum Treffen tragfähiger Aussagen über das Auftreten eines Gleichgewichtsprozesses in **D1** basiert auf den unterschiedlichen spektralen Signaturen der angeregten Zuständen, zwischen denen sich das Gleichgewicht ausbildet. Somit ist es möglich, den Populationstransfer zwischen den Zuständen spektroskopisch zu verfolgen.[60, 74, 75, 76, 77] Eine Vorraussetzung dafür ist jedoch eine hinreichend hohe experimentelle Zeitauflösung, die über der Zeitskala des Prozesses liegt. Daher wurden fs-zeitaufgelöste transiente Absorptionsexperimente an **D1** - **D3** durchgeführt.

Alle drei untersuchten Koordinationsverbindungen zeigen die erwarteten ähnlichen spektralen Signaturen in ihren transienten Absorptionsspektren. Das heißt, dass der spektrale Bereich unter 520 nm in der Regel durch eine starke Grundzustandsbleichung und der längerwellige Bereich von angeregter Zustandsabsorption dominiert wird, was Abbildung 5.3 am Beispiel von **D1** veranschaulicht. Dadurch unterscheiden sich die Komplexe nicht signifikant von den in Kapitel 3 diskutierten Verbindungen, die teilweise ein stark strukturverwandtes Chromophor als Liganden tragen. Bei genauerer Betrachtung der zeitlichen Änderung des Signals fällt auf, dass in allen Fällen zur Anpassung ein Modell mit vier Zeitkonstanten notwendig ist.

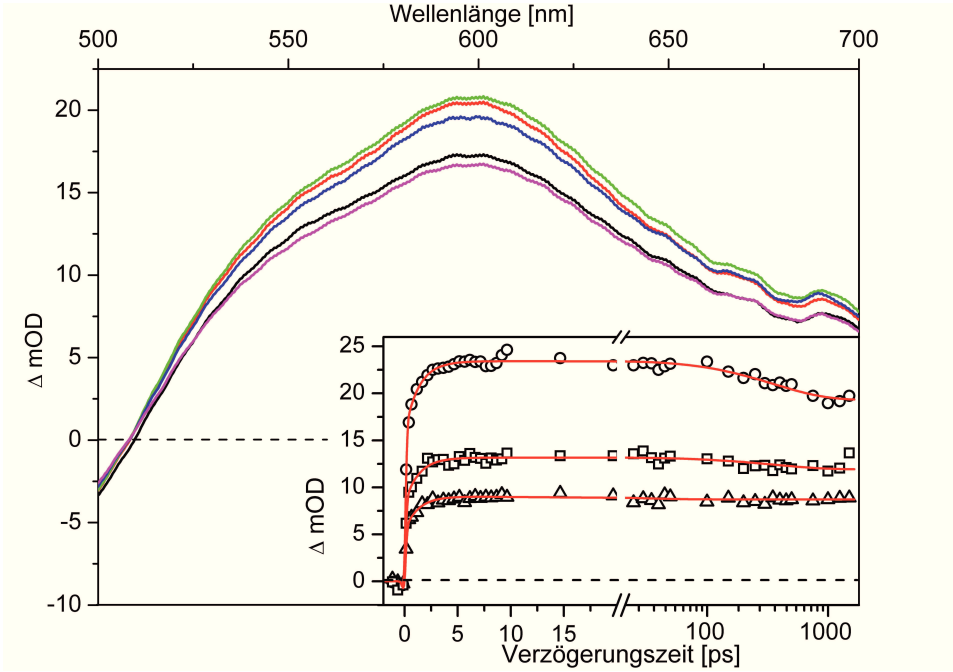


**Abbildung 5.3:** Transiente Absorptionsspektren des dinuklearen Metallkomplexes **D1** bei einer Verzögerungszeit von 1 ps (schwarz), 5 ps (rot), 10 ps (grün), 100 ps (blau) und 1000 ps (magenta) zwischen Pump- (488 nm) und Probepuls. Der Einsatz zeigt ausgewählte Kinetiken bei 550 nm (Rechtecke), 600 nm (Kreise) und 650 nm (Dreiecke), zusammen mit einem multiexponentiellen Fit (rote Linie).

Neben den schon bekannten Energiedissipationsprozessen $\tau_1 \approx 1\ ps$ , der angeregten Zustandsplanarisierung $\tau_2 \approx 6 - 27\ ps$, sowie dem langsamen Zerfall des angeregten Ensembles über verschiedene strahlende und nicht strahlende Zerfallskanäle $\tau_4 \approx 145 - 223\ ns$, die anhand der mononuklearen Komplexe in Kapitel 4 eindeutig identifiziert werden konnten, tritt hier ein weiterer Prozess in Erscheinung ($\tau_3 \approx 361 - 788\ ps$). Dieser läuft in allen Fällen auf einer Zeitskala von mehreren hundert ps ab und führt im experimentell zugänglichen Spektralbereich zu einer Abnahme der angeregten Zustandsabsorption des $^3$MLCT und gleichzeitig zum Aufbau von spektral verschiedenen Banden. Als Ursache dafür kann Triplett-Energietransfer aus dem $^3$MLCT in den $^3\pi\pi^*$ angesehen werden. Die dabei zu erwartende Intensitätszunahme im Bereich der angeregten Zustandsabsorption des $^3\pi\pi^*$ ist im Falle von **D1** und **D2** direkt bei Wellenlängen unterhalb von 510 nm sichtbar. Durch die Überlagerung dieses Effektes mit der angeregten Zustandsabsorption der $^3$MLCT-Zustände und der Grundzustandsbleichung fällt die Amplitude der Signaländerung jedoch gering aus. Für **D3** wird die $^3\pi\pi^*$ Absorption

im nahen Infrarot bei ca. 1000 nm erwartet. Die spektrale Lage dieses Übergangs wurde auf der Basis experimenteller Korrelationen zwischen der Lage des $S_0 \rightarrow S_1$-Übergangs der der angeregten Zustandsabsorption des $^3\pi\pi^*$ in konjugierten Systemen systematisch variierender Größe abgeschätzt.[78, 79, 80]

Auf diese experimentellen Befunde aufbauend lässt sich sagen, dass sich in allen drei untersuchten dinuklearen Metallkomplexen ein Gleichgewicht im angeregten Zustand einstellt, was die angeregte Zustandslebensdauer der Systeme verlängert. Dabei scheint die Struktur des jeweiligen *bis*-Terpyridins keinen signifikanten Einfluss zu haben. Dieses Ergebnis kann damit begründet werden, dass die Triplettzustände der Liganden im Allgemeinen energetisch tiefer liegen als die $^3$MLCT-Zustände, wodurch immer eine gewisse Triebkraft zur Gleichgewichtseinstellung vorhanden ist. Die exakte Lage der terpyridinzentrierten $^3\pi\pi^*$-Zustände konnte experimentell nicht bestimmt, sondern nur aus Simulationen oder Analogiebeziehungen abgeschätzt werden.[78, 79, 80] Dies macht letztlich eine quantitative Korrelation der Zeitkonstanten mit molekularen Strukturparametern unmöglich.

Um einen detaillierteren Einblick in die Abhängigkeit der Gleichgewichtseinstellung vom verwendeten konjugierten *bis*-Terpyridin zu bekommen, könnten temperaturabhängige transiente Absorptionsexperimente einen Beitrag leisten. Da der Prozess des Triplett-Energietransfers auch durch die Markustheorie beschrieben werden kann,[81] liefern temperaturabhängige Messungen der damit verbundenen Zeitkonstante genauere Einblicke. Diese Experimente können eine Weiterführung der vorliegenden Arbeit darstellen.

# 6 Einzelmolekülspektroskopie an Koordinationspolymeren konjugierter Terpyridine

## 6.1 Grundlegende spektroskopische Eigenschaften von Koordinationspolymeren konjugierter Terpyridine

Das hier untersuchte Koordinationspolymer besteht aus konjugierten *bis*-Terpyridinen, die durch Zinkionen verknüpft sind. Durch die Verwendung von Zink anstelle von Eisen, Ruthenium oder Osmium tragen keine MLCT-Übergänge zur angeregten Zustandsdynamik bei. Dadurch spiegeln die Koordinationspolymere im Wesentlichen die photophysikalischen Eigenschaften ihrer kleinsten Baueinheiten, den konjugierten *bis*-Terpyridinen wieder.[1, 21, 82] So unterscheiden sich weder Absorptions- noch Emissionsspektren der Monomere und des Polymers signifikant. Es kommt lediglich zu einer deutlichen Verringerung des Absorptionsquerschnitts je *bis*-Terpyridineinheit sowie zu einer deutlichen Verringerung der Fluoreszenzquantenausbeute bei nahezu unveränderter Fluoreszenzlebensdauer (siehe Abbildung 6.1). Diese in ihrerer Quantenausbeute verringerte, aber immer noch starke Emission ermöglicht die Untersuchung der hier vorgestellten Koordinationspolymere durch Einzelmolekülfluoreszenzspektroskopie.[83]

Allgemein ist der Kenntnisstand über die lichtinduzierten Prozesse in dieser Klasse von Koordinationspolymeren als gering einzustufen. Dem gegenüber steht eine Vielzahl von Arbeiten zur Synthese dieser Systeme.[18, 20] Die hohe strukturelle Ähnlichkeit des hier verwendeten *bis*-Terpyridins mit MEH-PPV, einem sehr intensiv untersuchten Vertreter organischer polymerer Halbleiter, ermöglicht einen direkten Vergleich beider Klassen von fluoreszierenden Polymeren. Eine zentrale Frage besteht darin, ob sich die lichtinduzierten Prozesse in MEH-PPV und den MEH-PPV analogen Koordinationspolymeren gleichen, oder ob die systematische Unterbrechung des konjugierten Systems durch oktaedrische Zink(II)-Terpyridinkomplexe eine föllig andere angeregte Zustandsdynamik induziert.

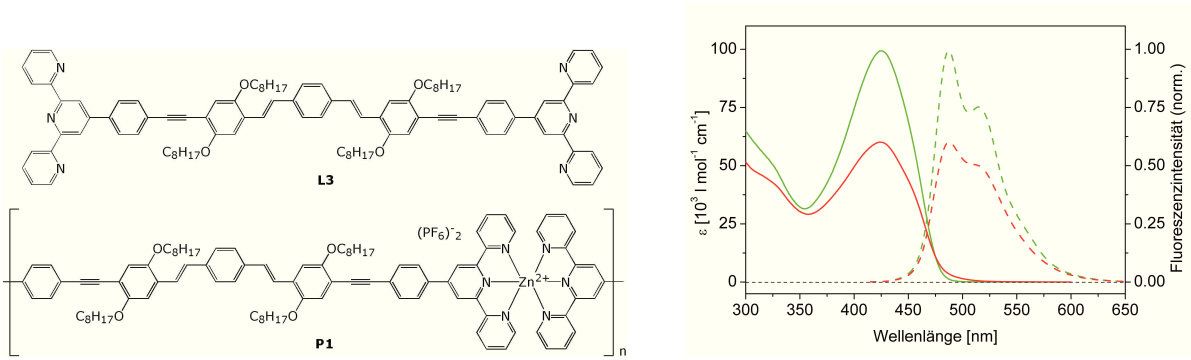


**Abbildung 6.1:** Struktur eines konjugierten *bis*-Terpyridins (**L3**) und dem sich daraus ableitenden Zink(II)-Koordinationspolymer **P1**, welches durch Einzelmolekülspektroskopie untersucht wurde. Weiterhin sind die Absorptions- und Emissionsspektren von **L3** (grün) und **P1** (rot) gezeigt.

## 6.2 Bestimmung der absoluten Fluoreszenzintensität isolierter Koordinationspolymere

Wie bereits erwähnt, besteht ein signifikanter Unterschied zwischen den hier untersuchten Koordinationspolymeren und deren kleinsten Baueinheiten in der deutlichen Verringerung der Fluoreszenzquantenausbeute nach der Polymerisierung. Für dieses Verhalten existieren zwei mögliche Erklärungen: Zum einen ist es möglich, dass die Komplexierung mit Zinkionen die angeregte Zustandsdynamik der entsprechenden *bis*-Terpyridine stark beeinflusst und somit zu einer Verringerung der Quantenausbeute jedes einzelnen, in das Polymer eingebauten, Chromophors führt. Auf der anderen Seite ist es denkbar, dass die angeregte Zustandsdynamik der *bis*-Terpyridine durch die Koordination nicht signifikant beeinflusst wird, also die individuelle Quantenausbeute der einzelnen Chromophore unverändert bleibt. Die verringerte Quantenausbeute des Polymermoleküls als Ganzes kann dann nur durch ein „Ausschalten“ einer bestimmten Anzahl von Chromophoren im Polymer erklärt werden.

Um dieser Frage auf den Grund zu gehen, wurde die absolute Helligkeit einer großen Anzahl isolierter Polymermoleküle in einer Matrixumgebung bestimmt.[84, 85] Die Matrix dient zum einen dazu, das Polymer vor unerwünschten Photoreaktionen zu schützen. Des Weiteren kann dadurch in guter Näherung eine lösungsmittelartige Umgebung simuliert werden.[83] Bei der Verwendung üblicher Matrixsysteme wie PMMA oder PS kam es aufgrund des polykationischen Charakters der Koordinationspolymere zur Entmischung während der Probenpräparation. Aus diesem Grund wurde ein statistisches PMMA/PMA (85%/15%) Kopolymer als Matrix verwendet, welches sich ausgezeichnet zur Abscheidung von Matrixpolymerfilmen mit statistisch verteilten, isolierten Koordinationspolymermolekülen eignete. Für die Statistik über die absolute Helligkeit einzelner Moleküle wurden die Werte für ca. 3000 Moleküle aus fluoreszenzmikroskopischen Aufnahmen ermittelt, wie sie exemplarisch in Abbildung 6.2 zu sehen sind. Unter Einbeziehung der für ein einzelnes Chromophor im Polymer erwarteten Fluoreszenzintensität konnte darüber hinaus der relative Gehalt an emittierenden Chromo-

phoren in einem Polymermolekül bestimmt werden. Demnach fluoreszieren in einem solchen Polymer nur durchschnittlich 33% der Chromophore. Die photophysikalischen Eigenschaften der enthaltenen *bis*-Terpyridine werden jedoch nur marginal beeinflusst, was anhand der nur geringfügigen Änderungen im Absorptions- und Emissionsspektrum sowie in der Emissionslebensdauer deutlich wird. Vielmehr scheint es in den Koordinationspolymeren einen „dunklen" Zustand zu geben, in dem sich im Durchschnitt 67% der Chromophore befinden. In diesem können die Chromophore zwar Photonen absorbieren aber nicht emittieren. Es kann jedoch ausgeschlossen werden, dass es sich bei diesen dunklen Zuständen um photoinduzierte Fluoreszenzlöscher handelt. Deren Häufigkeit hängt von der Anregungsrate eines Moleküls und somit direkt von der Anregungsleistung ab. Um den Einfluss solcher photoinduzierter Löscher auszuschließen, wurde die experimentelle Helligkeitsverteilung mit einem, der Anregungsleistung entsprechenden, experimentell bestimmten Korrekturfaktor verrechnet.

Eine vielversprechende Erklärung dafür, dass im Durchschnitt nur 33% der Chromophore emittieren, sind sterische Spannungen im Makromolekül. Aus den im Kapitel 3 präsentierten Ergebnissen geht hervor, das die Planarisierung des Terpyridinliganden im angeregten Zustand einen Schlüsselprozess innerhalb der angeregten Zustandsdynamik darstellt. Wird nun das Chromophor an der Planarisierung gehindert, ist die Emission eines Photons aus dem $S_1$ sehr unwahrscheinlich oder nicht möglich. Während die Planarisierung im isolierten Liganden eine freie, ungehinderte Bewegung darstellt, so wird sie durch den Einbau des Liganden in ein starres Koordinationspolymer signifikant gehindert. Die verringerte Fluoreszenzquantenausbeute von Chromophoren im Koordinationspolymer relativ zu ihren freien ungebundenen Gegenstücken, kann also durch eine gehinderte Planarisierung im angeregten Zustand erklärt werden.

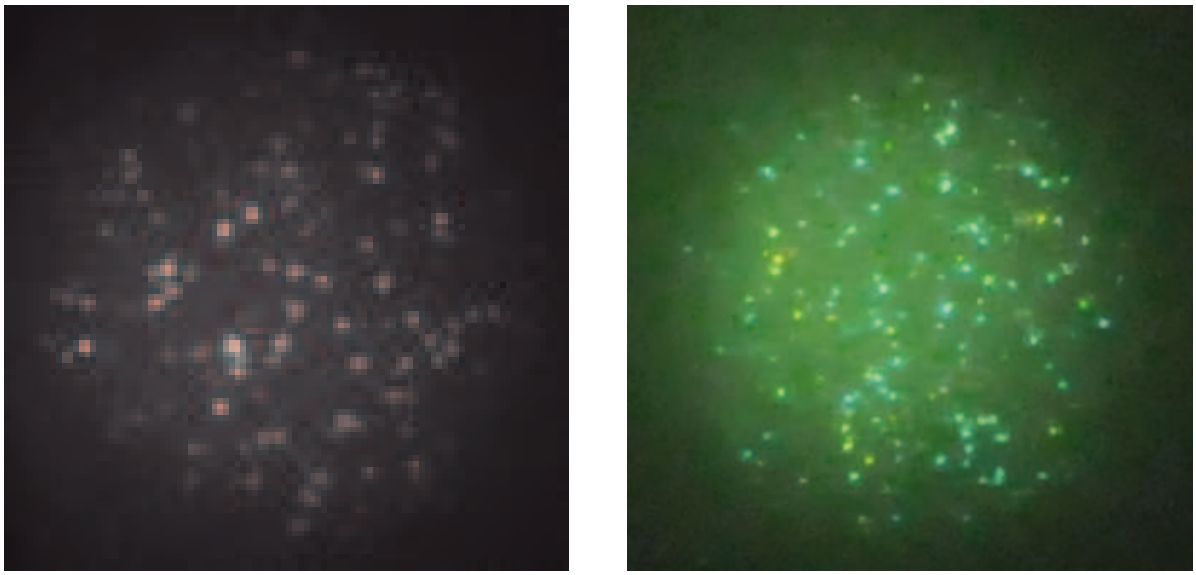

**Abbildung 6.2:** Grauwertbild (links) und Echtfarbenbild (rechts) einer typischen Probe für die Einzelmolekülspektroskopie, erhalten durch Aufschleudern einer verdünnten Koordinationspolymerlösung in DMF mit einem Matrixgehalt von 10mg/ml PMMA/PMA auf einem Glasträger.

Allgemein kann der durchschnittliche Gehalt an „aktiven“ Chromophoren mit ca. 33% als sehr hoch eingestuft werden. In MEH-PPV dagegen bewegt sich dieser Wert je nach DP zwischen 1% und 25%,[84] wobei der Anteil fluoreszierender Chromophore in einem Polymer mit dem DP zu korrelieren scheint. Das kann dadurch erklärt werden, dass kurze Makromoleküle weniger stark geknäult vorliegen. Das bedeutet, dass in Polymeren mit hohem DP der relative Anteil emittierender Chromophore geringer ist als in einem entsprechenden Polymer mit niedrigem DP. Im Fall der hier untersuchten Koordinationspolymere kann auf der Basis von AFM Experimenten und der hydrodynamischen Charakterisierung an stark strukturverwandten Zink- und Rutheniumkoordinationspolymeren ein geringer DP von ca. 35 sowie eine nahezu lineare Geometrie angenommen werden.[17, 23, 24] Dadurch sind intramolekulare Wechselwirkungen einzelner Chromophore innerhalb des Polymers vernachlässigbar. Diese Annahme konnte durch polarisationsabhängige Experimente für die hier untersuchten Systeme bestätigt werden, was anhand von Abbildung 6.3 deutlich wird. Dabei wurde eine starke Modulation der Fluoreszenzintensität mit periodisch variierender Anregungspolarisation mit Modulationstiefen um 1 gefunden. Dies spricht für eine streng parallele Ausrichtung aller Chromophore in einem Polymer, wie es nur in linearen Makromolekülen zu erwarten ist.

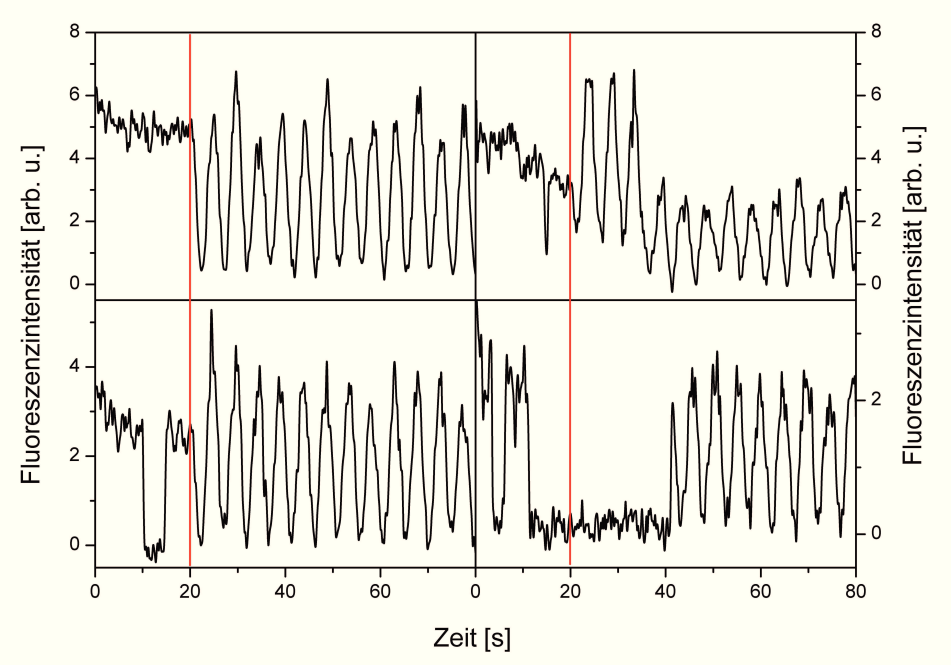


**Abbildung 6.3:** Abhängigkeit der Fluoreszenzintensität isolierter Polymermoleküle von der Polarisation des Anregungslichtes. Die rote Linie markiert den Zeitpunkt, ab dem die Anregungspolarisation durch Rotation einer $\lambda/2$-Platte kontinuierlich variiert wurde.

## 6.3 Zeitaufgelöste Fluoreszenzmessung an einzelnen, isolierten Koordinationspolymeren

Wie bereits bei den polarisationsabhängigen Experimentenim vorangegangenen Abschnitt zu erkennen war, ist die Fluoreszenzintensität eines einzelnen Polymermoleküls zeitlich nicht konstant. Vielmehr scheint sie zwischen diskreten Werten zu schwanken, sie „blinkt“.[86] Solche Fluktuationen der Fluoreszenzintensität stellen einen generellen Effekt in der Einzelmolekülspektroskopie dar, der sowohl bei Farbstoffmolekülen als auch in Multichromophorsystemen auftritt und verschiedene Ursachen haben kann. Eine allgemeingültige Erklärung stellt der Übergang eines Chromophors in einen nicht näher spezifizierten, nicht-lumineszierenden Zustand dar. Ist dieser Prozess reversibel, wie bei der Population von langlebigen Triplettzuständen oder der Bildung separierter Ladungsträger, kann das Molekül nach Verstreichen der Lebensdauer dieses Zustandes wieder Fluoreszenz aussenden. Ist der Prozess irreversibel, wie zum Beispiel bei Photoreaktionen die zur Zerstörung des Chromophors führen, bleibt das Chromophor dauerhaft dunkel.[87, 88] In ersterem Fall fluktuiert die Fluoreszenzintensität zwischen einem Maximal- und einem Minimalwert, während es im zweiten Fall zu einer steten Abnahme der Fluoreszenzintensität des Polymers kommt.

Bei zeitaufgelösten Einzelmolekülexperimenten im Millisekundenbereich an den hier beschriebenen Koordinationspolymeren konnten in einer schützenden Stickstoffatmosphäre zwei unterschiedliche Arten des Blinkens beobachtet werden. Zum Einen treten Sprünge kleiner Amplitude auf, deren Intensitätsschwankungen mit dem reversiblen An- und Ausschalten einzelner Chromophore korreliert werden können. Des Weiteren kommt es mit deutlich geringerer Häufigkeit zu globalen Ereignissen, bei denen der Großteil, oder sogar alle Chromophore eines Polymers simultan ausgeschaltet werden.

Das individuelle Blinken einzelner Chromophore kann durch strukturelle Fluktuationen der Chromophore erklärt werden. Es ist von detaillierten Studien an PBI-Farbstoffen und deren Derivaten bekannt, dass Geometrieänderungen, insbesondere Torsionen, einen starken Einfluss auf die spektroskopischen Eigenschaften haben.[89, 90] Auch die für den Aufbau der hier untersuchte Koordinationspolymere verwendeten *bis*-Terpyridine verfügen über ein solches flexibles Strukturelement, das die spektroskopischen Eigenschaften maßgeblich mitbestimmt. Dabei handelt es sich um die, im Grundzustand ca. 35° verdrillte, Verknüpfung der Terpyridineinheit mit dem sich anschließenden Chromophor.[28] Thermische Fluktuationen dieses Winkels sind die wahrscheinlichste Ursache für das individuelle Blinken einzelner Chromophore. Daneben kommt noch ISC in den $T_1$ in Betracht, wodurch ebenfalls einzelne Chromophore über mehrere $\mu$s in einen dunklen Zustand gelangen können.

Die Ursache für die drastischen Intensitätsschwankungen, bei denen teilweise die Emission des ganzen Moleküls über mehrere Sekunden ausgeschaltet wird, können auf Basis der experimentellen Daten nicht eindeutig geklärt werden. Prinzipiell ist dieses Verhalten wahrscheinlich auf die lichtinduzierte Bildung global wirkender statischer Fluoreszenzlöscher zurückzuführen,

deren Lebensdauer bis zu mehrere Sekunden beträgt. Die experimentell gefundene hohe Sensitivität dieser Löscher gegenüber Sauerstoff (siehe Abbildung 6.4) lässt vermuten, dass es sich dabei entweder wiederum um langlebige Triplett- oder ladungsseparierte Zustände handelt. Beim Wechsel der experimentellen Atmosphäre von reinem Stickstoff zu Luft (ca. 21% Sauerstoff) kommt es zu einer sofortigen Zunahme der Fluoreszenzintensität. Ein solcher Effekt wurde bereits für konjugierte Polymere, Nanopartikel und einzelne Farbstoffmoleküle beobachtet und beruht auf der Desaktivierung langlebiger statischer Fluoreszenzlöscher durch molekularen Sauerstoff. [91, 92, 93, 94] Es konnte in der Vergangenheit mehrfach gezeigt werden, dass sowohl freie Ladungsträger (Elektronen und Löcher) als auch Triplettzustände effektive die Fluoreszenz einzelner Moleküle/Chromophore ausschalten.[95, 96] In beiden Fällen wird durch Sauerstoff der statische Fluoreszenzlöscher vernichtet und das Polymer kann nach erneuter Anregung wieder fluoreszieren.

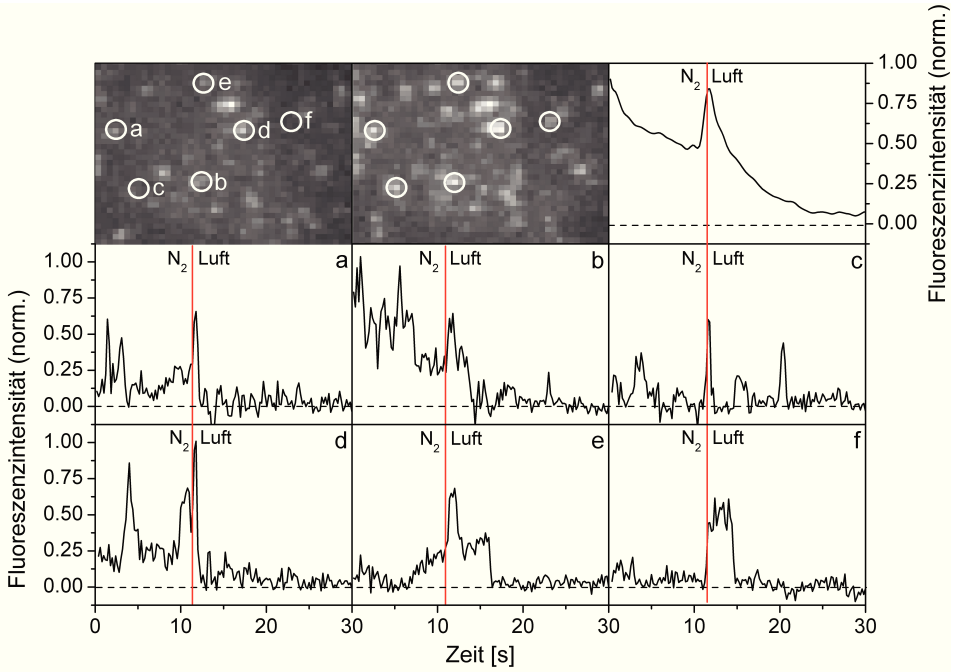


**Abbildung 6.4:** Abhängigkeit der Fluoreszenzintensität isolierter Polymermoleküle von der Zusammensetzung der umgebenden Atmosphäre. Die Bilder oben links und in der Mitte zeigen eine Anzahl von Polymermolekülen in einer Stickstoff- und in einer Luftatmosphäre. Die Ausschnitte a-f zeigen die Transienten von sechs ausgewählten Molekülen, während der Ausschnitt oben rechts die Summe der Transienten von ca. 100 Polymermolekülen zeigt. Die rote Linie markiert dabei den Zeitpunkt an dem die Atmosphäre geändert wurde.

Zwar macht die lange Dauer der dunklen Perioden Triplettzustände als Ursache unwahrscheinlich, jedoch konnte die Bildung ladungsseparierter Zustände bisher noch nicht experimentell bestätigt werden. In guter Übereinstimmung mit den experimentellen Befunden, sowie in Anlehnung an detaillierte Studien zu langlebigen statischen Fluoreszenzlöschern in isolierten Farbstoffmolekülen wird folgendes Modell vorgeschlagen:[91, 97, 98]

Durch die intrinsischen photophysikalischen Eigenschaften der *bis*-Terpyridinchromophore, verstärkt durch den Schweratomeffekt der Zinkionen, kommt es zu einer effektiven Bevölkerung von Triplettzuständen, die selbst nicht emittieren. Weiterhin kommt es zur Bildung

freier Ladungsträger, die eine Lebensdauer von mehreren Sekunden aufweisen, die als globale statische Fluoreszenzlöscher wirken und die in großen Bereichen des Polymermoleküls die Fluoreszenz ausschalten. Ob sich die ladungsseparierten Zustände aus Singulet- oder Triplettexzitonen bilden, kann derzeit noch nicht gesagt werden. Durch beide Effekte sowie durch strukturelle Fluktuationen einzelner Chromophore, ist in jedem Koordinationspolymermolekül nur ein bestimmter Anteil der enthaltenen Chromophore in einem „hellen“ Zustand und trägt zur emittierten Gesamtintensität bei. Die Quantenausbeute einzelner „heller“ Chromophore bleibt dabei unverändert zu der Quantenausbeute der isolierten Chromophore in Lösung.

# 7 Zusammenfassung und Ausblick

Auf der Basis der experimentellen Ergebnisse, die in dieser Arbeit vorgestellt wurden, kann die Eignung von konjugierten *bis*-Terpyridienen zum Aufbau von Koordinationspolymeren mit interessanten und vielversprechenden spektroskopischen Eigenschaften untermauert werden. Ein besonderer Schwerpunkt der Arbeit lag dabei auf der Untersuchung der angeregten Zustandsdynamik in den konjugierten Terpyridinen selbst, sowie in den sich daraus ableitenden mono-, di- und polynuklearen Koordinationsverbindungen mit Metallen der 6. Nebengruppe. Durch die Anwendung zeitaufgelöster spektroskopischer Techniken konnte zunächst der Relaxationspfad in den freien Terpyridinliganden aufgeklärt werden, wobei zum Teil die in der Literatur prognostizierten Effekten erstmals direkt nachgewiesen werden konnten.

Zum Einen ist das die relativ effiziente Population von langlebigen Triplettzuständen, die, zumindest in freien unkomplexierten Terpyridinen bisher nicht mit in die Beschreibung der angeregten Zustandsdynamik einbezogen wurden. Des Weiteren konnte durch die Verwendung von Lösungsmitteln, die sich systematisch in kritischen Parametern wie Polarität und Viskosität unterscheiden, eine signifikante Geometrieänderung im angeregten Zustand belegt werden. Dabei handelt es sich um die Planarisierung zwischen der Terpyrdineinheit und dem in 4‘-Position verknüfpften Chromophor. Dadurch kommt es zu einer Erhöhung der Konjugation beider Molekülfragmente, womit eine starke Rotverschiebung des Fluoreszenzspektrums einhergeht. Der starke Unterschied zwischen Grund- und angeregter Zustandsgeometrie in den hier untersuchten konjugierten Terpyridinen führt somit zu einer deutlichen Stabilisierung der angeregten Zustände, was sich in den hohen Emissionsquantenausbeuten manifestiert. Somit stellen diese Systeme geeignete Bausteine photoaktiver Koordinationspolymere dar, in denen die lichtinduzierte Bildung stabiler und langlebiger angeregter Zustände eine zentrale Rolle spielt.

Die Komplexierung dieser Terpyridinliganden mit Übergangsmetallen der 6. Nebengruppe führt zu einer dramatischen Änderung der angeregten Zustandsdynamik. Zwar konnte gezeigt werden, dass innerhalb der ligandzentrierten angeregten Zustände der Relaxationspfad nahezu identisch verläuft, jedoch kommt es nahe des Franck-Condon-Punktes zu einer fast quantitativen IC in die metallzentrierte $^1$MLCT-Zustände. Dies führt zu einer annähernd vollständigen Löschung der Fluoreszenz bei ansonsten nahezu unveränderter angeregter Zustandsdynamik in den ligandzentrierten $\pi\pi^*$-Zuständen. Diese fast unveränderte Dynamik ist ein starkes Indiz dafür, dass die elektronische Struktur des Liganden von den Metallkationen nur geringfügig beeinflusst wird und ein sehr effektives IC in die metallzentrierten $^3$MLCT-Zustände der dominanteste Effekt der Komplexierung ist. Innerhalb der metallzentrierten Zustände verläuft der

Relaxationspfad prinzipiell so, wie es für die meisten Polypyridinkomplexe der Fall ist: Nach Photoanregung des $^1$MLCT-Zustands, welcher unabhängig von der Größe des in 4‘-Position verknüpften Chromophors lediglich über die Terpyridineinheit selbst und den sich daran dierekt anschließenden Phenylring delokalisiert ist, kommt es zu einem schnellen ISC in den $^3$MLCT-Zustand. Dieser Prozess läuft im Allgemeinen auf einer Zeitskala kleiner als 100 fs ab, was durch den Schweratomeffekt der Übergangsmetallkationen erklärt wird. Innerhalb dieses Zustandes kommt es zu Energiedissipations- und Solvatisierungsprozessen, zu denen unter anderem die Planarisierung des konjugierten Terpyridinliganden gehört. Da der $^3$MLCT analog dem $^1$MLCT auf der Terpyridineinheit und dem direkt daran geknüpften Phenylring lokalisiert ist, führt diese Planarisierung zu einer besseren Delokalisierung des angeregten Zustands. Das bewirkt eine zusätzliche energetische Stabilisierung des lumineszierenden $^3$MLCT-Zustands, was sich in einer erhöhten Phosphoreszenzlebensdauer, einem rotverschobenen Emissionsspektrum, sowie in einer erhöhten Barriere für die strahlungslose Kopplung zu den $^{HS}$dd-Zuständen zeigt. Somit kann festgehalten werden, dass die hier untersuchten konjugierten Terpyridine einen deutlichen stabilisierenden Effekt auf den energetisch tiefsten $^3$MLCT-Zustand haben. Es kommt somit in den mononuklearen Komplexen zu einer effizienten, von der Anregungswellenlänge nahezu unabhängigen Bevölkerung eines langlebigen und stabilen ladungsseparierten Zustands.

Bei der Erweiterung der untersuchten Moleküle von mono- zu dinuklearen Komplexen kann ebenfalls die bereits bei den mononuklearen Komplexen diskutierte Stabilisierung des energetisch tiefsten $^3$MLCT-Zustands beobachtet werden. Die Population erfolgt nach einem identischen Muster, je nachdem ob liganden- oder metallzentrierte Übergänge angeregt werden. Darüber hinaus tritt hier ein zusätzlicher Prozess auf, der in den mononuklearen Systemen nicht beobachtet werden konnte. Dabei handelt es sich um die Einstellung eines Gleichgewichts zwischen dem tiefsten $^3$MLCT und einem ligandzentrierten Triplettzustand. Dieser Prozess wurde durch temperaturabhängige Lebensdauermessungen näher untersucht, wodurch auch quantitative Informationen über die relative Lage der Zustände und Aktivierungsenergien für die einzelnen Teilschritte erhalten wurden. Diese experimentellen Befunde stehen darüber hinaus in guter Übereinstimmung mit Simulationen der Topologie der angeregten Zustände, die in der Arbeitsgruppe von Prof. Leticia Gonzàlez angefertigt wurden. Durch transiente Absorptionsexperimente konnten diese Befunde weiterhin verifiziert werden, da sich der Populationstransfer aus dem $^3$MLCT in den $^3\pi\pi^*$ auch in der zeitlichen Änderung der transienten Absorptionsspektren wiederspiegelt. In allen untersuchten dinuklearen Komplexen kommt es demnach zur Einstellung des Gleichgewichtes auf einer Zeitskala von einigen 100 ps. Weiterhin kann festgestellt werden, dass dieser Prozess aus der entspannten und planarisierten angeregten Zustandsgeometrie des energetisch tiefsten $^3$MLCT stattfindet. Somit führt die Planarisierung im angeregten Zustand zur Stabilisierung und stellt einen Schlüsselprozess für die sich anschließende Gleichgewichtseinstellung dar.

Es kommt also in allen untersuchten dinuklearen Komplexen, die auch als Monomere von Koordinationspolymeren bezeichnet werden können, zur Ausbildung langlebiger Triplettzustände, die darüber hinaus einen deutlichen ladungsseparierten Charakter aufweisen. Damit erfüllen sie die zu Beginn formulierten Anforderungen an ein geeignetes System für eine effektive Anwen-

dung im Bereich der Photovoltaik, die in der photoinduzierten Bildung langlebiger Triplettexzitonen liegt. Ob dabei diese langlebigen Triplettexzitonen in den Koordinationspolymeren lokalisiert oder entlang des Polymerstrangs delokalisiert vorliegen konnte nur zum Teil durch Einzelmolekülexperimente untersucht werden und stellt einen Kernaspekt weiterführender Arbeiten dar.

Die Untersuchung einzelner, isolierter Polymermoleküle stellt einen weiteren wichtigen Schritt in Richtung photoaktiver Koordinationspolymere dar. Da sich die entsprechenden Verbindungen der Metalle der 6. Nebengruppe aufgrund ihrer sehr geringen Emissionsquantenausbeute nicht für derartige Untersuchungen eignen, wurden erste Untersuchungen anhand eines homologen Zink-Koordinationspolymers durchgeführt. Diese zeichnen sich durch eine intensive, ligandzentrierte Fluoreszenz aus, was eine Untersuchung mittels Einzelmolekülfluoreszenzspektroskopie ermöglicht. Durch derartige Experimente konnte auch in dieser Substanzklasse ein signifikanter Einfluss langlebiger Triplettzustände gefunden werden. In Analogie zu den bereits behandelten dinuklearen Rutheniumkomplexen, bei denen teilweise der selbe Ligand Verwendung fand, werden diese Triplettzustände mit denen korreliert, die an der Ausbildung eines Gleichgewichts im angeregten Zustand der dinuklearen Metallkomplexe beteiligt sind.

Die Beteiligung von Triplettzuständen an der angeregten Zustandsdynamik konnte durch zeitaufgelöste Einzelmolekülexperimente im Millisekundenbereich in unterschiedlichen Atmosphären bestätigt werden. Hier zeigten die dunklen Zustände, die in Teilen des Polymers die Fluoreszenz löschen, eine hohe Sensitivität gegenüber elementarem Sauerstoff. Beim Wechsel der Atmosphäre von Stickstoff zu Luft kam es zu einer unmittelbaren Zunahme der Fluoreszenzintensität, was durch die Desaktivierung langlebiger statischer Fluoreszenzlöscher erklärt werden kann. Bei diesen Löschern handelt es sich wahrscheinlich um Triplettzustände und um langlebige ladungsseparierte Zustände.

Abschließend lässt sich sagen, dass in den hier untersuchten konjugierten Terpyridinen langlebige Triplettzustände einen signifikanten Beitrag zur angeregten Zustandsdynamik leisten. Dieser Effekt hängt unter anderem von der Anwesenheit schwerer Metallkationen ab, die zum einen die ISC-Quantenausbeute (Zink) erhöhen oder zur effektiven Population ladungsseparierter $^3$MLCT-Zustände führen (Eisen, Ruthenium und Osmium). Diese experimentellen Befunde unterstreichen das hohe Potential terpyridinbasierter Koordinationspolymere für Anwendungen in der Photovoltaik, da sich die effektive Bildung langlebiger Triplettexzitonen im allgemeinen günstig auf die Leistungsparameter polymerer Solarzellen auswirkt.

# Literaturverzeichnis


[1] Schlütter, F.; Wild, A.; Winter, A.; Hager, M. D.; Baumgaertel, A.; Friebe, C.; Schubert, U. S. *Macromolecules* **2010**, *43*, 2759–2771.

[2] Winter, A.; Friebe, C.; Hager, M. D.; Schubert, U. S. *European Journal of Organic Chemistry* **2009**, 801–809.

[3] Brütting, W. *Physics of Organic Semiconductors*, 1st ed.; Brütting, W., Ed.; WILEY-VCH Verlag GmbH & Co. KGaA: Weinheim, 2005; Vol. 201.

[4] Thompson, B. C.; Frechet, J. M. J. *Angewandte Chemie* **2008**, *120*, 62–82.

[5] Brabec, C.; Dyakonov, V.; Scherf, U. *Organic Photovoltaics: Materials, Device Physics and Manufacturing Technologies.*, 1st ed.; Brabec, C.; Dyakonov, V.; Scherf, U., Eds.; WILEY-VCH Verlag GmbH & Co. KGaA: Weinheim, 2008.

[6] Hirsch, A.; Brettreich, M. *Fullerenes: Chemistry and Reactions*, 1st ed.; Hirsch, A.; Brettreich, M., Eds.; WILEY-VCH Verlag GmbH & Co. KGaA: Weinheim, 2005.

[7] Brütting, W.; Rieß, W. *Physik Journal* **2008**, *7*, 33–38.

[8] Lakowicz, J. R. *Principles of Fluorescence Spectroscopy*, 4th ed.; Springer Science+Busines Media, LLC, 2006.

[9] Padinger, F.; Rittberger, R. S.; Sariciftci, N. S. *Advanced Functional Materials* **2003**, *13*, 85–88.

[10] Yang, X.; Loos, J.; Veenstra, S. C.; Verhesss, W. J. H.; Wienk, M. M.; Kroon, J. M.; Michels, M. A. J.; Janssen, R. A. J. *Nano Letters* **2005**, *5*, 579–583.

[11] Scheblykin, I. G.; Yartsev, A.; Pullerits, T.; Gulbinas, V.; Sundström, V. *Journal of Physical Chemistry B* **2007**, *111*, 6303–6321.

[12] Lee, C. L.; Hwang, I. W.; Byeon, C. C.; Kim, B. H.; Greenham, N. C. *Advanced Functional Materials* **2010**, *20*, 2945–2950.

[13] Burrows, H. D.; Melo, J. S. D.; Serpa, C.; Arnaut, L. G.; Monkman, A. P. *Chemical Physics* **2001**, *115*, 9601–9606.

[14] Guo, F.; Kim, Y. G.; Reynolds, J. R.; Schanze, K. S. *Chemical Communications* **2006**, 1887–1889.

[15] Wong, W. Y.; Harvey, P. D. *Luminescence* **2010**, *31*, 671–713.

[16] Ng, W. Y.; Chan, W. K. *Advanced Materials* **1997**, *9*, 716–719.

[17] Kelch, S.; Rehahn, M. *Macromolecules* **1999**, *32*, 5818–5828.

[18] Dobrawa, R.; Würthner, F. *Journal of Polymer Scienc: Part A: Polymer Chemistry* **2005**, *43*, 4981–4995.

[19] Chiper, M.; Hoogenboom, R.; Schubert, U. S. *Macromolecular Rapid Communications* **2009**, *30*, 565–578.

[20] Wild, A.; Winter, A.; Schlütter, F. *Chemical Society Reviews* **2011**, *40*, 1459–1511.

[21] Winter, A.; Friebe, C.; Chiper, M.; Hager, M. D.; Schubert, U. S. *Journal of Polymer Scienc: Part A: Polymer Chemistry* **2009**, *3*, 4083–4098.

[22] Wild, A.; Friebe, C.; Winter, A.; Hager, M. D.; Grummt, U. W.; Schubert, U. S. *European Journal of Organic Chemistry* **2010**, 1859–1868.

[23] Wild, A.; Schlütter, F.; Pavlov, G. M.; Friebe, C.; Festag, G.; Winter, A.; Hager, M. D.; Cimrova, V.; Schubert, U. S. *Macromolecular Rapid Communications* **2010**, *31*, 868–874.

[24] Stepanenko, V.; Stocker, M.; Müller, P.; Büchner, M.; Würthner, F. *Journal of Materials Chemistry* **2009**, *19*, 6816–6826.

[25] Harriman, A.; Khatyr, A.; Ziessel, R.; Benniston, A. C. *Angewandte Chemie International Edition* **2000**, *39*, 4287–4290.

[26] El-ghayoury, A.; Harriman, A.; Khatyr, A.; Ziessel, R. *Angewandte Chemie International Edition* **2000**, *39*, 185–189.

[27] Baitalik, S.; Wang, X. Y.; Schmehl, R. H. *Journal of the American Chemical Society* **2004**, *126*, 16304–16305.

[28] Presselt, M.; Dietzek, B.; Schmitt, M.; Popp, J.; Winter, A.; Chiper, M.; Friebe, C.; Schubert, U. S. *Journal of Physical Chemistry C* **2008**, *112*, 18651–18660.

[29] Presselt, M.; Dietzek, B.; Schmitt, M.; Rau, S.; Winter, A.; Jäger, M.; Schubert, U. S.; Popp, J. *Journal of Physical Chemistry A* **2010**, *114*, 13163–13174.

[30] Constable, C.; Lewis, J.; Liptrot, C.; Raithby, P. R. *Inorganic Chimica Acta* **1990**, *178*, 47–54.

[31] Ziessel, R. *Synthesis* **1999**, *11*, 1839–1865.

[32] Winter, A.; Friebe, C.; Chiper, M.; Schubert, U. S.; Presselt, M.; Dietzek, B.; Schmitt, M.; Popp, J. *ChemPhysChem* **2009**, *10*, 787–798.

[33] Chen, Y. Y.; Tao, Y. T.; Lin, H.-C. *Macromolecules* **2006**, *39*, 8559–8566.

[34] Chen, Y. Y.; Lin, H. C. *Polymer* **2007**, *48*, 5268–5278.

[35] Schubert, U.; Hofmeier, H.; Newkome, G. R. *Modern Terpyridine Chemistry*, 1st ed.; WILEY-VCH Verlag GmbH & Co. KGaA: Weinheim, 2006.

[36] Burnworth, M.; Mendez, J. D.; Schroeter, M.; Rowan, S. J.; Weder, C. *Macromolecules* **2008**, *41*, 2157–2163.

[37] Tuccitto, N.; Delfanti, I.; Torrisi, V.; Scandola, F.; Chiorboli, C.; Stepanenko, V.; Würthner, F.; Licciardello, A. *Physical Chemistry Chemical Physics* **2009**, *11*, 4033–4038.

[38] Bässler, H.; Schweitzer, B. *Accounts of Chemical Research* **1999**, *32*, 173–182.

[39] Horng, M. L.; Gardecki, J. A.; Papazyan, A.; Maroncelli, M. *Journal of Physical Chemistry* **1995**, *99*, 17311–17337.

[40] Horng, M. L.; Gardecki, J. A.; Maroncelli, M. *Journal of Physical Chemistry A* **1997**, *101*, 1030–1047.

[41] Wang, X. Y.; Del Guerzo, A.; Schmehl, R. H. *Chemical Communications* **2002**, 2344–2345.

[42] Akesson, E.; Bergstrom, H.; Sundström, V.; Gillbro, T. *Chemical Physics Letters* **1986**, *126*, 385–393.

[43] Sluch, M. I.; Godt, A.; Bunz, U. H.; Berg, M. A. *Journal of the American Chemical Society* **2001**, *123*, 6447–6448.

[44] Di Paolo, R. E.; Seixas de Melo, J.; Pina, J.; Burrows, H. D.; Morgado, J.; Maçanita, A. L. *ChemPhysChem* **2007**, *8*, 2657–6264.

[45] Dietzek, B.; Tarnovsky, A. N.; Yartsev, A. *Chemical Physics* **2009**, *357*, 54–62.

[46] Engelman, R.; Jortner, J. *Molecular Physics* **1970**, *18*, 145–164.

[47] Juris, A.; Balzani, V.; Barigelletti, F.; Campagna, S.; Belser, P.; Zelewsky, A. *Coordination Chemistry Reviews* **1988**, *84*, 85–277.

[48] Balzani, V.; Juris, A.; Venturi, M.; Ciamician, C. G.; Campagna, S.; Serroni, S. *Chemical Reviews* **1996**, *96*, 759–833.

[49] Damrauer, N. H.; Cerullo, G.; Yeh, A.; Boussie, T. R.; Shank, C. V.; McCusker, J. K. *Science* **1997**, *275*, 54–57.

[50] Henry, W.; Coates, C. G.; Brady, C.; Ronayne, K. L.; Matousek, P.; Towrie, M.; Botchway, S. W.; Parker, A. W.; Vos, J. G.; Browne, W. R.; McGarvey, J. J. *Journal of Physical Chemistry A* **2008**, *112*, 4537–4544.

[51] Mc Cusker, J. K.; Walda, K. N.; Dunn, R. C.; Simon, J. D.; Magde, D.; Hendrickson, D. N. *Journal of the American Chemical Society* **1993**, *115*, 298–307.

[52] Gawelda, W.; Cannizzo, A.; Pham, V. T.; van Mourik, F.; Bressler, C.; Chergui, M. *Journal of the American Chemical Society* **2007**, *129*, 8199–8206.

[53] Bressler, C.; Milne, C.; Pham, V.-T.; El Nahhas, A.; van der Veen, R. M.; Gawelda, W.; Johnson, S.; Beaud, P.; Grolimund, D.; Kaiser, M.; Borca, C. N.; Ingold, G.; Abela, R.; Chergui, M. *Science* **2009**, *323*, 489–492.

[54] Medlycott, E. A.; Hanan, G. S. *Chemical Society Reviews* **2005**, *34*, 133–42.

[55] Medlycott, E. A.; Hanan, G. S. *Coordination Chemistry Reviews* **2006**, *250*, 1763–1782.

[56] Benniston, A. C.; Harriman, A.; Li, P.; Patel, P. V.; Rostron, J. P.; Sams, C. A. *Journal of Physical Chemistry A* **2006**, *110*, 9880–9886.

[57] Christensson, N.; Dietzek, B.; Yartsev, A.; Pullerits, T. *Vibrational Spectroscopy* **2010**, *53*, 2–5.

[58] Myers, A. B. *Chemical Reviews* **1996**, *96*, 911–926.

[59] Herrmann, C.; Neugebauer, J.; Presselt, M.; Uhlemann, U.; Schmitt, M.; Rau, S.; Popp, J.; Reiher, M. *Journal of Physical Chemistry B* **2007**, *111*, 6078–6087.

[60] Tschierlei, S.; Presselt, M.; Kuhnt, C.; Yartsev, A.; Pascher, T.; Sundström, V.; Karnahl, M.; Schwalbe, M.; Schäfer, B.; Rau, S.; Schmitt, M.; Dietzek, B.; Popp, J. *Chemistry a European Journal* **2009**, *15*, 7678–7688.

[61] Hansen, P. W.; Jensen, P. W. *Spectrochimica Acta Part A: Molecular Spectroscopy* **1994**, *50*, 169–183.

[62] Lain, P. P.; Campagna, S.; Loiseau, F. *Coordination Chemistry Reviews* **2008**, *252*, 2552–2571.

[63] Fang, Y. Q.; Taylor, N. J.; Laverdire, F.; Hanan, G. S.; Loiseau, F.; Campagna, S.; Nierengarten, H.; Leize-wagner, E.; Dorsselaer, A. V. *Inorganic Chemistry* **2007**, *46*, 2854–2863.

[64] Lumpkin, R. S.; Kober, E. M.; Worl, L. M.; Murtaza, Z.; Meyer, T. J. *Journal of Physical Chemistry* **1990**, *94*, 239–243.

[65] Coe, B. J.; Thompson, D. W.; Culbertson, C. T.; Schoonover, J. R.; Meyer, T. J. *Inorganic Chemistry* **1995**, *34*, 3385–3395.

[66] Benniston, A. C.; Chapman, G.; Harriman, A.; Mehrabi, M.; Sams, C. A. *Inorganic Chemistry* **2004**, *43*, 4227–4233.

[67] Brennaman, M. K.; Alstrum-Acevedo, J. H.; Fleming, C. N.; Jang, P.; Meyer, T. J.; Papanikolas, J. M. *Journal of the American Chemical Society* **2002**, *124*, 15094–15098.

[68] Wang, X. Y.; Guerzo, A. D.; Schmehl, R. H. *Journal of Photochemistry and Photobiology C: Photochemistry Reviews* **2004**, *5*, 55–77.

[69] Hissler, M.; Harriman, A.; Khatyr, A.; Ziessel, R. *Chemistry a European Journal* **1999**, *5*, 3366–3381.

[70] McClenaghan, N. D.; Leydet, Y.; Teresa, M.; Campagna, S. *Coordination Chemistry Reviews* **2005**, *249*, 1336–1350.

[71] El-ghayoury, A.; Harriman, A.; Khatyr, A.; Ziessel, R. *Journal of Physical Chemistry A* **2000**, *104*, 1512–1523.

[72] El-ghayoury, A.; Harriman, A.; Ziessel, R. *Journal of Physical Chemistry A* **2000**, *104*, 7906–7915.

[73] Benniston, A. C.; Harriman, A. *Coordination Chemistry Reviews* **2008**, *252*, 2528–2539.

[74] Benniston, A. C.; Harriman, A.; Pariani, C.; Sams, C. A. *Journal of Physical Chemistry A* **2007**, *111*, 8918–8924.

[75] Liu, Y.; Hammitt, R.; Lutterman, D. A.; Joyce, L. E.; Thummel, R. P.; Turro, C. *Inorganic Chemistry* **2009**, *48*, 375–385.

[76] Henrich, J. D.; Zhang, H.; Dutta, P. K.; Kohler, B. *Journal of Physical Chemistry B* **2010**, *114*, 14679–14688.

[77] Sun, Y.; Liu, Y.; Turro, C. *Journal of the American Chemical Society* **2010**, *132*, 5594–5595.

[78] Gelink, G. H.; Piet, J. J.; Wegewijs, B. R.; Müllen, K.; Wildeman, J.; Hadziioannou, G.; Warman, J. M. *Physical Review B* **2000**, *62*, 1489–1491.

[79] Candeias, L. P.; Wildeman, J.; Hadziioannou, G.; Warman, J. M. *Journal of Physical Chemistry B* **2000**, *104*, 8366–8371.

[80] De Melo, J. S.; Pina, J.; Burrows, H. D.; Di Paolo, R. E.; Macanita, A. L. *Chemical Physics* **2006**, *330*, 449–456.

[81] Voityuk, A. A. *Journal of Physical Chemistry C* **2010**, *114*, 20236–20239.

[82] Dobrawa, R.; Lysetska, M.; Ballester, P.; Grüne, M.; Würthner, F. *Macromolecules* **2005**, *38*, 1315–1325.

[83] Lupton, J. M. *Advanced Materials* **2010**, 1689–1721.

[84] Lin, H.; Tian, Y.; Zapadka, K.; Persson, G.; Thomsson, D.; Mirzov, O.; Larsson, P.-O.; Widengren, J.; Scheblykin, I. G. *Nano Letters* **2009**, *9*, 4456–4461.

[85] Lin, H.; Camacho, R.; Tian, Y.; Kaiser, T. E.; Würthner, F.; Scheblykin, I. G. *Nano Letters* **2010**, *10*, 620–626.

[86] Van den Bout, D. A.; Yip, W. T.; Hu, D.; Fu, D. K.; Swager, T. M.; Barbara, P. F. *Science* **1997**, *277*, 1074–1077.

[87] Scurlock, R. D.; Wang, B.; Ogilby, P. R.; Sheats, J. R.; Clough, R. L. *Journal of the American Chemical Society* **1995**, *117*, 10194–10202.

[88] Ma, L.; Wang, X.; Wang, B.; Chen, J.; Wang, J.; Huang, K.; Zhang, B.; Cao, Y.; Han, Z.; Qian, S.; Yao, S. *Chemical Physics* **2002**, *285*, 85–94.

[89] Hofkens, J.; Vosch, T.; Maus, M.; Köhn, F.; Cotlet, M.; Weil, T.; Herrmann, A.; Müllen, K.; De Schryver, F. C. *Chemical Physics Letters* **2001**, *333*, 255–263.

[90] Krause, S.; Kowerko, D.; Börner, R.; Hübner, C. G.; Borczykowski, C. *ChemPhysChem* **2011**, *12*, 303–312.

[91] Zondervan, R.; Kulzer, F.; Orlinskii, S. B.; Orrit, M. *Journal of Physical Chemistry A* **2003**, *107*, 6770–6776.

[92] Becker, B. K.; Lupton, J. M.; Feldmann, J.; Nehls, B. S.; Galbrecht, F.; Gao, D.; Scherf, U. *Advanced Functional Materials* **2006**, 364–370.

[93] Müller, J.; Lupton, J. M.; Rogach, A. L.; Feldmann, J.; Talapin, D. V.; Weller, H. *Applied Physics Letters* **2004**, *85*, 381–383.

[94] Schindler, F.; Lupton, J. M.; Feldmann, J.; Scherf, U. *Advanced Functional Materials* **2004**, *16*, 653–657.

[95] Cordes, T.; Vogelsang, J.; Tinnefeld, P. *Journal of the American Chemical Society* **2009**, *131*, 5018–5019.

[96] Bolinger, J. C.; Traub, M. C.; Adachi, T.; Barbara, P. F. *Science* **2011**, *331*, 565–567.

[97] Haase, M.; Hübner, C. G.; Nolde, F.; Müllen, K.; Basche, T. *Physical Chemistry Chemical Physics* **2011**, *13*, 1776–1785.

[98] Tinnefeld, P.; Buschmann, V.; Weston, K. D.; Sauer, M. *Journal of Physical Chemistry A* **2003**, *107*, 323–327.

# Publikationen

## [RS1] Spectroscopic Investigation of the Ultrafast Photoinduced Dynamics in $\pi$-Conjugated Terpyridines


R. Siebert, D. Akimov, M. Schmitt, A. Winter, U. S. Schubert, B. Dietzek and J. Popp, Spectroscopic Investigation of the Ultrafast Photoinduced Dynamics in $\pi$-Conjugated Terpyridines, *ChemPhysChem*, **2009**, *10*, 910-919.



### Autorenschaft der Publikation

| | |
|---|---|
| Ronald Siebert | stationäre Absorptions-, Emissions- und Ramanspektroskopie, zeitaufgelöste transiente Absorptions- und Emissionsspektroskopie, Auswertung und Diskussion der Daten, Erstellung des Manuskripts |
| Denis Akimov | Durchführung spektroskopischer Arbeiten |
| Michael Schmitt | Diskussion und Korrektur des Manuskripts |
| Andreas Winter | Synthese und Charakterisierung der untersuchten Substanzen, Diskussion und Korrektur des Manuskripts |
| Ulrich S. Schubert | Konzept- und Ergebnisdiskussion, Diskussion und Korrektur des Manuskripts |
| Benjamin Dietzek | Projektleitung, Konzept- und Ergebnisdiskussion, Diskussion und Korrektur des Manuskripts |
| Jürgen Popp | Konzept- und Ergebnisdiskussion, Diskussion und Korrektur des Manuskripts |

CHEMPHYSCHEM

DOI: 10.1002/cphc.200800847

# Spectroscopic Investigation of the Ultrafast Photoinduced Dynamics in π-Conjugated Terpyridines

Ronald Siebert,[a] Denis Akimov,[a, b] Michael Schmitt,[a] Andreas Winter,[c] Ulrich S. Schubert,[c, d] Benjamin Dietzek,*[a, b] and Jürgen Popp[a, b]

Time-resolved spectroscopy is applied to investigate the ultrafast relaxation dynamics of several π-conjugated *mono*-, *bis*-, *tris*- and *tetrakis*(terpyridine) derivatives. This particular series of structurally closely related systems was prepared applying efficient synthetic strategies and resembles key building blocks for a wide range of photoactive complexes, dendrimers and metallo-polymers with resulting potential applications, for example, in photovoltaics or as organic light-emitting diodes. Aiming for applications of supramolecular assemblies based on these recently presented terpyridine ligands a detailed knowledge of the light-induced processes of the ligands themselves represents a prerequisite. By applying femtosecond time-resolved absorption spectroscopy in concert with time-resolved fluorescence and Raman measurements, we detail the photophysical properties.

## 1. Introduction

In modern materials research, π-conjugated polymers are currently in the spotlight of interest since their rich electro-optical properties[1] make them promising candidates for possible applications in the fields of photovoltaic devices[2] and organic light emitting diodes (OLEDs).[3] Besides various types of organic polymers[1d,4] and small organic molecules,[5] also coordination compounds have gained much interest.[6] In particular, materials containing luminescent transition metal ions or rare-earth metal complexes are highly demanding due to their high stability and flexibility in structure design and modification.[7]

Therefore, recent work focuses on the combination of π-conjugated structures with photoactive transition metal complexes. Thus, a diverse variety of chelating ligands (e.g. 2,2′-bipyridine, 1,10-phenanthroline, 2,2′:6′,2″-terpyridine) bearing a π-conjugated backbone has been synthesized,[8–10] on the basis of which a number of transition metal complexes and metallopolymers have been realized.[11,12] Furthermore, such metallopolymers reveal interesting optical and photophysical properties like chirality,[13] electroluminescence[14] and self-organization.[15] Additionally, supramolecular antennas can be constructed by introducing branched ligands. Such dendritic structures feature unique light harvesting properties[16] making them interesting candidates for mimicking natural light harvesting antennas.[17,18] While photophysical characterization on the basis of steady-state absorption and emission spectroscopy yields considerable information about the electronic structure and excited-state properties, ultrafast time-resolved spectroscopy unravels the complex ultrafast energy and electron transfer processes in real time (see for example, ref. [17,18]).

The scope of this paper is the ultrafast photophysical characterization of structuarly related terpyridine ligand systems, with molar masses between 768 and 2838 g mol$^{-1}$ (Scheme 1). In extension of our previous work on the synthesis and characterization of these materials,[10b] all bearing a π-conjugated, in some cases branched, backbone consiting of a phenyl core, vinyl-dialkoxyphenyl-ethynyl-phenyl arms and capped with 2,2′:6′,2″-terpyridine moieties at the end of the extended π-conjugated system, we now utilize a wide variety of advanced spectroscopic techniques. The ligands themselves exhibit interesting photophysical properties, for example, high fluores-

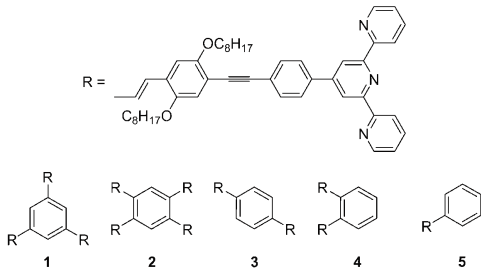


**Scheme 1.** Schematic representation of the investigated π-conjugated terpyridines **1**–**5**.

[a] *R. Siebert, Dr. D. Akimov, Dr. M. Schmitt, Dr. B. Dietzek, Prof. Dr. J. Popp*
*Institute for Physical Chemistry*
*Friedrich-Schiller-University Jena*
*Helmholtzweg 4, 07743 Jena (Germany)*
*Fax: (+49) 3641-206399*
*E-mail: benjamin.dietzek@uni-jena.de*

[b] *Dr. D. Akimov, Dr. B. Dietzek, Prof. Dr. J. Popp*
*Institute for Photonic Technology*
*Albert-Einstein-Str. 9, 07745 Jena (Germany)*

[c] *Dr. A. Winter, Prof. Dr. U. S. Schubert*
*Laboratory of Macromolecular Chemistry and Nanoscience*
*Eindhoven University of Technology*
*P.O. Box 513, 5600 MB Eindhoven (The Netherlands)*

[d] *Prof. Dr. U. S. Schubert*
*Laboratory of Organic and Macromolecular Chemistry*
*Friedrich-Schiller-University Jena*
*Humboldtstr. 10, 07743 Jena (Germany)*

   

cence quantum yields and a strongly red-shifted emission with respect to the lowest energy transition.[10b] These basic spectroscopic properties were investigated by steady-state emission- and absorption spectroscopy, but a real time investigation of the relaxation processes, following the electronic excitation, was lacking in previous studies. Such investigations are fundamental for further studies, since the perspective is the generation of metallo-polymers on the basis of these ligands using transition metal ions, such as $Fe^{II}$, $Ru^{II}$ and $Os^{II}$ because of their strong tendency to form octahedral complexes. The vision is to utilize them in photovoltaic and electroluminescent devices by substituting the most common conjugated organic polymers like poly(phenylenevinylene) and poly(phenylene-ethylynene)s derivatives (PPVs and PPEs, repectively). The high potential of combining such conjugated materials with photoactive terpyridine-based transition metal complexes (e.g. $Ru^{II}$) towards photovoltaic appications has been shown earlier by Krebs and co-workers.[12b,c] The main topic is to understand the processes starting with light absorption and ending with a charge transfer to an electrode. For this reason, time-resolved and steady-state spectroscopic methods have first been applied to the metal-free ligand systems to detail the light-triggered relaxation processes. This study is essential for future investigations, since a more complex relaxation path potentially is expected to arise from the complexation with metal ions; the spectroscopic interpretation thereof will be significantly facilated by detailed knowledge about the photophysics of the free ligands.

The presentation in this paper is organized as follows: We will first sketch the steady-state spectroscopic properties of **1–5** in solution. Subsequently, the time-resolved differential absorption ($\Delta A$) data will be presented and discussed in some detail. The rigid-linear *bis*(terpyridine) **3** is chosen as reference system for a most detailed discussion of the photophysical properties, because of the very similar behavior of all five systems under investigation.

## 2. Results and Discussion

### 2.1. Steady-State Spectroscopy

Representatively, the absorption spectrum of compound **3** (measured in THF) is depicted in Figure 1a. The absorption spectrum is divided into three main transitions, the first of which below 265 nm, the second at 265 to 355 nm and the long wavelength transition is located at 355 to 500 nm. All electronic transitions in the spectral region discussed show high extinction coefficients between $6\times10^4$ and $1\times10^5$. Thus, these extinction coefficients fall into the typical range for $\pi$–$\pi^*$ transitions. Hence, the transitions are accordingly assigned.[19] It has been shown in the literature, that the transition below 265 nm is located on the terpyridine structural moiety, while the other transitions are mainly centered on the $\pi$-conjugated backbone.[10b,c] This assignment is corroborated by the second-derivative spectrum, which is shown in Figure 1a additionally. Utilizing this method it is possible to highlight the fine structure of the electronic transition and to analyze the vibrations

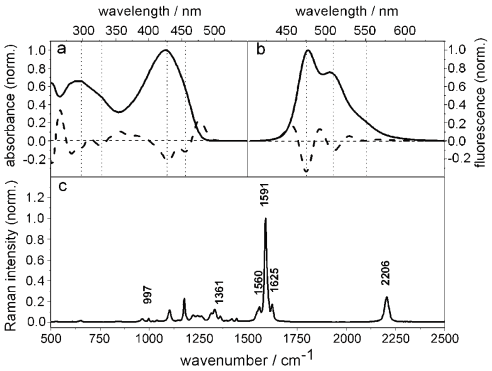


**Figure 1.** a) Absorption spectrum (solid line) of **3** dissolved in THF with the corresponding second derivative (dashed line). b) Emission spectrum (solid line) of **3** dissolved in tetrahydrofurane excited at 400 nm with the corresponding second derivative (dashed line). c) Raman spectrum of **3** excited at 1064 nm.

coupled to the electronic transition.[20] For the linear *bis*(terpyridine) **3**, a respective analysis reveals that the vibrations at 1550, 3070 and 1780 $cm^{-1}$ are coupled to the electronic transition. These can be assigned to the symmetric stretching mode of the C–C double bond at 1591 $cm^{-1}$ [20,21] and to the C–H stretching vibrations around 3000 $cm^{-1}$.

Similar results can be obtained from the emission spectrum of **3** and its second-derivative spectrum (Figure 1b). The emission peaks at 477 nm, that is, 20964 $cm^{-1}$ and, hence, is red-shifted by 2565 $cm^{-1}$ with respect to the absorption maximum. Similar to the absorption spectrum, the emission spectrum features a vibronic progression corresponding to a vibrational mode at 1450 $cm^{-1}$, which represents the symmetric stretching mode of the C–C double bond. While the second-derivative spectral analysis of absorption and emission spectra yields information about the vibrational modes, which are coupled to the respective electronic transition, a more complete vibrational information is obtained by Raman scattering and IR absorption spectroscopy.

From Figure 1c it becomes obvious that a few intense vibrations dominate the Raman spectra. In comparison to previous studies on related systems using Raman and resonance Raman spectroscopy combined with DFT methods, some Raman bands can be assigned.[21] Following the argumentation given in ref. [21] we assign the band at 997 $cm^{-1}$ to a ring breathing vibration of the terpyridine moiety. During this vibration the carbon-based aromatic pedestal remains unaffected. The vibration at 1361 $cm^{-1}$ is also caused by a ring breathing vibration, but in this case it involves only the central unit of the terpyridine sphere and the neighboured phenylene unit. This vibration is accompanied by strong movements of the interaromatic bonds between several carbon atoms and a pronounced stretching vibration of the phenylene and pyridine connecting bond. The Raman bands at 1560, 1591 and 1625 $cm^{-1}$ are assigned to aromatic in-plane vibrations in the same way. Another vibration, which can be unambiguously assigned is the 2206 $cm^{-1}$ vibration due to a symmetric stretching of the

  

ethynyl group. However, a direct comparison between the Raman data shown here and presented by Presselt et al.[21] reveals some differences. Figure 1c shows a much higher intensity for the vibrations at 1560, 1591 and 1625 $cm^{-1}$ and the detailed spectral structure appears altered, the reason being that the system discussed in the literature[21] is part of the extended chromophores, which are in the focus of this paper. The presence of a high number of non-aromatic double bonds together with the higher number of phenylene rings constitute the structural difference to this related system and cause the different shape of the spectrum in this region.

The deviation between the wavenumbers obtained from vibrational spectroscopy, that is, Raman and IR spectroscopy, and the fine-structure analysis, originates from the broad features typically observed in room temperature absorption and emission spectra. Spectroscopic techniques that will allow a better estimation of the high-frequency vibrations coupled to the electronic transition, such as resonance Raman spectroscopy,[22] three-pulse photon echo peak-shift spectroscopy or other four-wave mixing schemes,[23] low temperature fluorescence or single-molecule spectroscopy[24–26] will be performed in a later stage of our investigations. In particular, single molecular spectroscopy will additionally provide information on the molecular sub-ensembles, which are appearing underneath the broad features of the electronic transitions in our present measurements.

Having discussed the steady-state spectroscopic properties of **3** in detail, Figure 2 summarizes the absorption and emission spectra of the substances **1**–**5**. All systems reveal similar photophysical characteristics, for example, a high fluorescence quantum yield up to 85% and a strongly Stokes-shifted emission. The presented spectra are in agreement with data shown in our description of the synthesis of the materials.[10b]

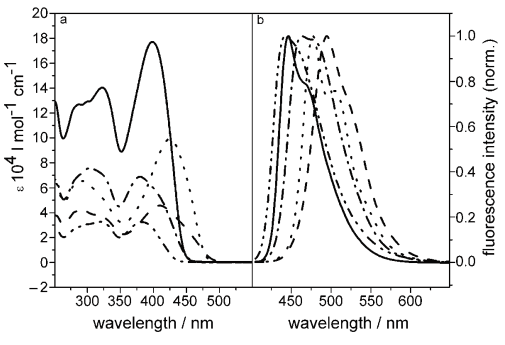


**Figure 2.** a) Absorption spectra of **1** (solid line), **2** (dashed line), **3** (dotted line), **4** (dashed-dotted line) and **5** (dashed-double-dotted line). b) Emission spectra of **1** (solid line), **2** (dashed line), **3** (dotted line), **4** (dashed-dotted line) and **5** (dashed-double-dotted line) obtained by excitation at 400 nm. All spectra have been measured in THF.

### 2.2 Femtosecond Time-resolved Differential Absorption Spectroscopy

To detail the photoinduced excited-state dynamics of the terpyridine systems, fs time-resolved transient absorption measurements have been performed. Photoexcitation is carried out at 400 nm, thus exciting the lowest energy $\pi$–$\pi^*$ transition. The photoinduced dynamics are subsequently interrogated using a white-light-supercontinuum probe. This procedure yields an overall picture of the photoinduced dynamics, while single-color probe experiments with probe-wavelengths in the spectral range between 500 to 700 nm are used for a precise fitting of kinetic rate constants. Figure 3 (left-hand side of each panel) summarizes the $\Delta A$ spectra for **1–5** for various delay times between pump and probe pulse, while the right-hand panels in Figure 3 display the results of a global fitting approach to be detailed below.

The overall appearance of the $\Delta A$ spectra is similar for terpyridines **1**–**5**: The spectra show negative $\Delta A$ changes in the blue part of the spectrum, corresponding to stimulated emission (SE). Dominant contributions from ground-state bleach to the negative $\Delta A$ feature can be excluded based on spectral considerations: As can be seen from Figure 2a, the extinction coefficient for any of the systems under investigation is negligibly small for wavelengths longer than 500 nm. As can be seen from a comparison of the steady-state absorption and emission data with the $\Delta A$ spectra (Figure 3), the negative $\Delta A$ changes are observed significantly red-shifted from the ground-state absorption, however they are in good agreement with the maxima of the corresponding fluorescence spectra. Hence, we assign this spectral feature to SE, which is neighboured by a broad and very intense positive $\Delta A$ signal at longer probe wavelengths. This positive band originates from excited-state absorption (ESA). Aside from the afore mentioned general trends observed in all spectra of this series, it is apparent that the exact spectral position of the zero-crossing between SE and ESA strongly depends on the actual substance under investigation. While it appears at around 505 and 520 nm for **5** and **1**, respectively, it experiences a strong bathochromic shift to about 580 nm for **3**. This effect correlates well with the overall trend observed in the relative positions of ground-state absorption and steady-state emission. However, detailed information about the shape of the ESA are not yet at hand, thus we cannot estimate the spectral dependence of the interplay of ESA and SE in detail.

Comparing the $\Delta A$ spectra for various delay times (Figure 3), the general spectral features do not change significantly. The dominant effect of temporal evolution is a signal intensity decrease. On top some spectral shifts are apparent, which become more pronounced, when considering the delay-time spectral shifts of the $\Delta$Abs = 0-points.

The delay-time dependence of the $\Delta$Abs = 0-point is exemplarily detailed in Figure 4 for *bis*(terpyridine) **3**. Initially, the $\Delta$Abs = 0-point shifts to the red, that is, the dynamics resembles features of a dynamic Stokes-shift under the assumption that the dominant part of the spectral shift originates from a shift of the SE maximum. In Figure 4b the zero-crossing is plotted as a function of the delay time. Interestingly, the change of the spectral position of the $\Delta$Abs = 0-point does not occur monotonically to the red, but it changes sign and for long delay times, at which also a decay of the overall $\Delta A$ signal becomes the dominant process, visible in the time-resolved spectra.

  

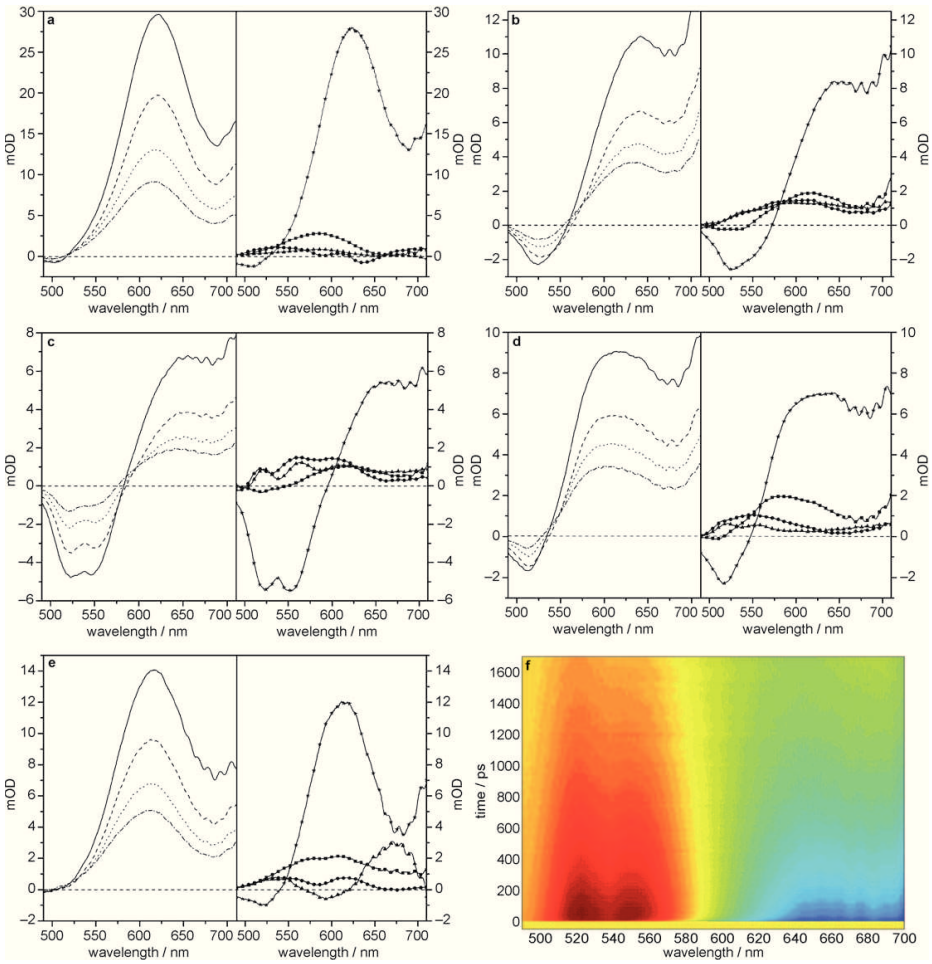


**Figure 3.** Transient absorption spectra (respective left-hand panels) for substances **1** (a), **2** (b), **3** (c), **4** (d) and **5** (e) excited at 400 nm at 0.5 ps (solid line), 500 ps (dashed line), 100 ps (dotted line) and 1500 ps (dashed-dotted line), respectively. All spectra have been measured in THF. Each right-hand panel shows the decay-associated spectra obtained from a global fit. The DAS associated with the time constants $\tau_1$, $\tau_2$ and $\tau_3$ are displayed as squares, triangles and stars, respectively. The spectrum, which appears as a constant within the time range of our measurements is shown as circles. Panel f) displays the full two-dimensional differential absorption data set of **3**. Differential absorption amplitudes are color coded from high negative (dark red) to positive (dark blue).

Therefore, it is obvious that more than a single process contributes to this complex temporal dependency. Initially, the system shows a dynamic red-shift during the first 50 ps which can be fitted by a bi-exponential function resulting in two time constants ($\tau_1 = 1.2$ ps and $\tau_2 = 17$ ps, respectively). Fitting of the long delay-time decay of the $\Delta Abs = 0$ spectral changes yields a time-constant $\tau_3$ of 1.5 ns.

In order to investigate the relationship between the time-scales obtained from the temporal evolution of the $\Delta Abs = 0$-point and the global kinetic process reflected in the $\Delta A$ data, a global-fitting approach of the transient-absorption spectra was pursued.[27] Prior to applying the global multi-exponential fit routine, the data matrix was numerically corrected for the chirp of the probe continuum. The use of a tri-exponential fitting function including an additional infinite time constant was required in order to obtain satisfactory fitting results. The results of this fitting approach are summarized in Table 1. The characteristic time constants fall in the range of $\tau_1 = 1.4$–$3.7$ ps, $\tau_2 = 20$–$45$ ps and $\tau_3 = 0.9$–$1.2$ ns depending on the particular system. Hence, the time-constants obtained from the global analysis are coherent with the kinetic estimations from the fit of the temporal shift of the $\Delta Abs = 0$-points. Consequently, we will discuss the photophysical processes underlying both measurements on the same basis. To facilitate this discussion, decay-associated spectra (DAS), representing the spectral weight of each individual kinetic component at a particular probe-wavelength, are summarized in the right-hand panels of Figure 3.

From the DAS it is obvious that the respective slowest component dominates the overall appearance of the $\Delta A$ spectra for all compounds in the series investigated. This ns-component reveals contributions of SE, which appear more pro-

  

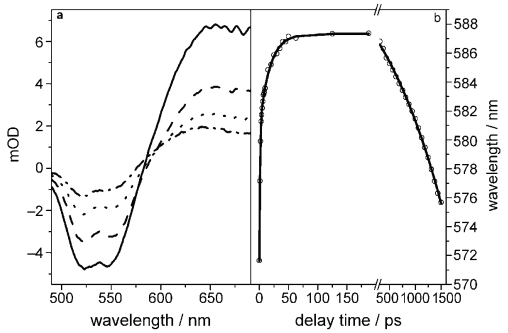


**Figure 4.** a) Transient absorption spectra for **3** in THF solution excited at 400 nm at 0.5 ps (solid line), 500 ps (dashed line), 1000 ps (dotted line) and 1500 ps (dashed-dotted line). b) Temporal evolution of the zero-crossing in the transient spectra as a function of time (black squares); additionally, the corresponding bi-exponential fit of the initial red-shift during the first picoseconds (solid line) and the fit of the long-time data (dashed line) are depicted.

**Table 1.** Time-constants for the tri-exponential decay of the kinetics obtained by global fitting of the transient spectra.

| Compound | $\tau_1$ [ps] | $\tau_2$ [ps] | $\tau_3$ [ps] |
|---|---|---|---|
| **1** | 1.4 | 20 | 1120 |
| **2** | 2.8 | 28 | 1020 |
| **3** | 2.7 | 33 | 920 |
| **4** | 3.7 | 44 | 1050 |
| **5** | 3.1 | 45 | 1060 |

nounced than in the actual spectral raw data. This finding is related to the positive ΔAbs-signals of the infinite component of any system. The DAS associated with $\tau_1$ and $\tau_2$ show absorption maxima at wavelengths shorter than those, at which the ns-component for **1–4** peak. Thus, they reflect the initial dynamic Stokes-shift, which is also seen in the temporal shift of the ΔAbs = 0-point. Contrary, the DAS($\tau_2$) of **5** reveals a spectrally intermediate minimum at 600 nm and, consequently, the DAS($\tau_2$) resembles here a kind of a mirror image of DAS($\tau_3$). This highlights the fact that the $\tau_2$-process populates the state, which decays on a ns-timescale. This general relaxation behavior is valid for all molecules, but its spectral manifestation is most pronounced for *mono*(terpyridine) **5**. This phenomenon might be correlated to the relatively simple molecular structure of **5** within the series of interest. Thus, the monomeric system **5** shows a more distinct photophysics than the oligomeric derivatives **1**–**4**. This might be attributed to the presence of more than one spectroscopic unit in the larger systems due to torsional disruption of the π-conjugation[10b,28] and the cross-shaped structure of the terpyridine-arms,[29] while for **5** a single spectroscopic unit is observed. It is apparent in the DAS of all systems, that the spectrum of the infinite component shows an ESA maximum, which is slightly shifted to the blue compared to the absorption of the ns-component. Generally, the spectral distribution of the different time-constants is, however, similar for the compounds **1**–**5**, that is, DAS($\tau_1$) and DAS($\tau_2$) show positive amplitudes and have only positive values in a similar course. Furthermore, $\tau_3$ has negative values in the region of SE and positive ones for the ESA.

It is noteworthy, that the DAS($\tau_3$) of *bis*(terpyridine) **3** (Figure 3c) nicely resembles the fine-structure of steady-state emission fluorescence (see Figure 3b). The double minimum in the DAS reflects the pronounced structure corresponding to the 1450 $cm^{-1}$ vibration, the coupling of this to the electronic transition has been discussed above.

To complement the photophysical data recorded with a supercontinuum white-light probe, transient absorption kinetics have been recorded with single-color probe pulses. Such an experimental approach combined with a detection scheme utilizing spectrally integrated detection of the probe light generally allows for experimental suppression of coherent artifact contributions to the signal.[30] Additionally, a better time-resolution and improved signal-to-noise ratios can in general be obtained. Thus, this approach has been pursued for **1–5** in probe-regions showing positive and negative Δ*A* signals. Exemplarily, the results of such single kinetic measurements of **3** recorded at 520, 550 and 650 nm, respectively, are shown in Figure 5. The kinetics recorded at 520 and 550 nm both reflects

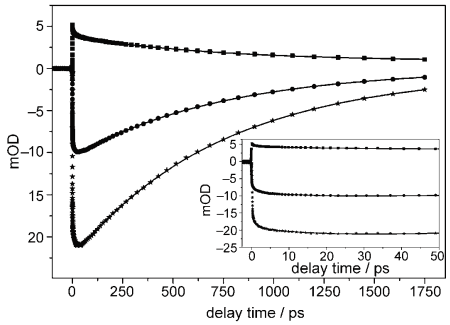


**Figure 5.** Transient absorption kinetics of **3** (measured in THF) upon pumping at 400 nm, probed at 520 nm (circles), 550 nm (stars) and 650 nm (squares) with the corresponding fits (solid lines). The inset shows an enlarged view of the initial part of the signals.

the time dependence of the SE and, hence, their temporal behavior is qualitatively very similar. On the other hand, the kinetics recorded at 650 nm represents the dynamics of the ESA band, hence showing positive Δ*A* changes (see also Figure 3). Irrespective of the probe-wavelength the temporal evolution of the kinetics can be numerically approximated by a tri-exponential fit function. The results of the respective fits are summarized in Table 2.

As can be seen from Table 2 and Figure 5 the first two components account for the initial rise of the signal during the first 30 ps. The third component on the other hand describes the decay of the radiative state. A different temporal dependence is observed for the ESA signal recorded at 650 nm: Here, the signal appears instantaneously within the experimental response and the Δ*A* changes subsequently decrease with a tri-exponential decay. By executing the fit of the ESA kinetics time-constants are retrieved, which are very similar to those

  

**Table 2.** Time-constants obtained from the multi-exponential fit of the single-color transient absorption kinetics.

| Compound | $\tau_1$ [ps] | | $\tau_2$ [ps] | | $\tau_3$ [ps] | | |
|---|---|---|---|---|---|---|---|
| | SE[a] | ESA[b] | SE[a] | ESA[b] | SE[a] | ESA[b] | F[c] |
| **1** | 1.6* | 1.2 | 11.7* | 19.2 | 0.89 | 0.96 | 1.3 |
| **2** | 0.9* | 1.8 | 14.7* | 23.6 | 0.81 | 0.98 | 1.3 |
| **3** | 0.8* | 1.0 | 15.1* | 20.0 | 0.74 | 0.72 | 1.1 |
| **4** | 1.4* | 1.4 | 16.0* | 19.1 | 0.76 | 0.72 | 1.4 |
| **5** | – | 2.1 | – | 19.0 | – | 0.83 | 1.4 |

[a] Stimulated emission. [b] Excited-state absorption. [c] Fluorescence. * Time-constants referring to rise-components.

obtained from SE kinetics (see Table 2). This finding indicates that either rate is associated with the same excited-state relaxation processes. As an exception, for *mono*(terpyridine) **5** only ESA kinetics have been observed in the spectral range of interest, since no SE contributes to the signal between 500 and 700 nm. Instead, ESA dominates the overall kinetics. Again it should be noted, that the slowest lifetimes obtained from the fit of the $\Delta A$ data are associated with some uncertainty as the delay-time range accessible with our delay line does not exceed 2 ns. More correct estimations of the slowest component are presented below in the context of ns-time-resolved streak-camera measurements.

### 2.3. Excited-State Wavepacket Dynamics

The data presented up to now solely reveal excited-state relaxation kinetics, without providing further insight into the photo-induced dynamics or the excited-state molecular geometry away from the Franck-Condon point, whose geometry can—in principle—be inferred from the modes coupled to the electronic transition, that is, visible in the finestructure of the absorption spectra. Aside from ultrafast time-resolved vibrational spectroscopic techniques,[31] the transient kinetics themselves bear—under suitable circumstances—some information about the excited-state structure. In the case of *bis*(terpyridine) **3** the transient kinetics recorded at 550 nm show residual oscillations after subtraction of the multi-exponential fitting function from the experimental data has been performed (Figure 6).[32] These oscillations stem from coherently excited vibrational wavepackets on the excited-state potential energy surface. Contributions to the wavepacket from ground-state coherences can be excluded by an appropriate selection of the probe wavelength, which is chosen to fall in the spectral region of pure SE.[33] A Fourier transformation analysis of these oscillations yields the vibrational modes representative of the excited-state structure.[34]

Interestingly, the fast-Fourier-transformation (FFT) analysis does not reveal identical low-wavenumber modes as the 1064 nm Raman spectrum of the identical substance. While the FFT is dominated by a vibration at 300 $cm^{-1}$, this mode does not appear in the non-resonant Raman spectrum (Figure 6, bottom). Nonetheless, the FFT identifies a very low-wavenumber contribution at around 80 $cm^{-1}$, which is correlated to the strong low-wavenumber mode in the Raman spectrum. However, the dominant peak in the FFT is clearly shifted to 300 $cm^{-1}$. This difference is attributed to different structures of the ground- and excited-state, whereas it is not possible at this stage to distinguish between two plausible explanations: Assuming that the 300 $cm^{-1}$ mode on the excited-state potential corresponds to the somewhat weaker mode at about 400 $cm^{-1}$ in the ground-state Raman spectrum, the effect it thought to be caused by the reduction on bond-strength of double and triple bonds upon the optical π–π* transition. Though these modes are visible in the Raman spectrum at significantly higher wavenumbers, that is, at typically 1590.6 and 2205.8 $cm^{-1}$, some collective and, thus, low-wavenumber modes involving double (or triple) bonds, might give rise to the observed phenomenon. A second possible rationalization is based on the correlation of the strong modes in wither spectrum, that is, the100 $cm^{-1}$ mode in the non-resonance Raman spectrum with the 300 $cm^{-1}$ oscillation visible in the time-resolved data. Starting from this assumption, the now hypsochromic shift of the mode, can be invoked by excited-state planarization.[35] This effect is well known for π-conjugated polymers and leads to an increase in the electronic delocalization upon photoexcitation and, therefore, an increase in the bond order of the respective molecular bonds. Hence, the corresponding Raman active modes reflecting the bonding situation will shift to higher wavenumbers. Though we aim at clarifying this open question in the course of further experimental and computational investigations, the data shown here present first insights in the significant photoinduced structural reorientations in the terpyridine systems under investigation.

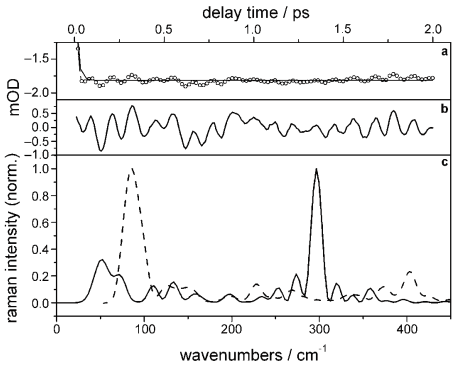


**Figure 6.** a) Time-resolved stimulated emission of **3** (measured in THF) recorded at 510 nm. Symbols represent data, while the fit result is shown as a solid line. b) Transient absorption data after subtraction of the multi-exponential kinetics. c) FFT of the residual oscillations in the stimulated emission (solid line) compared to the off-resonance Raman spectrum (dashed line) of the substance.

### 2.4. Time-Resolved Fluorescence Streak-Camera Measurements

Aside from the Δ- data, which—due to experimental limitations—have been recorded in a delay-time window of only 2 ns, time-resolved emission spectroscopy provides complementary information on the kinetics of the excited-state de-

  

population. Therefore, we recorded streak-camera data upon photoexcitation at 400 nm with a time-resolution of 30 ps.

The corresponding data are summarized in Figure 7. No spectral evolution of the emission has been visible with the time-resolution accessible in our streak-camera system. Therefore, Figure 7 presents spectrally integrated fluorescence kinetics reflecting the overall depopulation of the emissive excited state. It can be seen, that the temporal dependence of the fluorescence for **1**–**5** shows generally a very similar behavior: The kinetics reveal a response-function limited rise followed by a decay of the emission, which can be approximated as an exponential decay. As a results of this analysis Figure 7 shows the experimental fluorescence kinetics in concert with the fitted curves. The characteristic time-constants obtained from the fit range from 1.1 to 1.9 ns and agree well with the rough estimation obtained from the $\Delta A$ kinetics.

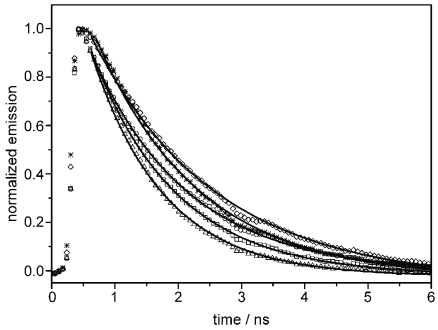


**Figure 7.** Time-resolved fluorescence kinetics (symbols) and exponential fits (lines) of **1** (squares), **2** (circles), **3** (triangles), **4** (diamonds) and **5** (stars). The substances were dissolved in THF and the emission was excited at 435 nm. As no spectral evolution of the emission spectrum has been observed with our time-resolution, the data are presented spectrally integrated.

### 2.5. Photophysical Model

We will start the discussion of a global photophysical picture from the observation that the emissive state decays relatively fast with radiative rates in the order of $7\times10^8\ s^{-1}$. The radiative transition (i.e. the fluorescence) can be assumed to leave the emitting molecules in the initial ground-state of the respective system. Thus, one has to note the presence of a long lived species in the $\Delta A$ spectra. As mentioned above, the corresponding DAS show an absorption band with a blue-shifted maximum compared to the ns-DAS spectrum. This spectral shift is also reflected by the long-time shift of the $\Delta Abs = 0$-point to shorter probe wavelengths. We rationalize these observations in terms of fluorescence quenching by inter-system crossing, that is, population of a triplet-state out of the thermally equillibrized emissive $S_1$ state, which has been frequently observed for conjugated $\pi$-systems. Hence, it provides a natural explanation for the experimental data.[36] Triplet quantum yields for comparable $\pi$-conjugated systems fall in the range of roughly 1 to 3%.[36a–d,37] Therefore, the constant-DAS spectra represent the triplet absorption spectra of **1**–**5**. Further characterization of the triplet state could be performed by pulse radiolysis coupled to triplet–triplet energy transfer involving triplet sensitizers[36c] or by means of photoacustic calorimetry.[36d] However, our attempt to measure the luminescence of the triplet-state in solvents containing heavy atoms like iodine at room temperature was unfortunately not successful. Therefore, we conclude that non-radiative decay of the triplet-state dominates the luminescence as the triplet-deactivation pathway. Similiarly, the ns-DAS represents the absorption spectrum of the equillibrized $S_1$ state, which is centered between 600 and 650 nm for **1** and **5**, while the systems **2**–**4** exhibit a broader $S_1 \rightarrow S_n$-absorption extending towards 700 nm.

From the data presented and discussed above it is apparent that in addition to the ns-lifetime two time-constants in the range of 1 to 5 and 15 to 40 ps, respectively, are required to fully account for the experimental data. The latter two represent rise-times in the SE kinetics and decay-times when monitoring the ESA. Based on the physical connection between these two processes, that is, considering that ESA is observed at any position of the excited-state surface but SE dominantly occurs from the energetic minimum of the $S_1$-potential any relaxation process such as cooling or solvation generally results in a spectral shift of the ESA contribution and the formation of the long-lived SE band.

Upon photoexcitation of the $\pi$–$\pi^*$ transition, molecules are promoted to the Franck-Condon point on the first excited-state potential energy surface. From the Franck-Condon point geometry, which is characterized by strong reorganization along the vibrational modes visible in the fine structure of the electronic absorption spectrum, the system relaxes to the emissive, that is, thermally relaxed, S1 state. Solvation generally contributes to the aforementioned initial excited-state dynamics and typically occurs on 100 fs to some-ps timescale,[38] wherein slow components generally contribute more dominantly for solvents with high viscosity and/or pronounced hydrogen-bonding capabilities.[38a] For tetrahydrofurane, the solvent used in this study, solvation is characterized by a bi-exponential process with the characteristic time-constants of 228 fs and 1.52 ps, respectively.[38a] Besides solvation intramolecular vibrational redistribution (IVR) contributes to the initial photo-induced kinetics, which rapidly, that is, within some ten to 100 fs, spreads the energy, initially placed in the photoactive modes, over all low-wavenumber vibrational degrees of freedom of the molecule.[39] Furthermore, cooling will contribute to the initial dynamics, that is, energy dissipation from the solute into the solvent—a process that can take between a few to some-ten ps, depending on the solvent, specific solute–solvent interactions and the vibrational excess energy.[39]

Based on these timescale arguments, the fastest component ($\tau_1 \approx 1.2$ ps) is assigned to the interplay of solvation and IVR. The slower $\tau_2$-component is associated to cooling—a process that finally leads to the emissive, vibrationally thermalized $S_1$-excited state.[40] The latter assignment is coherent with the shape of the DAS($\tau_2$) for terpyridines **1–4** showing a very broad ESA, which spectrally narrows down upon formation of the ns-component. Furthermore, the positive $\Delta A$ contributions,

  

in spectral regions, in which the ns-components reveal contributions from SE, indicate that $\tau_2$ corresponds to the formation of the emissive state and does not contribute to the overall emission in the visible spectrum. Associated with the decay of the emissive state ($\tau_3$) the formation of a long-lived non-emissive component is observed, that we assign this to a triplet state, the ESA of which appears blue-shifted compared to the absorption of the thermally relaxed $S_1$ state. Figure 8 schematically summarizes the photoinduced relaxation processes for the class of terpyridines investigated here.

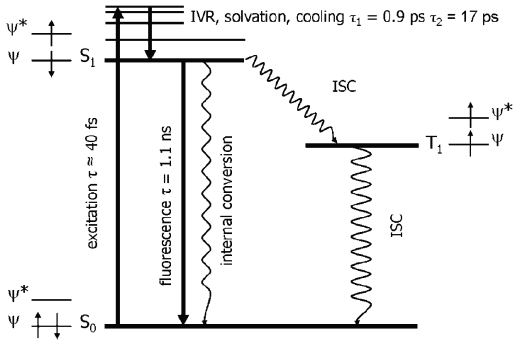


**Figure 8.** Schematic visualization of the excited-state dynamics of **1–5** (IVR = intramolecular vibrational redistribution, ISC = inter-system crossing).

We have to point out that the overall relaxation behavior is independent of the particular terpyridine. Despite some indications that *mono*(terpyridine) **5** shows slightly different spectral weights for the process associated with $\tau_2$ than the *bis*-, *tris*- and *tetrakis*(terpyridine)s **1**–**4**, this overall similarity indicates that the splitting of the larger systems into distinct spectroscopic units does not change the general relaxation behavior as also observed for **5**. Therefore, this study defines a clear starting point for on-going work, which will be focused on metal-complexes and metallo-polymers based on the building blocks studied here. Such metallo-polymers containing various transition metal centers will constitute structurally flexible supramolecular antennas, which can be designed in a variety of molecular geometries. The to-be-expected unique light-harvesting and energy- and charge-transfer processes in such assemblies make them promising candidates to be used as antennas in artificial light-harvesting systems. Hence, the work presented here constitutes the cornerstone for further spectroscopic investigations aiming for a detailed structure-dynamics correlation in such systems, which will potentially help to focus synthetic strategies to achieve most directed excited-state dynamics.

## 3. Conclusions

We have detailed the photoinduced excited-state dynamics of a series of structurally closely related π-conjugated *mono*-, *bis*-, *tris*- and *tetrakis*(terpyridine) derivatives utilizing complementary time-resolved spectroscopic techniques, such as femtosecond time-resolved $\Delta A$ and ns-time-resolved streak-camera measurements. The work presented here is in extension of previous work on the synthesis and application of advanced (supramolecular) terpyridine architectures. The results obtained reveal a complex non-exponential excited-state relaxation containing kinetic steps ranging over three orders of magnitude in time, irrespective of the individual terpyridine system. We have identify three distinct processes in the order of 1, 20 and 1000 ps, respectively. The first two of these we associate to solvation, a very fast process in THF—the solvent used in this study—and cooling. These processes drive the photoexcited systems to relax into equilibrated excited-state geometries, from where fluorescence is visible. Hence, the formation of the emissive-state is visible as an initial increase of SE, a decay of ESA and, as a joint effect, a dynamic Stokes-shift. Finally, the 1000 ps component, which appears as an overall decrease of the signal, is attributed to the decay of the radiative state. This decay does not only populate the initial ground-state but an additional long-lived $\Delta A$ component has been concluded from the data. The spectral features of this long-lived component are highly conserved among all five terpyridines studied. This component is assigned to triplet–triplet absorption. We anticipate that these results will be the basis for a detailed understanding of the photophysics of new metallo-polymers based on the terpyridine systems discussed here.

## Experimental Section

The synthesis of the series π-conjugated terpyridines (**1**–**5**) was recently published elsewhere.[10b]

The time-resolved transient absorption set-up was based on an amplified Ti:Sapphire oscillator (Libra, Coherent Inc.) producing a pulse-train of 80 fs 950 μJ pulses centered at 800 nm with a repetition rate of 1 kHz. The pulses were split by means of a 50:50 beamsplitter and one of the individual portions was used to independently pump a non-collinear optical-parametric amplifier (TOPASwhite, LightConversion Ltd.); the output of this was tuned between 500 and 700 nm and served as probe pulse in several experiments, while the other one was used to generate the pump pulse by second harmonic generation. For this reason the beam was focused in a 100 μm thick BBO crystal. In some experiments reported here, white light was used as probe. Therefore, 1% of the 800 nm fundamental beam was split away and focused into a Ti-sapphire plate to generate a supercontinuum. A chopper was inserted into the pump path to block every second pump pulse. The probe pulses were delayed in time with respect to the arrival of the pump pulses at the sample position by means of a delay line and split by means of a 30:70 beamsplitter to obtain probe and reference pulses. The probe pulses were focused into the sample by means of a 500 mm focal-length spherical mirror, while the reference pulses were biasing the sample and were directed onto the detector. Probe-pulses were spatially and temporally overlapped at the sample position with the pump pulses, which were focused into the sample by means of a 1000 mm focal-length quartz lens. The different focus conditions resulted in a larger focal spot of the pump beam as compared to the probe and ensured homogeneous excitation of the sample over the entire probe-focus volume. The polarization of the pump pulses was rotated to yield magic-angle polarization geometry. After the sample the pump pulse was blocked, while the probe pulse is re-collimated by a second

  

500 mm focal-length spherical mirror and—in concert with the reference beam—was sent to the detection system, which was obtained from Pascher Instruments AB and allows for simultaneous spectrally resolved detection of probe and reference intensities on a double-stripe diode array, each stripe consisting of 512 individual diodes. The diode array was read-out with the repetition rate of the laser and the $\Delta A$ signal was calculated from the probe and reference intensities for a pair of measurements corresponding to pump-on and pump-off conditions. It was ensured that the energy of the pump pulses was kept well below 0.5 μJ, while typical probe intensities fall into the range of a few hundred nJ. Autocorrelation of the probe pulses and the experimental response function was recorded at the sample position in a 1 mm thick BBO crystal. From this data the temporal duration of the probe pulses and the experimental response function could be estimated to be in the order of 30–40 fs.

The fluorescence lifetimes were obtained by streak camera measurements. Therefore, a Ti-Saphire Laser (Tsunami, Newport Spectra-Physics GmbH) was used as light source. Repetition rate was reduced to 4 kHz by a pulse selector (Model 3980, Newport Spectra-Physics GmbH) and afterwards the beam was frequency doubled in a second harmonic generator (Newport Spectra-Physics GmbH) to create the 435 nm pump beam. The emission was recorded using a CHROMEX 250IS spectrograph and a Hamamatsu HPD-TA streak-camera.

Steady-state absorption spectra were recorded on a Jasco V-670 spectrophotometer, the fluorescence spectra were measured from dilute solutions using a Jasco FP-6200 spectrofluorimeter. Infrared spectra were obtained with a Bruker IFS 66 spectrometer. The FT-Raman spectra were measured with a Bruker MultiRam II equipped with a Klastech CW Single Frequency DENICAFC 1064 nm ND:YAG Laser and a Olympus BX51 M Systemmikroskop.

The substances were dissolved in oxygen-free tetrahydrofurane (THF) of spectroscopic grade to yield an optical density of 0.3 in a 3 mm quartz-glass cuvette at the excitation wavelength. Absorption spectra of the sample were recorded prior and after the experimental runs to monitor the integrity of the samples.

## Acknowledgements

*The authors acknowledge financial support by the Fonds der Chemischen Industrie and the Nederlandse Organisatie voor Wetenschappelijk Onderzoek (VICI award to U.S.S.) We thank Roman Schmeißner and Sven Peters for assistance with the streak-camera measurements.*

**Keywords:** fluorescence · reaction dynamics · supramolecular chemistry · terpyridine ligands · ultrafast UV/Vis spectroscopy

[1] a) N. S. Sariciftci, L. Smilowitz, A. J. Heeger, F. Wudl, *Science* **1992**, *258*, 1474; b) R. H. Friend, M. Granstrom, K. Petritsch, A. C. Arias, A. Lux, M. A. Andersson, *Nature* **1998**, *395*, 257–260; c) B. Carbonnier, D. A. M. Egbe, E. Birckner, U. W. Grummt, T. Pakula, *Macromolecules* **2005**, *38*, 7546–7554; d) E. Tekin, D. A. M. Egbe, J. M. Kranenburg, C. Ulbricht, S. Rathgeber, E. Birckner, N. Rehmann, K. Meerholz, U. S. Schubert, *Chem. Mater.* **2008**, *20*, 2727–2735.

[2] a) B. C. Thompson, J. M. J. Frechet, *Angew. Chem.* **2008**, *120*, 62–82; *Angew. Chem. Int. Ed.* **2008**, *47*, 58–77; b) I. G. Scheblykin, A. Yartsev, T. Pullerits, V. Gulbinas, V. J. Sundström, *J. Phys. Chem. B* **2007**, *111*, 6303–6321.

[3] a) H. Yersin, *Highly Efficient OLEDs with Phosphorescent Materials*, Wiley-VCH, Weinheim, **2008**; b) K. Müllen, U. Scherf, *Organic Light Emitting Devices*, Wiley-VCH, Weinheim, **2006**.

[4] a) O. Nuyken, S. Jungermann, V. Wiederhirn, E. Bacher, K. Meerholz, *Monatsh. Chem.* **2006**, *137*, 811–824; b) C.-W. Chiu, T. J. Chow, C.-H. Chuen, H.-M. Lin, Y.-T. Tao, *Chem. Mater.* **2003**, *15*, 4527–4532; c) K. R. J. Thomas, J. T. Lin, Y. T. Tao, C.-H. Chuen, *Adv. Mater.* **2002**, *14*, 822–826.

[5] a) K. Walzer, B. Maennig, M. Pfeiffer, K. Leo, *Chem. Rev.* **2007**, *107*, 1233–1271; b) N. Koch, *ChemPhysChem* **2007**, *8*, 1438–1455; c) M. Pfeiffer, S. R. Forrest, X. Zhou, K. Leo, *Org. Electron.* **2003**, *4*, 21–26; d) M. T. Bernius, M. O'Brien, J. Inbasekaran, W. Wu, *Adv. Mater.* **2000**, *12*, 1737–1750; e) J. H. Burroughes, D. C. C. Bradley, A. R. Brown, R. N. Marks, K. Mackay, R. H. Friend, P. L. Burns, A. B. Holmes, *Nature* **1990**, *347*, 539–541.

[6] a) E. Holder, B. M. W. Langeveld, U. S. Schubert, *Adv. Mater.* **2005**, *17*, 1109–1121; b) R. Shunmugam, G. N. Tew, *Macromol. Rapid Commun.* **2008**, *29*, 1355–1362; c) P.-T. Chou, Y. Chi, *Chem. Eur. J.* **2007**, *13*, 380–395; d) R. Vivas-Reyes, F. Nunez-Zarur, E. Martinez, *Org. Electron.* **2008**, *9*, 625–634; e) V. Marin, E. Holder, R. Hoogenboom, U. S. Schubert, *Chem. Soc. Rev.* **2007**, *36*, 618–635; f) P.-T. Chou, Y. Chi, *Eur. J. Inorg. Chem.* **2006**, 3319–3332.

[7] a) B. C. Krummacher, V.-E. Choong, M. K. Mathai, S. A. Choulis, F. So, F. Jermann, T. Fiedler, M. Zachau, *Appl. Phys. Lett.* **2006**, *88*, 113506; b) R. C. Evans, P. Douglas, C. J. Winscom, *Coord. Chem. Rev.* **2006**, *250*, 2093–2126; c) J. Slinker, D. Bernards, P. L. Houston, H. D. Abruña, S. Bernhard, G. G. Malliaras, *Chem. Commun.* **2003**, 2392–2399; d) B. W. D'Andrade, J. Brooks, V. Adamovich, M. E. Thompson, S. R. Forrest, *Adv. Mater.* **2002**, *14*, 1032–1036.

[8] a) V. Balzani, G. Bergamini, F. Marchioni, P. Ceroni, *Coord. Chem. Rev.* **2006**, *250*, 1254–1266; b) R.-A. Fallaphour, *Curr. Org. Synth.* **2006**, *3*, 19–39; c) B.-H. Ye, M.-L. Tong, X.-M. Chen, *Coord. Chem. Rev.* **2005**, *249*, 545–565; d) G. R. Newkome, A. K. Patri. E. Holder, U. S. Schubert, *Eur. J. Org. Chem.* **2004**, 235–254; e) M. Heller, U. S. Schubert, *Eur. J. Org. Chem.* **2003**, 947–961; f) U. S. Schubert, C. Eschbaumer, *Angew. Chem.* **2002**, *114*, 3016–3050; *Angew. Chem. Int. Ed.* **2002**, *41*, 2892–2926; g) C. D. Eisenbach, U. S. Schubert, *Macromolecules* **1993**, *26*, 7372–7374.

[9] S. Bonnet, J.-P. Collin, M. Koizumi, P. Mobian, J.-P. Sauvage, *Adv. Mater.* **2006**, *18*, 1239–1250.

[10] a) U. S. Schubert, H. Hofmeier, G. R. Newkome, *Modern Terpyridine Chemistry*, Wiley-VHC, Weinheim, **2006**; b) A. Winter, C. Friebe, M. D. Hager, U. S. Schubert, *Eur. J. Org. Chem.* **2009**, 801–809; c) A. Winter, C. Friebe, M. D. Hager, U. S. Schubert, *Macromol. Rapid Commun.* **2008**, *29*, 1679–1686; d) M. Jäger, L. Eriksson, J. Bergquist, O. Johansson, *J. Org. Chem.* **2007**, *72*, 10227–10230; e) A. Winter, D. A. Egbe, U. S. Schubert, *Org. Lett.* **2007**, *9*, 2345–2348; f) S. H. Hwang, C. N. Moorefield, L. Dai, G. R. Newkome, *Chem. Mater.* **2006**, *18*, 4019–4024; g) M. Schmittel, V. Kalsani, P. Mal, J. W. Bats, *Inorg. Chem.* **2006**, *45*, 6370–6377; h) S.-C. Yuan, H.-B. Chen, J. Pei, *Org. Lett.* **2006**, *8*, 5701–5704; i) A. Barbieri, B. Ventura, F. Barigeletti, A. de Nicolar, M. Quesada, R. Ziessel, *Inorg. Chem.* **2004**, *43*, 7359–7368; j) H. Hofmeier, U. S. Schubert, *Chem. Soc. Rev.* **2004**, *33*, 373–399; k) M. Heller, U. S. Schubert, *Eur. J. Org. Chem.* **2003**, 947–961.

[11] For recent examples see: a) M. W. Cooke, G. S. Hanan, F. Loiseau, S. Campagna, M. Watanabe, Y. Tanaka, *J. Am. Chem. Soc.* **2007**, *129*, 10479–10488; b) X. Chen, Q. Zhou, Y. Chen, Y. Geng, D. Ma, Z. Xie, L. Wang, *J. Lumin.* **2007**, *126*, 81–90; c) F. Camerel, R. Ziessel, B. Donnio, C. Bourgogne, D. Guillon, M. Schmutz, C. Iacovita, J. P. Bucher, *Angew. Chem.* **2007**, *119*, 2713–2716; *Angew. Chem. Int. Ed.* **2007**, *46*, 2659–2662; d) C. N. Carlson, C. J. Kuehl, R. E. Da-Re, J. M. Veauthier, E. J. Schelter, A. E. Milligan, B. L. Scott, E. D. Bauer, J. D. Thompson, E. D. Morris, K. D. John, *J. Am. Chem. Soc.* **2006**, *128*, 7230–7241; e) B. Song, G. Wang, M. Tan, J. Yuan, *J. Am. Chem. Soc.* **2006**, *128*, 13442–13450; f) P. P. Lainé, F. Bedioiui, F. Louisseau, C. Chiorboli, S. Campagna, *J. Am. Chem. Soc.* **2006**, *128*, 7510–7521; g) P. Coppo, M. Duati, V. N. Kozhevnikov, J. W. Hofstraat, L. De Cola, *Angew. Chem.* **2005**, *117*, 1840–1844; *Angew. Chem. Int. Ed.* **2005**, *44*, 1806–1810; h) K. Sénéchal-David, J. P. Leonard, S. E. Plush, T. Gunlaugsson, *Org. Lett.* **2006**, *8*, 2727–2730; i) A. Barbieri, B. Ventura, F. Barigeletti, A. de Nicolar, M. Quesada, R. Ziessel, *Inorg. Chem.* **2004**, *43*, 7359–7368.

[12] a) A. Benniston, A. Harriman, P. Lei, P. V. Patel, C. A. Sams, *J. Org. Chem.* **2006**, *71*, 3481–3493; b) O. Hagemann, M. Jørgensen, F. C. Krebs, *J. Org. Chem.* **2006**, *71*, 5546–5559; c) V. Duprez, M. Biancardo, H. Spanggaard, F. C. Krebs, *Macromolecules* **2005**, *38*, 10436–10448; d) I. Ciofini, P. P.

  

Lainé, F. Bedioui, C. Adamo, *J. Am. Chem. Soc.* **2004**, *126*, 10763–10777; e) A. H. Flood, J. F. Stoddard, D. W. Steuerman, J. R. Heath, *Science* **2004**, *306*, 2055–2056; f) A. El-Ghayoury, A. P. H. J. Schenning, P. A. van Hal, C. H. Weidl, J. L. J. van Dongen, R. A. J. Janssen, U. S. Schubert, E. W. Meijer, *Thin Solid Films* **2002**, *403–404*, 97–101; g) O. Schmelz, M. Rehahn, *e-Polymers* **2002**, *47*, 1–29; h) A. El-Ghayoury, A. P. H. Schenning, E. W. Meijer, *J. Polym. Sci. Part A* **2002**, *40*, 4020–4023; i) V. Balzani, P. Ceroni, A. Juris, A. Venturi, M. Venturi, S. Campagna, F. Puntoriero, S. Serroni, *Coord. Chem. Rev.* **2001**, *219–221*, 545–572; j) R. Ziessel, M. Hissler, A. El-ghayoury, A. Harriman, *Coord. Chem. Rev.* **1998**, *178–180*, 1251–1298.

[13] M. Kimura, M. Sano, T. Muto, K. Hanabusa, H. Shirai, N. Kobayashi, *Macromolecules* **1999**, *32*, 7951–7953.

[14] a) Y.-Y. Chen, H.-C. Lin, *J. Polym. Sci. Part A Polym. Chem.* **2007**, *45*, 3234–3255; b) Y.-Y. Chen, Y. T. Tao, H.-C. Lin, *Macromolecules* **2006**, *39*, 8559–8565.

[15] B. G. G. Lohmeijer, U. S. Schubert, *Chem. Commun.* **2004**, 2886–2887.

[16] S. Campagna, C. Di Pietro, F. Loiseau, B. Maubert, N. McClenaghan, R. Passalacqua, F. Puntoriero, V. Ricevuto, S. Serroni, *Coord. Chem. Rev.* **2002**, *229*, 67–74.

[17] a) S. Tschierlei, M. Presselt, C. Kuhnt, A. Yartsev, T. Pascher, V. Sundström, M. Karnahl, M. Schwalbe, B. Schäfer, S. Rau, M. Schmitt, B. Dietzek, J. Popp, unpublished results; b) B. Dietzek, W. Kiefer, J. Blumhoff, L. Böttcher, S. Rau, D. Walther, U. Uhlemann, M. Schmitt, J. Popp, *Chem. Eur. J.* **2006**, *12*, 5105–5115.

[18] J. Andersson, F. Puntoriero, S. Serroni, A. Yartsev, T. Pascher, T. Polivka, S. Campagna, V. Sundström, *Chem. Phys. Lett.* **2004**, *386*, 336–341.

[19] H. G. O. Becker, *Einführung in die Photochemie*, Deutscher Verlag der Wissenschaften, Berlin, **1991**.

[20] M. Hesse, H. Meier, B. Zeeh, *Spektroskopische Methoden in der organischen Chemie*, Thieme, Stuttgart, **1995**.

[21] a) M. Presselt, B. Dietzek, M. Schmitt, J. Popp, A. Winter, M. Chiper, C. Friebe, U. S. Schubert, *J. Phys. Chem. C* **2008**, *112*, 18651–18660; b) A. Winter, C. Friebe, M. Chiper, U. S. Schubert, M. Presselt, B. Dietzek, M. Schmitt, J. Popp, *ChemPhysChem* **2009**, DOI: 10.1002/cpch.200800714.

[22] a) S. Tschierlei, B. Dietzek, M. Karnahl, S. Rau, F. M. MacDonnell, M. Schmitt, J. Popp, *J. Raman Spectrosc.* **2008**, *39*, 557–559; b) S. Lochbrunner, A. Szeghalmi, K. Stock, M. Schmitt, *J. Chem. Phys.* **2005**, *122*, 244315.

[23] a) B. Dietzek, N. Christensson, P. Kjellberg, T. Pascher, T. Pullerits, A. Yartsev, *Phys. Chem. Chem. Phys.* **2007**, *9*, 701–710; b) B. Dietzek, N. Christensson, T. Pascher, T. Pullerits, A. Yartsev, *J. Phys. Chem. B* **2007**, *111*, 5396–5404; c) B. Dietzek, R. Masimenka, W. Kiefer, G. Hermann, J. Popp, M. Schmitt, *Chem. Phys. Lett.* **2005**, *415*, 94–99.

[24] R. Ziessel, G. Ulrich, L. Charbonniere, D. Imbert, R. Scopelliti, J. C. G. Bünzli, *Chem. Eur. J.* **2006**, *12*, 5060–5067.

[25] Z. Yu, P. F. Barbara, *J. Phys. Chem. B* **2004**, *108*, 11321–11326.

[26] O. Mirzov, I. G. Scheblykin, *Phys. Chem. Chem. Phys.* **2006**, *8*, 5569–5576.

[27] B. Dietzek, S. Tschierlei, G. Hermann, A. Yartsev, T. Pascher, V. Sundström, M. Schmitt, J. Popp, *ChemPhysChem* **2009**, *1*, 144–150.

[28] M. M. L. Grage, Y. Zaushiytsin, A. Yartsev, M. Chachisvillis, V. Sundström, T. Pullerits, *Phys. Rev. B* **2003**, *67*, 205207.

[29] a) F. Terenziani, C. Katan, E. Badaeva, S. Tretiak, M. Blanchrad-Desce, *Adv. Mater.* **2008**, *20*, 1–38; b) M. Rumi, S. J. K. Pond, T. Meyer-Friedrichsen, Q. Zhang, M. Bishop, Y. Zhang, S. Barlow, S. R. Mader, J. W. Perry, *J. Phys. Chem. C* **2008**, *112*, 8061–8071; c) Y.-H. Sun, K. Zhao, C.-K. Wang, Y. Luo, Y. Ran, X.-T. Tao, M.-H. Jiang, *THEOCHEM* **2004**, *682*, 185–189.

[30] a) S. A. Kovalenko, A. L. Dobryakov, J. Ruthmann, N. P. Ernsting, *Phys. Rev. A* **1999**, *59*, 2369–2384; b) B. Dietzek, T. Pascher, V. Sundström, A. Yartsev, *Laser Phys. Lett.* **2007**, *4*, 38–43.

[31] a) D. W. McCamant, P. Kukura, S. Yoon, R. A. Mathies, *Rev. Sci. Instrum.* **2004**, *75*, 4971–4980; b) R. Maksimenka, B. Dietzek, A. Szeghalmi, T. Siebert, W. Kiefer, M. Schmitt, *Chem. Phys. Lett.* **2005**, *408*, 37–43.

[32] In order to enhance the visibility of the oscillating component to the $\Delta A$ kinetics the probe light was spectrally dispersed in a spectrometer and the oscillations were recorded at a single spectral position within the probe spectrum.

[33] K. Stock, C. Schriever, S. Lochbrunner, E. Riedle, *Chem. Phys.* **2008**, *349*, 197–203.

[34] a) H. G. L. Fragnito, J. Y. Bigot, P. C. Becker, C. V. Shank, *Chem. Phys. Lett.* **1989**, *160*, 101–104; b) C. J. Brabec, G. Zerza, G. Cerullo, S. De Silvestri, S. Luzatti, J. C. Hummelen, S. Sariciftci, *Chem. Phys. Lett.* **2001**, *340*, 232–236.

[35] S. Westenhoff, W. J. D. Beenken, A. Yartsev, N. C. Greenham, *J. Chem. Phys.* **2006**, *125*, 154903.

[36] a) H. D. Burrows, J. S. de Melo, C. Serpaa, L. G. Arnaut, M. G. Miguel, A. P. Monkman, I. Hamblett, I. Navaratnam, *Chem. Phys.* **2002**, *285*, 3–11; b) A. P. Monkman, H. D. Burrows, L. J. Hartwell, L. E. Horsburgh, I. Hamblett, S. Navaratnam, *Phys. Rev. Lett.* **2001**, *86*, 1358–1361; c) A. P. Monkman, H. D. Burrows, M. G. Miguel, I. Hamblett, S. Navaratnam, *Chem. Phys. Lett.* **1999**, *307*, 303–309; d) H. D. Burrows, J. S. Melo, C. Serpa, L. G. Arnaut, A. P. Monkman, I. Hamblett, S. Navaratman, *J. Chem. Phys.* **2001**, *115*, 9601–9606; e) J. Seixas de Melo, L. M. Silva, L. G. Arnaut, R. S. Becker, *J. Chem. Phys.* **1999**, *111*, 5427–5433; J. Seixas de Melo, F. Elisei, C. Gartner, G. G. Aloisi, R. S. Becker, *J. Phys. Chem. A* **2000**, *104*, 6907–6911.

[37] A simple straight forward estimate of the triplet quantum yield based on the ratio of early and long-time ground-state bleaching signal was impossible as we do not observe $\Delta A$ data in the spectral region of dominant ground-state absorption.

[38] a) M.-L. Horng, J. A. Gardecki, A. Papazyan, M. Maroncelli, *J. Phys. Chem.* **1995**, *99*, 17311–17337; b) M.-L. Horng, J. A. Gardecki, M. Maroncelli, *J. Phys. Chem. A* **1997**, *101*, 1030–1047.

[39] T. Elsaesser, W. Kaiser, *Annu. Rev. Phys. Chem.* **1991**, *42*, 83–107.

[40] A. Mokhtari, J. Chesnoy, A. Laubereau, *Chem. Phys. Lett.* **1989**, *155*, 593–598.

Received: December 16, 2008
Revised: February 5, 2009
Published online on March 19, 2009

  

# [RS2] Excited-State Planarization as Free Barrierless Motion in a $\pi$-Conjugated Terpyridine



Reproduced with permission from:
R. Siebert, A. Winter, U. S. Schubert, B. Dietzek and J. Popp, Excited-State Planarization as Free Barrierless Motion in a $\pi$-Conjugated Terpyridine, *Journal of Physical Chemistry C*, **2010**, *114*, 6841-6848.



## Autorenschaft der Publikation

| | |
|---|---|
| Ronald Siebert | stationäre Absorptions- und Emissionsspektroskopie, zeitaufgelöste viskositäts- und polaritätsabhängige transiente Absorptionsspektroskopie, zeitaufgelöste temperaturabhängige Emissionsspektroskopie, Auswertung der Daten, Ergebnisdiskussion und Erstellung des Manuskripts |
| Andreas Winter | Synthese und Charakterisierung der untersuchten Substanzen, Diskussion und Korrektur des Manuskripts |
| Ulrich S. Schubert | Konzept- und Ergebnisdiskussion, Diskussion und Korrektur des Manuskripts |
| Benjamin Dietzek | Projektleitung, Konzept- und Ergebnisdiskussion, Diskussion und Korrektur des Manuskripts |
| Jürgen Popp | Konzept- und Ergebnisdiskussion, Diskussion und Korrektur des Manuskripts |

J. Phys. Chem. C 2010, 114, 6841–6848 

# Excited-State Planarization as Free Barrierless Motion in a $\pi$-Conjugated Terpyridine

**Ronald Siebert,[†] Andreas Winter,[‡] Ulrich S. Schubert,[‡,§] Benjamin Dietzek,*[,†,∥] and Jürgen Popp[†,∥]**

*Institute of Physical Chemistry, Friedrich-Schiller-University Jena, Helmholtzweg 4, 07743 Jena, Germany, Laboratory of Macromolecular Chemistry and Nanoscience, Eindhoven University of Technology, P.O. Box 513, 5600 MB Eindhoven, The Netherlands, Laboratory of Organic and Macromolecular Chemistry, Friedrich-Schiller-University Jena, Humboldtstr. 10, 07743 Jena, Germany, and Institute of Photonic Technology, Albert-Einstein-Str. 9, 07745 Jena, Germany*

*Received: January 12, 2010; Revised Manuscript Received: February 24, 2010*

We present femtosecond time-resolved transient absorption data and results from nanosecond time-resolved emission studies for an extended terpyridine system (4′-(4-((2,5-bis(octyloxy)-4-styrylphenyl)ethynyl)phenyl)-2,2′:6′,2″-terpyridine). By variation of selected solvent properties, that is, solvent viscosity, polarity, and temperature, we can dissect kinetic components, which are due to photoinduced molecular structure rearrangements of the terpyridine system. This real-time observation allows us to quantify the influence of the solvent viscosity on the structural rearrangements, which becomes slowed from 20 to 100 ps when changing the solvent from methanol to *n*-butanol. By adding temperature-dependent time-resolved emission experiments to the study, we show that the relaxed $S_1$ state partially decays via a nonradiative channel which can be assigned to an intersystem crossing to a lower lying $T_1$ state. The data presented in this paper directly visualize excited-state planarization of the terpyridine sphere in real time. Such motion of the terpyridine with respect to the adjacent conjugated rest leads to a highly conjugated chromophore and is causative for the observed photophysical features of the ligands and their transition metal complexes.

## Introduction

The conversion of light into chemical and electrical energy by means of artificial photosynthesis[1] and organic solar cells with properties tailored on the molecular level[2] represents a major challenge in modern chemistry. One of the key steps in harvesting and conversion of sun light, which will greatly help dealing with the looming energy crisis,[1b] is efficient light harvesting by mimicking natural photosynthesis or in photovoltaic applications. There are several approaches to this problem using different strategies like supramolecular frameworks,[3] organic semiconductors,[4] or metal-organic polymers, in which photoactive transition-metal centers are connected by different photoactive bridging ligands.[2b,5] The design of such systems allows for spectral-spatial focusing of the absorbed photon energy to a reaction center or photoactive electron donor.

Generally, transition metal complexes of 2,2′:6′,2″-terpyridine ligands,[6] for example, $[Ru(tpy)_2]^{2+}$, exhibit less useful photophysical properties than their 2,2′-bipyridine-based counterparts in terms of application for luminescent devices.[7] However, they are structurally more appealing with respect to the realization of linear assemblies, for example, as molecular wires.[8] Therefore, much effort has been laid on the design and synthesis of terpyridine-based ligands and their transition metal complexes with enhanced photophysical properties.[7a,9] Approaches incorporating electron-withdrawing and electron-donating substituents,[10] replacing the external pyridines by other heterocyclic rings[11] and extending the $\pi$-conjugated system[12] have recently been discussed.

The approach followed here is to adopt the major structural features of the most common poly(phenylene-ethynylene)-*alt*-poly(phenylene-vinylene)-type polymers[13] and to connect them to phenyl-substituted terpyridine spheres, which can subsequently be coordinated to transition-metal centers.[14] Such systems are well-known to stabilize MLCT states in the resultant transition-metal complexes due to delocalization of the MLCT over the entire chromophore.[7a] A substantial prerequisite for the success of this approach is the introduction of sufficient conjugation between the terpyridine-unit and the conjugated substituent. In this context it was shown that the conjugation between the two molecular parts is perturbed by the torsion of the terpyridine-plane with respect to the chromophore and has a strong influence on the photophysical properties of the ligand systems and their metal complexes.[15]

To evaluate the light-harvesting properties of such terpyridine-based supramolecular systems in real time, femtosecond time-resolved spectroscopy is applied. We previously focused on investigating the photophysics of related terpyridine-based ligand systems, which consist of one up to four terpyridine spheres connected by a $\pi$-conjugated spacer.[16] These ligands will form the structural basis for building one- or two-dimensional metallo-organic polymers for potential light-harvesting applications and operation in organic light-emitting diodes. We have investigated their photophysical properties, which are expected to have strong influence on the spectroscopic features of supramolecular architectures based terpyridine coordination polymers. These first experiments showed the formation of an emissive molecular geometry within picoseconds, which decays on a ns time-scale into a long-lived nonemissive triplet state.

* To whom correspondence should be addressed. Phone: 0049-3641-206332. Fax: 0049-3641-206399. E-mail: benjamin.dietzek@uni-jena.de.
[†] Institute of Physical Chemistry, Friedrich-Schiller-University Jena.
[‡] Eindhoven University of Technology.
[§] Laboratory of Organic and Macromolecular Chemistry, Friedrich-Schiller-University Jena.
[∥] Institute of Photonic Technology.

10.1021/jp100313x 
Published on Web 03/10/2010

Here, we focus on solvent-dependent time-resolved experiments to obtain substantially more insight into the photoinduced excited-state processes in the structurally most simple terpyridine system 4′-(4-((2,5-*bis*(octyloxy)-4-styrylphenyl)ethynyl)phenyl)-2,2′:6′,2″-terpyridine, consisting of a conjugated backbone and one terpyridine sphere (abbreviated "monoterpyridine" in the following). The experiments presented aim at discriminating between ultrafast intramolecular charge-transfer dynamics from excited-state structural rearrangements. The latter process has been discussed extensively in the literature on conjugated terpyridine systems in the context of excited-state planarization, which enlarges the $\pi$-electron system and stabilizes the excited state by stronger conjugation. However, the importance of such excited-state planarization has been inferred from the luminescence properties of synthetically modified terpyridine systems, and transient absorption experiments on terpyridine metal complexes.[17] In these cases the importance of this motion as a gating process was realized. The study at hand aims at a detailed femtosecond time-resolved investigation of the photoinduced planarization in isolated terpyridine model systems, in particular with respect to the solvent dependence of this reaction. The formation of an intramolecular charge-transfer state, the spectroscopic properties of which strongly vary with solvent polarity takes place in several small conjugated systems such carbonyl-substituted polyenes[18] as well as in, for example, carbonyl-substituted chlorophyll-derivates.[19] To disentangle intramolecular charge-transfer (ICT) from excited-state structural rearrangements and from other possible ultrafast relaxation processes, the solvent properties are systematically varied here. Variation of the solvent viscosity will affect any process associated with large structural rearrangement due to the local friction asserted on the solute by the solvent cage, the stiffness of which is correlated with the solvent viscosity.

A detailed and in-depth knowledge about these processes and their manifestation within the excited-state relaxation pathway in terpyridine based systems such as monoterpyridine will provide the basic framework for the synthesis of organo-metallic polymers and complexes with tailored electro-optical properties.

## Experimental Section

The synthesis of the series of $\pi$-conjugated terpyridine was recently published elsewhere.[20] The time-resolved transient absorption setup, which was described previously,[16] is based on an amplified Ti:Sapphire oscillator (Libra, Coherent Inc.) producing a pulse-train of 80 fs 950 $\mu$J pulses centered at 800 nm with a repetition rate of 1 kHz. The pulses were split by means of a 50:50 beamsplitter. One pulse-train was used to pump a noncollinear optical-parametric amplifier (TOPASwhite, LightConversion Ltd.), while the other one generated the pump pulses by second harmonic generation a 100 $\mu$m thick BBO crystal. In some experiments reported here, white light was used as probe. Therefore, 1% of the 800 nm fundamental beam was split off and focused into a sapphire plate to generate a supercontinuum.

It was ensured that the energy of the pump pulses was kept well below 0.5 $\mu$J, while typical probe intensities fall into the range of a few hundred nJ. Autocorrelation of the probe pulses and the experimental response function were recorded at the sample position by noncollinear second harmonic generation in a BBO crystal. The temporal duration of the probe pulses and the experimental response function was estimated to be in the order of 50−60 fs. Steady-state absorption spectra were frequently recorded to monitor the sample integrity.

Fluorescence lifetimes were obtained by time-correlated single-photon counting. Therefore, a Ti-Sapphire Laser (Tsunami, Newport Spectra-Physics GmbH) was used as light source. The repetition rate was reduced to 800 kHz by a pulse selector (Model 3980, Newport Spectra-Physics GmbH) and afterward the beam was frequency doubled in a second harmonic generator (Newport Spectra-Physics GmbH) to create the 435 nm pump beam. The emission was detected using a Becker & Hickel PMC-100-4 photon-counting module with 150 ps response-limited time resolution. To control the temperature of the sample an Oxford Instruments ITC 503 intelligent temperature monitor and control unit was used.

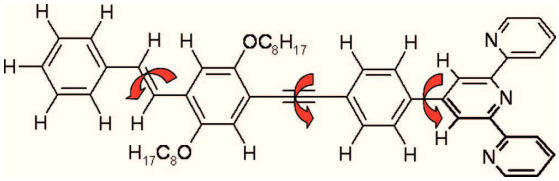


**Figure 1.** Schematic representation of the molecular structure of the investigated monoterpyridine.

Steady-state absorption spectra were recorded on a Jasco V-670 spectrophotometer, the fluorescence spectra were measured from dilute solutions using a Jasco FP-6200 spectrofluorimeter. All used solvents were of spectroscopic grade and purchased from Merck or Sigma Aldrich. The samples were prepared to yield an optical density of 0.1 in a 1 mm quartz-glass cuvette at the long wavelength absorption maximum.

## Results and Discussion

**Steady-State Spectroscopy.** Figure 2a shows the absorption and emission spectra of the tpy system dissolved in acetonitrile and toluene. These solvents represent the vertices of a number of binary mixtures of these highly polar and nonpolar solvents, which were used to investigate the effect of solvent polarity on the steady-state absorption and emission properties of the sample (Table 1).

Figure 2a shows that the spectral properties of the monoterpyridine strongly depend on the solvent polarity. This is reflected by the different shapes of the emission spectra when dissolving the sample in toluene and acetonitrile, respectively. The two main effects are a red shift of the emission maximum upon dissolution in the polar solvent and a loss of vibrational structure in the fluorescence spectrum, while the effect on the absorption spectra is weaker (see Figure 2). The qualitative solvent dependence becomes more quantitative in Figure 2b. Steady state spectra in different solvent environments with increasing polarity unravel the effect of polarity on the electronic transitions. To recover values for the Stokes shift as a function of solvent polarity, both absorption and emission spectra were deconvolved into two (absorption) and three (emission) Gaussian profiles to account for the vibrational structure (see the Supporting Information and ref 16 for details). From the deconvolved data, the Stokes shift was determined and plotted as a function of the solvent polarity, which was determined according to eq 1 [Equation 1: Polarity of the solvent ($\Delta f$), calculated from the static dielectric constant ($\varepsilon$) and the refractive index ($n$).] Linear regression of the data was carried out using the Lippert eq 2.[21] [Equation 2: Dependence of the Stokes shift ($\nu_{abs} - \nu_{em}$) from the solvent polarity, the difference in excited-state and ground-state dipole moment ($\mu_e - \mu_g$), and the radius of the solvent cage ($a$).]

$$\Delta f = \frac{\varepsilon - 1}{2\varepsilon + 1} - \frac{n^2 - 1}{2n^2 + 1} \quad (1)$$

$$v_{abs} - v_{em} = \frac{2}{hc}\left(\frac{\varepsilon - 1}{2\varepsilon + 1} - \frac{n^2 - 1}{2n^2 + 1}\right)\frac{(\mu_e - \mu_g)^2}{a^3} \quad (2)$$

Both the Stokes shift and the emission lifetime reveal a linear increase with increasing solvent polarity. This finding can be understood when invoking a higher dipole moment of the first excited state with respect to the electronic ground state. Such an excited state will be energetically more stabilized in polar environments compared to the electronic ground state. Hence, in more polar solvents, both the Stokes shift and the emission lifetime will increase. The linear dependences of Stokes shift and emission lifetime in concert with the minor effect of polarity on the absorption spectra indicate that absorption and emission involve the ground and the first excited state only: they occur between the electronic ground state and a $\pi\pi^*$ excited state without the contribution of a charge-transfer state.[22] It should be mentioned that the excitation is localized on the entire $\pi$-system and not only on the conjugated substituent of the terpyridine sphere, as corroborated by DFT calculations and Raman experiments on related systems.[15]

**Ultrafast Picosecond Photoinduced Dynamics.** The steady-state absorption and emission spectra as a function of solvent polarity reveal the nature of the electronic transitions observed. However, they do not yield direct insight into excited-state equilibration processes, which will take place upon photoexcitation. In order to monitor the dependence of such ultrafast processes on the molecular environment, we performed femtosecond time-resolved transient absorption experiments. Such experiments are presented and discussed in the following. In doing so, we aim at disentangling the effect of solvent polarity and solvent viscosity on the ultrafast, that is, sub-100-ps photoinduced dynamics of the tpy system. For the sake of clarity, we will present the results of polarity and viscosity-dependent transient-absorption experiments separately before suggesting an overall explanation for the observed behavior.

**TABLE 1: Comparison of the Data from the Solvent-Dependent Measurements**[a]

| solvent vol % toluene in acetonitrile | $\Delta f$ | $v_1$/cm$^{-1}$ | $v_2$/cm$^{-1}$ | $\Delta v$/cm$^{-1}$ |
|---|---|---|---|---|
| 0 | 0.71 | 24741 | 22609 | 2133 |
| 10 | 0.64 | 24682 | 22621 | 2061 |
| 20 | 0.57 | 24591 | 22644 | 1947 |
| 30 | 0.50 | 24621 | 22631 | 1990 |
| 40 | 0.43 | 24596 | 22664 | 1932 |
| 50 | 0.36 | 24642 | 22687 | 1955 |
| 60 | 0.29 | 24564 | 22722 | 1842 |
| 70 | 0.22 | 24571 | 22765 | 1806 |
| 80 | 0.15 | 24565 | 22817 | 1748 |
| 90 | 0.08 | 24587 | 22903 | 1,683 |
| 100 | 0.01 | 24597 | 23,050 | 1547 |
| methanol | 0.71 | 25018 | 22772 | 2245 |
| acetone | 0.65 | 24816 | 22744 | 2072 |
| THF | 0.44 | 24716 | 22754 | 1962 |

[a] Column one represents the solvent mixtures from toluene and acetonitrile or the pure solvents, $f$ refers to the polarity of the solvent system, and $v_1$ and $v_2$ are the maxima of the deconvolved absorption and emission spectra, respectively.

**Solvent-Polarity Dependence.** The formation of an intramolecular charge-transfer state upon photoexcitation has been discussed in the literature for terpyridines and terpyridine-related systems, in particular for their zinc(II) complexes.[12,14b,23] Furthermore, it is a common feature in other strongly conjugated systems such as carbonyl-substituted carotenoids[18] and chlorophyll derivates.[19] Commonly, all these systems exhibit a strongly solvent-polarity dependent excited-state behavior,[18b,24] which is indicative of an ICT state. This solvent-polarity dependence stems from the enlarged excited-state molecular dipole upon formation of an ICT state that is consequently more stabilized in polar solvents compared to nonpolar ones. Hence, ICT

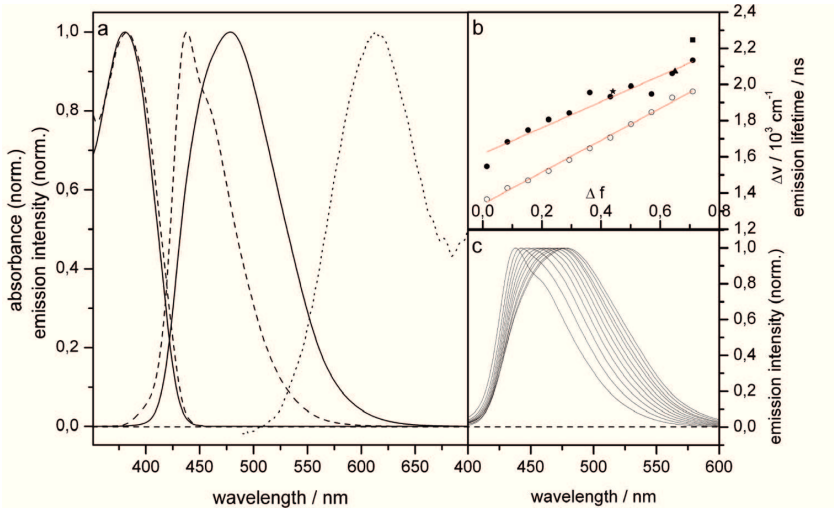


**Figure 2.** (a) Comparison of the absorption and emission spectra of the analyte using toluene (dashed line) and acetonitrile (solid line) as solvent with a transient absorption spectra at 500 ps recorded in THF (dotted line). (b) Polarity dependence of the Stokes shift in $10^3$ cm$^{-1}$ (solid circles represent binary mixtures of toluene and acetonitrile, while the square/triangle/star refers to methanol/THF/acetone as solvent, respectively) and the emission lifetime in ns (open circles). The red lines are the linear regression to the data points. (c) Comparison of the emission spectra recorded in the different binary mixtures. Here, it can be noted that the vibrational structure of the spectrum vanished, when the solvent polarity is gradually changed from nonpolar to highly polar.

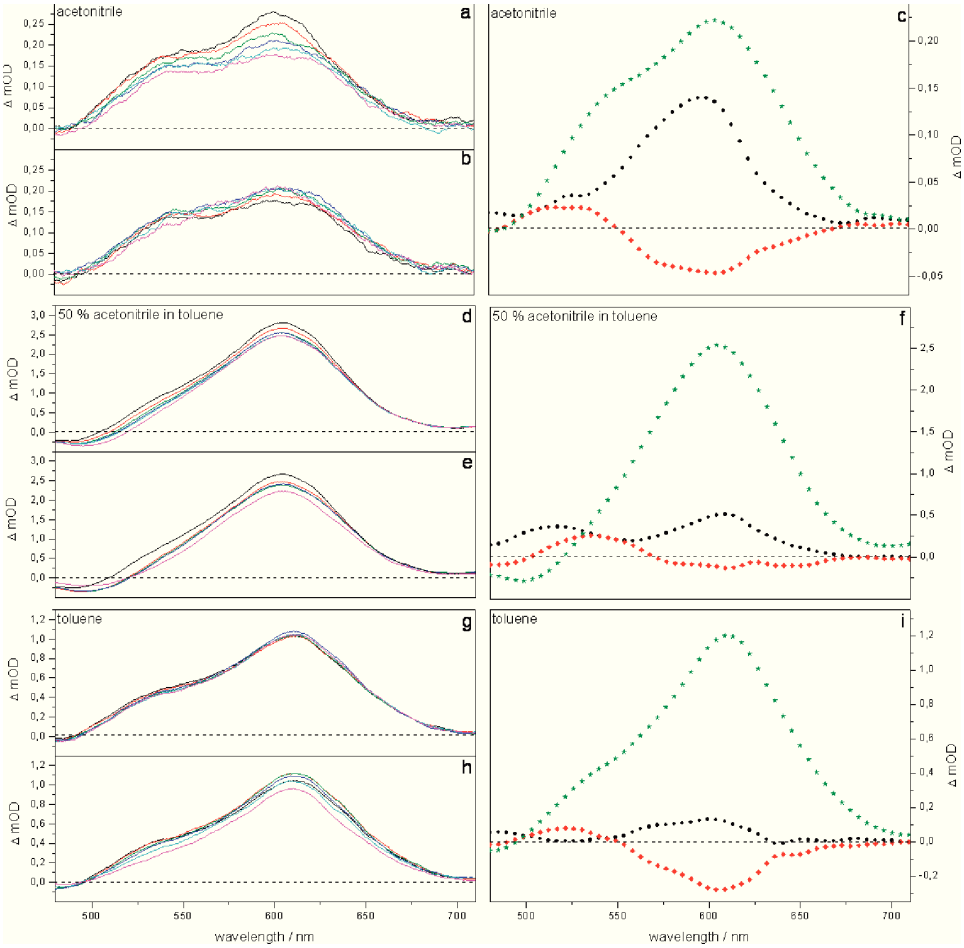


**Figure 3.** Transient-absorption spectra for the tpy dissolved in three solvents of different toluene content in acetonitrile (0% $\Delta f = 0.71$; 50% $\Delta f = 0.36$; 100% $\Delta f = 0.01$). Panels a, d, and g compare transient spectra between 0 and 10 ps after excitation (0.5 ps black; 1.0 ps red; 2.5 ps green; 5.0 ps blue; 7.5 ps cyan; and 10.0 ps magenta), while panels b, e, and h show transient spectra between 10 and 500 ps (10 ps black; 25 ps red; 50 ps green; 100 ps blue; 250 ps cyan; and 500 ps magenta). Panels c, f, and i depict the respective decay-associated spectra for a three-exponential decay with 2.0−3.0 ps (black squares), 15−20 ps (red circles), and a nanosecond component (green stars). Due to the limited delay-time range accessible in our experimental arrangement, a precise estimate of this time constant based on transient-absorption data is not possible. However, the results from time-resolved emission experiments allow us to provide more precise estimates (see ref 28).

formation will contribute to the transient-absorption kinetics with a strongly solvent-dependent component. To interrogate the system at hand with respect to the presence of an ICT state, transient-absorption experiments employing a supercontinuum white-light probe were carried out in different solvents, that is, toluene, acetonitrile, and a 50:50 mixture of both solvents (see Figure 3).

Figure 3a,b depicts transient-absorption spectra at different delay times for the monoterpyridine in acetonitrile, and panel c shows the decay-associated spectra, obtained from a triexponential global fitting procedure. Panels d−i show respective information for the monoterpyridine dissolved in toluene and the toluene−acetonitrile mixture. For all three solvent systems similar general decay behaviors are observed: Directly after photoexitation the signal decays during the first 10 ps. This process is followed by a slower decay in the blue part and a rise of the signal in the red part of the transient spectra which is completed after roughly 250 ps. Finally, a slow overall decay of the signal is observed, which extends over the experimentally accessible delay-time window. The amplitudes of the first two components relative to the slow component are larger for pure acetonitrile when compared to the other two solvent conditions. The decay in the blue and the rise in the red part of the spectrum on the intermediate time scale occur concertedly. A more quantitative description of the observed photophysics stems from a global fitting analysis, which resulted in three time-constants $\tau_1 = 2-3$ ps, $\tau_2 = 15-20$ ps, and $\tau_3 \approx$ ns. The corresponding decay-associated spectra are shown in panels c, f, and i. Considering the decay-associated spectra the spectral features associated with the kinetic components are discussed. It can be seen, that the fast component causes an overall decay of the signal, followed by a slower component, which corresponds to a rise between 550 and 750 nm and a decay below 500 nm. The third exponent again represents an overall decay on a long time scale. Furthermore, it is obvious that the spectral distribution of the exponentials is rather equal for all solvents, representing systems with a very high, medium and very low polarity. Finally, it should be noticed that the data obtained from monoterpyridine in several solvent mixtures correlate well with data from previous studies, which were restricted to an

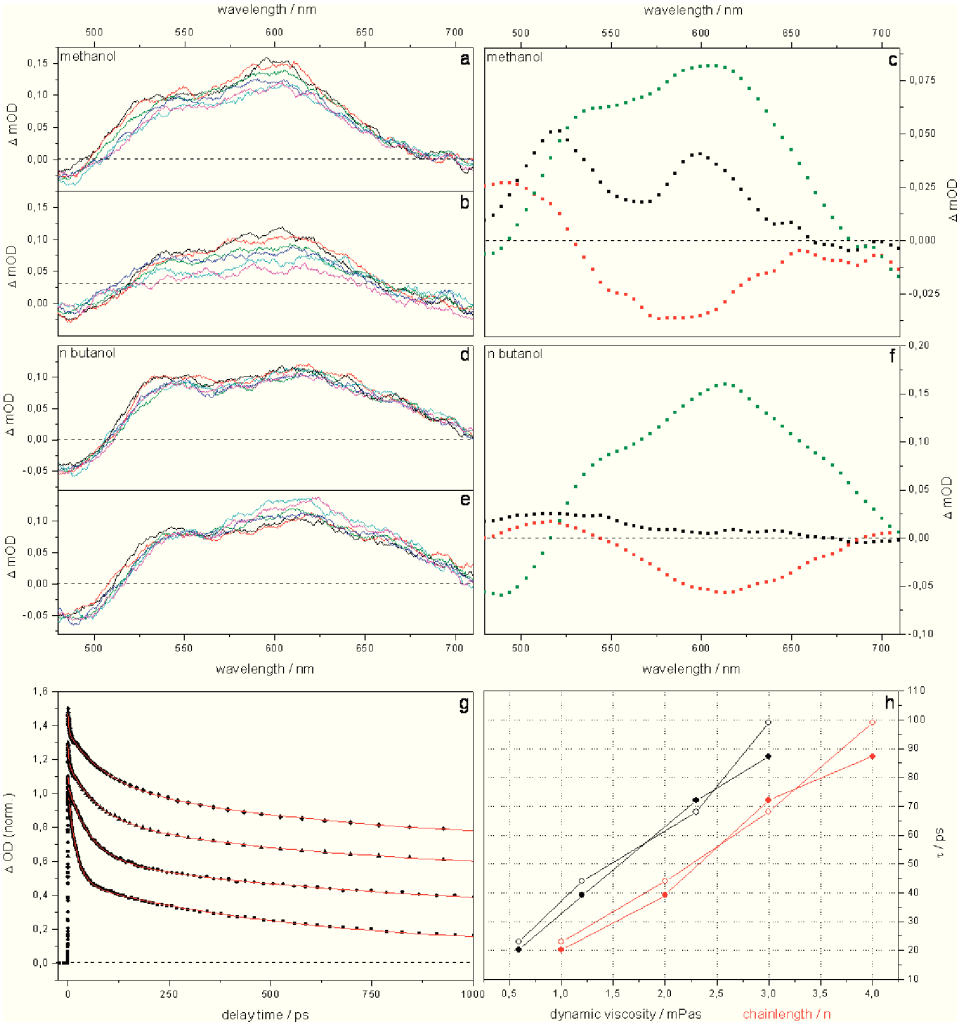


**Figure 4.** Transient-absorption spectra of monoterpyridine dissolved in methanol ($\Delta f = 0.71$) and *n*-butanol ($\Delta f = 0.61$). Panels a and d compare transient spectra between 0 and 10 ps after excitations (0.5 ps black; 1.0 ps red; 2.5 ps green; 5.0 ps blue; 7.5 ps cyan; and 10.0 ps magenta), while panels b and e show transient spectra between 10 and 500 ps (10 ps black; 25 ps red; 50 ps green; 100 ps blue; 250 ps cyan; and 500 ps magenta). Panels c and f depict the respective decay associated spectra for a three exponential decay with 2.0−3.0 ps (black squares), 20−100 ps (red circles), and a nanosecond component (green stars). Figure 4g compares single kinetic traces recorded at 550 nm for methanol (squares), ethanol (circles), *n*-propanol (triangles), and *n*-butanol (diamonds) together with the respective triexponential fit (red line). Figure 4h shows the medium time constant ($\tau_2$) as function of solvent viscosity (black) and the chain length of the alcohols (red). Full symbols represent data using single 550 nm as probe beam and the empty ones white light, respectively.

investigation of the photophysics of monoterpyridine in tetrahydrofuran.[16]

Thus, the solvent dependent transient-absorption data using a supercontinuums probe reveal no strong influence of the solvent polarity on the shape of the excited-state absorption spectra in the spectral observation window. This finding strongly indicates that the photophysics of monoterpyridine does not involve the formation of an ICT state. As spelled out before, in the latter case, we would expect strongly solvent polarity dependent spectral features.

**Solvent-Viscosity Dependence.** Aside from the formation of an ICT state, significant rearrangements of the molecular geometry in the excited electronic state of conjugated terpyridines have been discussed.[7a,9] Photoinduced structural rearrangements as well as conceptually related isomerization reactions[25] reveal a strong dependence on the solvent viscosity due to the interaction of the molecule with the surrounding solvent cage during the molecular motion.[26] Thus, recording differential absorption spectra as a function of solvent viscosity will help to distinguish ultrafast structural rearrangements from other photochemical or photophysical processes, because the kinetic components associated with severe geometrical changes of the solute are supposed to be slowed in the more viscous solvents.[27] To test if photoinduced structural rearrangements on the excited-state potential-energy surface are of significance for the terpyridine system, the tpy was dissolved in a series of *n*-alcohols ($n = 1-4$) and transient-absorption spectra as well as single wavelength kinetics were recorded.

Figure 4 compares the transient-absorption spectra for the monoterpyridine dissolved in the two alcohols methanol and

*n*-butanol. Panels a and b (d and e for butanol) depict transient-absorption spectra at different delay times, while panel c (f) shows decay-associated spectra, obtained from a triexponential global fit. Figure 3g compares single wavelength pump−probe kinetics recorded at 550 nm for methanol, ethanol, propanol, and butanol, while panel h summarizes the dependence of the time constant $\tau_2$ on solvent viscosity and alcohol chain length. For all alcohols the general decay behavior is similar (Figure 3a, b, d, e, and h) and comparable to the data observed when using acetonitrile and toluene as solvents: A fast sub-10 ps signal decay is followed by a slower decay in the blue part and a rise of the signal in the red part of the transient spectra. Subsequently, an overall decay of the differential absorption signal is observed, which extends over the rest of the experimentally accessible delay-time window. While the fast process can be characterized with a time constant $\tau_1 = 2-3$ ps, irrespective of the solvent viscosity, the second process ($\tau_2$) shows a drastic solvent viscosity dependence, yielding $\tau_2 = 20$ and 100 ps for methanol and butanol, respectively. To separately illustrate this behavior, Figure 4g compares single-wavelength kinetics recorded at 550 nm for the various alcohols. From these high S/N data, it is possible to determine precise values for the solvent-dependent characteristic time constants, which for $\tau_2$ are summarized in Figure 4h. Figure 4h summarizes the solvent-dependence of $\tau_2$ obtained from fitting the data shown in Figure 4. As can be seen, linear dependences of $\tau_2$ on both solvent viscosity and alcohol chain length are observed.

The pronounced deceleration of the kinetic associated with $\tau_2$ can be understood invoking a distinct change of the excited-state molecular geometry being associated with this component. Such an assignment is consistent with a number of publications, where strongly viscosity dependent time constants associated with isomerization reactions in solution have been reported.[25,26,27a,28] This being stated, the question arises if the molecular bond can be identified, at which structural rearrangement dominantly takes place. Inspection of the molecular structure (see Figure 1) reveals three positions, where steric interactions and repulsion of substituents cause a distorted, that is, nonplanar, geometry. Hence, a weakened double-bond character in the excited-state of the conjugated chromophore offers the possibility for photoinduced torsional relaxation. One of these positions is the PPV-related part of the molecule. Here, the planar geometry is disturbed by the large octyloxy substituents. From *p*-phenylene-vinylene trimer, used as model compounds for PPV polymers, it is known that excited state planarization occurs directly after photoexcitation on a time scale in the order of 10 ps.[29] A second position, at which changes in the molecular structure are possible, is the ethinylene part. At this position excited-state planarization was also reported for PPE derivatives.[30] Furthermore, the terpyridine sphere is twisted roughly 35° away from the almost planar conjugated backbone. Theoretical approaches to determine the molecular structure in the electronic ground state, however, showed that the part with the most disturbed geometry is the terpyridine part, while the other substructures show only minor deviations from the planar conformation. (The ground state geometry was determined by DFT calculations and their comparison to the corresponding Raman and IR-spectra.) Therefore, it appears most plausible to assign the photoinduced structural changes to the orientation of the terpyridine sphere, which is twisted by roughly 35° with respect to the rest of the chromophore. In some terpyridine−metal complexes, such motions could be identified as a gating process in the relaxation pathway, which occurs on a sub 10 ps time scale. These considerations further hint to excited-state planarization being responsible for the herein observed ultrafast solvent-viscosity dependent photophysics of the monoterpyridine.[17] The longer time scale for this process, observed in our experiments would be due to a more extended chromophor in this case, which causes a higher steric impact.

As a result of the twisted ground-state geometry, which is estimated based on DFT calculations on structurally related systems, the conjugation between the two parts of the molecular structure is decreased from its optimal value, that is, corresponding to the planar structure.[15] Nonetheless, molecular torsion in the electronic ground state is not severe enough to electronically decouple both parts of the molecule, which still act as a single chromophore. Photoinduced torsional motion, however, should result in drastically altered spectral properties of the tpy system: A reduction of the torsion angle would increase the conjugation, while an increase of the torsion angle shall lead to a broken conjugation on the time scale of the torsional motion. These expectations are corroborated by the experimental results, because the data show signal decay in the blue part and a rising differential absorption band in the red with the characteristic time constant $\tau_2$. As indicated before, this observation can be explained by excited-state planarization: A distorted, blue absorbing chromophor, the geometrical structure of which resembles the ground-state structure, is converted into a planar, red absorbing chromophore by torsional relaxation. The excited-state potential-energy surface along this reaction coordinate seems to be rather flat as indicated by the almost linear dependence of the characteristic time constant $\tau_2$ on the solvent viscosity ($\eta$)[26] and the local friction asserted by the solvent, which is reflected in the chain-length dependence of $\tau_2$.[28a] Such linear behavior of the reaction rate has been previously observed in isomerization reactions and indicates that the respective molecular process occurs barrierless.[25,28b]

**Ultrafast Photoinduced Processes.** The ultrafast sub-100-ps light-induced processes in the conjugated monoterpyridine derivative are dominated by two distinct time constants: $\tau_1 \approx 2.5$ ps and $\tau_2 = 20-100$ ps. While $\tau_1$ is unaffected by either solvent viscosity or polarity, the kinetic process associated with $\tau_2$ is slowed significantly in more viscous solvents. In agreement with previous work, the 2 ps component is assigned to cooling,[31] which is known to occur on similar time scales. The subsequent viscosity dependent ps-component ($\tau_2$) is assigned to excited-state planarization of the twisted terpyridine sphere, leading to a relaxed $S_1$ state. An overall red-shift of the $S_1$ excited-state absorption, which is independent of solvent polarity, is apparent from the spectral dependence of the $\tau_2$-associated amplitude. This finding indicates that $\tau_2$ is not associated with intramolecular charge transfer. Thus, we conclude that photoinduced excited-state planarization of the conjugated terpyridine system takes place after photoexcitation on a picosecond time scale, a process that has been predicted to dominate the photochemistry of such dyes.[9,32]

**Nanosecond Fluorescence Dynamics.** Having discussed the ultrafast formation of the emissive geometry above, the remainder of the paper will focus on the nanosecond fluorescence dynamics as observed in time-correlated single-photon counting experiments. In previous work, a nanosecond kinetic component was observed, which led to a decay of the fluorescence while populating a long-lived nonemissive triplet state.[16] To obtain a more detailed insight in the solvent dependence of this process, temperature-dependent experiments have been conducted. To do so, emission lifetimes of the monoterpyridine in tetrahydrofuran (THF) were recorded as a function of temperature in the range between 300 and 170 K.

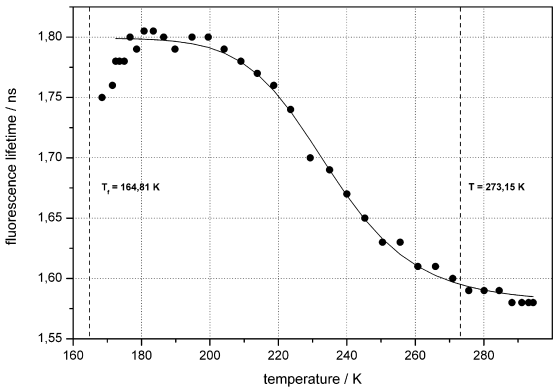


**Figure 5.** Temperature dependence of the emission lifetime of the monoterpyridine in THF. Symbols represent experimental data, while the solid line refers to the result of a fit. The vertical dashed lines indicate the fusion points of THF (164.8 K) and water (273.1 K), respectively.

Figure 5 summarizes the results of such experiments: At 300 K the emission lifetime is 1.58 ns. Reduction of the temperature below 290 K leads to an increase of the emission lifetime. The lifetime reaches its maximum values of roughly 1.80 nm at 180 K and decreases again slightly to 1.75 ns, when the temperature approaches the freezing point of THF at 164.8 K. Over the entire temperature range, the emission shows a monoexponential decay, the temperature dependence of which is typical for the presence of an excited-state barrier, dividing a radiative state and a nonradiative state. Monoexponential decay curves are recorded irrespective of the temperature, that is, no emission from $T_1$ is observed.

$$\tau(T) = \left[\frac{1}{\sum k + A\exp(-E_a/RT)}\right] + C \qquad (3)$$

Before estimating the barrier-height from the temperature-dependent data, we shall refer to experiments attempting to induce a similar barrier for the depopulation of the emissive state by variations of the macroscopic solvent viscosity at room temperature. Such experiments were performed by dissolution of monoterpyridine in a series of *n*-alcohols or in mixtures of acetone and acetylcellulose (see Supporting Information for details). While adding acetycellulose to acetone causes a drastic increase in viscosity, no effect on the emission lifetime could be observed. On the other hand, dissolution of the tpy in a series of *n*-alcohols causes only a slight decrease in the lifetime with increasing chain length, an effect that is assigned to the decreasing polarity of higher alcohols. This result indicates that quenching of the fluorescence does not involve major structural rearrangements of the molecular structure. The nonradiative decay of the long-lived species occurs by internal conversion (IC) or intersystem crossing (ISC) and does not alter the molecular geometry, while both processes compete with each other at room temperature. However, the nonradiative decay does not play the dominant role in the excited-state dynamics, because the sum over the quantum yields of IC and ISC is only about 26%. (The room temperature fluorescence quantum yield was determined to be 74%.) Upon a decrease in temperature, the IC quantum yield is reduced as vibrational fluctuations are thermally hindered and the promoter modes of the IC process are less efficiently populated. ISC on the other hand stemming from a purely electronic coupling is less affected by decreasing temperature.[33] Based on these considerations our experimental results can be understood as the balanced effect of strongly temperature, that is, fluctuation-dependent IC, and less temperature-dependent ISC.[16,34]

To evaluate the barrier height in a quantitative way, the functional form given in eq 3 was fitted to the data presented in Figure 5. In eq 3, the dependence of the emission lifetime $\tau(T)$ on the temperature and the energy barrier between the bright and a dark excited state is given.[35] $E_a$ refers to the activation energy needed for barrier crossing, $A$ is the Arrhenius factor, and $\Sigma k$ represents the sum over all temperature-independent rates. The constant $C$ accounts for the high-temperature offset of the temperature-dependent data. Following this approach, a barrier height of 36.5 kJ/mol for IC is obtained. The height of this barrier is a good explanation for the high fluorescence quantum yield of about 74%, because nonradiative deactivation directly to the ground state seems to be only a weak effect and the remaining about 26% have a significant contribution of ISC.[34]

## Conclusion

This contribution presents the direct observation of ultrafast excited-state planarization for a conjugated terpyridine system on the example of 4′-(4-((2,5-bis(octyloxy)-4-styrylphenyl)ethynyl)phenyl)-2,2′:6′,2″-terpyridine. Such motion has already been identified to have a strong influence on the excited-state dynamics. However, previously it was not investigated in detail on a model system by tuning solvent parameters such as polarity, viscosity and temperature. The solvent-dependent excited-state processes in the conjugated monoterpyridine derivative were investigated by femtosecond time-resolved absorption and nanosecond time-resolved emission spectroscopy. We report the observation of a 10−100 ps kinetic component, the actual rate of which is strongly solvent-viscosity dependent. Its viscosity dependence, that is, increased rate with decreasing viscosity, indicates that major structural rearrangements are associated with this component. Furthermore, the linear dependence of $\tau$ on the solvent viscosity indicates that the excited-state planarization occurs barrierless. The spectral amplitudes of this component do not vary significantly with the polarity of the environment and give no evidence for the contribution of any intramolecular charge-transfer state, which has been speculated to play a role in the excited-state photochemistry of conjugated terpyridine systems. Upon barrierless excited-state planarization a relaxed and emissive excited-state geometry is formed, the emission lifetime of which is found to increase with decreasing temperature. The underlying radiative decay competes with nonradiative processes such as internal conversion back to the ground state and intersystem crossing. Internal conversion, however, plays a minor role only, because this process was found to be thermally activated and to occur over a 36 kJ/mol barrier. However, the crossing of the barrier is not associated with large-scale structural rearrangement of the solute but rather due to thermally activated structural fluctuations.

We expect the direct observation of ultrafast photoinduced planarization in a conjugated terpyridine model system and its detailed dependence on solvent parameters such as viscosity and polarity might impact the design of terpyridine-based polymers with tailored electro-optical properties. Such polymers might find a broad range of applications in artificial light harvesting, polymer solar cells, and organic light-emitting diodes.

**Acknowledgment.** Financial support of the Fonds der Chemischen Industrie, the Dutch Polymer Institute, the Nederlandse Organisatie voor Wetenschappelijk Onderzoek (VICI award for U.S.S.) and the Thüringer Ministerium für Bildung, Wissenschaft und Kultur (Grant No. B 514-09049, PhotoMIC) for this work is highly acknowledged. We thank Dr. Denis Akimov for technical assistance with the experimental setup and Dr. Michael Schmitt and Prof. Dr. Ulrich-Walter Grummt for helpful discussions.

**Supporting Information Available:** Additional data and figures. This material is available free of charge via the Internet at http://pubs.acs.org.

## References and Notes

(1) (a) Rau, S.; Walther, D.; Vos, J. G. *Dalton Trans.* **2007**, *9*, 915–919, and references cited therein. (b) Lewis, N. S.; Nocera, D. G. *Proc. Natl. Acad. Sci. U.S.A.* **2006**, *103*, 15729–15735, and references cited therein.

(2) (a) Thompson, B. C.; Frechet, J. M. J. *Angew. Chem., Int. Ed.* **2008**, *120*, 62–82. (b) Duprez, V.; Biancardo, M.; Spanggaard, H.; Krebs, F. C. *Macromolecules* **2005**, *38*, 10436–10448. (c) O'Regan, B.; Grätzel, M. *Nature* **1991**, *353*, 737–739. (d) McNamara, W. R.; Snoeberger, R. C.; Li, G.; Schleicher, J. M.; Cady, C. W.; Poyatos, M.; Schmuttenmaer, C. A.; Crabtree, R. H.; Brudvig, G. W.; Batista, V. S. *J. Am. Chem. Soc.* **2008**, *130*, 14329–14338.

(3) Scandola, F.; Chiorboli, C.; Prodi, A.; Iengo, E.; Alessio, E. *Coord. Chem. Rev.* **2006**, *250*, 1471–1496.

(4) Hoppe, H.; Sacritiftci, N. S. *Adv. Polym. Sci.* **2008**, *214*, 1–86.

(5) Pefkianakis, E. K.; Tzanetos, N. T.; Chochos, C. L.; Andreapoulou, A. K.; Kallitsis, J. K. *J. Polym. Sci., Part A: Polym. Chem.* **2009**, *47*, 1939–1952.

(6) (a) Schubert, U. S.; Hofmeier, H.; Newkome, G. R. *Modern Terpyridine Chemistry*; VCH-Wiley: Weinheim, 2006. (b) Andres, P. R.; Schubert, U. S. *Adv. Mater.* **2004**, *16*, 1043–1068.

(7) (a) Medlycott, E. A.; Hanan, G. S. *Coord. Chem. Rev.* **2006**, *250*, 1763–1782. (b) Campagna, S.; Puntoriero, F.; Nastasi, F.; Bergamini, G.; Balzani, V. *Top. Curr. Chem.* **2007**, *280*, 117–214. (c) Tschierlei, S.; Presselt, M.; Kuhnt, C.; Yartsev, A.; Pascher, T.; Sundström, V.; Karnahl, M.; Schwalbe, M.; Schäfer, B.; Rau, S.; Schmitt, M.; Dietzek, B.; Popp, J. *Chem.—Eur. J.* **2009**, *15*, 7678–7688. (d) Siebert, R.; Winter, A.; Dietzek, B.; Schubert, U. S.; Popp, J. *Macromol. Rapid Commun.* **2010**, DOI: 10.1002/marc.200900894.

(8) Barbieri, A.; Ventura, B.; Barigelletti, F.; De Nicola, A.; Quesada, M.; Ziessel, R. *Inorg. Chem.* **2004**, *43*, 7359–7369.

(9) Medlycott, E. A.; Hanan, G. S. *Chem. Soc. Rev.* **2005**, *34*, 133–142.

(10) Maestri, M.; Armaroli, N.; Balzani, V.; Constable, E. C.; Cargill Thompson, A. M. W. *Inorg. Chem.* **1995**, *34*, 2759–2767.

(11) (a) Abrahamsson, M.; Jäger, M.; Österman, T.; Eriksson, L.; Persson, P.; Becker, H. C.; Johansson, O.; Hammarström, L. *J. Am. Chem. Soc.* **2006**, *128*, 12616–12617. (b) Schulze, B.; Friebe, C.; Hager, M. D.; Winter, A.; Hoogenboom, R.; Görls, H.; Schubert, U. S. *Dalton Trans.* **2009**, 787–794.

(12) Wang, X. Y.; Guerzo, A.; Tunuguntla, H.; Schmehl, R. H. *Res. Chem. Int.* **2007**, *33*, 63–77.

(13) (a) Egbe, D. A. M.; Carbonnier, B.; Birckner, E.; Grummt, U. W. *Prog. Polym. Sci.* **2009**, *34*, 1023–1067. (b) Grimsdale, A. C.; Chan, K. L.; Martin, R. E.; Jokisz, P. G.; Holmes, A. B. *Chem. Rev.* **2009**, *109*, 897–1091.

(14) (a) Winter, A.; Friebe, C.; Hager, M. D.; Schubert, U. S. *Macromol. Rapid Commun.* **2008**, *29*, 1679–1686. (b) Winter, A.; Friebe, C.; Chiper, M.; Hager, M. D.; Schubert, U. S. *J. Polym Sci., Part A: Polym. Chem.* **2009**, *47*, 4083–4098. (c) Chen, Y. Y.; Tao, Y. T.; Lin, H. C. *Macromolecules* **2006**, *39*, 8559–8566.

(15) (a) Winter, A.; Friebe, C.; Chiper, M.; Schubert, U. S.; Presselt, M.; Dietzek, B.; Schmitt, M.; Popp, J. *ChemPhysChem* **2009**, *10*, 787–798. (b) Presselt, M.; Dietzek, B.; Schmitt, M.; Popp, J.; Winter, A.; Chiper, M.; Friebe, C.; Schubert, U. S. *J. Phys. Chem. C* **2008**, *112*, 18651–18660.

(16) Siebert, R.; Akimov, D.; Schmitt, M.; Winter, A.; Schubert, U. S.; Dietzek, B.; Popp, J. *ChemPhysChem* **2009**, *10*, 910–919.

(17) (a) Damrauer, N. H.; Boussie, T. R.; Devenney, M.; McCusker, J. K. *J. Am. Chem. Soc.* **1997**, *119*, 8253–8268. (b) Damrauer, N. H.; McCusker, J. K. *J. Phys. Chem. A* **1999**, *103*, 8440–8446. (c) Lainé, P. P.; Campagna, S.; Loiseau, F. *Coord. Chem. Rev.* **2008**, *252*, 2552–2571. (d) Lainé, P. P.; Bedioui, F.; Loiseau, F.; Chiorboli, C.; Campagna, S. *J. Am. Chem. Soc.* **2006**, *128*, 7510–7521.

(18) (a) Polivka, T.; Sundström, V. *Chem. Rev.* **2004**, *104*, 2021–2071. (b) Zigmantas, D.; Hiller, R. G.; Yartsev, A.; Sundström, V.; Polivka, T. *J. Phys. Chem. B* **2003**, *107*, 5339–5348. (c) Zigmantas, D.; Hiller, R. G.; Sharples, F. P.; Frank, H. A.; Sundström, V.; Polivka, T. *Phys. Chem. Chem. Phys.* **2004**, *6*, 3009–3016.

(19) (a) Dietzek, B.; Tschierlei, S.; Herman, G.; Yartsev, A.; Pascher, T.; Sundström, V.; Schmitt, M.; Popp, J. *ChemPhysChem* **2009**, *10*, 144–150. (b) Dietzek, B.; Kiefer, W.; Yartsev, A.; Sundström, V.; Schellenberg, P.; Grigaravicius, P.; Herman, G.; Popp, J.; Schmitt, M. *ChemPhysChem* **2006**, *7*, 1727–1733.

(20) Winter, A.; Friebe, C.; Hager, M. D.; Schubert, U. S. *Eur. J. Org. Chem.* **2009**, 801–809.

(21) Lippert, E. Z. *Elektrochem.* **1957**, *61*, 962–975.

(22) (a) Nad, S.; Pal, H. *J. Phys. Chem. A* **2001**, *105*, 1097–1106. (b) Grummt, U. W.; Weiss, D.; Birckner, E.; Beckert, R. *J. Phys. Chem. A* **2007**, *111*, 1104–1110. (c) Fery-Forgues, S.; Fayet, J. P.; Lopez, A. *J. Photochem. Photobiol. A* **1993**, *70*, 229–243.

(23) (a) Chen, X.; Zhou, Q.; Cheng, Y.; Geng, Y.; Ma, D.; Xie, Z.; Wang, L. *J. Lumin.* **2007**, *126*, 81–90. (b) Wang, X. Y.; Guerzo, A.; Schmehl, R. H. *Chem. Commun.* **2002**, 2344–2345. (c) Leroy, S.; Soujanya, T.; Fages, F. *Tetrahedron Lett.* **2001**, *42*, 1665–1667. (d) Tessore, F.; Roberto, D.; Ugo, R.; Pizzotti, M. *Inorg. Chem.* **2005**, *44*, 8967–8978.

(24) Dietzek, B.; Kiefer, W.; Hermann, G.; Popp, J.; Schmitt, M. *J. Phys. Chem. B* **2006**, *110*, 4399–4406.

(25) Akesson, E.; Bergström, H.; Sundström, V.; Gillbro, T. *Chem. Phys. Lett.* **1986**, *126*, 385–393.

(26) (a) Bagchi, B.; Fleming, G. R. *J. Phys. Chem.* **1990**, *94*, 9–20. (b) Bagchi, B.; Fleming, G. R.; Oxtoby, D. W. *J. Chem. Phys.* **1983**, *78*, 7375–7385.

(27) (a) Dietzek, B.; Tarnovsky, A. N.; Yartsev, A. *Chem. Phys.* **2009**, *357*, 54–62. (b) Dietzek, B.; Christensson, N.; Pascher, T.; Pullerits, T.; Yartsev, A. *J. Phys. Chem. B* **2007**, *111*, 5396–5404. (c) Akers, W.; Haidekker, M. A. *Trans. ASME* **2004**, *126*, 340–345.

(28) (a) Todd, D. C.; Fleming, G. R. *J. Chem. Phys.* **1993**, *98*, 269–279. (b) Aberg, U.; Sundström, V. *Chem. Phys. Lett.* **1991**, *185*, 461–467.

(29) (a) Di Paolo, R. E.; Seixas de Melo, J.; Pina, J.; Burrows, H. D.; Morgado, J.; Macanita, A. L. *ChemPhysChem* **2007**, *8*, 2657–2664. (b) Di Paolo, R. E.; Burrows, H. D.; Morgado, J.; Macanita, A. L. *ChemPhysChem* **2009**, *10*, 448–454.

(30) Sluch, M. I.; Godt, A.; Bunz, U. H.; Berg, M. A. *J. Am. Chem. Soc.* **2001**, *123*, 6447–6448.

(31) (a) Horng, M. L.; Gardecki, J. A.; Papazyan, A.; Maroncelli, M. *J. Phys. Chem.* **1995**, *99*, 17311–17337. (b) Horng, M. L.; Gardecki, J. A.; Maroncelli, M. *J. Phys. Chem. A* **1997**, *101*, 1030–1047.

(32) Aleman, E. A.; Shreiner, C. D.; Rajesh, C. S.; Smith, T.; Garrison, S. A.; Modarelli, D. A. *Dalton Trans.* **2009**, 6562–6577.

(33) (a) Larson, E. J.; Johnson, C. K. *J. Phys. Chem. B* **1999**, *103*, 10917–10923. (b) Mac, M.; Kwiatkowski, P.; Pischel, U. *Chem. Phys. Lett.* **2002**, *357*, 440–449.

(34) (a) Burrows, H. D.; Seixas de Melo, J.; Serpa, C.; Arnaut, L. G.; Miguel, M. G.; Monkman, A. P.; Hamblett, I.; Navaratnam, S. *Chem. Phys.* **2002**, *285*, 3–11. (b) Pina, J.; Seixas, M.; Burrows, H. D.; Galbrecht, F.; Bilge, A.; Kudla, C. J.; Scherf, U. *J. Phys. Chem. B* **2008**, *112*, 1104–1111.

(35) (a) Lewis, F. D.; Zuho, X. *J. Am. Chem. Soc.* **2003**, *125*, 8806–8813. (b) Yang, J. S.; Liau, K. L.; Hwang, C. Y.; Wang, C. M. *J. Phys. Chem. A* **2006**, *110*, 8003–8010.

JP100313X

## [RS3] Dual Emission from Highly Conjugated 2,2‘:6‘:2“-Terpyridine Complexes - a potential Route to White Emitters


R. Siebert, A. Winter, B. Dietzek, U. S. Schubert and J. Popp, Dual Emission from Highly Conjugated 2,2‘:6‘:2“-Terpyridine Complexes - A Potential Route to White Emitters, *Macromolecular Rapid Communications*, **2010**, *31*, 883-888.



### Autorenschaft der Publikation

| | |
|---|---|
| Ronald Siebert | stationäre Absorptions- und Emissionsspektroskopie, Auswertung der Daten, Ergebnisdiskussion und Erstellung des Manuskripts |
| Andreas Winter | Synthese und Charakterisierung der untersuchten Substanzen, Diskussion und Korrektur des Manuskripts |
| Benjamin Dietzek | Projektleitung, Konzept- und Ergebnisdiskussion, Diskussion und Korrektur des Manuskripts |
| Ulrich S. Schubert | Konzept- und Ergebnisdiskussion, Diskussion und Korrektur des Manuskripts |
| Jürgen Popp | Konzept- und Ergebnisdiskussion, Diskussion und Korrektur des Manuskripts |

Communication

Macromolecular Journals

Macromolecular Rapid Communications

# Dual Emission from Highly Conjugated 2,2′:6′:2″-Terpyridine Complexes — A Potential Route to White Emitters

Ronald Siebert, Andreas Winter, Benjamin Dietzek,* Ulrich S. Schubert,* Jürgen Popp

Here, we present a new class of terpyridine complexes of the transition-metal ions, iron(II), ruthenium(II), and osmium(II), overcoming the poor emission properties typical for this class of polypyridyl complexes. These complexes show, besides an increased room-temperature emission quantum yield and a prolonged lifetime of the metal-to-ligand charge-transfer (MLCT) states, dual emission from two well-separated excited states of the same molecule. These experimental findings are attributed to a highly stabilized ligand chromophore, where photoinduced excited-state planarization causes an enhancement of electron delocalization. This planarization, in turn, reduces the potential energy of the $S_1$ state and minimizes electronic coupling to the MLCT state, which is prone to non-radiative deactivation via metal-centered excited states. Due to their dual emission the complexes presented here show emission covering the entire Vis spectral range upon excitation of the $\pi\pi^*$ states in the near UV. Thus, by structurally tuning the electronic coupling of the $\pi\pi^*$ and the MLCT states a new synthetic route toward white emitters, which can subsequently be incorporated into polymers, is opened.

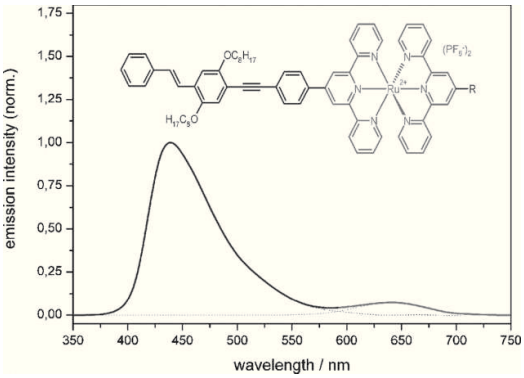


R. Siebert, B. Dietzek, J. Popp
Institute for Physical Chemistry, Friedrich-Schiller-University Jena, Helmholtzweg 4, 07743 Jena, Germany
Fax: (+49) 0 3641 206399; E-mail: benjamin.dietzek@uni-jena.de
A. Winter, U. S. Schubert
Laboratory of Macromolecular Chemistry and Nanoscience, Eindhoven University of Technology, P.O. Box 513, 5600 MB Eindhoven, The Netherlands; Dutch Polymer Institute (DPI), P.O. Box 902, 5600 AX Eindhoven, The Netherlands
B. Dietzek, J. Popp
Institute for Photonic Technology Jena, Albert-Einstein-Str. 9, 07745 Jena, Germany
U. S. Schubert
Laboratory of Organic and Macromolecular Chemistry, Friedrich-Schiller-University Jena, Humboldtstr. 10, 07743 Jena, Germany
Fax: (+49) 0 3641 948202; E-mail: ulrich.schubert@uni-jena.de

*Macromol. Rapid Commun.* **2010**, *31*, 883–888




DOI: 10.1002/marc.200900894

## Introduction

In modern materials research, π-conjugated polymers are currently in the spotlight of interest, since their rich electro-optical properties[1] make them promising candidates for applications in the fields of photovoltaic devices[2] and organic light-emitting diodes (OLEDs).[3] Besides various types of organic polymers and small organic molecules, also coordination compounds have recently gained increased interest.[4] This contribution focuses on the luminescence properties of a set of transition-metal ion complexes of a 2,2′:6′:2″-terpyridine bearing π-conjugated substituent.[5] These materials have a great potential to be used in photovoltaic and electroluminescent devices by substituting the commonly applied conjugated organic polymers, such as PPVs and PPEs.[6] The herein presented complexes represent model systems for a number of supra- and macromolecular compounds, which are the topic of ongoing work. Several synthetic strategies have been developed to implement such coordination compounds into macromolecular frameworks, e.g., the formation of coordination polymers, the attachment of macromolecular side chains to the ligand systems, or the encapsulation in a carrier polymer.[7] In particular, coordination polymers, i.e., individual ligand units connected by metal ions forming a macromolecular assembly, are of great interest due to the possibility of utilizing the spectral properties of both the metal center and the ligand framework. Such systems could potentially constitute approaches toward artificial light harvesting by coordinating different metal ions in order to generate an energy and electron transfer gradient along the polymer chain. Another promising approach to utilize the terpyridine metal complexes presented in this work is the embedding in polymer matrices for inkjet printing and for the formation of OLED materials.[8] In any case, synthetic fine tuning of the electro-optical properties of such polymers requires detailed knowledge of the spectral properties of the supramolecular building blocks, i.e., the transition-metal complexes of conjugated terpyridine systems, as presented here.

In general, terpyridine complexes exhibit only poor luminescence, originating from emission of an excited metal-to-ligand charge-transfer (MLCT) state.[9] The terpyridine MLCT emission is characterized by very low quantum yields and short lifetimes because of an effective electronic coupling between the emissive MLCT state and metal-centered (MC) excited states which has its origin in the distorted octahedral structure of the terpyridine complexes as compared to the structure of related bipyridine complexes.[10] However, several synthetic strategies exist to improve the luminescence properties of terpyridine complexes. One promising approach focuses on creating an excited-state equilibrium between the $^3$MLCT and the ligand-centered (LC) triplet state, even if conjugated chromophores are attached to the terpyridine sphere. Furthermore, substitution with electron-accepting or electron-donating groups can be utilized to tune the emission properties of terpyridine transition-metal complexes.[11] Yet another approach to improve the luminescence properties is to introduce heterocyclic components, which result in a reduced torsion angle between the terpyridine sphere and the substituent. Such a planar conformation causes a significant delocalization of the excitation and, consequently, stabilizes the excitation in a way that even at room temperature phosphorescence can be observed.

Although terpyridine MLCT emission bands are generally spectrally quite broad, a further extension of the spectral range of emission is desired. This is particularly true when designing molecular white emitters for potential OLED applications. While transition-metal complexes with different metal centers have shown to exhibit significantly broadened emission spectra,[12] another approach to molecular white emitters would be the design of a system bearing two distinct emitting states, where the electronic coupling between these two states can be ideally controlled by structural variations. Along these lines, this contribution presents new terpyridine complexes that show dual emission from the $\pi\pi^*$ as well as from the MLCT state and, hence, suggest a potential route to supramolecular white emitters.

## Experimental Part

### Materials and Instrumentation

All chemicals were of reagent grade and used as received unless otherwise specified. The solvents were obtained from Biosolve and were dried and distilled according to standard procedures. Preparative size exclusion chromatography was performed using SX-3 BioBeads™ and acetone as eluent. The synthesis and characterization of (*E*)-4-(4-((2,5-*bis*-(octyloxy)-4-styrylphenyl)-ethynyl)phenyl)-2,2′:6′,2″-terpyridine (**L**)[5a] and $Ru(DMSO)_4Cl_2$ was carried out according to the literature.[13]

$^1$H NMR spectra were recorded on a Varian Mercury 400 MHz spectrometer at 298 K. Chemical shifts are given in ppm relative to tetramethylsilane ($Me_4Si$). Matrix-assisted laser desorption-ionization time-of-flight mass spectrometry (MALDI-TOF MS) was performed on a Voyager-DE PRO biospectrometry workstation (Applied Biosystems) TOF mass spectrometer, with dithranol as matrix. Elemental analyses were carried out on a EuroVector EuroEA3000 elemental analyzer configured for CHNS. The steady-state absorption spectra were recorded using a UV–Vis-NIR-spectrometer Varian Cary 5000. For this purpose, $2 \times 10^{-5}$ mol/L solutions were measured in a 10-mm quartz glass sample cell. The emission spectra were obtained from solutions with a similar concentration using a Jasco FP 6200 Spectrofluorometer. The relative quantum yields were determined versus quinine sulfate in 0.1 M sulfuric acid as standard ($\Phi_F = 0.55$, $n_D = 1.333$). In doing so, the spectra were recorded with a Perkin-Elmer LS 50 spectrometer


*Macromol. Rapid Commun.* **2010**, *31*, 883–888

Macromolecular Journals
DOI: 10.1002/marc.200900894

and corrected according to the spectral sensitivity function of the detector.

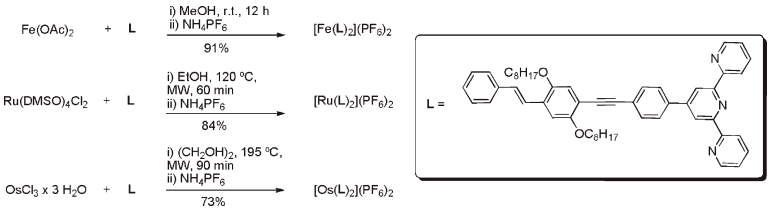


*Figure 1.* Schematic representation of the investigated transition-metal complexes.

### Synthesis of the Transition-Metal Complexes

$[Fe(\mathbf{L})_2](PF_6)_2$

A suspension of **L** (76.8 mg, 0.1 mmol) and $Fe(CH_3COO)_2$ (8.7 mg, 0.05 mmol) in methanol (15 mL) was stirred at room temperature for 12 h. Subsequently, the purple solution was filtered and the filtrate was treated with an excess of $NH_4PF_6$. After stirring at room temperature for 2 h, the precipitate was filtered off. The crude product was recrystallized from methanol/acetonitrile to yield $[Fe(\mathbf{L})_2](PF_6)_2$ as a purple powder (85.6 mg, 91%). $^1$H NMR ($d_6$-acetone, 300 MHz): $\delta = 9.72$ (s, 4H), 9.07 (d, $^3J = 8.0$ Hz, 4H), 8.55 (d, $^3J = 7.9$ Hz, 4H), 8.11 ($m_c$, 4H), 7.936 (d, $^3J = 8.2$ Hz, 4H), 7.64–7.57 (m, 12H), 7.48 ($m_c$, 4H), 7.41 ($m_c$, 4H), 7.30 ($m_c$, 6H), 7.21 (s, 2H), 4.24 (t, $^3J = 6.0$ Hz, 4H), 4.14 (t, $^3J = 6.3$ Hz, 4H), 1.93 ($m_c$, 8H), 1.64 ($m_c$, 4H), 1.52–1.30 (m, 32H), 0.91 ($m_c$, 12H). MALDI-TOF MS (dithranol): $m/z = 1735.76$ ($[M–PF_6]^+$), 1590.81 ($[M–(PF_6)_2]^+$). $C_{106}H_{114}F_{12}FeN_6O_4P_2$ (1881.85): Calcd. C 67.65, H 6.11, N 4.47; Found C 67.95, H 5.88, N 4.31.

$[Ru(\mathbf{L})_2](PF_6)_2$

A suspension of **L** (76.8 mg, 0.1 mmol) and $Ru(DMSO)_4Cl_2$ (24.2 mg, 0.05 mmol) in ethanol (10 mL) was heated under microwave irradiation at 120 °C for 60 min. The red solution was filtered and the filtrate was treated with an excess of $NH_4PF_6$. After stirring at room temperature for 2 h, the precipitate was filtered off. The crude product was purified by preparative size exclusion chromatography (SX-3 BioBeads, acetone as eluent), followed by precipitation into diethyl ether to yield $[Ru(\mathbf{L})_2](PF_6)_2$ as a deep red powder (81.0 mg, 84%). $^1$H NMR ($d_6$-acetone, 300 MHz): $\delta = 9.50$ (s, 4H), 9.07 (d, $^3J = 8.1$ Hz, 4H), 8.44 (d, $^3J = 8.3$ Hz, 4H), 8.11 ($m_c$, 4H), 7.88 (d, $^3J = 8.6$ Hz, 4H), 7.84 (d, $^3J = 6.1$ Hz, 4H), 7.65–7.56 (m, 10H), 7.46 ($m_c$, 4H), 7.41 ($m_c$, 4H), 7.36 ($m_c$, 4H), 7.20 (s, 2H), 4.23 (t, $^3J = 6.1$ Hz, 4H), 4.14 (t, $^3J = 6.6$ Hz, 4H), 1.91 ($m_c$, 8H), 1.64 ($m_c$, 4H), 1.46 ($m_c$, 4H), 1.42–1.25 (m, 32H), 0.91 ($m_c$, 12H). MALDI-TOF MS (dithranol): $m/z = 1871.90$ ($[M–PF_6]^+$), 1726.84 ($[M–(PF_6)_2]^+$). $C_{106}H_{114}F_{12}N_6O_4P_2Ru$ (1927.08): Calcd. C 66.07, H 5.96, N 4.36; Found C 65.81, H 6.32, N 4.68.

$[Os(\mathbf{L})_2](PF_6)_2$

A suspension of **L** (76.8 mg, 0.1 mmol) and $OsCl_3 \times 3\ H_2O$ (17.5 mg, 0.05 mmol) in ethylene glycol (10 mL) was heated under microwave irradiation at 195 °C for 90 min. The dark brown solution was filtered and the filtrate was treated with an excess of $NH_4PF_6$. After stirring at room temperature for 2 h, the precipitate was filtered off. The crude product was purified by preparative size exclusion chromatography (SX-3 BioBeads, acetone as eluent), followed by precipitation into diethyl ether to yield $[Os(\mathbf{L})_2](PF_6)_2$ as a dark brown powder (73.6 mg, 73%). $^1$H NMR ($d_6$-acetone, 300 MHz): $\delta = 9.53$ (s, 4H), 9.08 (d, $^3J = 8.0$ Hz, 4H), 8.40 (d, $^3J = 7.9$ Hz, 4H), 8.00 ($m_c$, 4H), 7.88 (d, $^3J = 8.2$ Hz, 4H), 7.73 (d, $^3J = 5.5$ Hz, 4H), 7.63–7.55 (m, 10H), 7.46 ($m_c$, 4H), 7.41 ($m_c$, 4H), 7.31 ($m_c$, 4H), 7.19 (s, 2H), 4.25 (t, $^3J = 6.4$ Hz, 4H), 4.15 (t, $^3J = 6.3$ Hz, 4H), 1.91 ($m_c$, 8H), 1.64 ($m_c$, 8H), 1.48–1.21 (m, 32H), 0.89 ($m_c$, 12H). MALDI-TOF MS (dithranol): $m/z = 1871.90$ ($[M–PF_6]^+$), 1726.84 ($[M–(PF_6)_2]^+$). $C_{106}H_{114}F_{12}N_6O_4OsP_2$ (2016.24): Calcd. C 63.14, H 5.70, N 4.17; Found C 62.97, H 5.98, N 4.44.

## Results and Discussion

The complexation of the terpyridine **L** was carried out as depicted in Figure 1; depending on the nature of the transition-metal ion different reaction conditions were applied. The complexes of the general structure $[M(\mathbf{L})_2](PF_6)_2$ (M = Fe, Ru, Os) were isolated after anion exchange with $NH_4PF_6$ in high yields (73–91%) and characterized by NMR spectroscopy, MALDI-TOF MS, as well as by elemental analysis. The formation of the desired complexes could be concluded from the characteristic chemical shifts of the terpyridine moiety. As shown in Figure 2, the signals of the $H^{3',5'}$-protons of the central pyridine ring are shifted from 8.77 (uncomplexed ligand L) to 9.72 ppm ($Fe^{II}$ complex), 9.50 ppm ($Ru^{II}$ complex), and 9.53 ppm ($Os^{II}$ complex), respectively.

These transition-metal ions also induce significant alterations of the photophysical properties of the systems as compared to the free ligands that were characterized

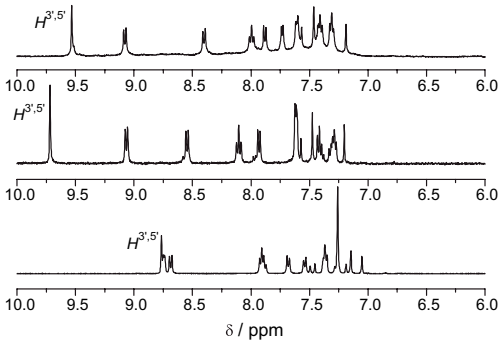


*Figure 2.* $^1$H NMR spectra (aromatic region) of terpyridine **L** (bottom, $CDCl_3$), $Fe^{II}$ complex (middle, $d_6$-acetone), and $Os^{II}$ complex (top, $d_6$-acetone). For all spectra: 400 MHz, 298 K.

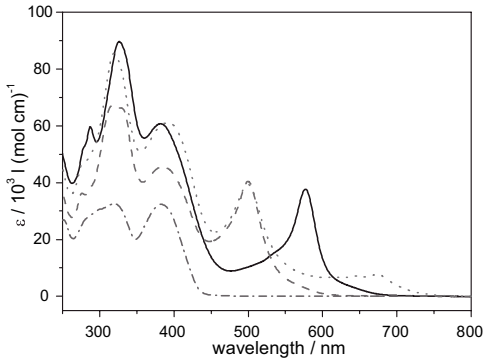


*Figure 3.* Comparison of the steady-state absorption spectra of the investigated $Fe^{II}$ (solid line), $Ru^{II}$ (dashed line), and $Os^{II}$ complexes (dotted line) with the absorption spectrum of the free ligand (dashed-dotted line).

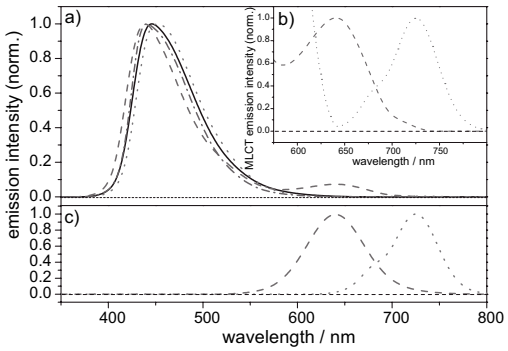


*Figure 4.* (a) Comparison of the steady-state emission spectra of the investigated $Fe^{II}$ (solid line), $Ru^{II}$ (dashed line), and $Os^{II}$ complexes (dotted line) with the one of the free ligand (dashed line) upon excitation at 330 nm. (b) Red emission bands observed for the $Ru^{II}$ (dashed line) and $Os^{II}$ complex (dotted line) upon excitation at 330 nm. (c) Emission spectra of the $Ru^{II}$ and $Os^{II}$ complex after direct excitation of the MLCT transition at 500 nm.

previously.[14] The steady-state absorption spectra complexes are shown in Figure 3. As can be seen, one dominant feature due to complexation is the appearance of new ground-state absorption band.

In either case the absorption spectrum is dominated by LC $\pi\pi^*$ transitions in the blue part (<450 nm) and a new intensive transition within the visible part of the spectrum. This new transition which can be assigned to an MLCT transition is centered at 500 nm for $Ru^{II}$, at 577 nm for $Fe^{II}$, and shows for the $Os^{II}$ complex a pronounced bi-modal structure with two maxima at 500 and 674. Furthermore, the blue shoulders of these MLCT bands correspond to vibronic fine structures and weak MC transitions[15] while the respective long-wavelength shoulders can be assigned to spin-forbidden transitions into the triplet MLCT state. The assignment was experimentally verified for the $Os^{II}$ complexes and is assumed to hold true also for the analogous complexes with $Ru^{II}$ and $Fe^{II}$ as central ions.[16]

Complexation of the free ligands not only affects the steady-state absorption spectra, but also the emission properties as can be seen in Figure 4. Figure 4a and b compare the emission spectrum of the free ligand with the luminescence spectra of the transition-metal complexes upon excitation of the $\pi\pi^*$ transition of the conjugated terpyridine ligand at 330 nm. All systems exhibit a strong emission band centered between 440 and 450 nm with a spectral shape that is consistent with its assignment to $\pi\pi^*$ fluorescence commonly observed for this class of conjugated terpyridine ligands.[5a,17] As summarized in Table 1, the fluorescence-excitation spectra for the free ligand system ($\Phi_F = 0.74$) and the weakly emitting $Fe^{II}$ complex ($\Phi_F = 0.024$) reveal that excitation within the range of 321 and 383 nm leads to the population of the same emissive state (data not shown).

The blue emission following excitation at 330 nm is observed for all systems investigated here. However, upon complexation with ruthenium(II) and osmium(II) ions, the luminescence quantum yield drops at least two orders of magnitude down to $2 \times 10^{-5}$ and $1 \times 10^{-4}$, while the spectral shape of the blue emission band remains rather unaffected by complexation. But, as can be seen in Figure 4, the $Ru^{II}$ and $Os^{II}$ complexes show additional emission bands at 640 and 725 nm, respectively. The spectral characteristics of these additional emission bands indicate that they stem from radiative relaxation of a $^3$MLCT state induced by the presence of the heavy metal ions.[9] This assignment is further corroborated by the fact, that it is possible to directly excite the $^3$MLCT transition as shown in Figure 4c. The spectroscopic features of this weak emission fit very well to those observed for the closely related 4′-toluoyl-2,2′:6′:2″-terpyridine ($\lambda_{max} = 640$ nm). This similarity can be explained by the fact that the excited-state properties,

*Table 1.* Emission quantum yields and lifetimes observed for the free ligand systems and the respective metal complexes.

| Sample | $\Phi_F$ | $\tau_F$[a)] | $\tau_P$[a)] |
|---|---|---|---|
| | | ns | ns |
| Ligand L | 0.74 | 1.59 | – |
| $[Fe(L)_2](PF_6)_2$ | 0.024 | 1.56 | – |
| $[Ru(L)_2](PF_6)_2$ | 0.00002 | 1.64 | 36.5 |
| $[Os(L)_2](PF_6)_2$ | 0.0001 | 1.61 | 136.7 |

[a)]The subscripts $\tau_F$ and $\tau_P$ denote lifetimes of the $\pi\pi^*$ fluorescence and MLCT-centered phosphorescence, respectively.


*Macromol. Rapid Commun.* **2010**, *31*, 883–888

Macromolecular Journals
DOI: 10.1002/marc.200900894

i.e., delocalization of the MLCT excitation, are exclusively dominated by the close periphery of the terpyridine unit, which is very similar in both systems.[9b,11b,18]] The dramatic difference in the emission lifetimes between these two complexes (0.95 ns for the 4′-toluoyl-2,2′:6′:2″-terpyridine complex) can be explained by the fact that delocalization of the MLCT excitation is not the only effect influencing the luminescence lifetime. If, for example, heterocyclic, electron-donating, or electron-withdrawing substituents are introduced in the 6′-position, the emission wavelength of such complexes can be tuned significantly.[11]

To the best of our knowledge, the unprecedented observation of dual luminescence from terpyridine transition-metal complexes can be mechanistically rationalized considering the following relaxation pathway. Excitation of the ligand-based $\pi\pi^*$ transition induces excited-state planarization of the entire chromophore[14] leading to a highly stabilized excited-state geometry, which causes the high emission quantum yield ($\Phi_F = 0.74$) and the long lifetime ($\tau_F = 1.59$ ns) observed for the free ligand (Table 1).[14b] Furthermore, the formation of the more planar excited-state geometry compared to the electronic ground state results in a large emission Stokes shift of the free ligand ($\Delta\nu = 1932\ cm^{-1}$), because of the significant geometry differences between excited state and ground state which itself reduce the vibronic coupling and the non-radiative decay. For some metal complexes it has been reported that such planarization motions seem to function as a gating process for internal conversion between the relaxed $\pi\pi^*$, i.e., the cooled state in its energetically most favorable geometrical configuration, and the MLCT state.[14,19] In most cases this internal conversion process is very fast and efficient and, thus, LC emission is quenched effectively and only weak phosphorescence is observed. However, for the complexes reported here, significant residual population remains in the $\pi\pi^*$ state and LC emission still occurs. A likely explanation for this behavior is the effective stabilization of the $\pi\pi^*$ excited state by photoinduced planarization, which enhances electronic delocalization in the conjugated system.

Dual luminescence has been reported for some selected bipyridine heteroleptic transition-metal complexes, in which emission occurs simultaneously from both LC and MLCT states.[20] Such unusual emission is mostly found under extreme conditions, i.e., in particular not at room temperature and in solution.[9] In addition, dual emission from different MLCT states in heteroleptic complexes was reported in literature.[10a,21] However, to the best of our knowledge the rigid electron-rich $\pi$-conjugated ligands used for complex formation in this paper constitute the first terpyridine system, which features dual luminescence. The apparent room-temperature phosphorescence of these terpyridine complexes arises most likely from the stabilization of the MLCT-excited state by electronic delocalization over the extended $\pi$-system and by an equilibrium between MLCT and LC triplet states.[11] If now an energetically stabilized MLCT state coexists with the LC excited states, dual emission occurs as it is observed in the herein investigated complexes. Such dual emission might constitute a route to new supramolecular white emitters.

Therefore, tuning the electronic coupling between the excited states to achieve a higher quantum yield for both emitting chromophores constitutes the major challenge for a synthetic strategy to this kind of supramolecular white emitters. In particular, this might be achieved by choosing a more appropriate conjugated terpyridine ligand — a class of ligands, which offers an enormous structural variety both with respect to the conjugated backbone[17a,22] and the terpyridine moiety.[23] Thereby, fine tuning of the electro-optical properties, e.g., the HOMO–LUMO bandgap, is possible and direct impact on the stability of the LC excited states can be achieved. On the other hand, the $^3$MLCT needs to be stabilized in order to obtain MLCT-quantum yields in the order of 10%, which also might be obtained by variation of the terpyridine ligand. As discussed above, highly conjugated systems are known to stabilize the $^3$MLCT by charge delocalization and by a secondary equilibrium with an LC triplet state. Additionally, direct linkage of the adjacent chromophore to the terpyridine by an ethynylspacer results in very high room-temperature lifetimes — a phenomenon which is assigned to an improved electronic coupling because of minor steric impact.[24] In general, it can be stated that the photophysical features of interest benefit from a coplanar excited-state geometry. Another factor that is expected to contribute to the design of supramolecular white emitters is an increased electronic coupling between the $^3$MLCT and an $^3$LC state, which — in turn — also depends at least in part on the torsion angle between the terpyridine moiety and the substituent.

## Conclusion

As series of new transition-metal complexes bearing a highly $\pi$-conjugated ligand system was synthesized and characterized. The systems investigated here adapt the major structural features of the most common semiconducting polymers. These complexes reveal dual luminescence — a phenomenon, which to the best of our knowledge has not been observed before for terpyridine transition-metal complexes. Such complexes can be used as molecular building blocks for the construction of electro-optically active coordination polymers or can be doped into polymer matrices for inkjet printing of OLED materials.

We suggest that the finding of dual luminescence can be rationalized on the basis of photoinduced excited-state planarization of the ligand, which strongly impacts the electronic properties and reduces the coupling to the MLCT

excited states. Furthermore, the extended π-system of the ligand stabilizes the $^3$MLCT against non-radiative decay back to the electronic ground state, an effect which is supported by the stabilizing influence of LC triplet states. As a net effect dual emission is observed from the $^3$MLCT and the $S_1$ excited state of the ligand itself. We suggest that modifications of the ligand systems will enable structural control of the electronic coupling between the relevant excited states in such complexes. Thereby, the observation of dual luminescence of terpyridine transition-metal complexes might open a new synthetic route toward supramolecular and macromolecular white emitters.

Acknowledgements: Financial support of the *Fonds der Chemischen Industrie*, the *Dutch Polymer Institute*, and the *Nederlandse Organisatie voor Wetenschappelijk Onderzoek* (VICI award for U.S.S.) is highly acknowledged.

Received: December 14, 2009; Revised: January 15, 2010; Published online: March 19, 2010; DOI: 10.1002/marc.200900894

Keywords: conjugated polymers; dual emission; luminescence; metallo-polymer complexes; spectroscopy

[1] [1a] T. A. Skotheim, J. R. Reynolds, *Conjugated Polymers – Theory, Synthesis, Properties and Characterization*, CRC Press, Boca Raton 2007; [1b] E. Tekin, D. A. M. Egbe, J. M. Kranenburg, C. Ulbricht, S. Rathgeber, E. Birckner, N. Rehmann, K. Meerholz, U. S. Schubert, *Chem. Mater.* **2008**, *20*, 2727.
[2] B. C. Thompson, J. M. J. Frechet, *Angew. Chem., Int. Ed.* **2008**, *120*, 62.
[3] K. Müllen, U. Scherf, *Organic Light Emitting Devices*, Wiley-VCH, Weinheim 2006.
[4] [4a] E. Holder, B. M. W. Langeveld, U. S. Schubert, *Adv. Mater.* **2005**, *17*, 1109; [4b] V. Marin, E. Holder, R. Hoogenboom, U. S. Schubert, *Chem. Soc. Rev.* **2007**, *36*, 618; [4c] C. Ulbricht, B. Beyer, C. Friebe, A. Winter, U. S. Schubert, *Adv. Mater.* **2009**, *21*, 4418.
[5] [5a] A. Winter, C. Friebe, M. D. Hager, U. S. Schubert, *Eur. J. Org. Chem.* **2009**, *12*, 801; [5b] A. Winter, C. Friebe, M. D. Hager, U. S. Schubert, *Macromol. Rapid Commun.* **2008**, *29*, 1679; [5c] A. Winter, D. A. M. Egbe, U. S. Schubert, *Org. Lett.* **2007**, *9*, 2345.
[6] [6a] A. C. Grimsdale, K. L. Chan, R. E. Martin, P. G. Jokisz, A. B. Holmes, *Chem. Rev.* **2009**, *109*, 897; [6b] D. A. M. Egbe, B. Carbonnier, E. Birckner, U.-W. Grummt, *Prog. Polym. Sci.* **2009**, *34*, 1023.
[7] [7a] M. Chiper, R. Hoogenboom, U. S. Schubert, *Macromol. Rapid Commun.* **2009**, *30*, 565; [7b] B. Happ, C. Friebe, A. Winter, M. D. Hager, R. Hoogenboom, U. S. Schubert, *Chem.–Asian J.* **2009**, *4*, 154.
[8] [8a] E. Tekin, P. J. Smith, U. S. Schubert, *Soft Matter* **2008**, *4*, 703; [8b] B.-J. de Gans, P. C. Duineveld, U. S. Schubert, *Adv. Mater.* **2004**, *16*, 203; [8c] E. Holder, V. Marin, M. A. R. Meier, U. S. Schubert, *Macromol. Rapid Commun.* **2004**, *25*, 1491; [8d] E. Tekin, E. Holder, V. Marin, B.-J. de Gans, U. S. Schubert, *Macromol. Rapid Commun.* **2005**, *26*, 293.
[9] [9a] A. Islam, N. Ikeda, K. Nozaki, Y. Okamoto, B. Gholamkhass, A. Yoshimura, T. Ohno, *Coord. Chem. Rev.* **1998**, *171*, 355; [9b] A. C. Benniston, G. Chapman, A. Harriman, M. Mehrabi, C. A. Sams, *Inorg. Chem.* **2004**, *43*, 4227.
[10] [10a] J. P. Sauvage, J. P. Collin, J. C. Chambron, S. Guillerez, C. Coudret, V. Balzani, F. Barigelletti, L. De Cola, L. Flamigni, *Chem. Rev.* **1994**, *94*, 993; [10b] S. Tschierlei, M. Presselt, C. Kuhnt, A. Yartsev, T. Pascher, V. Sundström, M. Karnahl, M. Schwalbe, B. Schäfer, S. Rau, M. Schmitt, B. Dietzek, J. Popp, *Chem. –Eur. J.* **2009**, *15*, 7678; [10c] M. Schwalbe, M. Karnahl, H. Görls, D. Chartrand, F. Laverdiere, G. S. Hanan, S. Tschierlei, B. Dietzek, M. Schmitt, J. Popp, J. G. Vos, S. Rau, *Dalton Trans.* **2009**, *38*, 4012; [10d] B. Dietzek, W. Kiefer, J. Blumhoff, L. Böttcher, S. Rau, D. Walther, U. Uhlemann, M. Schmitt, J. Popp, *Chem. –Eur. J.* **2006**, *12*, 5105.
[11] [11a] E. A. Medlycott, G. S. Hanan, *Chem. Soc. Rev.* **2005**, *34*, 133; [11b] E. A. Medlycott, G. S. Hanan, *Coord. Chem. Rev.* **2006**, *250*, 1763.
[12] P. Coppo, M. Duati, V. N. Kozhevnikov, J. W. Hofstraat, L. De Cola, *Angew. Chem., Int. Ed.* **2005**, *44*, 1806.
[13] G. Canard, C. Piguet, *Inorg. Chem.* **2007**, *46*, 3511.
[14] [14a] R. Siebert, D. Akimov, M. Schmitt, A. Winter, U. S. Schubert, B. Dietzek, J. Popp, *ChemPhysChem* **2009**, *10*, 910; [14b] R. Siebert, A. Winter, U. S. Schubert, B. Dietzek, J. Popp, *J. Phys. Chem. C* (submitted).
[15] [15a] R. J. H. Claerk, P. C. Turtle, D. P. Strommen, B. Streusand, J. Kincaid, K. Nakamoto, *Inorg. Chem.* **1997**, *16*, 84; [15b] W. Gawelda, A. Cannizzo, V. T. Pham, F. V. Mourik, C. Bressler, M. Chergui, *J. Am. Chem. Soc.* **2007**, *129*, 8199.
[16] [16a] D. Graff Thompson, J. R. Schoonover, C. J. Timpson, T. J. Meyer, *J. Phys. Chem. A* **2003**, *107*, 10250; [16b] X. Y. Wang, A. Guerzo, H. Tunuguntla, R. H. Schmehl, *Res. Chem. Intermed.* **2007**, *33*, 63.
[17] [17a] A. Winter, C. Friebe, M. Chiper, U. S. Schubert, M. Presselt, B. Dietzek, M. Schmitt, J. Popp, *ChemPhysChem* **2009**, *10*, 787; [17b] M. Presselt, B. Dietzek, M. Schmitt, J. Popp, A. Winter, M. Chiper, C. Friebe, U. S. Schubert, *J. Phys. Chem. C* **2008**, *112*, 18651.
[18] [18a] E. Amouyal, M. Bahout, G. Calzaferri, *J. Phys. Chem.* **1991**, *95*, 7641; [18b] A. C. Benniston, A. Harriman, P. Li, P. V. Patel, J. P. Rostron, C. A. Sams, *J. Phys. Chem. A* **2006**, *110*, 9880.
[19] [19a] P. P. Lainé, F. Bedioui, F. Loiseau, C. Chiorboli, S. Campagna, *J. Am. Chem. Soc.* **2006**, *128*, 7510; [19b] P. P. Lainé, S. Campagna, F. Loiseau, *Coord. Chem. Rev.* **2008**, *25*, 22552.
[20] [20a] G. J. Wilson, A. Launikonis, W. H. F. Sasse, A. W. H. Mau, *J. Phys. Chem. A* **1997**, *101*, 4860; [20b] D. S. Tyson, C. R. Luman, X. Zhou, F. N. Castellano, *Inorg. Chem.* **2001**, *40*, 4063; [20c] L. Song, J. Feng, X. Wang, J. Yu, Y. Hou, P. Xie, B. Zhang, J. Xiang, X. Ai, J. Zhang, *Inorg. Chem.* **2003**, *42*, 3393.
[21] [21a] T. E. Keyes, C. M. O'Connor, U. O'Dwyer, C. G. Coates, P. Callaghan, J. J. McGarvey, J. G. Vos, *J. Phys. Chem. A* **1999**, *103*, 8915; [21b] E. C. Glazer, D. Magde, Y. Tor, *J. Am. Chem. Soc.* **2007**, *129*, 8544.
[22] A. Winter, C. Friebe, M. Chiper, M. D. Hager, U. S. Schubert, *J. Polym. Sci., Part A: Polym. Chem.* **2009**, *47*, 4083.
[23] B. Schulze, C. Friebe, M. D. Hager, A. Winter, R. Hoogenboom, H. Goerls, U. S. Schubert, *Dalton Trans.* **2009**, *38*, 787.
[24] M. Hissler, A. Harriman, A. Khatyr, R. Ziessel, *Chem. –Eur. J.* **1999**, *5*, 3366.




DOI: 10.1002/marc.200900894

# [RS4] The Molecular Mechanism of Dual Emission in Terpyridine Transition Metal Complexes - Ultrafast Investigation of Photoinduced Dynamics



Reproduced with permission from:
R. Siebert, A. Winter, U. S. Schubert, B. Dietzek and J. Popp, The Molecular Mechanism of Dual Emission in Terpyridine Transition Metal Complexes - Ultrafast Investigation of Photoinduced Dynamics, *Physical Chemistry Chemical Physics*, **2011**, *13*, 1606-1617.



## Autorenschaft der Publikation

| | |
|---|---|
| Ronald Siebert | stationäre Absorptions- und Emissionsspektroskopie, zeitaufgelöste transiente Absorptionsspektroskopie, zeitaufgelöste temperaturabhängige Emissionsspektroskopie, Auswertung der Daten, Ergebnisdiskussion und Erstellung des Manuskriptes |
| Andreas Winter | Synthese und Charakterisierung der untersuchten Substanzen, Diskussion und Korrektur des Manuskripts |
| Ulrich S. Schubert | Konzept- und Ergebnisdiskussion, Diskussion und Korrektur des Manuskripts |
| Benjamin Dietzek | Projektleitung, Konzept- und Ergebnisdiskussion, Diskussion und Korrektur des Manuskripts |
| Jürgen Popp | Konzept- und Ergebnisdiskussion, Diskussion und Korrektur des Manuskripts |

PCCP

View Online
Dynamic Article Links

Cite this: *Phys. Chem. Chem. Phys.*, 2011, **13**, 1606–1617

www.rsc.org/pccp

**PAPER**

# The molecular mechanism of dual emission in terpyridine transition metal complexes—ultrafast investigations of photoinduced dynamics†

**Ronald Siebert,[a] Andreas Winter,[bcd] Ulrich S. Schubert,*[bcd] Benjamin Dietzek*[ae] and Jürgen Popp[ae]**

***Received 9th July 2010, Accepted 9th November 2010***
**DOI: 10.1039/c0cp01134g**

Temperature dependent luminescence experiments are combined with femtosecond time-resolved transient absorption spectroscopy to decipher the photoinduced excited-state relaxation pathway in mononuclear Fe, Ru and Os terpyridine complexes bearing a conjugated chromophore within the ligand framework. The herein presented complexes constitute a class of coordination compounds, which overcome the poor emission properties commonly observed for most terpyridine transition metal complexes. As reported earlier, the complexes reveal dual emission at room temperature stemming from ligand centered and metal-to-ligand charge-transfer states. The molecular mechanism of the room temperature dual luminescence is addressed experimentally in this contribution. The experimental results indicate an ultrafast branching reaction within the excited-state manifold upon photoexcitation of the ligand-centered $S_1$ state. This branching occurs from a "hot" excited state geometry close to the Franck–Condon point of absorption and within ~100 fs, *i.e.* the temporal resolution of our experimental setup. The combination of ultrafast differential absorption experiments and temperature-dependent luminescence data allows not only to draw conclusions about the molecular mechanism underlying the observed dual emission but also to construct quantitative Jablonski diagrams and, thereby, to detail the excited-state topology determining the remarkable luminescence properties of the systems at hand.

## Introduction

Conjugated polymers like poly[phenylene–vinylene], poly[phylene–ethinylene] and polythiophene play an important role in the field of organic photovoltaic (OPV) and organic light emitting devices (OLEDs).[1] This is due to their excellent film forming properties and the high potential for device design by deposition of layers with defined composition and thickness. In such polymers the photophysics, *e.g.* formation and dissociation, diffusion and recombination of charge carriers, is dominated by the singlet character of the excitons.[2] Therefore, a relatively short lifetime and diffusion length seem to limit the efficiency of solar cells based on such polymers. Recently, it could be shown that coordination polymers derived from heavy transition metal ions like platinum and palladium revealed a high photovoltaic performance, which was assigned to the formation of triplet excitons and, consequently, an enhanced exciton lifetime and diffusion length.[3–5] Beside the reported palladium and platinum polymers, which generally consists of different heterocyclic chromophores connected by direct carbon metal bonds, another class of semiconducting polymers with a high potential for photovoltaic applications is available—conjugated bis-terpyridine systems. Here the organic subunits are coordinatively connected by various transition metal ions. Hence, in such systems the choice of the metal ion strongly impacts the photophysical properties: while the use of $Zn^{2+}$ ions yields highly fluorescent polymers,[6–8] respective polymers containing $Fe^{2+}$, $Ru^{2+}$ and $Os^{2+}$ ions show strong contributions of metal-to-ligand charge-transfer (MLCT) excited-states and, therefore, reduced fluorescence quantum yields.[9–11] However, the appearance of MLCT excited-states can be utilized for light-induced generation of charge carriers, *e.g.* in photovoltaic devices.[12] Therefore, the large structural variety of coordination polymers, derived from conjugated bis-terpyridines and group 6 transition metal ions, opens a doorway to a new class of photoresponsive materials.[13–15]

[a] *Institute for Physical Chemistry, Friedrich-Schiller-University Jena, Helmholtzweg 4, 07743 Jena, Germany. E-mail: benjamin.dietzek@uni-jena.de; Fax: +49 3641 206399*
[b] *Laboratory of Macromolecular Chemistry and Nanoscience, Eindhoven University of Technology, P.O. Box 513, 5600 MB Eindhoven, The Netherlands*
[c] *Dutch Polymer Institute (DPI), P.O. Box 902, 5600 AX Eindhoven, The Netherlands*
[d] *Laboratory of Organic and Macromolecular Chemistry, Friedrich-Schiller-University Jena, Humboldtstr. 10, 07743 Jena, Germany*
[e] *Institute for Photonic Technology (IPHT) Jena, Albert-Einstein-Str. 9, 07745 Jena, Germany*

† Electronic supplementary information (ESI) available: Temperature-dependent phosphorescence lifetimes in comparison with data from model systems, quantitative Jablonski schemata for **Os** and **Fe**, differential absorption kinetics for **Fe**, and general information regarding handling of transient-absorption data. See DOI: 10.1039/c0cp01134g

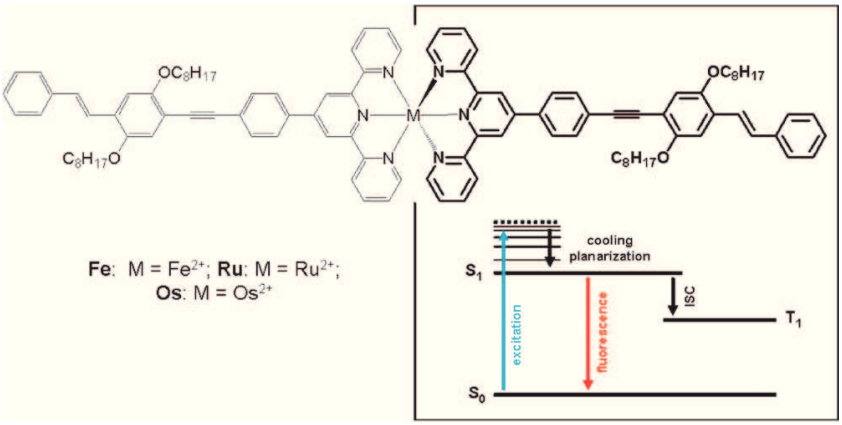


**Fig. 1** Schematic representation of the molecular structure of the complexes investigated together with an illustration of the ultrafast processes occurring upon photoexcitation of the free ligand.

The approach followed in our own research is to utilize bis-terpyridines as bridging ligands bearing a chromophore, which is related to the most common poly[phenylene–vinylene], poly[phylene–ethinylene] derivatives. These systems combine the promising photophysical properties of their chromophores with the chelating properties of the terpyridine sphere. Together with several transition metals they can easily form coordination polymers.[16,17] This contribution focuses on a number of coordination compounds, derived from 4′-(4-{[2,5-bis(octyloxy)-4-styrylphenyl]ethynyl}phenyl)-2,2′:6′,2″-terpyridine and the transition metal iron, ruthenium and osmium. These complexes, the structures of which are depicted in Fig. 1, constitute the smallest, periodically repeating unit of a coordination polymer based on 1,4-bis(4-{[4-(2,2′:6′,2″-terpyridin-4′-yl)phenyl]ethynyl}-2,5-bis(octyloxy)styryl)benzene. The spectroscopic properties of the ligand system itself were the topic of detailed previous studies.[18,19] These studies revealed an excited-state planarization as an important relaxation process, leading from the Franck–Condon point into a highly stabilized and bright excited state. This planarization represents a barrierless motion as substantiated by the viscosity dependence of the ultrafast process. Furthermore, intersystem crossing from the $S_1$ state to a long-lived non-emissive triplet state quenches the fluorescence (see Fig. 1).

This contribution reveals photoinduced excited-state dynamics, which is induced by complexation of the ligand with transition metal ions. The photophysical properties are investigated by the application of various spectroscopic techniques such as transient absorption and time-correlated single-photon-counting.

## Results and discussion

### Steady-state absorption and emission spectroscopy

The steady-state absorption and emission spectra of the $Fe^{2+}$, $Ru^{2+}$ and $Os^{2+}$ complexes (abbreviated as **Fe**, **Ru** and **Os**, respectively) investigated here are shown in Fig. 2. For

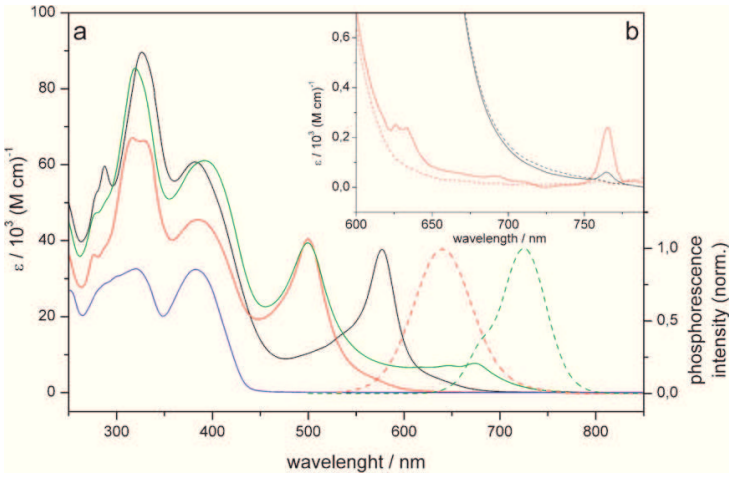


**Fig. 2** (a) UV/Vis absorption spectra (solid lines) of **Fe** (black), **Ru** (red), **Os** (green) as well as of the uncomplexed ligand (blue) compared to the phosphorescence spectra after excitation at 500 nm (dashed line) for the complexes **Ru** (red) and **Os** (green). (b) Absorption spectra under 200 bar oxygen pressure (solid line) and after oxygen release (dashed line) for **Fe** (black) and **Ru** (red), respectively.

comparison the absorption spectrum of the uncoordinated tpy-ligand is included in the figure.

**Absorption spectroscopy.** The absorption spectra of the complexes show qualitatively identical bandshapes in the blue part of the spectrum between 280 and 450 nm also agreeing with the absorption spectrum of the uncomplexed ligand (see Fig. 2). Thus, the transitions in this spectral range ($\lambda < 450$ nm) are assigned to π–π* transitions located on the conjugated chromophore of the ligand.[18,20] The electronic properties of this part of the ligand are rather unaffected by the complexation as can be judged by a comparison of the emission–excitation spectra of the free and complexed ligand.[21] In the metal complexes the ligand centered transitions have a higher molar extinction coefficient than in the free form. These changes in intensity cannot solely be ascribed to the fact that two ligands are coordinated to the respective metal ion, because even for **Ru**, bearing the most intense π–π* transitions, these transitions do not show twice the oscillator strength of the free ligand. However, such behavior has been observed before and was attributed to the polarizing effect of the transition dipole moment of one chromophore on the electron density of the second chromophore. By this an additional dipole moment with opposite sign is induced causing a reduced net dipole moment.[17]

Besides an altered intensity pattern of the ligand-centered transitions, complexation induces additional electronic transitions in the visible part of the absorption spectra with maxima at 577 (**Fe**), 500 (**Ru**) and 496 nm (**Os**). These transitions are assigned to transitions to the $^1$MLCT excited-state and the long and short wavelength shoulders are caused by the vibronic finestructure. In the case of **Os** an additional pronounced long wavelength absorption can be observed at 674 nm, which stems from direct excitation of a $^3$MLCT state. In general, such excitations are spin-forbidden but this selection rule is efficiently relaxed for **Os** because of effective spin–orbit coupling induced by the heavy metal ion.[22] The direct excitation of the dd states is symmetry forbidden and therefore overwhelmed by the much more intense (allowed) π–π* and $^1$MLCT transitions.

**Oxygen perturbation spectroscopy.** In the case of **Ru** the spin-forbidden transitions involving the $^3$MLCT excited state, which are invisible under ambient conditions, can be visualized under high oxygen pressure (200 bar) because of the magnetic perturbation of the singlet–triplet transition in the presence of a paramagnetic gas.[23] Fig. 2b compares steady-state absorption data for **Ru** and **Fe** recorded under high oxygen pressure. By applying such extreme conditions a set of new transitions appears at 626, 633 and 765 nm (**Ru**) and 764 nm (**Fe**), respectively, which are invisible under ambient conditions. The extinction coefficients of these $^3$MLCT transitions amount to roughly 0.5% of the $^1$MLCT transitions under 200 bar oxygen pressure, *i.e.* their transition dipole moment is still rather low even under such drastic conditions. Therefore, direct excitation to the $^3$MLCT excited states in **Ru** appears only as the shoulder at 626 and 633 nm, respectively. In the case of **Fe** such a transition cannot be observed even under high oxygen pressure, because iron represents the lightest transition metal. Based on these considerations it can be ruled out that the long-wavelength shoulder, observed for the MLCT absorption for **Fe** and **Ru** under ambient conditions, is due to a direct $^3$MLCT transition. Furthermore, in both spectra another transition is induced by magnetic perturbation at roughly 765 nm, which can be assigned to direct excitation of the ligand-centred $T_1$ state. This assignment is supported by comparison of the spectra with the experimental data of conjugated polymers bearing the same or a similar chromophore.[24,25] In the free ligand this state has a pure $T_1$ character, which is reflected by its influence on the excited-state dynamics of the free ligand.[18,19] As this state is non-luminescent even at 77 K, its lifetime is estimated to be in the range of about 20 to 200 μs, which are typical values for corresponding conjugated polymers.[24,25]

**Steady-state emission spectroscopy.** After excitation of the aforementioned transitions all three complexes show emission at room temperature, *i.e.* independent on the nature of the excited transition. However, it is necessary to distinguish between fluorescence and phosphorescence, because as a function of the excitation wavelength only a single or both processes are observed.[21] **Ru** and **Os** show very weak phosphorescence at room temperature after excitation of the $^1$MLCT state at 500 nm, while **Fe** is non-phosphorescent. The phosphorescence maxima are found at 640 (**Ru**) and 725 nm (**Os**), which—aside from the oxygen-induced absorption bands—also contain information about the energetic position of these excited states. Here, the maximum of the short wavelength shoulder represents the energetic position of the luminescent excited state. Comparing the data from steady-state absorption and emission spectroscopy it is possible to calculate the energetic position of the singlet and triplet excited-states, which, in turn, determine the shape of the spectra shown in Fig. 2. The results of such estimations are summarized in Table 1.

### Time-dependent and temperature-dependent emission spectroscopy

Previously it could be shown that **Ru** and **Os** reveal dual emission upon excitation of the π–π* transition.[21] As a possible explanation for this behavior, branching between two deactivation channels from a hot excited-state has been invoked. This feature requires excitation transfer between the initially π–π* excited state of the conjugated chromophore, which is fluorescent, and a phosphorescent $^3$MLCT state to occur. While the fluorescence is centered at roughly 450 nm the

**Table 1** Comparison of the position of the energy levels of the excited-states contributing to the UV/Vis absorption and emission spectra as obtained from the absorption and emission spectra (italic), respectively[a]

| Sample | $E_{S1}$/eV ($10^3$ cm$^{-1}$) | $E_{T1}$/eV ($10^3$ cm$^{-1}$) | $\Delta E_{S1T1}$/eV ($10^3$ cm$^{-1}$) |
|---|---|---|---|
| **L** | 3.05; *2.8* (24.6; *22.6*) | 1.62 (13.1) | 1.18 (9.5) |
| **Fe** | 1.86 (15.0) | — | — |
| **Ru** | 2.09 (16.9) | 1.96; *1.94* (15.8; *15.6*) | 0.14 (1.1) |
| **Os** | 2.09 (16.9) | 1.84; *1.83* (14.8; *14.8*) | 0.26 (2.1) |

[a] The values for the free ligand refer to the $S_0 \rightarrow S_1$ transition, while the ones for **Fe**, **Ru** and **Os** are due to the $^1$MLCT transition.

 

phosphorescence of **Ru** and **Os** is strongly redshifted to 640 (**Ru**) and 725 nm (**Os**). This spectral separation between these two radiative transitions makes it easy to observe and measure both processes separately. To obtain more detailed information about the excited-state topology, temperature-dependent emission experiments are performed. Aside from the aforementioned excited-state branching, which is proposed to result in the observed dual emission, other non-radiative deactivation channels seem to be present in the excited-state dynamics in **Fe**, **Ru** and **Os** as will be detailed in the following.

For the free ligand it could be shown that IC and ISC are the dominant non-radiative deactivation pathways, quenching the luminescent excited state and repopulating the ground state.[19] In the ligand IC involves a barrier of 0.34 eV. This huge barrier is attributed to a significant difference between excited-state and ground-state geometries: the fluorescent excited state is characterized by a planar excited-state geometry as opposed to the distorted ground state, where the terpyridine moiety is tilted by $\sim 35^{\circ}$ out of the plane of the conjugated side chain.[19,26,27]

To estimate the barrier height in the activation of such a non-radiative process in the complexed ligands, temperature-dependent fluorescence lifetime measurements are performed on **Fe**, **Ru** and **Os**. From the fluorescence experiments it is possible to estimate the impact of complexation on the photophysical properties of the ligand, *i.e.* to decipher if the planar and stable fluorescent $S_1$ excited state is affected by non-radiative deactivation channels. For **Ru** and **Os** additional temperature-dependent phosphorescence measurements were carried out, which provide conceptually identical information on the phosphorescent $^3$MLCT excited state. In particular, the barrier for non-radiative decay of the $^3$MLCT is of importance, because the lifetime of this charge-separated excited state is of great interest with respect to potential applications of the complexes in organic photovoltaic devices.[3–5] The results of the emission experiments are summarized in Fig. 3.

**Time-dependent and temperature-dependent fluorescence spectroscopy.** Fig. 3a shows the evolution of the fluorescence lifetime as a function of temperature in the range between 295 and 165 K for **Ru**, **Os**, **Fe** and the free ligand. All four sets of experimental data exhibit a temperature dependence characterized by an increase of the fluorescence lifetime up to 180 K followed by a decrease. The fluorescence-lifetime increase with decreasing temperature is due to freezing IC by minimizing vibrational energy in the excited state.[28] This behavior is similar for the free ligand as well as the complexes, because the influence of complexation on the conjugated chromophore of the ligand is quite low and the fluorescent state is associated with the $S_1$ state of the chromophore. The decrease in lifetime below 180 K can be explained by arresting the excited molecules in a "hot" excited-state geometry close to the Franck–Condon point (FC), which is prone to decay non-radiatively. Relaxation from the "hot" geometry at the FC point into the planar excited-state represents a barrierless process but the increasing viscosity near the friction point of the solvent (165 K) impacts, *e.g.* solvation and planarization.[29] This is a possible explanation for the decay of the fluorescence lifetime in this region. Characteristic values of the data discussed as well as the calculated activation barriers for non-radiative decay, obtained by fitting an Arrhenius expression (eqn (1)) to the data are summarized in Table 2.

$$\tau(T) = \left[\frac{1}{\sum k + A\exp(-\Delta E/k_{\mathrm{B}}T)}\right] \qquad (1)$$

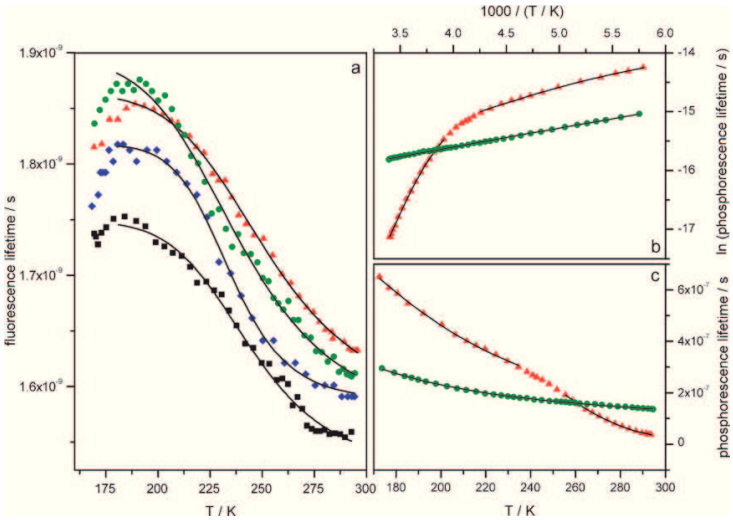


**Fig. 3** (a) Comparison of temperature dependent fluorescence lifetimes of the free ligand (blue diamonds) and the complexed ligand as part of **Fe** (black squares), **Ru** (red triangles) and **Os** (green circles). Black lines represent results of nonlinear fits according to eqn (1). (b and c) Temperature dependent phosphorescence lifetime of **Ru** (red triangles) and **Os** (green circles) on a logarithmic scale (b) and on a linear scale (c). For both sets of experiments a 435 nm laser beam was used for excitation. In the case of **Ru** and **Os** a set of short- and longpass filters was employed to separate the phosphorescence (620 nm longpass filter) from the fluorescence (440 nm longpass filter in combination with a 500 nm shortpass filter) and *vice versa*.

**Table 2** Summary of the fluorescence lifetimes of **L**, **Fe**, **Ru** and **Os** at low and high temperatures and the barriers for IC fitted to the temperature dependence of the fluorescence lifetimes

| Sample | $\tau_{300\ K}$/ns | $\tau_{180\ K}$/ns | $\Delta E$/eV ($cm^{-1}$) |
|---|---|---|---|
| **L**[19] | 1.59 | 1.81 | 0.34 (2800) |
| **Fe** | 1.56 | 1.74 | 0.26 (2100) |
| **Ru** | 1.64 | 1.84 | 0.22 (1800) |
| **Os** | 1.61 | 1.87 | 0.20 (1700) |

Eqn (1) reflects the dependence of the emission lifetime ($\tau$) from the temperature ($T$). $\sum k$ is the sum over all radiative and non-radiative rate constants, which do not involve an activation barrier, $A$ is a pre-exponential factor, $\Delta E$ represents the activation energy for the non-radiative decay, and $k_B$ is the Boltzmann constant.

Table 2 depicts the fluorescence lifetime at room temperature (300 K) and near the friction point of the solvent (180 K). Furthermore, Table 2 gives the calculated barrier heights for the non-radiative decay.

The very similar fluorescence lifetimes of all four samples (see Table 2) are due to the minor influence of complexation with transition metals on the structurally relaxed, *i.e.* the planarised $S_1$ excited-state. However, the fluorescence quantum yield of the complexed ligand is orders of magnitude lower compared to $\Phi$ of the free ligand. This is ascribed to efficient deactivation of the photoexcited $S_1$ state by $S_1 \rightarrow {}^1$MLCT IC from a "hot" excited-state geometry close to the FC followed by ultrafast $^1$MLCT $\rightarrow {}^3$MLCT ISC. Upon excitation of $S_1$ the $^3$MLCT states are thereby populated with an efficiency of roughly 90%. This value is estimated from the difference in fluorescence quantum yields comparing the free ligand ($\Phi$ = 0.74) with the complexed one ($\Phi$ = 0.024–0.00002).[21] This estimation assumes a subsequent $^1$MLCT $\rightarrow {}^3$MLCT intersystem crossing (ISC) with an efficiency of 100%—as typically observed for ruthenium polypyridyl complexes.[30,31] Thereby only a small fraction of the molecules photoexcited to the $\pi\pi^*$ state remain on the $S_1$ part of the potential surface (some % in the case of **Fe**, some ‰ in the case of **Ru** and **Os**) which can be detected by emission spectroscopy.[21]

If IC occurred from the relaxed $S_1$ excited-state, *i.e.* if the emissive singlet-state would be significantly quenched non-radiatively, the fluorescence lifetime (and not only the fluorescence quantum yields) of the complexes should be lowered compared to the free ligand. The by ~0.1 eV lower barrier for IC in the complexed ligand compared to the free one (see Table 2) is attributed to the reduction of the angle between the terpyridine sphere and the adjacent conjugated rest upon complexation, which minimizes the geometry differences between $S_1$ and $S_0$.[26]

**Time-dependent and temperature-dependent phosphorescence spectroscopy.** While the temperature-dependent fluorescence experiments help to decipher non-radiative pathways leading to a decay of the ligand centred $S_1$ excited state, phosphorescence measurements are used to detail the decay characteristics of the phosphorescent $^3$MLCT states in **Ru** and **Os**. Fig. 3b and c depict the phosphorescence lifetimes of **Ru** and **Os** as a function of temperature. Similar to the analysis of the fluorescence data an Arrhenius expression, fitted to the experimental data, yields the height of the barriers corresponding to non-radiative deactivation processes.[32–34] Characteristic values obtained from the fit are summarized in Table 3, which contains the phosphorescence lifetimes at room temperature (300 K) and near the friction point of the solvent (180 K) for the two phosphorescent complexes **Ru** and **Os** as well as for analogous 2,2′:6′,2″-terpyridine reference complexes. In addition the barrier heights, determining the excited-state lifetime of the $^3$MLCT, *i.e.* $\Delta E_A$ and $\Delta E_B$, are given.

**Table 3** Summary of the phosphorescence lifetimes of **Ru** and **Os** at low and high temperatures as well as the calculated barriers for IC between the $^3$MLCT and $^{HS}$d–d excited-state. Furthermore, the data for the corresponding bis-terpyridine complexes, taken from ref. 34 and 33, are given for comparison

| Sample | $\tau_{300\ K}$/ns | $\tau_{180\ K}$/ns | $\Delta E_A$/eV ($cm^{-1}$) | $\Delta E_B$/eV ($cm^{-1}$) |
|---|---|---|---|---|
| **Ru** | 36.5 | 585 | 0.07 (600) | 0.4 (3200) |
| **Os** | 136 | 279 | 0.03 (240) | — |
| **$[Ru(tpy)_2]^{2+}$** | — | 48 | 0.07 (560) | 0.21 (1700) |
| **$[Os(tpy)_2]^{2+}$** | 270 | — | 0.08 (640) | 0.43 (3500) |

**Ru based phosphorescence.** The data for **Ru** show a biexponential increase of the phosphorescence lifetime from 36.5 to 650 ns in the range between 295 and 165 K. In general this can be ascribed to freezing two distinct non-radiative deactivation pathways. These processes involve a barrier and are consequently hindered by reducing the temperature. The higher room temperature phosphorescence lifetime of **Ru** compared to its unsubstituted analogue $[Ru(tpy)_2]^{2+}$ [34] is due to stabilization of the $^3$MLCT by partial delocalization of the excited-state over parts of the conjugated chromophore attached to the terpyridine moiety. Furthermore, the formation of an equilibrium between the $^3$MLCT and other triplet states present stabilizes the $^3$MLCT and contributes to the prolonged luminescence.[35] Both effects have been considered in the literature and are known to have the observed effect on the phosphorescence lifetime of ruthenium terpyridine complexes.[35,36] Furthermore, the data summarized in Table 3 reveal an increased phosphorescence lifetime upon decreasing the temperature, a common feature for ruthenium and osmium polypyridyl complexes. Here, data analysis reflects two activated processes, which impact the luminescence properties of **Ru**. In accordance with the literature one process occurs over a low barrier ($\Delta E_A$) while the other one involves a significantly higher barrier ($\Delta E_B$).[37–39] The increase in lifetime with decreasing temperature is a result of the IC between the $^3$MLCT and the $^{HS}$d–d excited-state, which is suppressed in a cooled environment because of its high activation energy ($\Delta E_B$ = 0.4 eV). This barrier is almost twice as high as in **$[Ru(tpy)_2]^{2+}$** what is attributed to the effective stabilization of the $^3$MLCT excited-state by the herein presented ligand. Furthermore, a second thermally activated process becomes apparent at low temperatures, which involves only a reduced barrier ($\Delta E_A$ = 0.07 eV). This process is also detectable for **$[Ru(tpy)_2]^{2+}$** where it is found to occur across a similar barrier than in **Ru**.[34] This process is assigned to IC into a higher lying MLCT excited-state.[33–39] This excited-state is

 

assumed to be also a $^3$MLCT, however, with an increased singlet character, which favors rapid IC to the $^{HS}$d–d excited-states and represents therefore an additional deactivation pathway of the phosphorescent $^3$MLCT.

**Os based phosphorescence.** The results obtained for **Os** are different to those of **Ru**, as here a single activated process seems to determine the luminescence properties ($\Delta E_A$ = 0.03 eV). This process is also to be found for **[Os(tpy)$_2$]$^{2+}$**, but its activation energy is higher in the latter complex. In analogy to **Ru** we assign this process to IC between the phosphorescent $^3$MLCT and a higher lying MLCT excited state. The absence of the second activated process, *i.e.* $^3$MLCT → $^{HS}$d–d IC, can be explained by the effective stabilization of the $^3$MLCT and the consequently increased energy gap between these two states. The lack of influence of the $^{HS}$d–d excited state on the luminescence properties resembles the photophysics of osmium(II) tris-bipyridine complexes and related systems, for which such a result has been reported.[37] However, for **[Os(tpy)$_2$]$^{2+}$** the effect of the $^{HS}$d–d state has been reported.[33] Because of the distorted octahedral geometry typically observed for terpyridine complexes the $^{HS}$d–d excited state is lower in energy and, hence, accessible from the phosphorescent $^3$MLCT. For **Os** the effective stabilization of the $^3$MLCT compensates this effect and causes the absence of this deactivation channel. However, the room temperature lifetime of **Os** (136 ns) is lower than in **[Os(tpy)$_2$]$^{2+}$** (270 ns) due to a reduced barrier between the $^3$MLCT and higher lying MLCT states, which are prone to decay non-radiatively. The underlying assumption that the extended chromophore at the 4′-position of the terpyridine causes the decreased barrier between these two excited states is inline with work by Alemán *et al.*, who obtained lifetimes of about roughly 220 ns for osmium complexes with an adjacent chromophore of intermediate length (see ESI†).[40]

**Nature of triplet states responsible for the temperature-dependent phosphorescence properties.** In **Ru** and **Os** phosphorescent $^3$MLCT excited-states contribute to the emission spectra. These metal-induced states are highly stabilized by delocalization over the extended ligand and formation of an equilibrium with another triplet excited state. This point raises the question if the ligand-centered triplet state, which is discussed to prolong the phosphorescence lifetime, is the same state that is apparent in steady-state absorption spectroscopy ($T_1$). In this case the equilibrium between the phosphorescent state and the secondary triplet state at room temperature would be suppressed by the large energy gap of 0.33 (**Ru**) and 0.22 eV (**Os**) as deduced from the oxygen-perturbation spectra (Fig. 2, Table 1). In such a situation, back transfer from the $T_1$ into the $^3$MLCT excited state would be suppressed due to the large energetic difference or—at least—a significant temperature dependence of this effect should be visible. However, this contradicts the experimental results, which show that only a lifetime increase is observed with decreasing temperature. Nevertheless, the comparison of the luminescence lifetimes of **Ru** and **[Ru(tpy)$_2$]$^{2+}$** points to the stabilizing net effect of the secondary triplet-state, because of the relatively long (36.5 ns) room temperature luminescence lifetime of **Ru** compared to the non-luminescent **[Ru(tpy)$_2$]$^{2+}$** complex. In the complexes presented here, one might speculate that the presence of heavy metal ions perturbs the ligand excited-state potential surface and induces a ligand-centred triplet-state with pronounced charge transfer-character ($^3$LCCT).[41–43] This excited-state could have a more appropriate energy to be in a thermal equilibrium with the $^3$MLCT excited-state than $T_1$ even at very low temperatures. A further indication in favour of this assumption stems from the comparison of the lifetimes of **Ru** and **[Ru(tpy)$_2$]$^{2+}$** at around 100 K. At this temperature the lifetime of the **[Ru(tpy)$_2$]$^{2+}$** model system is much longer than the one of **Ru** as can be estimated from the temperature dependences observed experimentally (see ESI†). As already mentioned above, the experimentally observed lifetime is a weighted average of both $^3$LCCT and $^3$MLCT decays for **Ru**, while it is the pure $^3$MLCT lifetime for **[Ru(tpy)$_2$]$^{2+}$**. If additionally the $T_1$ would be in equilibrium with the $^3$MLCT the lifetime of **Ru** should be orders of magnitude longer, because most molecules would rest in this low lying excited state, the lifetime of which can be estimated to be approximately 100 μs.[24,25] As this contradicts the experimental findings it might be more plausible to assume a $^3$LCCT with a similar energy and lifetime being in thermal equilibrium with the $^3$MLCT state. At the same time $^3$MLCT → $^{HS}$d–d IC requires a large activation energy and is consequently strongly suppressed for **Ru** and completely absent for **Os**.

**Molecular origin of dual emission—decay of luminescent states.** Having discussed the luminescence lifetime data, we shall now turn our attention to argue on the molecular origin of dual room-temperature luminescence in the herein presented metal complexes, which stems from an effective IC from a "hot" geometry close to the FC between the initially photoexcited $S_1$ and the $^1$MLCT states. This interpretation is corroborated by the ligand-centred fluorescence, the spectral shape, lifetime and temperature dependence of which are almost unaffected by complexation. If the branching in the excited state occurred from the relaxed $S_1$ state, *i.e.* the fluorescent state was quenched by interconversion into the MLCT moiety, one would expect significant alterations of the fluorescence lifetime upon complexation, which is not observed.

### Femtosecond transient absorption spectroscopy

While temperature-resolved TCSPC measurements help to understand the energetics of radiative and non-radiative deactivation of long-lived luminescent states, femtosecond time-resolved measurements unravel the relaxation pathway from the FC to these states. Therefore, all three metal complexes were investigated by transient absorption spectroscopy following photoexcitation of the ligand centred $S_0$ → $S_1$ transition (at 400 nm) and the $^1$MLCT transition (at 575 nm for **Fe** and at 525 nm for **Ru** and **Os**). The excitation of the ππ* excited states is assumed to be followed by branching of the excited state between two different relaxation pathways causing the dual emission upon excitation of the ππ* state. On the other hand, excitation in the red part of the spectra directly populates MLCT excited

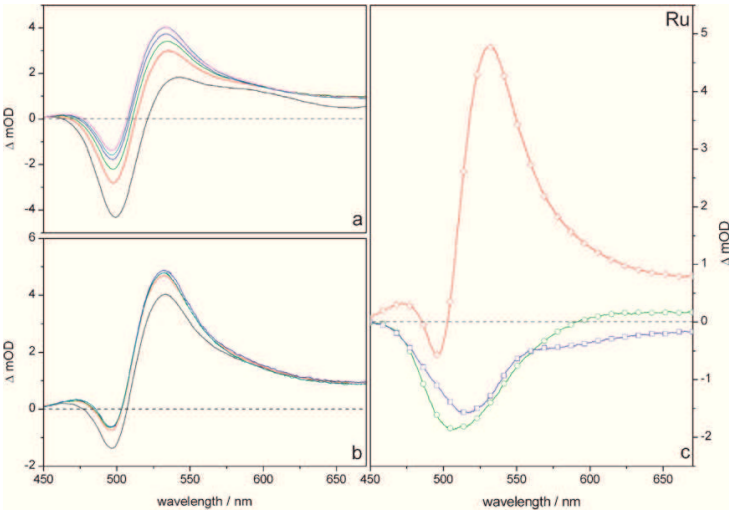


**Fig. 4** Transient absorption spectra for **Ru** dissolved in THF after excitation at 400 nm. Panel a compares transient spectra between 0 and 10 ps after excitation (0.1 ps black; 1.0 ps red; 2.5 ps green; 5.0 ps blue; 7.5 ps cyan and 10.0 ps magenta) while panels b shows transient spectra between 10 and 1000 ps (10 ps black; 50 ps red; 100 ps green; 500 ps blue; 1000 ps cyan). Panel c depicts the respective decay associated spectra for the multi-exponential decay with approx. 2–6 ps (green circles), 20–25 ps (blue squares) and a long lived nanosecond component‡ (red diamonds).

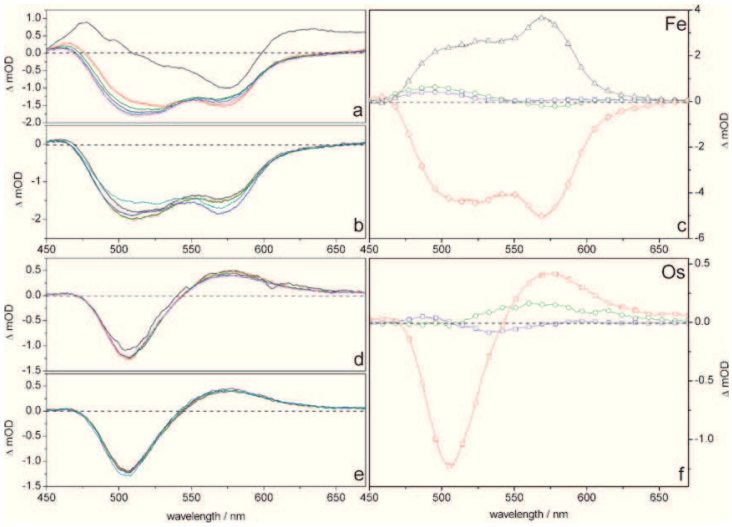


**Fig. 5** Transient absorption spectra for **Fe** (a–c) and **Os** (d–f) dissolved in THF after excitation at 400 nm. Panels a and d compare transient spectra between 0 and 10 ps after excitation (0.1 ps black; 1.0 ps red; 2.5 ps green; 5.0 ps blue; 7.5 ps cyan and 10.0 ps magenta) while panels b and e show transient spectra between 10 and 1000 ps (10 ps black; 50 ps red; 100 ps green; 500 ps blue; 1000 ps cyan). Panels c and f depict the respective decay associated spectra for the multi-exponential decay with 2–6 ps (green circles), 20–25 ps (blue squares), 700 ps (black triangles) and a long lived nanosecond component‡ (red diamonds).

states, which represent one of the two deactivation channels accessible upon blue excitation. Comparing results obtained from experiments at different excitation wavelengths is therefore helpful to investigate the branching process close to the FC point. The results of such measurements, *i.e.* the transient absorption spectra at different delay times and the decay associated spectra (DAS), obtained by global fitting, are summarized in Figs. 4 to 7.

**Excitation of the ππ*-transition at 400 nm.** Fig. 4a and b depicts transient-absorption spectra for **Ru** at different delay

‡ Due to the limited delay-time range accessible in our experimental arrangement, a precise estimate of this time-constant based on transient-absorption data is not possible. However, the results from time-resolved emission experiments allow us to provide more precise estimates (see ref. 28).

 

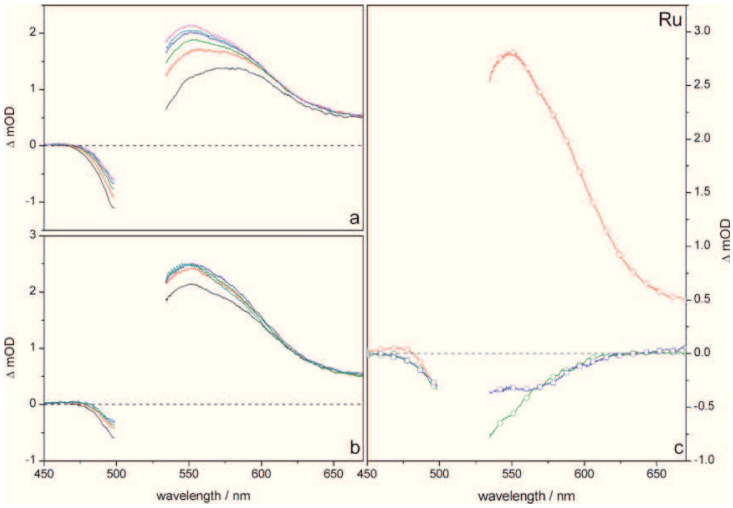


**Fig. 6** Transient absorption spectra for **Ru** dissolved in THF after excitation at 525 nm. Panel a compares transient spectra between 0 and 10 ps after excitation (0.1 ps black; 1.0 ps red; 2.5 ps green; 5.0 ps blue; 7.5 ps cyan and 10.0 ps magenta) while panels b shows transient spectra between 10 and 1000 ps (10 ps black; 50 ps red; 100 ps green; 500 ps blue; 1000 ps cyan). Panel c depicts the respective decay associated spectra for the multi-exponential decay with approx. 2–6 ps (green circles), 20–25 ps (blue squares) and a long lived nanosecond component‡ (red diamonds).

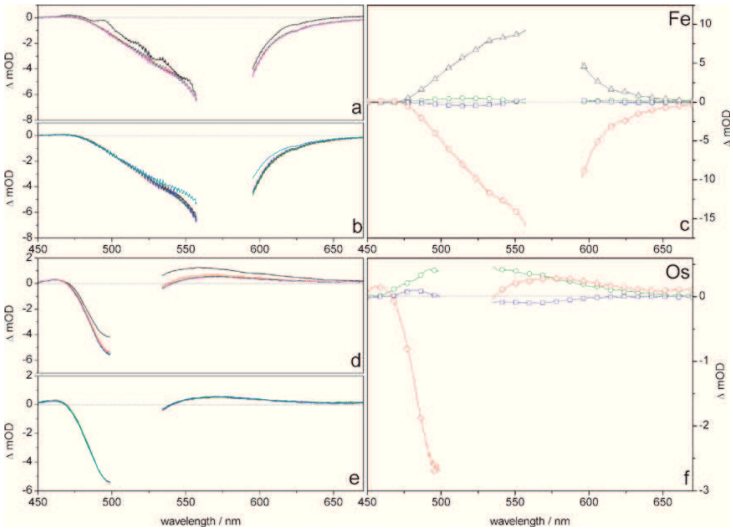


**Fig. 7** Transient absorption spectra for **Fe** (a–c) and **Os** (d–f) dissolved in THF after excitation at 575 nm (**Fe**) and 525 nm (**Os**). Panels a and d compare transient spectra between 0 and 10 ps after excitation (0.1 ps black; 1.0 ps red; 2.5 ps green; 5.0 ps blue; 7.5 ps cyan and 10.0 ps magenta) while panels b and e show transient spectra between 10 and 1000 ps (10 ps black; 50 ps red; 100 ps green; 500 ps blue; 1000 ps cyan). Panels c and f depict the respective decay associated spectra for the multi-exponential decay with 2–6 ps (green circles), 20–25 ps (blue squares), 700 ps (black triangles) and a long lived nanosecond component‡ (red diamonds).

times and Fig. 4c shows the respective DAS. Here the transient spectra are dominated by positive values from 510 nm to longer wavelength with a maximum at 530 nm, while negative contributions with a minimum at 500 nm are revealed. In the blue part of the spectra towards 450 nm a weak positive differential absorption band is discernible. Between 600 and 500 nm the signal increases during the first 10 ps accompanied by a decrease below 500 nm with apparently the same temporal dependence. Furthermore, the dominant positive band undergoes a blueshift on the same timescale. Afterwards the signal remains nearly unchanged up to long delay times with positive bands at roughly 475 and 530 nm and a negative differential absorption feature at 500 nm. The global fitting analysis reveals three kinetic components. The first one is characterized by 2-ps time constant and causes a rise (decay) of the signal below (above) 580 nm. The second component

corresponds to a 20–25 ps process and causes an overall rise of the signal with a maximum at 510 nm. The third DAS reflects the long-lived differential absorption signal with positive contributions above 500 nm and below 480 nm and the residual ground-state bleach visible at 490 nm.

In the case of **Os** a similar behavior can be observed (Fig. 5): a 2 ps component decreases the signal in the spectral range above 500 nm. This decrease is followed by a 20–25 ps component causing a decay (rise) of the signal below (above) 500 nm. In contrast to **Ru** no blueshift of the positive differential absorption band is observed for **Os** associated with $\tau_2$. The infinite component reveals a negative (positive) differential absorption band at 505 (575) nm.

For **Fe**, the transient absorption spectrum is dominated by a broad negative band spanning almost the entire spectral observation window (Fig. 5). Only at the blue (approx. 450–480 nm) and red edges (approx. 640–680 nm) of the probe spectrum, positive differential absorption changes are recorded. During the first 10 ps after photoexcitation the signal rises at around 510 nm and decays at around 575 nm. This process is followed by a rise at around 500–575 nm during the next few hundred picoseconds. Finally, an overall slow decay of the signal is observed, which extends over the experimentally accessible delay time window. Fig. 5c depicts the DAS representing the four processes determining the spectral–temporal evolution of the signal: a 6 ps component can be identified to cause the fast rise (decay) of the signal in the blue (red) part of the spectrum. Furthermore a 20–25 ps component is responsible for the additional increase in intensity with the strongest contributions around 500 nm. Subsequently, the signal evolution is determined by another rise component, which is characterized by a 600 ps time constant. Finally an overall decay on a several nanosecond timescale is observed. The latter two processes represent mirror-imaged DAS.

**Excitation of the $^1$MLCT-transition at 525 and 575 nm, respectively.** Having summarized the transient absorption results for excitation of the ligand-centred $S_1$ state, our attention shall be turned to transient absorption measurements upon direct pumping of the $^1$MLCT transition to test for the presence of pump-wavelength dependent excited-state dynamics. Fig. 6 and 7 compare the respective data and the DAS for **Ru** (Fig. 6a–c), **Fe** (Fig. 7a–c) and **Os** (Fig. 7d–f).

Comparing Fig. 4 and 6 it becomes apparent that no drastic differences can be observed between the transient spectra or the DAS recorded for pumping the $\pi\pi^*$ and the $^1$MLCT transition of **Ru**. This pump-wavelength independent photoinduced dynamics indicates that the observed kinetics arise from MLCT excited states. These states are either pumped directly at 525 nm or are populated by IC from the photoexcited ligand-centred $S_1$ excited-state (pumped at 400 nm). However, we observe characteristic MLCT transient absorption features immediately (within the time resolution of the differential absorption spectrometer) after photoexcitation of the $S_1$ state. This finding points to the fact that $S_1 \rightarrow {}^1$MLCT IC occurs rapidly within the time resolution accessible and originates from molecular geometries close to the FC, *i.e.* IC occurs before cooling and relaxation into the emissive geometry are observed. Comparing the transient spectra with the data for the free ligand[18,19] it is possible to assign the 2–6 ps component to cooling. The 20–25 ps component is associated with the photoinduced planarization of, in the ground state, the distorted terpyridine ligand.[19,26] The major discrepancy between the DAS obtained from the free ligand and the metal complexes is the different dispersion of the component assigned to the planarization. A possible explanation for this finding is that the transient spectrum is dominated by $S_1$ excited-state absorption in the case of the ligand and by $^3$MLCT excited-state absorption in the case of the respective metal complexes. Both excited states are strongly affected by the light-induced planarization motion, but show different spectral features. However, the rate of the photoinduced planarization is only weakly affected by complexation, *i.e.* it seems to be slightly decelerated from 20 ps in the free ligand to 20–25 ps in the complexes, which might be rationalized by the higher mass of the rotating part in the complex. The $^3$MLCT is populated by IC between the $S_1$ and the $^1$MLCT and a subsequent $^1$MLCT $\rightarrow$ $^3$MLCT ISC (upon excitation at 400 nm) or by direct ISC between the photoexcited $^1$MLCT (upon excitation at 525 nm) and the $^3$MLCT. The observed blueshift of the differential absorption spectra occurs on the same timescale as the formation of a structurally relaxed $^3$MLCT. These two processes, *i.e.* cooling and planarization, minimize the potential energy of the $^3$MLCT and thus increase the energy gap between higher lying excited-states, resulting in the observed blueshift of the differential absorption band. The infinite component as identified in the differential absorption data and the DAS can be assigned to the absorption of the thermalised $^3$MLCT. As this state in **Ru** reveals a very long lifetime of 36.5 ns its decay is not visible within the delay-time window accessible in our experiment.

Similar to **Ru** there is a good agreement between the spectral shape of the DAS for both excitation wavelengths for **Fe** and **Os**. Only the two fast components, *i.e.* the 2–6 and 20–25-ps, show a slightly altered dispersion when comparing the two pump wavelengths. In particular, the 20–25 ps component has positive contributions for **Fe** around 500 nm after excitation at 400 nm while there are negative values in this region upon excitation at 575 nm. Furthermore, there are slight differences in the relative intensities of the components and small spectral shifts, *e.g.* the maximum of the 2–6 ps component for **Os** is at 575 for 400 nm and at 525 for 525 nm excitation. Nonetheless, the transient-absorption kinetics of **Os** are very similar to those of **Ru** and hence are rationalized in an analogous manner. The major differences between the data observed for **Os** and **Ru** are the absolute amplitude of the differential absorption signals and the lack of a dynamic blueshift, which was prominently observed for **Ru**. The absence of the blueshift can be explained by different relative energetic positions of the "hot" and "cool" $^3$MLCT excited state for **Os** compared to **Ru** (see Table 1). Consequently, the excited-state absorption features are spectrally shifted. Therefore, the main effect of cooling and planarization should also occur at a different wavelength, which apparently is outside the experimentally accessible range between 450 and 700 nm.

In **Fe**, however, a further component with an intermediate decay time is present aside from the fast components and the relative slow recovery of the ground state. This component is characterized by a 600–700 ps time constant and shows

 

significant amplitudes only between 450 and 650 nm (see Fig. 5c and 7c). This process can be ascribed to IC between the $^3$MLCT excited-state and the $^{HS}$d–d excited-state, which, in turn, relaxes on a $>2$ ns timescale. In **Fe** the $^3$MLCT does not show such a long lifetime as in **Ru** and **Os** because of its high energy and, therefore, the good match with the $^{HS}$d–d excited-state. To put the observed lifetimes into the context of related complexes, we refer to work of Chergui and coworkers on $[Fe(bpy)_3]^{2+}$.[44] In comparison to their work, the excited-state lifetime of both the $^3$MLCT and the $^{HS}$d–d excited-state in **Fe** is much longer than in the related $[Fe(bpy)_3]^{2+}$ complex. Again this finding points to the significant stabilizing effect of the conjugated ligand system in **Fe**.

**Molecular origin of dual emission—ultrafast formation of emissive states.** In summary, the transient-absorption kinetics of **Ru**, **Os** and **Fe** show strong contributions of both a 2–6 ps and a 20–25 ps component irrespective of excitation into the $S_1$ or the $^1$MLCT state. These processes are assigned to cooling and planarization of the $^3$MLCT excited state, respectively. The close similarity of the differential absorption data for **Ru**, **Os** and **Fe** at different excitation wavelengths is, therefore, evidence for a branching of the excited-state dynamics into the $S_1$ and the $^1$MLCT occurring from a "hot" geometry close to the FC: irrespective of the excitation wavelength features characterisitic for MLCT related dynamics are observed immediately after photoexcitation. As a consequence of this branching, only a minor fraction of molecules initially placed into the $S_1$ state remains within the $S_1$ manifold. If the population of the MLCT manifold took place from a cool and relaxed, *i.e.* luminescent $S_1$, a change from the well known transient-absorption features of the free ligand to the ones observed upon direct excitation of the MLCT states of **Ru**, **Os** and **Fe** should be observable. This, however, is not observed. In contrast, upon excitation of the $S_1$ **Ru** and **Os** show a transient absorption spectrum typical for their $^3$MLCT excited state[40] even 100 fs after photoexcitation. The same observation holds true for **Fe**. Furthermore, if population of the MLCT state took place from the luminescent $S_1$ state the $S_1$ fluorescence lifetime of the metal complexes should be reduced as compared to the free ligand. As outlined above in detail this behavior is also not observed. Thus, upon photoexitation of the $S_1$ state ultrafast $S_1 \rightarrow {}^1$MLCT IC takes place close to the FC. This IC is then followed by an ultrafast ISC to the $^3$MLCT. Subsequently, cooling and excited-state planarization takes place within the $^3$MLCT and a relaxed and stabilized luminescent $^3$MLCT is formed. This state shows room-temperature luminescence with lifetimes of 0.6–0.7 ns (**Fe**), 36.5 ns (**Ru**) and 135.6 ns (**Os**). In the case of **Ru** the excited-state relaxation into the energetic minimum of the $^3$MLCT causes the blueshift of excited-state absorption (see Fig. 4 and 6), which is not visible in the case of **Os** most likely due to different relative energetic positions of the relevant excited states.

It should be noticed that excited-state planarization of the terpyridine ligand causes the excitation to be delocalized over both the terpyridine sphere and the adjacent chromophore. Hence, it is important for the stabilization of the $^3$MLCT. Therefore, planarization acts as a gating process for a partial charge delocalization and the resultant stabilization of the excited state and is thus crucial for the photophysics of these compounds.[45,46]

Summarizing the data presented in this manuscript it is possible to reconstruct the photoinduced relaxation pathway of the metal complexes: upon photoexcitation of the $S_1$ state branching from a "hot" excited state close to the FC occurs leaving a small fraction of excited molecules in the $S_1$ state while the majority of molecules populates the MLCT manifold by ultrafast IC within the temporal resolution of the experiment. Depending on the metal center the fraction of molecules undergoing $S_1 \rightarrow {}^1$MLCT IC can be estimated to $>90\%$ of the photoexcited molecules based on the emission quantum yields. IC from the $S_1$ to the $^1$MLCT is followed by an ultrafast ISC to the $^3$MLCT. Both processes occur within the $\sim 100$ fs temporal resolution of the transient absorption experiment. By planarization of the terpyridine ligand on a 20 ps time-scale excitation delocalizes over the conjugated ligand. In addition to planarization the formation of an equilibrium between the $^3$MLCT and a secondary triplet state stabilizes the $^3$MLCT against IC to $^{HS}$d–d states, which is the most efficient non-radiative deactivation channel in terpyridine complexes. The nature of this secondary triplet-state is presently undefined though its assignment to an $^3$LCCT can be favored based on the afore given arguments.

The excited molecules remaining in the $S_1$ state undergo cooling and planarization leading to a planarized ligand geometry with an excited-state lifetime of roughly 1.6 ns. The excited-state absorption of this state is too weak to be detected because of the low population, and can only be observed in the case of **Fe** (see ESI†), where the ligand-centered excited-state absorption is visible by the positive values in the transient spectra above 650 nm (see Fig. 3a and b). In **Fe** IC between the $S_1$ and the $^1$MLCT is apparently less effective than in **Ru** and **Os**.

Finally, Fig. 6 comprises the experimental results for **Ru** into a representative quantitative Jablonski diagram (see ESI† for **Fe** and **Os**). These schemes reflect the fact that the relaxation pathway is quite similar for all three complexes and dominated by the interplay of ligand centred and MLCT excited states. The major difference between the different complexes is the energetic position of the singlet and triplet MLCT with respect to the $^{HS}$d–d excited states. The relative position of the $^3$MLCT is one of the most sensitive parameters influencing the photophysical properties of the complexes as it determines the $T_1(^3\text{LCCT}) \leftrightarrow {}^3$MLCT equilibrium as well as the interplay between the $^3$MLCT and the $^{HS}$d–d state. In the case of **Os**, *i.e.* the complex with the longest phosphorescence lifetime, the energy of the $^3$MLCT excited-state is quite low and, therefore, a good match with the secondary triplet-state. This energetic match in energy is accompanied by a small barrier for the thermal equilibrium between both states and a high activation barrier for IC to the $^{HS}$d–d state. Both features result in a particularly long room temperature luminescence lifetime. In the case of **Fe** (see ESI†) this does not hold true, since the high energy of the $^3$MLCT promotes IC to the high $^{HS}$d–d excited state and curbs the equilibrium between the $^3$MLCT and the secondary triplet state. Therefore, the lifetime of the $^3$MLCT state is just about 600–700 ps. Finally, **Ru** is situated

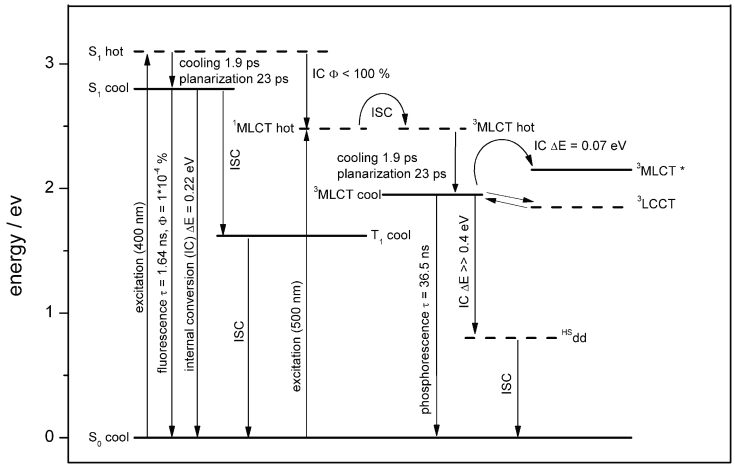


**Fig. 8** Representative Jablonski scheme for **Ru** reconstructed from the experimental data. Solid lines represent energy levels with defined energetic positions, while dashed ones indicate excited states, the energy of which can only be indirectly inferred or depends on excitation wavelength.

somewhere in between these two extremes showing a room temperature luminescence lifetime of 36.5 ns, which is still remarkably long for **Ru** terpyridine complexes (Fig. 8).

## Conclusion

This work presents a detailed temperature-dependent luminescence study in concert with femtosecond time-resolved transient absorption spectroscopy to decipher the molecular mechanism of the dual emission observed for ruthenium(II) bis[4′-(4-{[2,5-bis(octyloxy)-4-styrylphenyl]ethynyl}phenyl)-2,2′:6′,2″-terpyridine] (**Ru**) and osmium(II) bis[4′-(4-{[2,5-bis(octyloxy)-4-styrylphenyl]ethynyl}phenyl)-2,2′:6′,2″-terpyridine] (**Os**). These complexes represent coordination compounds with two highly stabilized triplet excited states resulting in a remarkably long room temperature luminescence lifetime. Upon excitation of the ligand-centred $S_1$ state the MLCT moiety is populated from a ''hot'' excited-state geometry close to the Franck–Condon point leaving only a minor fraction (sub 10%) of excited molecules within the $S_1$ state. These molecules undergo cooling and planarization leading to the formation of a fluorescent $S_1$ state, while the majority of photoexcited molecules undergo $S_1 \rightarrow {}^1$MLCT IC and subsequent ISC to a $^3$MLCT, which is followed by cooling and planarization of the ligand geometry. The stabilization especially of the resultant phosphorescent $^3$MLCT state is due to delocalization over parts of the adjacent chromophore and an equilibrium with a secondary triplet-state, which is speculated to have charge-transfer character. It could be shown that the planarization of the terpyridine ligand is a gating process for the formation of long-lived excited states and thus impacts the excited-state features of **Ru**, **Os** and **Fe** (iron(II) bis[4′-(4-{[2,5-bis(octyloxy)-4-styrylphenyl]ethynyl}phenyl)-2,2′:6′,2″-terpyridine]).

Non-radiative deactivation of $^3$MLCT excited states back to the ground state is suppressed with respect to related polypyridine complexes because of high activation barriers, which are quantified by temperature dependent fluorescence and phosphorescence experiments. Finally, it should be pointed out that the formation of excited-states with a prolonged room temperature lifetime and charge-transfer character is a prerequisite for light-induced electron transfer to strong electron acceptors, *i.e.* fullerene derivatives, and opens the doorway for applications of the herein investigated complexes in electrooptical devices.

## Experimental

The synthesis of the π-conjugated terpyridine ligand and the respective iron(II), ruthenium(II) and osmium(II) complexes was recently published elsewhere.[20,21] The time-resolved transient absorption set-up, which was described previously in detail,[18] is based on an amplified Ti:Saphire oscillator (Libra, Coherent Inc.), which produces a pulse train of 80 fs 950 μJ pulses centered at 800 nm with a pulse repetition rate of 1 kHz. The pulses are split by means of a 50 : 50 beamsplitter. One pulse train is used to generate the pump beam by either using a non-collinear optical-parametric amplifier (TOPASwhite, LightConversion Ltd., $\lambda_{excitation}$ = 525 or 575 nm) or second harmonic generation in a 100 μm thick BBO crystal ($\lambda_{excitation}$ = 400 nm). In all the experiments reported here white light is used as a probe, which is generated by splitting of a minor fraction of the residual amplifier output and focusing of this small fraction into a sapphire plate.

It is ensured that the energy of the pump pulses is kept well below 0.5 μJ, while typical probe intensities fall into the range of a few hundred nJ. Autocorrelation of the probe pulses and the experimental response function are recorded at the sample position by non-collinear second harmonic generation in a BBO crystal. The temporal duration of the pump pulses was estimated to be in the order of 50–60 fs, while the experimental response function is determined by the supercontinuum and therefore is in the range of 100 fs. Steady-state absorption spectra are frequently recorded to ensure sample integrity. Prior to analysis the experimental differential absorption data are chirp corrected and afterwards fitted with a global fitting routine. The

 

differential absorption spectra shown in Fig. 4 and 5 were smoothed by a 5 point smoothing average algorithm (see ESI†) to eliminate noise from the spectrometer for better visualization, while the fitting algorithm was applied to the raw data.

Fluorescence lifetimes are obtained by time-correlated single-photon counting on a setup previously described.[47] Here, a Ti–Sapphire laser (Tsunami, Newport Spectra-Physics GmbH) is used as the light source. The repetition rate is reduced to 400 kHz by a pulse selector (Model 3980, Newport Spectra-Physics GmbH). Afterwards the fundamental beam of the Ti–Sapphire oscillator is frequency doubled in a second harmonic generator (Newport Spectra-Physics GmbH) to create the 435-nm pump beam. The emission is detected by a Becker & Hickel PMC-100-4 photon-counting module with 150 ps response-limited time resolution. To control the temperature of the sample an Oxford Instruments ITC 503 intelligent temperature monitor and control unit is used.

Steady-state absorption spectra under ambient conditions are recorded on a Jasco V-670 spectrophotometer, while spectra under high oxygen pressure are recorded employing a high-pressure UV cell (F-076 from Research & Industrial Instruments Company England) and a UV-Vis-NIR-spectrometer (Varian Cary 5000). The fluorescence spectra are measured from dilute solutions using a Jasco FP-6200 spectrofluorimeter. All solvents utilized in this study are of spectroscopic grade (Merck and Sigma Aldrich). The samples are prepared to yield an optical density of 0.1 in a 1 mm quarz-glass cuvette at the long wavelength absorption maximum.

## Acknowledgements

Financial support of the Fonds der Chemischen Industrie, the Dutch Polymer Institute, the Nederlandse Organisatie voor Wetenschappelijk Onderzoek (VICI award for U.S.S.) and the Thüringer Ministerium für Bildung, Wissenschaft und Kultur (Grant No. B 514-09049, PhotoMIC) for this work is highly acknowledged. We thank Dr Denis Akimov for technical assistance with the experimental setup and Alfred Jacobi for assistance with the high pressure experiments.

## References

1 K. Müllen and U. Scherf, *Organic Light Emitting Devices*, Wiley-VCH, Weinheim, 2006.
2 I. G. Scheblykin, A. Yartsev, T. Pullerits, V. Gulbinas and V. Sundström, *J. Phys. Chem. B*, 2007, **111**, 6303.
3 J. S. Wilson, A. S. Dhoot, A. J. A. B. Seeley, M. S. Khan, A. Köhler and R. H. Friend, *Nature*, 2001, **413**, 828.
4 F. Guo, Y. Kim, J. R. Reynolds and K. S. Schanze, *Chem. Commun*., 2006, 1887.
5 X. Wang, Q. Wang, L. Yan, W. Wong, K. Cheung, A. Ng, A. B. Djurišić and W. K. Chan, *Macromol. Rapid Commun*., 2010, **31**, 861.
6 S. Yu, C. Kwok, W. K. Chan and C. Ming, *Adv. Mater*., 2003, **15**, 1643.
7 Y. Chen and H. Lin, *J. Polym. Sci., Part A: Polym. Chem*., 2007, **45**, 3243.
8 A. Winter, C. Friebe, M. Chiper, M. D. Hager and U. S. Schubert, *J. Polym. Sci., Part A: Polym. Chem*., 2009, **47**, 4083.
9 S. Kelch and M. Rehahn, *Macromolecules*, 1999, **32**, 5818.
10 A. El-Ghayoury, A. P. H. J. Schenning and E. W. Meijer, *J. Polym. Sci., Part A: Polym. Chem*., 2002, **40**, 4020.
11 V. Duprez, M. Biancardo, H. Spanggaard and F. C. Krebs, *Macromolecules*, 2005, **38**, 10436.
12 A. El-Ghayoury, A. P. H. J. Schenning, P. A. van Hal, C. H. Weidl, J. L. J. van Dongen, R. A. J. Janssen, U. S. Schubert and E. W. Meijer, *Thin Solid Films*, 2002, **403**, 97.
13 W. Y. Ng, X. Gong and W. K. Chan, *Chem. Mater*., 1999, **11**, 1165.
14 P. D. Vellis, J. A. Mikroyannidis, C. Lo and C. Hsu, *J. Polym. Sci., Part A: Polym. Chem*., 2008, **46**, 7702.
15 R. Dobrawa and F. Würthner, *J. Polym. Sci., Part A: Polym. Chem*., 2005, **43**, 4981.
16 F. Schlütter, A. Wild, A. Winter, M. D. Hager, A. Baumgaertel, C. Friebe and U. S. Schubert, *Macromolecules*, 2010, **43**, 2759.
17 A. Wild, F. Schlütter, G. M. Pavlov, C. Friebe, G. Feslag, A. Winter, M. D. Hager, V. Cimrová and U. S. Schubert, *Macromol. Rapid Commun*., 2010, **31**, 868.
18 R. Siebert, D. Akimov, M. Schmitt, A. Winter, U. S. Schubert, B. Dietzek and J. Popp, *ChemPhysChem*, 2009, **10**, 910.
19 R. Siebert, A. Winter, U. S. Schubert, B. Dietzek and J. Popp, *J. Phys. Chem. C*, 2010, **114**, 6841.
20 A. Winter, C. Friebe, M. D. Hager and U. S. Schubert, *Eur. J. Org. Chem*., 2009, 801.
21 R. Siebert, A. Winter, U. S. Schubert, B. Dietzek and J. Popp, *Macromol. Rapid Commun*., 2010, **31**, 883–888.
22 D. Graff Thompson, J. R. Schoonover, C. J. Timpson and T. J. Meyer, *J. Phys. Chem. A*, 2003, **107**, 10250.
23 D. F. Evans, *J. Chem. Soc*., 1961, 1987.
24 A. P. Monkman, H. D. Burrows, L. J. Hartwell, L. E. Horsburgh, I. Hamblett and S. Navaratnam, *Phys. Rev. Lett*., 2001, **86**, 1358.
25 H. D. Burrows, J. Seixas de Melo, C. Serpa, L. G. Aarnaut, M. da G. Miguel, A. P. Monkman, I. Hamblett and S. Navaratnam, *Chem. Phys*., 2002, **285**, 3.
26 M. Presselt, B. Dietzek, M. Schmitt, J. Popp, A. Winter, M. Chiper, C. Friebe and U. S. Schubert, *J. Phys. Chem. C*, 2008, **112**, 18651.
27 A. Winter, C. Friebe, M. Chiper, U. S. Schubert, M. Presselt, B. Dietzek, M. Schmitt and J. Popp, *ChemPhysChem*, 2009, **10**, 787.
28 R. Englman and J. Jortner, *Mol. Phys*., 1970, **18**, 145.
29 B. Dietzek, A. N. Tarnovsky and A. Yartsev, *Chem. Phys*., 2009, **357**, 54.
30 N. H. Damrauer, G. Cerullo, A. Yeh, T. R. Boussie, C. V. Shank and J. K. McCusker, *Science*, 1997, **275**, 54.
31 B. Dietzek, W. Kiefer, J. Blumhoff, L. Böttcher, S. Rau, D. Walther, U. Uhlemann, M. Schmitt and J. Popp, *Chem.–Eur. J*., 2006, **12**, 5105.
32 J. P. Sauvage, J. P. Collin, J. C. Chambron, S. Guillerez, C. Coudret, V. Balzani, F. Barigeletti, L. De Cola and L. Flamigni, *Chem. Rev*., 1994, **94**, 993.
33 A. C. Benniston, A. Harriman, P. Li and C. A. Sams, *J. Phys. Chem. A*, 2005, **109**, 2302.
34 A. Amini, A. Harriman and A. Mayeux, *Phys. Chem. Chem. Phys*., 2004, **6**, 1157.
35 E. A. Medlycott and G. S. Hanan, *Chem. Soc. Rev*., 2005, **34**, 133, and references cited therein.
36 P. P. Lainé, S. Campagna and F. Loiseau, *Coord. Chem. Rev*., 2008, **252**, 2552, and references cited therein.
37 R. S. Lumpkin, E. M. Kober, L. A. Worl, Z. Murtaza and T. J. Meyer, *J. Phys. Chem*., 1990, **94**, 239.
38 B. J. Coe, D. W. Thompson, C. T. Culbertson, J. R. Schoonover and T. J. Meyer, *Inorg. Chem*., 1995, **34**, 3385.
39 A. C. Benniston, G. Chapman, A. Harriman, M. Mehrabi and C. A. Sams, *Inorg. Chem*., 2004, **43**, 4227.
40 E. A. Alemán, C. D. Shreiner, C. S. Rajesh, T. Smith, S. A. Garrison and D. A. Modarelli, *Dalton Trans*., 2009, (33), 6562.
41 A. C. Benniston, A. Harriman, D. J. Lawrie and A. Mayeux, *Phys. Chem. Chem. Phys*., 2004, **6**, 51.
42 S. Tschierlei, M. Presselt, C. Kuhnt, A. Yartsev, T. Pascher, V. Sundström, M. Karnahl, M. Schwalbe, B. Schäfer, S. Rau, M. Schmitt, B. Dietzek and J. Popp, *Chem.–Eur. J*., 2009, **15**, 7678.
43 Alternatively, it is also possible to assign the secondary triplet-state to an additional ligand centered charge-transfer excited-state, which is induced by the presence of the coordinated metal ion. Such findings have been reported for $Zn^{2+}$ complexes.
44 W. Gawelda, A. Cannizzo, V. T. Pham, F. van Mourik, C. Bressler and M. Chergui, *J. Am. Chem. Soc*., 2007, **129**, 8199.
45 N. R. Damrauer, T. R. Boussie, M. Devenney and J. K. McCusker, *J. Am. Chem. Soc*., 2006, **119**, 8253.
46 P. P. Lainé, F. Bedioui, F. Loiseau, C. Chiorboli and S. Campagna, *J. Am. Chem. Soc*., 2006, **128**, 7510.
47 B. Dietzek, W. Kiefer, A. Yartsev, V. Sundström, P. Schellenberg, P. Grigaravicius, G. Hermann, J. Popp and M. Schmitt, *ChemPhysChem*, 2006, **8**, 1727.

# [RS5] Direct Observation of Temperature Dependent Excited-State Equilibrium in Dinuclear Ruthenium Terpyridine Complexes Bearing Electon-Poor Bridging Ligands



Reproduced with permission from:
R. Siebert, C. Hunger, J. Guthmuller, F. Schlütter, A. Winter, U. S. Schubert, L. Gonzàlez, B. Dietzek and J. Popp, Direct Observation of Temperature Dependent Excited-State Equilibrium in Dinuclear Ruthenium Terpyridine Complexes Bearing Electron-Poor Bridging Ligands, *Journal of Physical Chemistry C*, **2011**, **115**, 12677-12688.



## Autorenschaft der Publikation

| | |
|---|---|
| Ronald Siebert | Durchführung experimenteller Arbeiten, Auswertung der temperaturabhängigen Emissionsexperimente, Ergebnisdiskussion und Erstellung des Manuskripts |
| Christoph Hunger | stationäre Absorptions- und Emissionsspektroskopie, zeitaufgelöste transiente Absorptionsspektroskopie, temperaturabhängige zeitaufgelöste Emissionsspektroskopie, Auswertung experimenteller Daten |
| Julien Guthmuller | TDDFT-Rechnungen, Beiträge zur Erstellung des Manuskripts |
| Florian Schlütter | Synthese und Charakterisierung eines Teils der untersuchten Substanzen |
| Andreas Winter | Synthese und Charakterisierung eines Teils der untersuchten Substanzen, Diskussion und Korrektur des Manuskripts |
| Ulrich S. Schubert | Konzept- und Ergebnisdiskussion, Diskussion und Korrektur des Manuskripts |
| Leticia Gonzàlez | Konzept- und Ergebnisdiskussion, Diskussion und Korrektur des Manuskripts |
| Benjamin Dietzek | Projektleitung, Konzept- und Ergebnisdiskussion, Diskussion und Korrektur des Manuskripts |
| Jürgen Popp | Konzept- und Ergebnisdiskussion, Diskussion und Korrektur des Manuskripts |

THE JOURNAL OF PHYSICAL CHEMISTRY C

ARTICLE

pubs.acs.org/JPCC

# Direct Observation of Temperature-Dependent Excited-State Equilibrium in Dinuclear Ruthenium Terpyridine Complexes Bearing Electron-Poor Bridging Ligands

Ronald Siebert,[†] Christoph Hunger,[†] Julien Guthmuller,[†] Florian Schlütter,[‡] Andreas Winter,[‡] Ulrich S. Schubert,[‡,§] Leticia González,[*,†] Benjamin Dietzek,[*,†,⊥] and Jürgen Popp[†,⊥]

[†]Institute for Physical Chemistry, Jena Center for Soft Matter (JCSM), and Abbe Center of Photonics (ACP), Friedrich-Schiller-University Jena, Helmholtzweg 4, 07743 Jena, Germany

[‡]Laboratory of Organic and Macromolecular Chemistry (IOMC) and Jena Center for Soft Matter (JCSM), Friedrich-Schiller-University Jena, Humboldtstrasse 10, 07743 Jena, Germany

[§]Dutch Polymer Institute (DPI), P.O. Box 902, 5600 AX Eindhoven, The Netherlands

[⊥]Institute of Photonic Technology (IPHT), Jena Albert-Einstein-Strasse 9, 07745 Jena, Germany

Supporting Information

**ABSTRACT:** Dinuclear ruthenium−terpyridine complexes, bearing highly conjugated bridging ligands, have been investigated by time- and temperature-dependent emission spectroscopy, femtosecond time-resolved transient-absorption spectroscopy, and time-dependent density functional theory calculations. These terpyridine compounds show room-temperature emission around 640 nm and lifetimes between 140 and 230 ns. Reduction of the temperature results in an overall increase of emission lifetime. However, the specific temperature dependence of the luminescence lifetime depends on the particular bridging ligand. This ligand-specific behavior is found to correlate with the electronic structure of the ligand, which indicates an excited-state equilibrium between a highly delocalized $^3$MLCT and a ligand-centered $^3\pi\pi^*$ excited-state. Due to this equilibrium a prolonged room-temperature lifetime is observed.

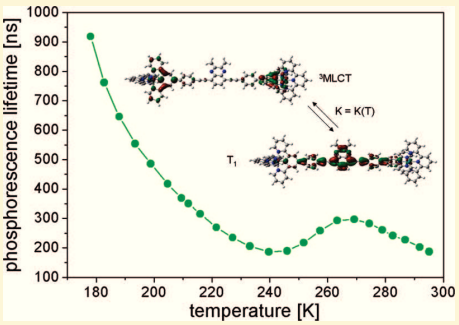


## 1. INTRODUCTION

The formation of long-lived charge-separated states represents a key challenge in organic semiconductor research due to the positive effect of such states on the exciton diffusion length,[1] which presents a central metric for the performance of organic semiconductors. Several approaches dealing with this challenge are focused on the connection of coordination compounds to well-known conjugated polymeric structures.[2] One of the simplest ways to achieve long-lived charge-separated excited states is to create coordination polymers from conjugated linker segments and a suitable metal ion, e.g., from conjugated bis-terpyridines and ruthenium(II) ions.[3] Conjugated bis-terpyridines represent the most suitable bridging ligand systems as they are readily synthesized and combine a great deal of structural variation of the chromophore with a high affinity to form ruthenium-based coordination polymers.[4−8] Furthermore, following this strategy the unfavorable photophysical properties of $[Ru(terpy)_2]^{2+}$, i.e., a short room-temperature lifetime and a low emission quantum yield,[9] can be overcome. These properties, which limit the use of $[Ru(terpy)_2]^{2+}$ in, e.g., luminescent devices, are caused by efficient internal conversion between the lowest metal-to-ligand charge transfer ($^3$MLCT) excited-state and the $^3$MC excited-states,[10,11] which are prone to decay nonradiatively back to the ground-state. However, by introducing a conjugated chromophore into the ligand structure, prolonged lifetimes and increased quantum yields are observed. The chromophore adjacent to the terpyridine leads to a partial delocalization of the $^3$MLCT state, which, in turn, causes a significantly prolonged room temperature lifetime.[12,13]

Aside from excited-state delocalization, the substitution of an extended conjugated system to the terpyridine unit can induce an excited-state equilibrium between the $^3$MLCT, which is mainly localized on the terpyridine sphere, and a triplet state ($^3\pi\pi^*$) localized on the adjacent chromophore.[12,14,15] In these cases, where such an equilibrium exists, especially when aromatic systems such as naphthalene, anthracene, and pyrene with long-lived triplet-state are used as substituents, a significant increase in excited-state lifetime can be observed.[16,17] Here, the observed excited-state lifetime is a weighted average of both the $^3$MLCT and the $^3\pi\pi^*$ lifetime. Such an excited-state energy transfer from

Received: April 28, 2011
Revised: May 18, 2011
Published: June 06, 2011

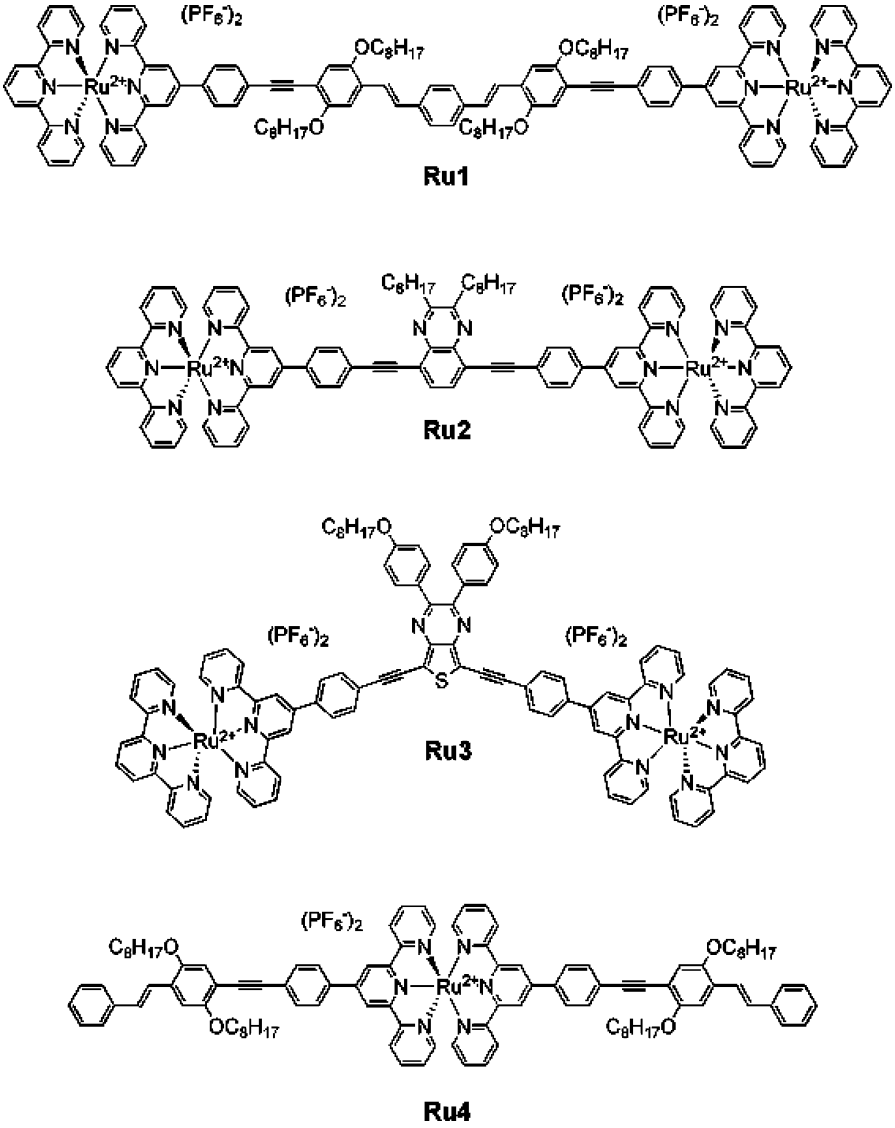


**Figure 1.** Schematic representation of the molecular structures of the dinuclear complexes (**Ru1**, **Ru2**, **Ru3**) derived from bis-terpyridines with different electronic structures together with the mononuclear reference complex **Ru4**.

the $^3$MLCT to a secondary triplet-state associated with the ligand is a common feature in coordination compounds of extended ligands and has been observed up to now in a few selected mononuclear[18−23] and dinuclear coordination compounds.[24−28]

Thus, it is intriguing to investigate and decipher the excited-state dynamics and the formation of an excited-state equilibrium in the complexes presented here (see Figure 1), which present building blocks of photoactive coordination polymers. The considered set of dinuclear ruthenium complexes contains bridging ligands with different electronic properties. Temperature-dependent emission and femtosecond transient-absorption experiments are performed in concert with time-dependent density functional theory (TDDFT) studies. The work focuses on the influence of the bridging ligands on the excited-state dynamics of the lowest $^3$MLCT excited-state, in particular if an excited-state equilibrium and the dynamics of its formation can be observed. The paper is organized as follows:

Section 2 describes the overall photophysics of the ruthenium(II) terpyridine complexes and the employed photophysical model as well as the experimental and theoretical methods. Sections 3.1 and 3.2 present the results of temperature-dependent emission experiments (using time-correlated single-photon counting, TCSPC). Theoretical calculations of the triplet excited-states are given and analyzed in section 3.3. The transient absorption data to unravel the photoinduced dynamics leading to the population of the emissive state observed in TCSPC measurements are presented and discussed in section 3.4. Finally, section 4 provides a conclusive discussion summarizing the results.

**Scheme 1. Schematic Summary of the Excited-States Relevant for the Photophysics of Ruthenium Terpyridine Complexes with Extended Ligand Structures[a]**

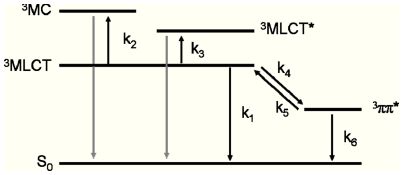


[a] In addition to the electronic states, the relevant rates corresponding to the interconversion between individual states are indicated as black arrows. $k_2-k_6$ represent processes, which are thermally activated, while $k_1$ does not require any activation energy. Thus, the scheme presents a simplified model for the deactivation dynamics of the lowest luminescent $^3$MLCT state in ruthenium terpyridyl complexes.

## 2. METHODOLOGIES

**2.1. Conceptual Model.** To unravel the complex photoinduced relaxation dynamics in transition metal complexes, various experimental approaches can be pursued.[27,29] This contribution particularly focuses on temperature-dependent phosphorescence lifetime measurements because such data allow for detailing the deactivation channels coupled to the luminescent excited-state. Together with femtosecond transient-absorption spectroscopy, it is possible to reconstruct all the photoinduced relaxation pathways. These time-resolved spectroscopic studies are accompanied by TDDFT calculations yielding energies for the relevant excited-state and a detailed assignment of the experimentally observed decay processes to electronic states.

Prior to presenting the experimental data, the complex deactivation channels of the luminescent $^3$MLCT states in Ru(II)−terpyridine complexes shall be exemplified for cases, in which a chromophore is in conjugation with the coordinating terpyridine unit.

Scheme 1 compares the relevant deactivation channels of the energetically lowest $^3$MLCT excited state of Ru(II)−terpyridine complexes.[10,13,14,30] The following processes contribute to the decay of the luminescent $^3$MLCT state: Phosphorescence ($k_1$), internal conversion to a metal-centered $^3$MC ($k_2$) and a higher lying $^3$MLCT* state ($k_3$), and the equilibrium with a secondary triplet-state ($k_4$ and $k_5$), which is assumed to be localized on the extended chromophore of the ligand. The latter state, which is termed $^3\pi\pi^*$ in Scheme 1, is nonemissive, i.e., decays nonradiatively to the ground-state ($k_6$). As will be detailed below, the processes $k_2-k_6$ require activation energy, i.e., they are associated with barrier crossing along the relevant reaction coordinates. Only the radiative process ($k_1$) does not require thermal activation. The lifetime of the $^3\pi\pi^*$ state (see Scheme 1), the exact nature of which will be discussed in the context of the TDDFT results, should be in the order of 50−100 $\mu$s as extrapolated from structurally related compounds.[31] Therefore, the contribution of the nonradiative decay of the $^3\pi\pi^*$ state, i.e., $k_6$, to the nanosecond dynamics of the system, which is at the core of this paper, is negligible. For a quantitative evaluation of the experimental lifetime data the model summarized in Scheme 1 can be comprised into a fit function reflecting the influence of the various deactivation channels on the measured luminescence lifetime (see Supporting Information). To use such a fit model to account for the temperature-dependent changes in emission lifetime ($\tau$), it should be noted that the rates $k_2-k_5$ are assumed to be thermally activated and to follow the Arrhenius temperature dependence. In case an excited-state equilibrium (determined by the interplay of $k_4$ and $k_5$) contributes to the observed luminescence, the radiative properties and in particular the luminescence lifetime should be strongly temperature-dependent: Thus, this equilibrium should respond to any temperature change, due to the fact that $k_4$ as well as $k_5$ are thermally activated. Hence, it affects the overall lifetime of the $^3$MLCT, which, according to literature, can be expressed as a weighted average of the fractional population and lifetimes of both excited-state involved in the equilibrium.[14] Therefore, luminescence lifetime measurements as a function of temperature help to identify the influence of this equilibrium on the observed lifetime, as decreasing the temperature results in freezing the $^3$MLCT ↔ $^3\pi\pi^*$ equilibrium and consequently causes a decreased lifetime. In general, $k_2$, $k_3$, and $k_6$ are processes that reduce the emission lifetime while $k_4$ and $k_5$ represent a thermal equilibrium among excited-state, which acts as a reservoir of luminescent molecules and hence prolongs the luminescence lifetime. Upon reducing the temperature, the rates of all processes, which involve an activation energy barrier, will be affected. Blocking $k_2$, $k_3$, and $k_6$ should result in an increase of lifetime while suppression of the excited-state equilibrium ($k_4$ and $k_5$) should cause a decrease. After this brief general introduction into the photophysics of ruthenium terpyridine complexes, the $\pi$-conjugated terpyridine complexes studied here and their temperature-dependent emission shall be discussed in detail.

**2.2. Experimental Methods.** The synthesis of the $\pi$-conjugated terpyridine ligands and their respective ruthenium(II) complexes **Ru1**−**Ru4** (see Figure 1) was published elsewhere.[2,30,32] Luminescence lifetimes are obtained by time-correlated single-photon counting using a setup that has been described previously.[13] Briefly, a Ti-sapphire laser (Tsunami, Newport Spectra-Physics GmbH), whose repetition rate is reduced to 400 kHz by a pulse selector (Model 3980, Newport Spectra-Physics GmbH), is used as the light source. Therefore, the fundamental beam of the Ti-sapphire oscillator is doubled in frequency in a second harmonic generator (Newport Spectra-Physics GmbH) to create the 435-nm pump beam. The emission is detected by a Becker & Hickel PMC-100-4 photon-counting module with 150 ps response-limited time resolution. The sample temperature is controlled by an Oxford Instruments ITC 503 intelligent temperature monitor and control unit. An exponential decay is fit to the experimentally recorded phosphorescence kinetics, and the resultant lifetimes are analyzed as a function of temperature.

The time-resolved transient absorption setup is based on an amplified Ti:sapphire oscillator (Legend-Elite, Coherent Inc.), which produces a pulse train of 30-fs 3.5-mJ pulses centered at 800 nm with a pulse repetition rate of 1 kHz. The pulses are split by means of a 50:50 beam splitter. One pulse train is used to generate the pump beam having a wavelength of $\lambda_{pump}$ = 488 nm by means of a noncollinear optical-parametric amplifier (TOPAS-C, LightConversion Ltd.). White light is used as the probe, which is generated by focusing a minor fraction of the amplifier output into a sapphire plate. The white light is split by means of a beam splitter to obtain the probe and reference beams. The pump pulses are delayed in time by means of an optical delay line, and their polarization was rotated by 54.7° (magic angle) with respect to the probe beam by using a Berek compensator. The pump pulse is blocked after the sample, while the probe pulse is recollimated and sent to a double-stripe diode-array detection system

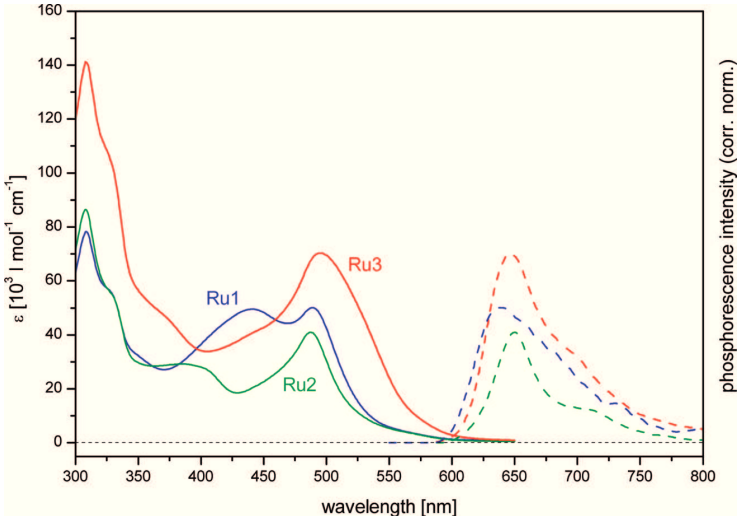


**Figure 2.** Absorption spectra from dilute solutions in acetonitrile at room temperature (solid lines) as well as the emission spectra in a butyronitrile glass at 77 K (dashed lines) of **Ru1** (blue), **Ru2** (green), and **Ru3** (red).

(Pascher Instruments AB) together with the reference pulse. The diode array is read out with the repetition rate of the laser and the $\Delta A$ signal is calculated for individual pairs of laser pulses corresponding to pump-on and pump-off conditions. It is ensured that the energy of the pump pulses is kept well below 0.5 $\mu$J, while typical probe intensities fall into the range of a few hundred nanojoules. Steady-state absorption spectra are frequently recorded to ensure sample integrity. Prior to data analysis, the experimental differential absorption data is chirp corrected and afterward fitted with a global fitting routine.

Steady-state absorption spectra under ambient conditions are recorded on a UV−vis−NIR spectrometer (Varian Cary 5000). The luminescence spectra are measured from dilute butyronitrile glasses at 77 K using a Perkin Ellmer LS50-B spectrofluorimeter. All solvents utilized in this study are of spectroscopic grade (Merck and Sigma Aldrich). The solvents for temperature-dependent measurements are distilled under an argon atmosphere prior to use to minimize oxygen and water content.

**2.3. Theoretical Methods.** Quantum chemical calculations were performed with the Gaussian 09 program.[33] The geometries of the ground-state ($S_0$) and of the lowest triplet-state ($T_1$) were optimized by means of density functional theory using the exchange-correlation functional B3LYP.[34,35] The 28-electron relativistic effective core potential MWB[36] was used with its basis set for the ruthenium atoms, that is, 4s, 4p, 4d, and 5s electrons are treated explicitly, whereas the three first inner shells are described by the core pseudopotential. The 6-31G(d) double-$\zeta$ basis set was employed for the ligands. The singlet−triplet excitation energies at the $S_0$ and $T_1$ geometries were obtained from time-dependent density functional theory within the adiabatic approximation, applying the same functional, pseudopotential, and basis set. The effects of the interaction with a solvent (butyronitrile, $\varepsilon$ = 24.291, $n$ = 1.384) on the geometries and excitation energies were taken into account by the integral equation formalism of the polarizable continuum model.[37] The nonequilibrium procedure of solvation was used for the calculation of the excitation energies, which is well adapted for processes where only the fast reorganization of the electronic distribution of the solvent is important. In order to reduce the computational complexity, the aliphatic chains ($C_8H_{17}$) located on the bridging ligands (Figure 1) were approximated in the calculations by methyl groups. This allows for a reduction of the computational cost of the simulations without affecting the spectroscopic properties of the complexes.

## 3. RESULTS

**3.1. Steady-State Spectroscopy.** Steady-state absorption and emission spectra were recorded to obtain the fundamental spectroscopic signatures of **Ru1**−**Ru3** (see Figure 1).

Figure 2 compares the UV/vis absorption spectra of the binuclear complexes **Ru2** and **Ru3** (both having electron-poor bridging ligands) to that of **Ru1** with an electron-rich bridging ligand. These steady-state spectra show similar global structures for each of the complexes. The blue part of the spectra ($\leq$350 nm) is dominated by $\pi\pi^*$ transitions located at the terpyridine sphere, while at longer wavelength the spectra contain contributions from the $\pi\pi^*$ transition located on the extended conjugated system as well as from the $^1$MLCT transition.[4,8,38] The unusual shapes of the absorption spectra compared to $[Ru(terpy)_2]^{2+}$, i.e., the presence of pronounced short wavelength shoulders at roughly 400 (445) nm for **Ru2** (**Ru1**) or long wavelength shoulders (ca. 525 nm for **Ru3**), are due to the superposition of the $^1$MLCT transitions with $\pi\pi^*$ transitions of the extended chromophore, which are absent for $[Ru(terpy)_2]^{2+}$. In addition to the absorption data, emission spectra upon excitation at 475 nm are shown in Figure 2. The observed emission originates from the triplet manifold of the complexes, which is populated rapidly upon excitation of the $^1$MLCT transition by intersystem crossing due to the presence of the heavy metal ion ruthenium.[39,40] The emission spectra are centered around 640 nm, i.e., roughly 40 nm (1030 cm$^{-1}$) red-shifted with respect to the emission of $[Ru(terpy)_2]^{2+}$.[9] This shift is due to the stabilizing effect of the extended $\pi$-system, which is connected to the

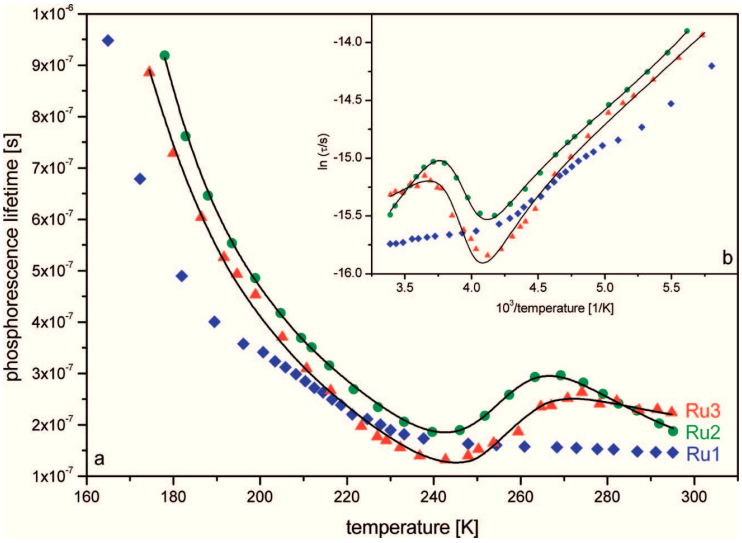


**Figure 3.** Phosphorescence lifetime of **Ru1** (blue diamonds), **Ru2** (green circles), and **Ru3** (red triangles) with their corresponding nonlinear fits (black lines) as a function of temperature in the range between ca. 300 K and 150 K. Figure 3b shows the same information on a logarithmic scale and a reciprocal temperature axis.

terpyridine in 4′-position, causing an enhanced excitation delocalization over parts of the adjacent chromophore. The shape of the emission spectra for **Ru2** and **Ru3** is due to an intense 0−0 transition accompanied by a broad long-wavelength shoulder, arising from several vibrations coupled to the electronic transition. On the other, hand, **Ru1** shows a much less structured emission due to the spectral overlap of phosphorescence from the lowest $^3$MLCT and a $^3$MLCT* with slightly higher energy. The existence of this excited state in ruthenium(II) complexes was substantiated by temperature and polarization-dependent emission spectroscopy.[10,41] Furthermore, it has been reported to decay radiatively in some systems,[10,41] **Ru1** being one of them. For **Ru1** the emission from the $^3$MLCT* state can be observed at low temperatures where nonradiative deactivation of this state is suppressed. The spectral shape of this $^3$MLCT* emission is comparable to the shape of the **Ru1** $^3$MLCT emission; however, it appears shifted bathochromically by approximately 600 cm$^{-1}$. The overlap of these two contributions causes the broader emission spectra of the reference compound **Ru1** with respect to the spectra of **Ru2** and **Ru3**, which bear electron-poor heterocycles in their bridging ligand.

**3.2. Temperature-Dependent TCSPC Measurements.** Reducing the temperature in these terpyridine systems is known to have a positive effect on intensity and lifetime of the $^3$MLCT-based phosphorescence. Measuring the emission lifetime or quantum yield dependence on temperature allows further examination of the deactivation dynamics of the energetically lowest luminescent $^3$MLCT state. In particular, as argued above, the number of dark relaxation channels and their respective activation energies can be estimated. Following this approach the lifetimes of the complexes were measured in the temperature range between 300 K and 150 K. The respective experimental results are depicted in Figure 3, which compares the temperature-dependent phosphorescence characteristics of **Ru2** and **Ru3** to **Ru1**. The temperature-dependent phosphorescence lifetime of all three samples reveals a complex slope with an overall increase in lifetime upon decreasing temperature. While **Ru1** shows a steady rise in lifetime with decreasing temperature **Ru2** and **Ru3** reveal a more complex behavior, indicating a complex structure of triplet-states involved in the deactivation of the luminescent $^3$MLCT state. For these two systems, the lifetime increases up to a temperature of about 275 K, followed by a decrease between ca. 275 K and 245 K. Finally the lifetime increases again with decreasing temperature. This qualitatively different temperature dependence of the luminescence lifetime for **Ru2**/**Ru3** and **Ru1** suggests qualitatively different excited-state topologies. Therefore, a separate discussion of the luminescence properties of all three complexes is performed in the following, starting with the conceptually straightforward luminescence properties of **Ru1**.

(i) **Ru1** exhibits a small increase in lifetime from 145 to 230 ns between 300 K and 220 K, followed by a more pronounced lifetime rise for temperatures below 220 K. This dependence of the luminescence lifetime on the temperature can be understood by the contribution of two distinct dark deactivation channels, which are inhibited for decreasing temperatures. One of these two dark deactivation pathways is internal conversion (IC) of the lowest lying $^3$MLCT to a $^3$MC state ($k_2$), a process that needs activation energy of a few thousand wavenumbers.[13,42] The observed steeper increase for lower temperatures is caused by freezing the second deactivation route, namely IC from the lowest lying $^3$MLCT to an additional, slightly higher lying $^3$MLCT* ($k_3$ see Scheme 1). This deactivation process needs only a few hundred wavenumbers for activation and hence is suppressed for lower temperatures.[9,42] The temperature-dependent emission data for **Ru1** do not show any immediate indication for the presence of an excited-state equilibrium ($k_4$ and $k_5$). Nonetheless, **Ru1** reveals an unusually long room temperature lifetime of 146 ns, which might be explained as involving a stabilizing effect due to the presence of a secondary triplet state.

(ii) In the case of **Ru2**, bearing an electron-poor bridging ligand, the temperature-dependent lifetime shows a general increase when reducing the temperature, which steepens for low temperatures, i.e., below ca. 200 K. Nevertheless, the temperature-dependent lifetime curve possesses distinct differences as compared to **Ru1**, especially in the temperature range between 270 and 240 K. Here the slope turns from an increase into a decrease before the lifetime rises up again below 240 K upon decreasing temperatures. According to literature, the lifetime increase between 300 K and 270 K and between 220 K and 200 K can be attributed to the inhibition of IC between the lowest $^3$MLCT and the $^3$MC state and IC between the lowest lying $^3$MLCT and the $^3$MLCT*, respectively. The lifetime decrease between 270 K and 240 K can be explained by invoking an additional $^3\pi\pi^*$ state (see Scheme 1), which has an energy close or lower to the $^3$MLCT state but a significantly longer lifetime. Upon formation of a $^3$MLCT$\leftrightarrow{}^3\pi\pi^*$ equilibrium a significant fraction of the excited ensemble is residing in this additional triplet-state, which is separated from the $^3$MLCT by an activation barrier, that can be overcome at ambient temperatures. Therefore, this triplet state $^3\pi\pi^*$ acts as a "storage basin" for excited molecules due to its longer lifetime as compared to the $^3$MLCT. Hence, the experimentally determined luminescence lifetime is a weighted average of both the lifetimes of the $^3$MLCT and the secondary triplet-state $^3\pi\pi^*$.[14] Decreasing the temperature reduces the thermal energy present in the system, which is needed as activation energy for the formation of the equilibrium. Therefore, upon decreasing temperature, the $^3\pi\pi^*$ state cannot be accessed anymore and hence its stabilizing effect is lost. Consequently, the measured luminescence lifetime decreases with increasing temperature.

(iii) **Ru3** shows qualitatively the same temperature dependence as **Ru2**, i.e., a lifetime increase up to 275 K is followed by a decrease down to 240 K. Upon further reduction of the temperature, the phosphorescence lifetime increases steadily. Similar to that for **Ru1** and **Ru2**, the initial rise is due to freezing the IC between the lowest $^3$MLCT and a $^3$MC excited-state, the process with the highest activation energy. Subsequently, the thermal equilibrium between the lowest $^3$MLCT and a more ligand-centered triplet-state $^3\pi\pi^*$ is impacted for decreasing temperatures. Similar to that for **Ru2**, the overall lifetime benefits from this equilibrium. Thus, inhibition of the interplay between $^3$MLCT and $^3\pi\pi^*$ leads to a faster decay of the phosphorescence. Finally, IC from the lowest $^3$MLCT to the $^3$MLCT* is suppressed for lower temperatures.

In order to obtain quantitative information on the remarkable excited-state landscape of the complexes **Ru1**−**Ru3** the phosphorescence lifetime as a function of temperature was fitted to a model, taking into account the $^3$MLCT deactivation channels depicted in Scheme 1 (see Supporting Information for details). The results of such a fitting approach are shown as black lines in Figure 3 and summarized in Table 1. Table 1 includes the luminescence data of reference complexes **Ru4** and $[Ru(terpy)_2]^{2+}$ are included for comparison.

As a general feature of ruthenium terpyridine complexes, two distinct processes contribute to the excited-state deactivation, internal conversion to a $^3$MC excited-state ($\Delta E_2$), and a slightly higher lying $^3$MLCT* excited-state ($\Delta E_3$).[30,42] The activation energies $\Delta E_2$ of 2800 and 3120 cm$^{-1}$ for **Ru2** and **Ru3**, respectively, are much higher than that for $[Ru(terpy)_2]^{2+}$ (1700 cm$^{-1}$)[30,42] and close to the one obtained for the related mononuclear complex **Ru4**.[13] The increased activation energies in the complexes containing conjugated terpyridines are due to the effective stabilization of the $^3$MLCT by the related ligand systems. Furthermore, also the second deactivation process, i.e., $^3$MLCT−$^3$MLCT* IC shows activation energies $\Delta E_3$ in the same range for all complexes. The close similarity of the terpyridine ligands in **Ru2** and **Ru3** as well as in **Ru4** suggests that both values for **Ru1** are similar. In contrast, IC from the $^3$MLCT into the second triplet-state ($^3\pi\pi^*$ in Scheme 1) takes place only for **Ru2** and **Ru3** and is activated by 940 (**Ru2**) and 320 cm$^{-1}$

**Table 1. Comparison of the Activation Energies for Nonradiative Deactivation Channels Affecting the Excited-State Lifetime**[a]

| complex | $\Delta E_2$ [cm$^{-1}$] | $\Delta E_3$ [cm$^{-1}$] | $\Delta E_4$ [cm$^{-1}$] | $\Delta E_5$ [cm$^{-1}$] |
|---|---|---|---|---|
| $[Ru(terpy)_2]^{2+}$[9] | 1700 | 560 | – | – |
| **Ru2** | 2800 | 420 | 940 | 7280 |
| **Ru3** | 3120 | 670 | 320 | 8230 |
| **Ru4**[13] | 3200 | 600 | – | – |

[a] The indices $i$ in $\Delta E_i$ refer to the respective rates in Scheme 1.

**Table 2. Singlet−Triplet Excitation Energies ($E$) of Ru2 Calculated at the Singlet Ground-State Geometry ($S_0$) and at the Lowest Triplet-State Geometry ($T_1$)**

| | $S_0$ geometry | | | $T_1$ geometry | | |
|---|---|---|---|---|---|---|
| state | transition | weight (%) | $E$ (cm$^{-1}$) | transition | weight (%) | $E$ (cm$^{-1}$) |
| $T_1$ | $\pi_B(350) \rightarrow \pi^*_B(351)$ | 61 | 14431 | $\pi_B(350) \rightarrow \pi^*_B(351)$ | 84 | 9627 |
| | $\pi_B(350) \rightarrow \pi^*_{B,terpy}(359)$ | 24 | | $\pi_B(350) \rightarrow \pi^*_{B,terpy}(355)$ | 12 | |
| $T_2$ | $d_{Ru}(349) \rightarrow \pi^*_B(351)$ | 38 | 16771 | $d_{Ru}(349) \rightarrow \pi^*_B(351)$ | 30 | 16044 |
| | $d_{Ru}(344) \rightarrow \pi^*_{terpy}(352)$ | 22 | | $d_{Ru}(344) \rightarrow \pi^*_{terpy}(352)$ | 17 | |
| | $d_{Ru}(349) \rightarrow \pi^*_{B,terpy}(359)$ | 5 | | $d_{Ru}(349) \rightarrow \pi^*_{B,terpy}(355)$ | 10 | |
| | $\pi_B(350) \rightarrow \pi^*_{terpy}(352)$ | 25 | | $\pi_B(350) \rightarrow \pi^*_{terpy}(352)$ | 34 | |
| $T_3$ | $d_{Ru}(349) \rightarrow \pi^*_{terpy}(352)$ | 36 | 17215 | $d_{Ru}(349) \rightarrow \pi^*_{terpy}(352)$ | 33 | 16584 |
| | $d_{Ru}(344) \rightarrow \pi^*_B(351)$ | 31 | | $d_{Ru}(344) \rightarrow \pi^*_B(351)$ | 24 | |
| | $\pi_B(350) \rightarrow \pi^*_{B,terpy}(359)$ | 16 | | $d_{Ru}(344) \rightarrow \pi^*_{B,terpy}(355)$ | 9 | |
| | | | | $\pi_B(350) \rightarrow \pi^*_{B,terpy}(355)$ | 22 | |

**Table 3. Singlet−Triplet Excitation Energies ($E$) of Ru3 Calculated at the Singlet Ground-State Geometry ($S_0$) and at the Lowest Triplet-State Geometry ($T_1$)**

| | $S_0$ geometry | | | $T_1$ geometry | | |
|---|---|---|---|---|---|---|
| state | transition | weight (%) | $E$ ($cm^{-1}$) | transition | weight (%) | $E$ ($cm^{-1}$) |
| $T_1$ | $\pi_B(399) \rightarrow \pi^*_B(400)$ | 86 | 9359 | $\pi_B(399) \rightarrow \pi^*_B(400)$ | 91 | 4826 |
| | $\pi_B(399) \rightarrow \pi^*_{B,terpy}(404)$ | 10 | | | | |
| $T_2$ | $d_{Ru}(394) \rightarrow \pi^*_{terpy}(401)$ | 14 | 16339 | $\pi_B(398) \rightarrow \pi^*_B(400)$ | 88 | 14811 |
| | $d_{Ru}(397) \rightarrow \pi^*_B(400)$ | 9 | | | | |
| | $d_{Ru}(397) \rightarrow \pi^*_{B,terpy}(404)$ | 9 | | | | |
| | $\pi_B(399) \rightarrow \pi^*_{terpy}(401)$ | 25 | | | | |
| | $\pi_B(398) \rightarrow \pi^*_B(400)$ | 24 | | | | |
| $T_3$ | $d_{Ru}(397) \rightarrow \pi^*_{terpy}(401)$ | 21 | 16660 | $d_{Ru}(397) \rightarrow \pi^*_B(400)$ | 11 | 15768 |
| | $d_{Ru}(394) \rightarrow \pi^*_B(400)$ | 17 | | $d_{Ru}(394) \rightarrow \pi^*_{terpy}(401)$ | 10 | |
| | $d_{Ru}(394) \rightarrow \pi^*_{B,terpy}(404)$ | 11 | | $d_{Ru}(397) \rightarrow \pi^*_{B,terpy}(402)$ | 7 | |
| | $d_{Ru}(395) \rightarrow \pi^*_{terpy}(401)$ | 7 | | $\pi_B(399) \rightarrow \pi^*_{terpy}(401)$ | 46 | |
| | $\pi_B(399) \rightarrow \pi^*_{B,terpy}(404)$ | 26 | | | | |
| $T_4$ | $\pi_B(398) \rightarrow \pi^*_B(400)$ | 55 | 16792 | $d_{Ru}(397) \rightarrow \pi^*_{terpy}(401)$ | 11 | 15890 |
| | $\pi_B(398) \rightarrow \pi^*_{B,terpy}(404)$ | 11 | | $d_{Ru}(394) \rightarrow \pi^*_B(400)$ | 10 | |
| | | | | $d_{Ru}(394) \rightarrow \pi^*_{B,terpy}(402)$ | 7 | |
| | | | | $\pi_B(399) \rightarrow \pi^*_{B,terpy}(402)$ | 44 | |

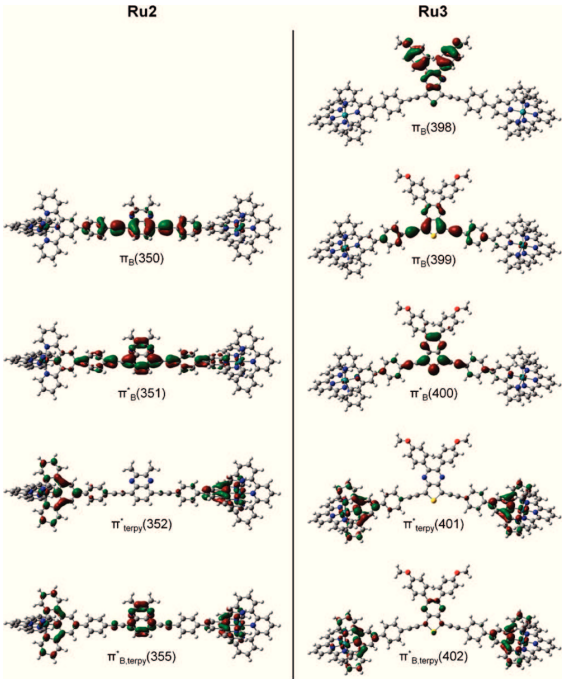


**Figure 4.** Molecular orbitals involved in the dominant configurations of the lowest lying triplet excited states of **Ru2** (left) and **Ru3** (right). The depicted orbitals are calculated at the $T_1$ geometry. Similar orbital shapes and ordering are obtained for the $S_0$ geometry, with the exception that at this geometry $\pi^*_{B,terpy}(355)$ for **Ru2** and $\pi^*_{B,terpy}(402)$ for **Ru3** correspond to the orbitals $\pi^*_{B,terpy}(359)$ and $\pi^*_{B,terpy}(404)$, respectively.

(**Ru3**), respectively; IC in the opposite direction requires much higher activation energy (7280 $cm^{-1}$ for **Ru2** and 8230 $cm^{-1}$ for **Ru3**). Taking into account that **Ru1** contains an electron-donating bridging ligand while **Ru2** and **Ru3** contain electron-accepting ones, there seems to be a correlation between structural parameters and the observed temperature dependence of the luminescence lifetime. Despite this correlation, the electronic character of the involved excited-states cannot be derived from such an energetic analysis. In order to do so, theoretical calculations were performed to gain a more detailed insight into the nature of the triplet excited-states involved in the equilibrium.

**Table 4. Comparison between the Calculated Energy Differences $E(^3MLCT) - E(^3\pi\pi^*)$ ($cm^{-1}$) and the Experimental Activation Energy Differences $\Delta E_5 - \Delta E_4$ ($cm^{-1}$)**

| complex | $S_0$ geometry | $T_1$ geometry | experimental |
|---|---|---|---|
| **Ru2** | 2340 | 6417 | 6340 |
| **Ru3** | 6980 | 10942 | 7910 |

**3.3. Theoretical Investigation of the Lowest Triplet-States.** TDDFT calculations were carried out to determine the lowest singlet−triplet excitation energies and the associated molecular orbital character of the states (Tables 2 and 3). In order to estimate the effect of geometrical relaxation in the excited-state, the calculations were performed at both the singlet ground-state geometry ($S_0$) and at the geometry of the lowest triplet state ($T_1$).

From Table 2 it can be seen that the lowest triplet-state ($T_1$) of **Ru2** mainly involves a transition between the $\pi_B(350)$ and the $\pi^*_B(351)$ orbitals (Figure 4), which are both localized on the center of the bridging ligand (B). Therefore, this state is identified as the ligand-centered $^3\pi\pi^*$ state discussed in the previous sections. Then, the next excited-state ($T_2$) shows a dominant MLCT character, with transitions to orbitals ($\pi^*_B(351)$, $\pi^*_{terpy}(352)$, and $\pi^*_{B,terpy}(355)$) localized both on the center and on the terpyridine groups of the bridging ligand where this state can be identified as the emissive $^3$MLCT state. Additionally, $T_2$ presents a non-negligible contribution of a $\pi\pi^*$ excitation going from the

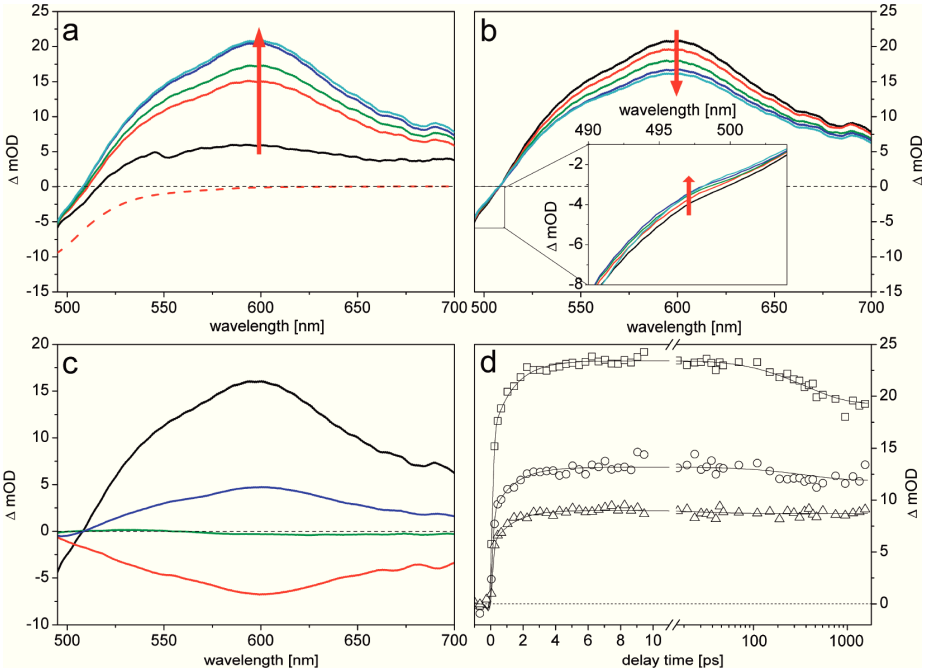


**Figure 5.** Transient-absorption spectra of **Ru1** at 0.1 (black), 0.5 (red), 1 (green), 5 (dark blue), 10 ps (cyan) (panel a) and at 10 (black), 100 (red), 500 ps (green), 1 ns (dark blue) and 1.5 ns (cyan) (panel b) after excitation at 488 nm together with an inverted and normalized absorption spectrum (red dashed line). The inset in panel b highlights the changes in the blue part of the transient-absorption spectra. Panel c compares the decay-associated spectra obtained by global fitting, showing processes on a 1.3 (red), 27 (green), and 361 ps (dark blue) time scale as well as an infinite component (black). Panel d shows three representative transient kinetics at 550 (open triangle), 600 (open circles), and 650 nm (open squares) together with the multiexponential fit (solid lines). The experimentally recorded differential absorption spectra shown were smoothed by a five points smoothing average algorithm[13] to eliminate noise from the spectrometer for better visualization, while the fitting algorithm was applied to the raw data.

center of the bridging ligand ($\pi_B(350)$) to the terpyridines ($\pi^*_{terpy}(352)$). The next triplet excited-state ($T_3$) is found close in energy to $T_2$ and presents a more pronounced MLCT character than $T_2$. Therefore, $T_3$ could be identified as the $^3$MLCT* state. Finally, from Table 2 it can be also noticed that the excitation energy of $T_1$ is significantly decreased when going from the $S_0$ geometry to the $T_1$ geometry. This behavior is associated with the geometrical relaxation occurring in the center of the bridging ligand when going from the $S_0$ to the $T_1$ geometry. In contrast, the $T_2$ and $T_3$ excitation energies show a much smaller decrease in energy between both geometries.

The triplet states obtained for the **Ru3** (Table 3) present comparable characteristics as those obtained for the **Ru2**, as anticipated from the spectroscopic similarities between the two complexes. However, some differences should be mentioned: (i) An additional state with a $\pi\pi^*$ character ($T_4$ at the $S_0$ geometry, $T_2$ at the $T_1$ geometry) is stabilized while going from the $S_0$ to the $T_1$ geometry, and it appears below the MLCT type excitations at the $T_1$ geometry; (ii) $T_1$ is obtained for both geometries at a significantly lower energy in comparison to **Ru2**; (iii) $T_2$ and $T_3$ ($T_3$ and $T_4$ at the $T_1$ geometry) have a more pronounced $\pi\pi^*$ character than **Ru2**. These facts indicate that $\pi\pi^*$ excitations located in the center of the bridging ligand are more stabilized in comparison to **Ru2**. However, despite noticeable $\pi\pi^*$ contributions, the MLCT type excitations show only a limited decrease in their excitation energies with respect to **Ru2**. This fact is in agreement with the similar experimental emission wavelengths obtained for both complexes at about 640 nm. Indeed, the calculated emission wavelengths, which can be estimated from the $^3$MLCT excitation energies, are found nearly constant for **Ru2** and **Ru3** with values of 596 nm (16771 cm$^{-1}$) and 612 nm (16339 cm$^{-1}$) at the $S_0$ geometry and of 623 nm (16044 cm$^{-1}$) and 634 nm (15768 cm$^{-1}$) at the $T_1$ geometry, respectively. This agreement with the experimental emission wavelength, which is about 640 nm for both complexes, is remarkable considering the employed level of theory and the fact that no vibronic structure was included.

It is also of central interest to investigate how the calculated relative energetic positions of the $^3\pi\pi^*$ and $^3$MLCT states correlate to the activation energy differences deduced from the experimental data. Thus, from Table 4 it can be seen that the theoretical energy differences show a reasonable agreement with the experimental activation energy differences. Indeed, the calculated energy of **Ru2** at the $T_1$ geometry (6417 cm$^{-1}$) is in excellent agreement with the experimental value (6340 cm$^{-1}$), whereas the experimental value for **Ru3** (7910 cm$^{-1}$) is in between the calculated energies at the $S_0$ and $T_1$ geometries. It is also obvious that the increase of the experimental activation energy difference going from **Ru2** to **Ru3** is qualitatively reproduced by the calculations and can be associated to the stabilization of the $^3\pi\pi^*$ state for **Ru3**.

A quantitative agreement between theory and experiment can, however, not be expected for such large complexes at the present level of approximations. For example, a better characterization of

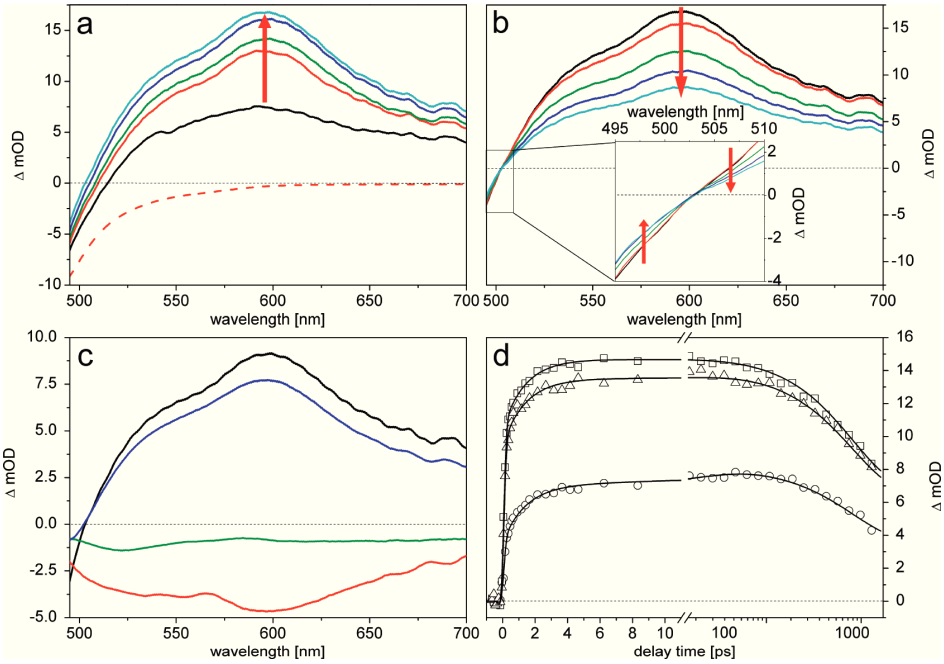


**Figure 6.** Transient-absorption spectra of **Ru2** at 0.1 (black), 0.5 (red), 1 (green), 5 (dark blue), 10 ps (cyan) (panel a) and at 10 (black), 100 (red), 500 ps (green), 1 ns (dark blue) and 1.5 ns (cyan) (panel b) after excitation at 490 nm together with an inverted and normalized absorption spectrum (red dashed line). The inset in panel b highlights the changes in the blue part of the transient-absorption spectra. Panel c compares the decay-associated spectra obtained by global fitting, showing processes on a 1.3 (red), 23 (green), and 813 ps (dark blue) time scale as well as an infinite component (black). Panel d shows representative transient kinetics at 550 (open triangle), 600 (open circles), and 650 nm (open squares) together with the multiexponential fit (solid lines). The experimentally recorded differential absorption spectra shown were smoothed by a five points smoothing average algorithm[13] to eliminate noise from the spectrometer for better visualization, while the fitting algorithm was applied to the raw data.

the emissive state $^3$MLCT would require an optimization of the $T_2$ geometry. However, our attempts in doing so for the **Ru2** complex were not conclusive due to numerical reasons. Nevertheless, it is encouraging to notice that the present calculations are able to identify the nature of the excited-states involved in the unusual emission properties of both complexes and are able to qualitatively reproduce the experimental trends related to the activation energy differences. This highlights the usefulness of theoretical calculations and corroborates the presence of an excited-state equilibrium, which explains the temperature-dependent emission lifetimes of both complexes in the 275−245 K range.

**3.4. Formation of the Excited-State Equilibrium.** It has been reported in recent work on terpyridine−porphyrin architectures[43,44] and dinuclear metal complexes[24,26,25,45] that transitions between triplet-states require orbital overlap of the donor and the acceptor states, which is indicated for the complexes investigated here by TDDFT calculations. Thus, to study the dynamic formation of the excited-state equilibrium, which was discussed to significantly impact the luminescent properties of the complexes at hand, transient-absorption spectroscopy was performed. Following excitation at 488 nm in resonance with the $^1$MLCT transition, white-light differential absorption spectra are recorded for different delay times. This allows the refinement of equilibration time-constants as obtained from TCSPC measurements and the investigation of spectral characteristics of the equilibrium process. Similar to the previous discussion, the data for complex **Ru1** will be presented first (Figure 5).

Figure 5 a and 5b shows the transient absorption spectra of **Ru1** at selected delay times between pump and probe beam, visualizing the overall evolution of the signal. In general, the transient spectra can be divided into two parts: (i) The part below 510 nm shows negative signals where no changes in intensity can be observed during the first 50 ps, while afterward the signal increases; (ii) above 510 nm the signal increases during the first 10 ps after excitation and decays afterward, reaching a constant level for delay times of 1.5 ns. This dynamical behavior can be best fitted using a three-exponential global-fitting routine. The two fastest components are characterized by time constants of 1.3 and 27 ps and show negative amplitudes. In contrast, the decay-associated spectra (DAS) associated with $\tau_3$ = 361 ps exhibits positive contributions with a maximum at 600 nm. Finally, a component with infinite lifetime contributes to the positive signal, representing the superposition of luminescence and excited-state absorption of the long-lived equilibrated triplet states. Due to the limited range of delay times accessible in the experiment, the decay of this state manifests itself as a constant in the analysis.

The observed DAS can be associated to distinct molecular processes based on experiments on the bridging ligand itself and on closely related complexes.[13,46] Directly after excitation of the $^1$MLCT and within the temporal resolution of the experiment, intersystem crossing (ISC) populates the $^3$MLCT state.[29,40] Afterward, the hot $^3$MLCT excited state undergoes cooling,

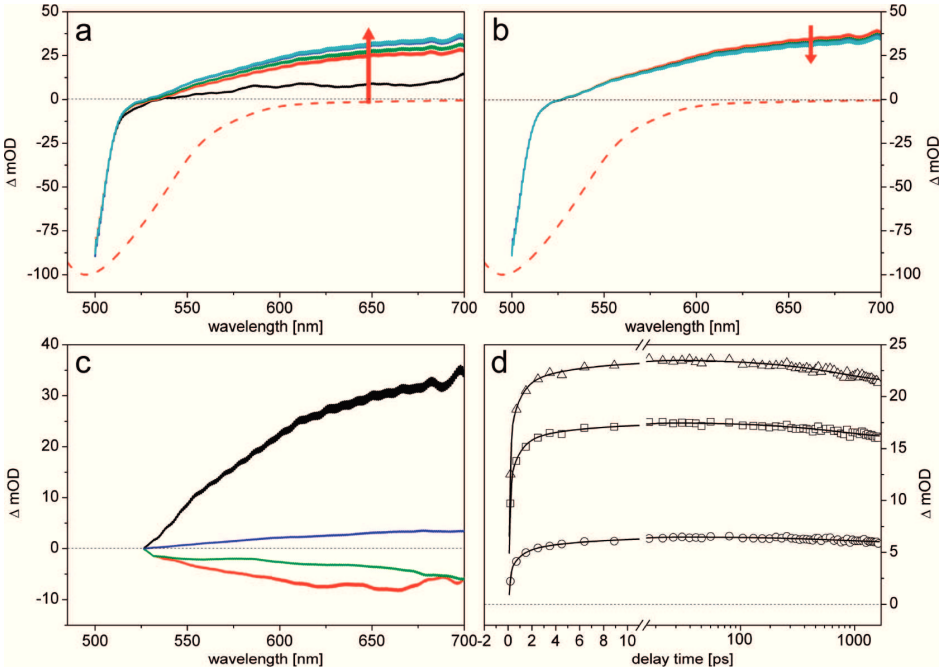


**Figure 7.** Transient-absorption spectra of **Ru3** at 0.1 (black), 0.5 (red), 1 (green), 5 (dark blue), 10 ps (cyan) (panel a) and at 10 (black), 100 (red), 500 ps (green), 1 ns (dark blue) and 1.5 ns (cyan) (panel b) after excitation at 490 nm together with an inverted and normalized absorption spectrum (red dashed line). Panel c compares the decay-associated spectra obtained by global fitting, showing processes on a 0.8 (red), 6 (green), and 788 ps (dark blue) time scale as well as an infinite component (black). Panel d shows representative transient kinetics at 550 (open triangle), 600 (open circles), and 650 (open squares) together with the multiexponential fit (solid lines). The experimentally recorded differential absorption spectra shown were smoothed by a five points smoothing average algorithm[13] to eliminate noise from the spectrometer for better visualization, while the fitting algorithm was applied to the raw data.

assigned to the 1.3 ps process, which is followed by excited-state planarization with a characteristic time constant of 27 ps.[13,46] The latter process reduces the angle between the terpyridine and the adjacent phenyl ring in the bridging ligand[47] and causes an increased excited-state delocalization of the $^3$MLCT over these molecular fragments, forming a thermalized $^3$MLCT state.[48] Typically this thermalized $^3$MLCT state relaxes back to the ground-state either radiatively or nonradiatively.[11] However, in the complexes investigated here an additional process on a 361 ps time scale is observed, which is assigned to the formation of an excited-state equilibrium between the $^3$MLCT and the $^3\pi\pi^*$ excited state. While the $^3\pi\pi^*$ state is located on the conjugated spacer in the bridging ligand, the $^3$MLCT state is centered on the terpyridine sphere and the directly adjacent phenyl ring.

On the basis of the description of the molecular processes leading to the $^3$MLCT$\leftrightarrow^3\pi\pi^*$ equilibrium, we shall now reconsider the spectral characteristics in more detail. Formation of the equilibrium reduces (increases) the population of the $^3$MLCT ($^3\pi\pi^*$) state. Therefore, the differential absorption signal decreases in the range of the $^3$MLCT absorption, i.e., at around 590 nm, and the absorption of the $^3\pi\pi^*$ is expected to increase. On the basis of previous studies on the free ligand,[49] estimations on the triplet-absorption energies in *p*-phenylenevinylene oligomers,[50,51] and assessment of work on PPV oligomers,[31] the $^3\pi\pi^*$ of the bridging ligand in **Ru1** should absorb below 620 nm.[49] Despite the expected overlap between $^3$MLCT and $^3\pi\pi^*$ absorptions, a spectral region can be identified in the data (Figure 5), in which the extinction coefficient of the $^3\pi\pi^*$ state exceeds the one of the $^3$MLCT state, i.e., at around 495 nm. In this spectral region an increase in the differential absorption signal appears correlated with the decay of the broad positive differential absorption band at 590 nm assigned to $^3$MLCT absorption. This shift of excited-state absorption from 590 to 495 nm occurs on the 361 ps time scale and is a characteristic feature for the formation of the $^3$MLCT$\leftrightarrow^3\pi\pi^*$ equilibrium.

The electronic structure of the ligands strongly impacts the photophysical properties of Ru−bis-terpyridine complexes. Therefore, **Ru2** and **Ru3** bearing electron-poor ligands are investigated in the following. The experimental data are depicted in Figures 6 and 7.

The differential absorption dynamics of **Ru2** and **Ru3** generally show comparable features to those obtained for **Ru1** (see Figure 5): Negative signals below 510 nm are accompanied by positive bands at longer wavelength, and the excited-state absorption rises during the first 10 to 20 ps after excitation and decreases afterward on a several hundred picosecond time scale, leveling off after a few nanoseconds. The characteristic time constants to describe this dynamical behavior are summarized in Table 5.

Despite these similarities, a notable difference between the differential absorption data of **Ru2** and **Ru3** is found: For **Ru2** a signal increase at 500 nm accompanies the decay of the main band at 600 nm on a 813 ps time scale. Such a feature is absent for **Ru3**. Nonetheless, the spectral shift in the transient absorption spectra of **Ru2** corresponds to the population of the

**Table 5. Comparison of the Characteristic Time Constants for the Observed Excited-State Relaxation Processes Obtained from Global Fitting of the Transient-Absorption Data ($\tau_1$, $\tau_2$, and $\tau_3$) and from TCSPC Experiments ($\tau_4$)**

| sample | $\tau_1$ (ps) | $\tau_2$ (ps) | $\tau_3$ (ps) | $\tau_4$ (ns) |
|---|---|---|---|---|
| **Ru1** | 1.3 | 27 | 361 | 145 |
| **Ru2** | 1.2 | 23 | 813 | 187 |
| **Ru3** | 0.8 | 6 | 788 | 223 |

$^3\pi\pi^*$ upon the decay of the $^3$MLCT. The spectral position of the $^3\pi\pi^*$ absorption maximum matches well with estimates based on work by Warman and co-workers[50,51] (see also Supporting Information). For **Ru3** the differential absorption signatures do not show a maximum in the visible spectral range, but the signal intensity increases toward the near-IR edge of the probing window. Furthermore, for **Ru3** the build-up of an excited-state absorption band in concert with the decay of the main band ($\tau_3$ = 788 ps) is not observed. On the basis of the estimation of the $^3\pi\pi^*$ absorption based on related polymeric systems (see Supporting Information), we suppose that the **Ru3**-$^3\pi\pi^*$ state absorbs only in the near-IR spectral region at roughly 1000 nm; hence, the characteristic turnover between two distinctly absorbing electronic states upon the formation of the excited-state equilibrium is not observed with our experimental settings.

On the basis of these considerations, it can be concluded that the formation of the excited-state equilibrium between the $^3$MLCT and a $^3\pi\pi^*$ state could be directly resolved by transient absorption spectroscopy. The kinetic analysis reveals time constants for this process ranging from 361 (**Ru1**, electron-rich bridging ligand) to roughly 800 ps (**Ru2** and **Ru3**, electron-poor bridging ligands). Notably, the complexes with electron-poor bridging ligands show a slower formation of the equilibrium. This is attributed to the different electronic situations introduced by the heterocycles of the ligands. The spectral characteristics associated with the formation of the $^3$MLCT$\leftrightarrow^3\pi\pi^*$ equilibrium show for **Ru1** and **Ru2** a clear transition between two distinct states. However, for **Ru3** only the decay of the $^3$MLCT state by its characteristic absorption features is observed, as the $^3\pi\pi^*$ state is expected to absorb outside the probe window accessible in the experiment.

## 4. CONCLUSION

The formation of an excited-state equilibrium in dinuclear bisterpyridine Ru-complexes bearing electron-poor bridging ligands has been investigated in a joint experimental and theoretical study. The time-resolved spectroscopic data point toward the presence of an excited-state equilibrium between the emitting $^3$MLCT state and a ligand-centered $^3\pi\pi^*$ excited-state. The population of the latter $^3\pi\pi^*$ state increases the observed luminescence lifetime by serving as a reservoir for the emissive $^3$MLCT state. For the complexes with electron-poor bridging ligands, temperature-dependent time-correlated single-photon data can be used to detail the excited-state topology, i.e., the activation energies needed for interconversion of various excited-states. The deduced experimental activation energy differences are in reasonable agreement with the theoretical results. While the experimental data only show the existence of an equilibrium between the luminescent $^3$MLCT and a secondary triplet state, the nature of this secondary triplet state as a $^3\pi\pi^*$ state is inferred from the TDDFT calculations. A complex with an electron-rich bridging ligand (**Ru1**) did not reveal the characteristic turnover of the luminescence lifetime as a function of temperature, which was indicative of the excited-state equilibrium in the case of the other complexes. Nevertheless, a $^3\pi\pi^*$ is assumed to contribute to the luminescence properties of this compound, because of its quite long room-temperature emission lifetime. Femtosecond transient absorption spectroscopy was used to yield direct insight into the formation kinetics of the $^3$MLCT$\leftrightarrow^3\pi\pi^*$ equilibrium. This process shows spectral characteristics revealing the partial disappearance of one state and the population of a second one. The respective characteristic time constants vary from 360 ps for the reference compound **Ru1** to roughly 800 ps for the complexes bearing an electron-poor bridging ligand. This value is in agreement with rates obtained from fitting the temperature-dependent TCSPC data. The work at hand significantly refines the photophysical picture established for such complexes in detailing the nature of the excited-triplet states characteristic for the photophysical properties of the dinuclear ruthenium-bisterpyridine complexes and adding information on the topology of the triplet manifold.

## ■ ASSOCIATED CONTENT

**Supporting Information.** Luminescence-excitation spectra, a detailed description of the fit of the temperature-dependent lifetime data, and an estimation of the energy for excited-state triplet−triplet absorption. This material is available free of charge via the Internet at http://pubs.acs.org.

## ■ AUTHOR INFORMATION

**Corresponding Author**

*E-mail: leticia.gonzalez@uni-jena.de (L.G.); benjamin.dietzek@uni-jena.de (B.D.).

## ■ ACKNOWLEDGMENT

Financial support from the Fonds der Chemischen Industrie, the Carl Zeiss Stiftung, the Dutch Polymer Institute, the Nederlandse Organisatie voor Wetenschappelijk Onderzoek (VICI award for U.S.S.), and the Thüringer Ministerium für Bildung, Wissenschaft und Kultur (grant no. B 514-09049, PhotoMIC) for this work is greatly appreciated. All the calculations have been performed at the Universitätsrechenzentrum of the Friedrich-Schiller-University Jena.

## ■ REFERENCES

(1) Thompson, B. C.; Fréchet, J. M. J. *Angew. Chem., Int. Ed.* **2008**, *120*, 62–82.
(2) Duprez, V.; Biancardo, M.; Spanggaard, H.; Krebs, F. C. *Macromolecules* **2005**, *38*, 10436–10448.
(3) Kelch, S.; Rehahn, M. *Macromolecules* **1999**, *32*, 5818–5828.
(4) Schlütter, F.; Wild, A.; Winter, A.; Hager, M. D.; Baumgaertel, A.; Friebe, C.; Schubert, U. S. *Macromolecules* **2010**, *43*, 2759–2771.
(5) Wild, A.; Friebe, C.; Winter, A.; Hager, M. D.; Grummt, U. W.; Schubert, U. S. *Eur. J. Org. Chem.* **2010**, 1859–1868.
(6) Wild, A.; Schlütter, F.; Pavlov, G. M.; Friebe, C.; Festag, G.; Winter, A.; Hager, M. D.; Cimrová, V.; Schubert, U. S. *Macromol. Rapid Commun.* **2010**, *31*, 868–874.
(7) Presselt, M.; Dietzek, B.; Schmitt, M.; Popp, J.; Winter, A.; Chiper, M.; Friebe, C.; Schubert, U. S. *J. Phys. Chem. C* **2008**, *112*, 18651–18668.

(8) Winter, A.; Friebe, C.; Chiper, M.; Schubert, U. S.; Presselt, M.; Dietzek, B.; Schmitt, M.; Popp, J. *Chem. Phys. Chem.* **2009**, *10*, 787–798.
(9) Amini, A.; Harriman, A.; Mayeux, A. *Phys. Chem. Chem. Phys.* **2004**, *6*, 1157–1164.
(10) Lumpkin, R. S.; Kober, E. M.; Worl, L. A.; Murtaza, Z.; Meyer, T. J. *J. Phys. Chem.* **1990**, *94*, 239–243.
(11) Sauvage, J. P.; Collin, J. P.; Chambron, J. C.; Guillerez, S.; Courdet, C.; Balzani, V.; Barigelletti, F.; De Cola, L.; Flamigni, L. *Chem. Rev.* **1994**, *94*, 993–1019.
(12) Medlycott, E. A.; Hanan, G. S. *Chem. Soc. Rev.* **2005**, *34*, 133–142.
(13) Siebert, R.; Winter, A.; Schubert, U. S.; Dietzek, B.; Popp, J. *Phys. Chem. Chem. Phys.* **2011**, *13*, 1606–1617.
(14) Wang, X.; Del Guerzo, A.; Schmehl, R. H. *Photochem. Rev.* **2004**, *5*, 55–77.
(15) Lainé, P. P.; Campagna, S.; Loiseau, F. *Coord. Chem. Rev.* **2008**, *252*, 2552–2571.
(16) Hissler, M.; Harriman, A.; Khatyr, A.; Ziessel, R. *Chem.—Eur. J.* **1999**, *5*, 3366–3381.
(17) McClenaghan, N. D.; Leydet, Y.; Maubert, B.; Indelli, M. T.; Campagna, S. *Coord. Chem. Rev.* **2005**, *249*, 1336–1350.
(18) Brennaman, M. K.; Alstrum-Acevedo, J. H.; Fleming, C. N.; Jang, P.; Meyer, T. J.; Papanikolas, J. M. *J. Am. Chem. Soc.* **2002**, *124*, 15094–15098.
(19) Brennaman, M. K.; Meyer, T. J.; Papanikolas, J. M. *J. Phys. Chem. A* **2004**, *108*, 9938–9944.
(20) Kuhnt, C.; Karnahl, M.; Tschierlei, S.; Griebenow, K.; Schmitt, M.; Schäfer, B.; Krieck, S.; Görls, H.; Rau, S.; Dietzek, B.; Popp, J. *Phys. Chem. Chem. Phys.* **2010**, *12*, 1357–1368.
(21) Henrich, J. D.; Zhang, H.; Dutta, P. K.; Kohler, B. *J. Phys. Chem. B* **2010**, *114*, 14679–14688.
(22) Sun, Y.; El Ojaimi, M.; Hammitt, R.; Thummel, R. P.; Turro, C. *J. Phys. Chem. B* **2010**, *114*, 14664–14670.
(23) Sun, Y.; Liu, Y.; Turro, C. *J. Am. Chem. Soc.* **2010**, *132*, 5594–5595.
(24) El-ghayoury, A.; Harriman, A.; Khatyr, A.; Ziessel, R. *J. Phys. Chem. A* **2000**, *104*, 1512–1523.
(25) Benniston, A. C.; Harriman, A. *Coord. Chem. Rev.* **2008**, *252*, 2528–2539.
(26) El-Ghayoury, A.; Harriman, A.; Ziessel, R. *J. Phys. Chem. A* **2000**, *104*, 7906–7915.
(27) Dietzek, B.; Kiefer, W.; Blumhoff, J.; Böttcher, L.; Rau, S.; Walther, D.; Uhlemann, U.; Schmitt, M.; Popp, J. *Chem.—Eur. J.* **2006**, *12*, 5105–5115.
(28) Tschierlei, S.; Presselt, M.; Kuhnt, C.; Yartsev, A.; Pascher, T.; Sundström, V.; Karnahl, M.; Schwalbe, M.; Schäfer, B.; Rau, S.; Schmitt, M.; Dietzek, B.; Popp, J. *Chem.—Eur. J.* **2009**, *15*, 7678–7688.
(29) Gawelda, W.; Cannizzo, A.; Pham, V. T.; van Mourik, F.; Bressler, C.; Chergui, M. *J. Am. Chem. Soc.* **2007**, *129*, 8199–8206.
(30) Benniston, A. C.; Chapman, G.; Harriman, A.; Mehrabi, M.; Sams, C. A. *Inorg. Chem.* **2004**, *43*, 4227–4233.
(31) Seixas de Melo, J.; Pina, J.; Burrows, H. D.; Di Paolo, R. E.; Macanita, A. L. *Chem. Phys.* **2006**, *330*, 449–456.
(32) Winter, A.; Friebe, C.; Hager, M. D.; Schubert, U. S. *Eur. J. Org. Chem.* **2009**, 801–809.
(33) Frisch, M. J.; Trucks, G. W.; Schlegel, H. B.; Scuseria, G. E.; Robb, M. A.; Cheeseman, J. R.; Scalmani, G.; Barone, V.; Mennucci, B.; Petersson, G. A.; Nakatsuji, H.; Caricato, M.; Li, X.; Hratchian, H. P.; Izmaylov, A. F.; Bloino, J.; Zheng, G.; Sonnenberg, J. L.; Hada, M.; Ehara, M.; Toyota, K.; Fukuda, R.; Hasegawa, J.; Ishida, M.; Nakajima, T.; Honda, Y.; Kitao, O.; Nakai, H.; Vreven, T.; Montgomery, J. A.; Peralta, J. E.; Ogliaro, F.; Bearpark, M.; Heyd, J. J.; Brothers, E.; Kudin, K. N.; Staroverov, V. N.; Kobayashi, R.; Normand, J.; Raghavachari, K.; Rendell, A.; Burant, J. C.; Iyengar, S. S.; Tomasi, J.; Cossi, M.; Rega, N.; Millam, J. M.; Klene, M.; Knox, J. E.; Cross, J. B.; Bakken, V.; Adamo, C.; Jaramillo, J.; Gomperts, R.; Stratmann, R. E.; Yazyev, O.; Austin, A. J.; Cammi, R.; Pomelli, C. J.; Ochterski, W.; Martin, R. L.; Morokuma, K.; Zakrzewski, V. G.; Voth, G. A.; Salvador, P.; Dannenberg, J. J.; Dapprich, S.; Daniels, A. D.; Farkas, Ö.; Foresman, J. B.; Ortiz, J. V.; Cioslowski, J.; Fox, D. J. *Gaussian 09 (Revision A.02)*; Gaussian, Inc., Wallingford, CT, 2009.
(34) Becke, A. D. *J. Chem. Phys.* **1993**, *98*, 5648–5652.
(35) Lee, C.; Yang, W.; Parr, R. G. *Phys. Rev. B* **1988**, *37*, 785–789.
(36) Andrae, D.; Häußermann, U.; Dolg, M.; Stoll, H.; Preuß, H. *Theor. Chim. Acta* **1990**, *77*, 123–141.
(37) Tomasi, J.; Mennucci, B.; Cammi, R. *Chem. Rev.* **2005**, *105*, 2999–3094.
(38) Stone, M. L.; Crosby, G. A. *Chem. Phys. Lett.* **1981**, *79*, 169–173.
(39) Damrauer, N. H.; Cerullo, G.; Yeh, A.; Boussie, T. R.; Shank, C. V.; McCusker, J. K. *Science* **1997**, *275*, 54–57.
(40) Bressler, C.; Milne, C.; Pham, V. T.; El-Nahhas, A.; van der Veen, R. M.; Gawelda, W.; Johnson, S.; Beaud, P.; Grolimund, D.; Kaiser, M.; Borca, C. N.; Ingold, G.; Abela, R.; Chergui, M. *Science* **2009**, *323*, 489–492.
(41) Yersin, H.; Gallhuber, E.; Vogler, A.; Kunkelyt, H. *J. Am. Chem. Soc.* **1983**, *105*, 4155–4156.
(42) Hecker, C. R.; Guthurst, A. K. I.; McMillin, D. R. *Inorg. Chem.* **1991**, *30*, 538–541.
(43) Benniston, A. C.; Harriman, A.; Pariani, C.; Sams, C. A. *Phys. Chem. Chem. Phys.* **2006**, *8*, 2051–2057.
(44) Benniston, A. C.; Harriman, A.; Pariani, C.; Sams, C. A. *J. Phys. Chem. A* **2007**, *111*, 8918–8924.
(45) Benniston, A. C.; Harriman, A.; Li, P.; Sams, C. A. *J. Am. Chem. Soc.* **2005**, *127*, 2553–2564.
(46) Siebert, R.; Winter, A.; Schubert, U. S.; Dietzek, B.; Popp, J. *J. Phys. Chem. C* **2010**, *114*, 6841–6848.
(47) Presselt, M.; Dietzek, B.; Schmitt, M.; Rau, S.; Winter, A.; Jäger, M.; Schubert, U. S.; Popp, J. *J. Phys. Chem. A* **2010**, *114*, 13163–13174.
(48) Meylemans, H. A.; Damrauer, N. H. *Inorg. Chem.* **2009**, *48*, 11161–11175.
(49) Siebert, R.; Akimov, D.; Schmitt, M.; Winter, A.; Schubert, U. S.; Dietzek, B.; Popp, J. *ChemPhysChem* **2009**, *10*, 910–919.
(50) Candeias, L. P.; Wildeman, J.; Hadziioannou, G.; Warman, J. *J. Phys. Chem. B* **2000**, *104*, 8366–8371.
(51) Gelinck, G. H.; Piet, J. J.; Wegewijs, B. R.; Müllen, K.; Wildeman, J.; Hadziioannou, G.; Warman, J. *Phys. Rev. B* **2000**, *62*, 1489–1491.

# [RS6] Ruthenium(II)-bis(4‘-(4-ethinylphenyl)-2,2‘:6‘,2“ -terpyridine) - A Versatile Synthon in Supramolecular Chemistry. Synthesis and Characterization


R. Siebert, F. Schlütter, A. Winter, M. Presselt, H. Görls, U. S. Schubert, B. Dietzek, J. Popp, Ruthenium(II)-*bis*(4‘-(4-ethinylphenyl)-2,2‘:6‘,2“-terpyridine) - A Versatile Synthon in Supramolecular Chemistry. Synthesis and Characterization. *Cent. Eur. J. Chem.*, **2011**, 9, online.



## Autorenschaft der Publikation

| | |
|---|---|
| Ronald Siebert | stationäre Absorptions- und Emissionsspektroskopie, zeitaufgelöste Emissionsspektroskopie bei 77K, Resonanz-Ramanspektroskopie, Auswertung der Daten, Ergebnisdiskussion und Erstellung des Manuskripts |
| Florian Schlütter | Synthese und Charakterisierung eines Teils der verwendeten Substanzen |
| Andreas Winter | Synthese und Charakterisierung eines Teils der verwendeten Substanzen, Diskussion und Korrektur des Manuskripts |
| Martin Presselt | DFT-Rechnungen mit entsprechender Modenzuordnung, Diskussion und Korrektur des Manuskripts |
| Helmar Görls | Röntgenstrukturanalyse eines der untersuchten Metallkomplexe |
| Ulrich S. Schubert | Projektleitung, Konzept- und Ergebnisdiskussion, Diskussion und Korrektur des Manuskripts |
| Benjamin Dietzek | Projektleitung, Konzept- und Ergebnisdiskussion, Diskussion und Korrektur des Manuskripts |
| Jürgen Popp | Konzept- und Ergebnisdiskussion, Diskussion und Korrektur des Manuskripts |

Cent. Eur. J. Chem.
DOI: 10.2478/s11532-011-0087-6

VERSITA

Central European Journal of **Chemistry**

# Ruthenium(II)-*bis*(4'-(4-ethynylphenyl)-2,2':6',2''-terpyridine) – A versatile synthon in supramolecular chemistry. Synthesis and characterization

**Research Article**

Ronald Siebert[1], Florian Schlütter[2], Andreas Winter[2], Martin Presselt[3], Helmar Görls[4], Ulrich S. Schubert[2,5*], Benjamin Dietzek[1,6**], Jürgen Popp[1,6]

[1]*Institute for Physical Chemistry, Jena Center for Soft Matter (JCSM), and Abbe Center of Photonics (ACP) Friedrich-Schiller-University Jena, 07743 Jena, Germany*

[2]*Laboratory of Organic and Macromolecular Chemistry (IOMC) and Jena Center for Soft Matter (JCSM) Friedrich-Schiller-University Jena, 07743 Jena, Germany*

[3]*Institute for Physics, Ilmenau University of Technology, 98693 Ilmenau, Germany*

[4]*Laboratory of Inorganic and Analytical Chemistry, Friedrich-Schiller-University Jena, 07743 Jena, Germany*

[5]*Dutch Polymer Institute (DPI) P.O. Box 902, 5600 AX Eindhoven, The Netherlands*

[6]*Institute of Photonic Technology (IPHT) Jena, 07745 Jena, Germany*

**Received 26 May 2011; Accepted 29 June 2011**

**Abstract:** A homoleptic ethynyl-substituted ruthenium(II)-*bis*terpyridine complex representing a versatile synthon in supramolecular chemistry was synthesized and analyzed by NMR spectroscopy, mass spectrometry and X-ray diffractometry. Furthermore, its photophysical properties were detailed by UV/Vis absorption, emission and resonance Raman spectroscopy. In order to place the results obtained in the context of the vast family of ruthenium coordination compounds, two structurally related complexes were investigated accordingly. These reference compounds bear either no or an increased chromophore in the 4`-position. The spectroscopic investigations reveal a systematic bathochromic shift of the absorption and emission maximum upon increasing chromophore size. This bathochromic shift of the steady state spectra occurs hand in hand with increasing resonance Raman intensities upon excitation of the metal-to-ligand charge-transfer transition. The latter feature is accompanied by an increased excitation delocalization over the chromophore in the 4`-position of the terpyridine. Thus, the results presented allow for a detailed investigation of the electronic effects of the ethynyl substituent on the metal-to-ligand charge-transfer states in the synthon for click reactions leading to coordination polymers.

**Keywords:** •



## 1. Introduction

Coordination polymers derived from transition metal ions and *bis*-terpyridine ligands are in the spotlight of smart-material research due to their widely tunable electronic and spectroscopic properties [1]. The tunability of the spectroscopic properties is achieved by varying the electronic structure of the terpyridine ligand or the connecting metal ion. These degrees of freedom open a doorway for potential applications of coordination polymers in the field of optoelectronic applications, *i.e.*, as in OLEDs or in polymer solar cells [2-6]. First ruthenium based coordination polymers have been synthesized in the 1990's [1]. Since then a rapidly

* *E-mail: ulrich.schubert@uni-jena.de*
** *E-mail: benjamin.dietzek@uni-jena.de*

growing variety of coordination polymers and oligomers based on transition metals and *bis*-terpyridine ligands have been reported [1,7-11]. The most common synthetic approach to coordination polymers and oligomers is polymerization of a *bis*-terpyridine in solution by adding metal salts and subsequent heating. Beside this widely used approach, several other strategies to create supramolecular architectures exist, *i.e.*, interconnecting of mononuclear terpyridine complexes by the formation of covalent bonds between substituents in the periphery of the terpyridine ligand. These approaches include, *e.g.*, the connection of small ruthenium(II)-*bis*terpyridine synthons by electrochemical polymerization [12], polycondensation [4], or Heck and Suzuki reactions [3,13,14]. It has further been demonstrated that click reactions can be utilized to this end [15]. This highly efficient and mild reaction was recently introduced as a synthetic tool in (supramolecular) polymer chemistry [16,17]. There, ethynyl-substituted terpyridines represent versatile substrates for the formation of 1*H*-1,2,3-triazoles by reaction with azide-functionalized derivatives (small organic molecules as well as macromolecules). Nevertheless, the synthesis of homoleptic mononuclear ruthenium(II)-*bis*terpyridine complexes, with side chains applicable for click reactions, presents an unsolved problem up to now. Herein the synthesis and characterization of a versatile precursor (**Ru2**, see Fig. 1) for coordination polymers to be derived by click reactions is presented. Furthermore, the synthon's photophysical properties are investigated by means of absorption and emission spectroscopy as well as resonance Raman spectroscopy. The spectroscopic results obtained are placed into context by a comparative evaluation of two reference complexes (**Ru1** and **Ru3**, see Fig. 1) bearing either no or an extended conjugated chromophore in the 4'-position of the terpyridine unit.

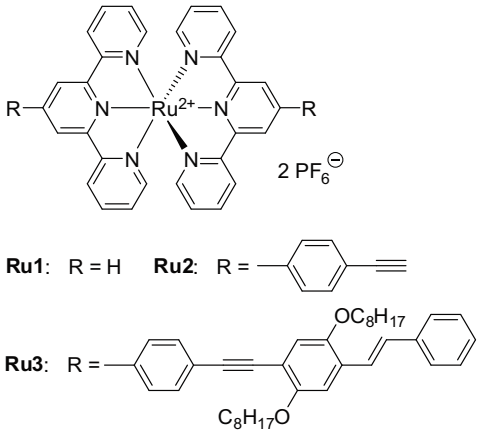


**Figure 1.** Molecular structure of the mononuclear ruthenium complexes (Ru1-Ru3), investigated in this contribution. Ru2 bears an ethynyl function rendering it a suitable reactant for click reactions.

# 2. Experimental procedure

## 2.1. General

All chemicals were of reagent grade, purchased from commercial suppliers and used as received unless specified otherwise. The solvents were purchased from Biosolve and were dried and distilled according to standard procedures. Chromatographic separation was performed with standardized silica gel 60 (Merck); the reaction progress was controlled by thin layer chromatography (TLC) using aluminum sheets pre-coated with silica gel 60 F254 (Merck). Microwave-assisted reactions were carried out in a Biotage Initiator ExpEU (max. power: 400 W, frequency: 2.450 MHz) using closed reaction vials. During the reaction, the temperature and the pressure profiles were detected. The synthesis and characterization of **Ru1** and **Ru3** has been reported elsewhere in detail [38,49]. 4'-(4-Ethynylphenyl)-2,2':6',2''-terpyridine [22], (*E*)-4-(4-((2,5-*bis*(octyloxy)-4-styrylphenyl)ethynyl)phenyl)-2,2':6',2''-terpyridine [50] and $Ru(DMSO)_4Cl_2$ [20] were prepared according to the literature.

## 2.2. Instrumentation

$^1$H NMR spectra were recorded on a Bruker AC 300 spectrometer (300 MHz) at 298 K; chemical shifts are reported in parts per million (ppm, $\delta$ scale) relative to the residual signal of the deuterated solvent; the coupling constants are given in Hz. Matrix-assisted laser desorption/ionization time-of-flight (MALDI-ToF) mass spectra were obtained from an Ultraflex III TOF/TOF mass spectrometer by dithranol as matrix in reflector and linear mode. Elemental analyses were carried out on a CHN-932 Automat Leco instrument. UV/Vis absorption spectra were measured using a UV-Vis-NIR Spectrometer (Model Varian Cary 5000), while emission spectra at 77 K were acquired using a spectrofluorimeter (Model Perkin Ellmer LS50-B). Resonance Raman spectra were measured with a conventional 90°-scattering arrangement. The lines of an argon ion laser (Model Coherent Innova 300C MotoFred Ion Laser) were used for excitation. A rotating cell was utilized to prevent heating of the samples. The scattered light was collected by a lens and focused to the slit of an Acton SpectraPro 2758i spectrometer, which was assembled with a back illuminated CCD from Princeton instruments. No changes in the absorption spectra could be observed after exposure to resonant laser light.

**Ru2:** A suspension of $Ru(DMSO)_4Cl_2$ (60 mg, 0.12 mmol) and 4'-(4-ethynylphenyl)-2,2':6',2''-terpyridine (83 mg; 0.24 mmol) in ethanol (15 mL) was degassed with argon for 2 hours. This mixture was heated under microwave irradiation for 2.5 hours at 105°C. After filtration and dilution with water an excess of $NH_4PF_6$ (150 mg) was added to precipitate the crude product. Final purification was achieved by column chromatography (silica gel, eluent: $CH_3CN/H_2O$/sat. aq. $KNO_3$ 40:4:1). The combined fractions were dissolved in an ethanol/acetonitrile mixture, filtrated and an excess of $NH_4PF_6$ (150 mg) was added to precipitate the product. Filtration and intensive washing with water, ethanol and methanol yielded the desired complex as red powder (40 mg, 0.04 mmol, 32%). Single crystals were obtained by slow diffusion of diethyl ether into a concentrated solution of **Ru2** in $CH_3CN$. $^1H$ NMR (300 MHz, $CD_3CN$, 25 °C): $\delta$ = 9.01 (s, 4 H), 8.66 (d, $J$ = 7.6 Hz, 4 H), 8.22 (d, $J$ = 8.3 Hz, 4 H), 7.95 (t, $J$ = 8.3 Hz, 4 H), 7.88 (d, $J$ = 8.3 Hz, 4 H), 7.44 (d, $J$ = 4.9 Hz, 4 H), 7.19 (t, $J$ = 6.3 Hz, 4 H), 3.66 (s, 2 H). MALDI-ToF MS (dithranol): $m/z$ = 913.15 [M-$(PF_6)^+$], 768.17 [M-2$(PF_6)^+$]. $C_{46}H_{30}F_{12}N_6P_2Ru$ (1057.77): calcd. C 52.53, H 2.86, N 7.95; found C 52.18, H 2.57, N 7.62.

**Ru3:** As reported in [38], a suspension of (*E*)-4-(4-((2,5-*bis*(octyloxy)-4-styrylphenyl)ethynyl) phenyl)-2,2':6',2''-terpyridine (76.8 mg, 0.1 mmol) and $Ru(DMSO)_4Cl_2$ (24.2 mg, 0.05 mmol) in ethanol (10 mL) was heated under microwave irradiation at 120°C for one hour. The red solution was filtered and the filtrate was treated with an excess of $NH_4PF_6$. After stirring at room temperature, the precipitate was filtered off. The crude product was purified by preparative size exclusion chromatography (SX-3 BioBeads™, acetone as eluent), followed by precipitation into diethyl ether to yield **Ru3** as a deep red powder (81.0 mg, 84%). $^1H$ NMR ($d_6$-acetone, 300 MHz): $\delta$ = 9.50 (s, 4H), 9.07 (d, $^3J$ = 8.1 Hz, 4H), 8.44 (d, $^3J$ = 8.3 Hz, 4H), 8.11 ($m_c$, 4H), 7.88 (d, $^3J$ = 8.6 Hz, 4H), 7.84 (d, $^3J$ = 6.1 Hz, 4H), 7.65–7.56 (m, 10H), 7.46 ($m_c$, 4H), 7.41 ($m_c$, 4H), 7.36 ($m_c$, 4H), 7.20 (s, 2H), 4.23 (t, $^3J$ = 6.1 Hz, 4H), 4.14 (t, $^3J$ = 6.6 Hz, 4H), 1.91 ($m_c$, 8H), 1.64 ($m_c$, 4H), 1.46 ($m_c$, 4H), 1.42–1.25 (m, 32H), 0.91 ($m_c$, 12H). MALDI-TOF MS (dithranol): $m/z$ = 1871.90 ([M–$PF_6]^+$), 1726.84 (M–$(PF_6)_2]^+$). $C_{106}H_{114}F_{12}N_6O_4P_2Ru$ (1927.08): Calcd. C 66.07, H 5.96, N 4.36; Found C 65.81, H 6.32, N 4.68.

## 2.3. Crystal structure determination.

The intensity data were collected on a Nonius Kappa CCD diffractometer, using graphite-monochromated Mo-$K_\alpha$ radiation. Data were corrected for Lorentz and polarization effects, but not for absorption [51,52]. The structure was solved by direct methods (SHELXS) and refined by full-matrix least squares techniques against $Fo^2$ (SHELXL-97). Only the hydrogen atoms at *C*3 and *C*8 were included at calculated positions with fixed thermal parameters. All other hydrogen atoms were located by difference Fourier synthesis and refined isotropically [52]. XP (SIEMENS Analytical X-ray Instruments, Inc.) was used for structure representations.

### 2.3.1. Crystal data for Ru2.

$[C_{46}H_{30}N_6Ru]^{2+}$, 2 $[F_6P]^-$, 0.5 $C_2H_3N$, $M_r$ = 1078.30 g mol$^{-1}$, Bordeaux-red prism, size 0.04×0.04×0.04 mm$^3$, triclinic, space group P$\bar{1}$, $a$ = 9.1841(2), $b$ = 12.5232(3), $c$ = 19.7614(5) Å, $\alpha$ = 96.969(2), $\beta$ = 99.435(2), $\gamma$ = 92.532(1)°, V = 2220.76(9) Å$^3$, T= -140°C, $Z$ = 2, $\rho_{calcd.}$ = 1.613 g cm$^{-3}$, μ (Mo-$K_\alpha$) = 5.19 cm$^{-1}$, F(000) = 1082, 15004 reflections in h(-11/11), k(-16/16), l(-25/21), measured in the range 2.65° ≤ Θ ≤ 27.52°, completeness $\Theta_{max}$ = 95.6%, 9755 independent reflections, $R_{int}$ = 0.0269, 8757 reflections with $F_o > 4\sigma(F_o)$, 665 parameters, 0 restraints, $R1_{obs}$ = 0.0518, $wR^2_{obs}$ = 0.1275, $R1_{all}$ = 0.0603, $wR^2_{all}$ = 0.1367, GOOF = 1.053, largest difference peak and hole: 1.101 / -1.162 e Å$^{-3}$.

# 3. Results and discussion

## 3.1. Synthesis and characterization.

Various methods for the preparation of ruthenium(II)-*bis*terpyridine complexes are known in the literature. In most cases, $RuCl_3 \bullet xH_2O$ is utilized for the synthesis of homoleptic (under reducing conditions in a one-step procedure) or heteroleptic species (in a directed two-step protocol) [11,18,19]. However, the comparably harsh reaction conditions often hinder the accessibility of complexes bearing (thermo)sensitive ligands. In order to overcome this limitation, Ziessel and co-workers introduced $Ru(DMSO)_4Cl_2$, as a versatile precursor complex, for the synthesis of ruthenium-*bis*tridentate complexes under relatively mild conditions [20,21]. The ethynyl moiety is a common structural motif in many terpyridine ligands with extended π-conjugated substituents (*e.g.* in so-called "molecular wires" or in arrays for artificial photosynthesis), but the homoleptic parent complex **Ru2** has not been described in the literature before.

The synthesis of **Ru2** has been carried out in moderate yield (32%) under microwave irradiation in degassed ethanol, utilizing $Ru(DMSO)_4Cl_2$ and 4'-(4-ethynylphenyl)-2,2':6',2''-terpyridine [22], as ligand. **Ru2** was characterized by $^1H$ NMR spectroscopy, MALDI-TOF mass spectrometry and elemental analysis (see supporting information for details). Moreover, single crystals suited for X-ray structure analysis have been

obtained, revealing the distorted octahedral geometry of the complex (Fig. 2). The structural parameters of **Ru2** (Fig. 3) have been compared to those of structurally related homoleptic complexes known from literature [23,24]: very little deviations with respect to the interligand angles and bond lengths have been observed. Furthermore, the strong deviations from a planar geometry in the ligand are directly obvious from the crystal structure, given in Fig. 2. This effect can directly be related to the steric impact between the terpyridine sphere and the ethynylphenyl moiety.

## 3.2. Absorption and emission spectroscopy.

Steady-state absorption spectra at room temperature as well as emission and excitation spectra at 77 K were measured to unravel the effect of the structural modifications of the terpyridine ligand. Particularly, the effect of the substituent in the 4'-position is a relevant parameter for the photophysical properties of such complexes. There are several empirical studies concerned with systematic variations of the spectroscopic parameters by varying the substitution in the 4'-position [11]. In the paper at hand, the focus is on the effect of an elongated conjugated system on the overall photophysical properties, especially on the extent of excitation delocalization over the adjacent chromophore. Such an effect has been studied on other systems before [25-27]: Some of these studies showed no effect of an elongated conjugated chromophore in the 4'-position on the absorption and emission spectra of the complexes [25,26], while other cases have been reported, in which the substitution in the 4'-position had a significant impact on the spectroscopic properties of the complexes [27]. Furthermore, it has been detailed that not only the size of the conjugated system, but also the torsional stress of the chromophore has to be taken into account because of its significant influence on the overall conjugation in the ligand system [10,28-30].

To start the discussion of the experiments presented here, Fig. 4 summarizes the absorption and emission spectra of **Ru1** – **Ru3**. Additionally, the positions of the $^1$MLCT absorption and $^3$MLCT emission maxima are shown. The apparent trend, *i.e.*, the absorption maxima appear bathochromically shifted upon increasing the length of the chromophore in the 4'-position, highlights the effect of the substituent on the energetic separation between $S_0$ and $^1$MLCT and the respective $^3$MLCT.

In general, the absorption spectra are dominated by intense transitions below 350 nm, assigned to ππ*-transitions of the terpyridine sphere. In **Ru1**, the pure terpyridine absorption can be observed, while for **Ru2** the ππ*-transitions of the entire conjugated system, *i.e.*, the terpyridine and the ethynylbenzene residue

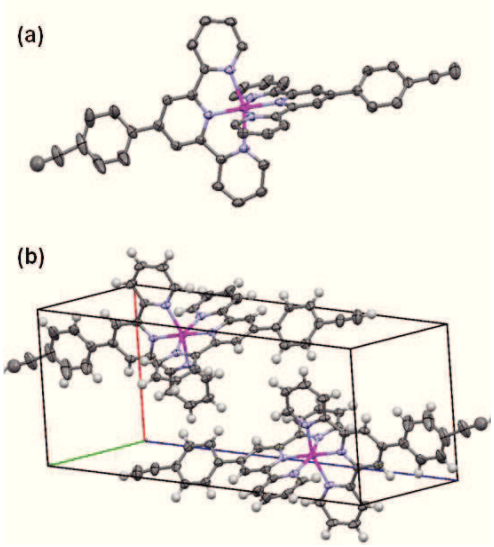


**Figure 2.** a) Representation of the X-ray single crystal structure of Ru2 (thermal ellipsoids at 50% probability level, hydrogen atoms omitted for clarity). (b) Elemental cell and packing of Ru2 (counterions and solvent molecules are not shown).

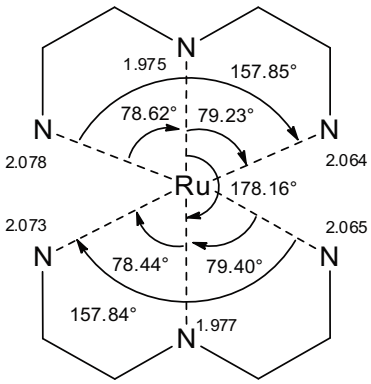


**Figure 3.** Selected structural parameters (bond lengths and angles) of Ru2 as determined by X-ray single crystal analysis.

contribute to the spectrum. **Ru3** reveals transitions of the entire conjugated chromophore, which are centered at about 380 nm as indicated by the isolated absorption band solely visible for **Ru3**. The bathochromic shift of this band with respect to **Ru2** arises from the increased conjugated system of the ligand. Due to the missing contribution of an adjacent chromophore in **Ru1**, the weak symmetry-forbidden dd-transitions at 350 nm are observed in this complex. As a general feature for **Ru1**–**Ru3** intense transitions appear in the visible part of the spectra, *i.e.*, at 475 (**Ru1**), 492 (**Ru2**) and 497 nm (**Ru3**). These bands, which show mutually identical vibronic fine structures due to vibrations at around 1600 cm$^{-1}$, are assigned to $^1$MLCT transitions [31].

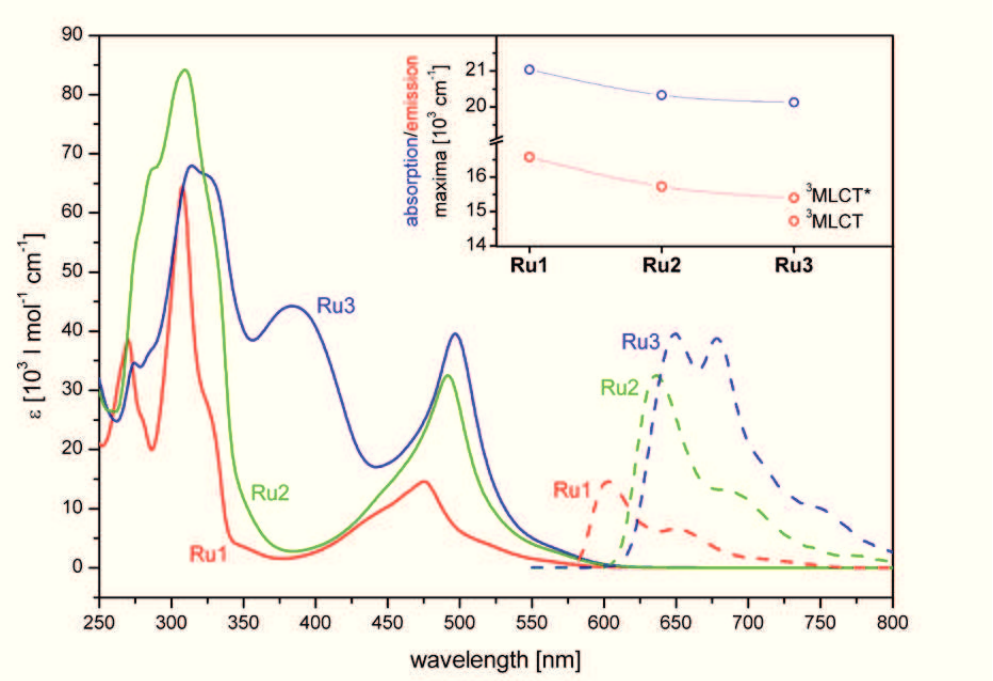


**Figure 4.** Room temperature absorption spectra of Ru1 (red solid line), Ru2 (green solid line) and Ru3 (blue solid line) in acetonitrile together with the emission spectra, recorded at 77 K for Ru1 (red dashed line), Ru2 (green dashed line) and Ru3 (blue dashed line). At room temperature the complexes Ru1 and Ru2 are not emissive. Furthermore, the spectral position of the $^1$MLCT absorption maximum (blue) and the $^3$MLCT emission maximum (red) are shown in the inset. Here, $^3$MLCT' refers to a secondary emissive MLCT excited state in Ru3 (see main text for discussion).

The fine structure of the $^1$MLCT transitions becomes only slightly enhanced at low temperatures (see Supporting Information). Thus, it is not possible to identify defined vibrations coupled to the electronic transition as it is possible in, *e.g.*, rigid conjugated chromophores. In the series, not only do the $^1$MLCT absorption of **Ru1**, **Ru2** and **Ru3** shift to longer wavelengths but also the absorption cross-section increases upon increasing the size of the conjugated chromophore. Previous studies showed that the torsion angle between the terpyridine sphere and the adjacent chromophore represents a significant parameter in determining the spectroscopic features of such systems: in the electronic ground state the torsion angle is roughly 35°, while dynamic planarization of the ligand structure both in the isolated ligand and in the related transition-metal-*bis*terpyridine complexes takes place upon photoexcitation [32-35]. The 35° angle in the ground state of the complex, as obvious from the crystal structure of **Ru2**, is large enough to reduce conjugation between the terpyridine sphere and the chromophore but does not inhibit conjugation between these two molecular fragments [29,30]. Following this argumentation, the absorption spectra indicate that for **Ru2** and **Ru3** an increased excitation delocalization and, therefore, stabilization of the $^1$MLCT should be observed. This is indicated by the bathochromic and hyperchromic shift of the $^1$MLCT transitions compared to **Ru1**.

The emission spectra of **Ru1**–**Ru3,** recorded at 77 K, are depicted in Fig. 4. The emission is due to the radiative decay of the lowest (thermalized) $^3$MLCT state. The emission maximum as a function of conjugated-chromophore size shows the same trend as the absorption data (inset Fig. 4). The trend also reflects the enhanced excitation delocalization in the excited state. **Ru1** and **Ru2** show similar shapes of the emission revealing an intense ($v_0$*-$v_0$)-transition at 603 (**Ru1**) and 636 nm (**Ru2**) in concert with two broad long wavelength shoulders. These are caused by vibronic progressions at around 1300 cm$^{-1}$ – a value typical for terpyridine complexes [36,37]. Table 1 compares the spectroscopic parameters obtained from absorption and emission experiments.

The 77 K emission spectra of **Ru1** and **Ru2** reveal band shapes typical for ruthenium polypyridyl complexes [36]. On the contrary, the 77 K spectrum

**Table 1.** Comparison of selected spectroscopic parameters for Ru1, Ru2 and Ru3. At room temperature no emission could be detected for Ru1 and Ru2 [36].

| sample | $\lambda_{max}$ [nm] (absorption) | $\lambda_{max}$ [nm] (emission) | | emission lifetime | | |
|---|---|---|---|---|---|---|
| | | 300 K | 77 K | 300 K [ns] | 77 K [μs] | |
| **Ru1** | 475.2 | - | 603 | - | 10.4 [36] | |
| **Ru2** | 491.8 | | 636 | | 14,2 | |
| **Ru3** | 496.8 | 640 [38] | 647, 677 | 36.5 [38] | 12 | 214 |

for **Ru3** shows qualitative differences when compared to the spectra of **Ru1** and **Ru2** [38]. The emission spectrum of **Ru3** reveals two transitions of roughly equal intensity dominating the spectrum with maxima at 647 and 677 nm. These maxima are accompanied by a broad and relatively unstructured long-wavelength shoulder. This shape – atypical for ruthenium polypyridyl complexes – cannot be explained by simple vibronic progression. This is further corroborated by the emission-decay characteristics of **Ru3**, for which the emission cannot be fit by a monoexponential function. Instead the emission decays biexponentially, characterized by two lifetimes $\tau_1$ = 12 μs and $\tau_2$ = 214 μs (see Fig. 5). The biexponential decay of the phosphorescence shows that for **Ru3** emission does not originate from a simple radiative decay of a single $^3$MLCT state.

One possible explanation for the luminescence properties of **Ru3** is simultaneous phosphorescence from two non-degenerate $^3$MLCT excited states as has been observed for some ruthenium(II)-*tris*bipyridine complexes. This dual emission has – in some reports – been assigned to simultaneous emission from two distinct $^3$MLCT states localized on different ligands in a heteroleptic complex [39,40]. However, the herein presented coordination compounds are homoleptic complexes. Therefore, such explanation cannot apply. Instead, we follow the line of arguing presented by Yersin *et al*. [41], who observed dual phosphorescence from two distinct states, termed $^3$MLCT and $^3$MLCT', which are associated with the same ligand structure. Thus, in **Ru3** we assign the observed emission to the $^3$MLCT and a secondary MLCT ($^3$MLCT') state, which – due to the presence of state specific deactivation channels – are supposed to reveal different luminescence lifetimes.

## 3.3. Resonance Raman spectroscopy

While emission experiments can provide indications about the stabilizing effect of the conjugated chromophore in the 4'-position of the terpyridine ligand, resonance Raman (rR) spectroscopy directly yields information about the localization of the initially excited $^1$MLCT state [42,43]. By utilizing a Raman-excitation wavelength in resonance with an electronic transition, Franck-Condon active vibrations become enhanced as compared to electronically non-resonant excitation. As these Franck-Condon active vibrations can be assigned to distinct structural features of the molecule, rR helps to identify the localization of the electronic excited state [42,44]. For recording rR spectra of **Ru1**–**Ru3**, the samples were excited in resonance with the $^1$MLCT absorption band. It was validated that the rR intensities of Franck-Condon active vibrations, as a function of rR excitation wavelength, follow the shape of the absorption spectrum (see Supporting Information) [45,46]. Based on the agreement of the absorption spectrum and the rR intensities, the following discussion will focus on the rR spectra obtained upon excitation at 476 nm (see Fig. 6). After acquisition of the raw data, the spectra were corrected for experimental differences in the excitation power and deviations between the absorbencies at 476 nm of individual samples. The corrected rR spectra of **Ru1–Ru3** are depicted in Fig. 6 together with a non-resonant Raman spectrum of the solvent.

It is directly obvious that there are differences between the spectra of **Ru2** and **Ru1**: A number of vibrations contribute to the spectra of **Ru2**, which are absent or only very weakly visible for **Ru1** [45]. In detail, such vibrations are located at 1064 ($\delta_{ip}(py_p)$), 1254 ($\nu(py_p\text{-}py_c)$, $\delta_{ip}(py_c\text{-}H)$), 1355 ($\nu(ph\text{-}py_{trig})$) and 1532 cm$^{-1}$ ($\delta_{ip}(py_c\text{-}ph)$). On the other hand the spectra of **Ru2** and **Ru3** are quite similar and dominantly differ only in the intensities of individual peaks. Contrary, vibrations at 1099 ($\delta_{ip}(tpy)$), 1166 ($\delta_{ip}(C_{tpy}H)$), 1473 ($\delta_{ip}(py_p)$) and 1606 cm$^{-1}$ ($\delta_{ip}(py_c)$) appear in **Ru1**, **Ru2** and **Ru3** and get increasingly enhanced in the rR spectra taken at 476 nm with increasing chromophore size in the order **Ru1**, **Ru2**, **Ru3**. The mode assignment was done by comparison of the rR spectra with literature reports on DFT calculations and non-resonant Raman measurements on the respective ruthenium(II) and zinc(II) complexes [29,45,47].

The differences in the rR spectra can be rationalized by different localizations of the initially photoexcited $^1$MLCT states in **Ru2** and **Ru1**. In **Ru2**, the excitation appears to be more delocalized, *i.e*., spread over the adjacent conjugated substituent at the 4'-position of the terpyridine. Consequently, Raman-active vibrations

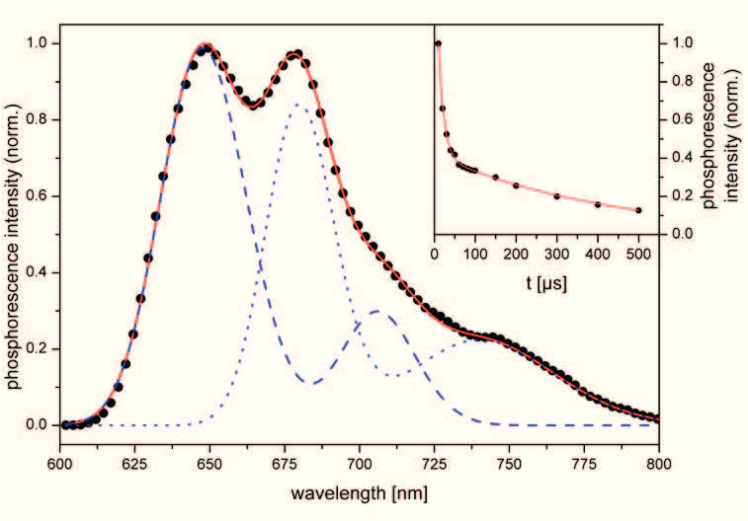


**Figure 5.** Deconvolution of the emission spectrum of Ru3 at 77 K (full circles) into two separate emissive species with different lifetimes of 12 $\mu$s (dashed line) and 214 $\mu$s (dotted line). The solid line refers to the resulting fit of the entire emission spectrum. The integrated emission intensity (integration between 630 and 760 nm) as a function of time is depicted in the inset of Fig. 5. The time-dependence of the emission is fit with a biexponential function.

associated with the structural elements present in **Ru2** but absent in **Ru1** become visible in the rR spectrum. However, further increase of the conjugated system from **Ru2** to **Ru3** does not lead to the appearance of vibrations in the rR spectrum, which could be assigned to direct excitation of the stilbene part of the chromophore in **Ru3**. The net effect of increasing the chromophore from **Ru2** to **Ru3** on the rR spectra is an increase of band intensities for most vibrations. This finding and the missing v(C≡C) vibration in both **Ru2** and **Ru3** – expected at about 2200 $cm^{-1}$ – suggest that the initial excitation is delocalized over the terpyridine sphere and the directly linked phenyl ring only. This finding is in agreement with previous theoretical studies on related systems [30,35]. A further increase of the conjugated system beyond the phenyl ring directly attached to the terpyridine causes no further delocalization of the $^1$MLCT. However, a higher degree of conjugation between the terpyridine sphere and the adjacent phenyl ring is observed [47] causing higher rR intensities.

In previous studies on closely related zinc(II) complexes, a vibration at about 1350 $cm^{-1}$ served as indicator for the conjugation between the terpyridine sphere and the adjacent phenyl ring. This vibration corresponds to the symmetric and asymmetric v(ph-py(trig)) vibration [29,47]. The spectral position of this band was analyzed for the different ligand structures to deduce the effect of structural variations on the conjugation within the chromophore. For **Ru2** and **Ru3**, two vibrations are overlapping yielding the band at 1350 $cm^{-1}$. Therefore, the rR intensities of the v(ph-py(trig)) vibrations are analyzed by deconvoluting the respective spectra in the region between 1320 and 1390 $cm^{-1}$ into three Lorentz profiles [48]. The results are given in Fig. 7, which shows the original data together with the results of the fit.

From Fig. 7 it appears that the v(ph-py(trig)) peak at 1355 $cm^{-1}$ can be deconvoluted into two separate bands, the peak areas of which increase from **Ru2** to **Ru3** (inset Fig. 7). An altered rR intensity correlates with a change in electron density upon photoexcitation and, hence, with the localization of the electronic transition in the fraction of the molecular architecture where the molecular vibration resides. Consequently, the higher rR intensities of the 1355 $cm^{-1}$ band is assigned to an enhanced localization of the $^1$MLCT on the terpyridine and the adjacent phenyl ring. This structural motif is apparent in both **Ru2** and **Ru3**. The different localizations of the photoexcited states and increased rR cross sections are caused by a higher conjugation. This, in turn, causes a smaller dihedral angel between the terpyridine and the phenyl ring as predicted by theory [47]. Therefore, rR allows to obtain detailed information about the initially photoexcited $^1$MLCT state in **Ru2**. The ethynyl-phenyl substituent causes a dramatic change in localization of the $^1$MLCT state and hence in the rR spectrum. Thus,

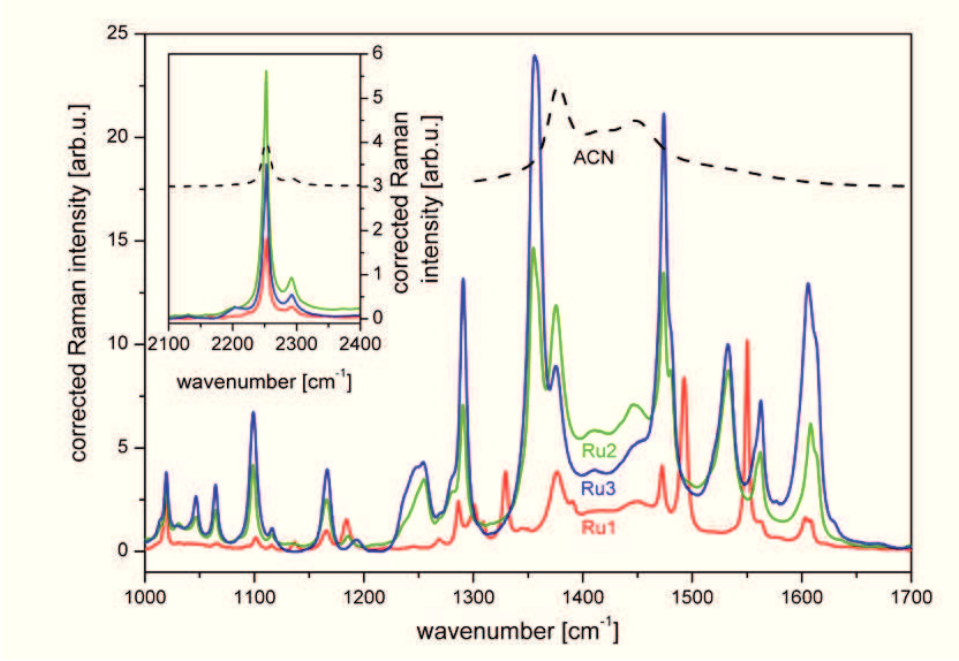


**Figure 6.** Resonance Raman spectra of Ru1 (red solid line), Ru2 (green solid line) and Ru3 (blue solid line) from solutions in acetonitrile (excitation at 476 nm). The non-resonant Raman spectrum of the solvent is given as reference (black dashed line, offset). The inset displays the resonance Raman spectra of Ru1–Ru3 and the nonresonant Raman spectrum of the solvent in the spectral region between 2100 and 2400 $cm^{-1}$. The spectral resolution of the spectrometer was approximated to 1 $cm^{-1}$.

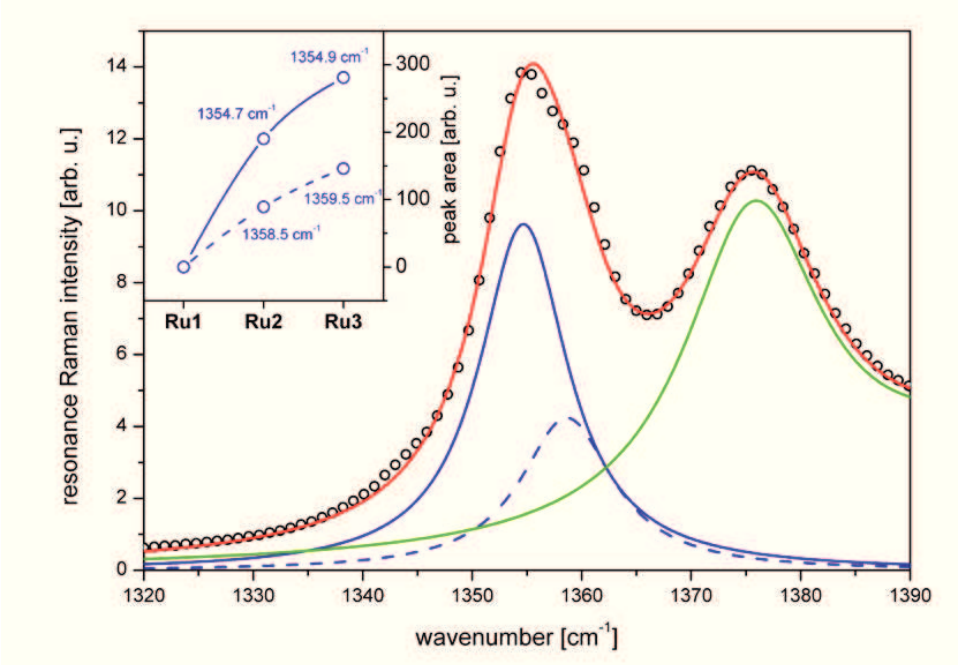


**Figure 7.** Fit of the resonance Raman spectra of Ru2 (circles) in the spectral region between 1320 and 1390 $cm^{-1}$ by a sum of three Lorentz bands (red solid line). Two peaks correspond to molecular vibrations of Ru2 (blue solid and dashed line) while the solid green line represents solvent signals (acetonitrile). The inset shows the respective integrated peak areas for the series Ru1, Ru2 and Ru3.

the data show that the stabilizing effect of the ethynyl-phenyl substitution on the electronic properties of the **Ru2** is directly associated with a more delocalized photoexcited state.

## 4. Conclusion

A versatile synthon for supramolecular chemistry, *i.e.*, click reactions, to engineer coordination polymers, has been synthesized and spectroscopically characterized. To this extent, NMR, mass spectrometry and crystal structure determination have been performed. Due to its potential application in photoactive coordination polymers, its photophysical properties were investigated by UV/Vis absorption and emission spectroscopy as well as resonance Raman spectroscopy. The results illustrate that the conjugated substituent connected in the 4'-position has significant impact on the spectroscopic properties of the complex. This is reflected in bathochromic shifts of the absorption and emission spectra and by an increased luminescence lifetime with respect to ruthenium(II)-*bis*terpyridine. Furthermore, the delocalization of the MLCT excited states over the adjacent phenyl ring increases upon introducing the phenyl-ethynyl-substituent in the 4'-position of the ligands – a central structural motif employed in click chemistry. Further elongation of the chromophore stabilizes the $^3$MLCT states only slightly more. However, it causes a higher conjugation in the MLCT state. A further increase of the size of the substituent in the 4'-position of the terpyridine, here a stilbene-derived chromophore was used, does not further enhance the excited-state delocalization.

### References

[1] A. Wild, A. Winter, F. Schlütter, U.S. Schubert, Chem. Soc. Rev. 40, 1459 (2011)
[2] W.K. Chan, X. Gong, W.Y. Ng, Appl. Phys. Lett. 71, 2919 (1997)
[3] W.Y. Ng, W.K. Chan, Adv. Mater. 9, 716 (1991)
[4] W.Y. Ng, X. Gong, W.K. Chan, Chem. Mater. 11, 1165 (1999)
[5] P.D. Vellis, J.A. Mikroyannidis, C.N. Lo, C.S. Hsu, J. Polym. Sci., Part A: Polym. Chem. 46, 7702 (2008)
[6] A. Wild, F. Schlütter, G.M. Pavlov, C. Friebe, G. Festag, A. Winter, M.D. Hager, V. Cimrova, U.S. Schubert, Macromol. Rapid Commun. 31, 868 (2010)
[7] U.S. Schubert, C. Eschbaumer, G. Hochwimmer, Synthesis 779 (1999)
[8] V. Grosshenny, A. Harriman, R. Ziessel, Angew. Chem. Int. Ed. 34, 2705 (1995)
[9] B.G.G. Lohmeijer, U.S. Schubert, Macromol. Chem. Phys. 204, 1072 (2003)
[10] A.C. Benniston, A. Harriman, P. Li, C.A. Sams, J. Am. Chem. Soc. 127, 2553 (2005)
[11] U.S. Schubert, H. Hofmeier, G.R. Newkome, Modern Terpyridine Chemistry (Wiley-VHC, Weinheim, 2006)
[12] J. Hjelm, E.C. Constable, E. Figgemeier, A. Hagfeldt, R. Handel, C.E. Housecroft, E. Mukhtarb, E. Schofield, Chem. Commun. 284 (2002)
[13] S. Kelch, M. Rehahn, Macromolecules 32, 5818 (1999)
[14] O. Schmelz, M. Rehahn, e-Polymers 47, 1 (2002)
[15] A. Winter, A. Wild, R. Hoogenboom, M.W.M. Fijten, M.D. Hager, R.A. Fallahapour, U.S. Schubert, Synthesis 1506 (2009)
[16] D. Fournier, R. Hoogenboom, U.S. Schubert, Chem. Soc. Rev. 36, 1369 (2007)
[17] U. Mansfeld, C. Pietsch, R. Hoogenboom, C.R. Becer, U.S. Schubert, Polym. Chem. 1, 1560 (2010)
[18] H. Hofmeier, S. Schmatloch, D. Wouters, U.S. Schubert, Macromol. Chem. Phys. 204, 2197 (2003)
[19] V. Marin, E. Holder, R. Hoogenboom, U.S. Schubert, Chem. Soc. Rev. 36, 618 (2007)
[20] R. Ziessel, V. Grosshenny, M. Hissler, C. Stroh, Inorg. Chem. 43, 4262 (2004)
[21] E. Alessio, Chem. Rev. 104, 4203 (2004)
[22] A. Winter, D. A.M. Egbe, U.S. Schubert, Org. Lett. 9, 2345 (2007)
[23] D. Chartrand, I. Theobald, G.S. Hanan, Acta Crystallogr., Sect. E: Struct. Rep. Online 63, 1561 (2007)
[24] A.C. Benniston, G. Chapman, A. Harriman, M. Mehrabi, C.A. Sams, Inorg. Chem. 43, 4227 (2004)
[25] A. Harriman, A. Khatyr, R. Ziessel, A.C. Benniston, Angew. Chem. Int. Ed. 39, 4287 (2000)
[26] S. Welter, N. Salluce, A. Benetti, N. Rot, P. Belser, P. Sonar, A.C. Grimsdale, K. Müllen, M. Lutz, A.L. Spek, L. De Cola, Inorg. Chem. 44, 4706 (2005)
[27] J.S. Bair, R.G. Harrison, J. Org. Chem. 72, 6653 (2007)
[28] M. Hissler, A. El-ghayoury, A. Harriman, R. Ziessel, Angew. Chem. Int. Ed. 37, 1717 (1998)

[29] M. Presselt, B. Dietzek, M. Schmitt, J. Popp, A. Winter, M. Chiper, C. Friebe, U.S. Schubert, J. Phys. Chem. C 112, 18651 (2008)
[30] M. Preselt, B. Dietzek, M. Schmitt, S. Rau, A. Winter, M. Jäger, U.S. Schubert, J. Popp, J. Phys. Chem. A 114, 13163 (2010)
[31] A. Cannizzo, F. van Mourik, W. Gawelda, G. Zgrablic, C. Bressler, M. Chergui, Angew. Chem. Int. Ed. 45, 3174 (2006)
[32] R. Siebert, D. Akimov, M. Schmitt, A. Winter, U.S. Schubert, B. Dietzek, J. Popp, ChemPhysChem 10, 910 (2009)
[33] R. Siebert, A. Winter, U.S. Schubert, B. Dietzek, J. Popp, J. Phys. Chem. C 114, 6841 (2010)
[34] R. Siebert, A. Winter, U.S. Schubert, B. Dietzek, J. Popp, Phys. Chem. Chem. Phys. 13, 1606 (2011)
[35] R. Siebert, C. Hunger, J. Guthmuller, F. Schlütter, A. Winter, U.S. Schubert, L. González, B. Dietzek, J. Popp, J. Phys. Chem. C, 115, 12677 (2011)
[36] A. Amini, A. Harriman, A. Mayeux, Phys. Chem. Chem. Phys. 6, 1157 (2004)
[37] B. J. Coe, D.W. Thompson, C.T. Cilbertson, J.R. Schoonover, T.J. Meyer, Inorg. Chem. 34, 3385 (1995)
[38] R. Siebert, A. Winter, B. Dietzek, U.S. Schubert, J. Popp, Macromol. Rapid Commun. 31, 883 (2010)
[39] E.C. Glazer, D. Magde, Y. Tor, J. Am. Chem. Soc. 127, 4190 (2005)
[40] E.C. Glazer, D. Magde, Y. Tor, J. Am. Chem. Soc. 129, 8544 (2007)
[41] H. Yersin, E. Gallhuber, A. Vogler, H. Kunkelyt, J. Am. Chem. Soc. 105, 4155 (1983)
[42] A.B. Myers, Chem. Rev. 96, 911 (1996)
[43] M. Schwalbe, M. Karnahl, H. Görls, D. Chartrand, F. Laverdiere, G.S. Hanan, S. Tschierlei, B. Dietzek, M. Schmitt, J. Popp, J. G. Vos, S. Rau, Dalton Trans. 4012 (2009)
[44] S. Tschierlei, B. Dietzek, M. Karnahl, S. Rau, F.M. MacDonnell, M. Schmitt, J. Popp, J. Raman Spectrosc. 39, 557 (2008)
[45] P.W. Hansen, P.W. Jensen, Spectrochim. Acta. 50A, 169 (1993)
[46] R.J.H. Clark, P.C. Turtle, D.P. Strommen, B. Streusand, J. Kincaid, K. Nakamoto, Inorg. Chem. 16, 84 (1977)
[47] A. Winter, C. Friebe, M. Chiper, U.S. Schubert, M. Presselt, B. Dietzek, M. Schmitt, J. Popp, ChemPhysChem 10, 787 (2009)
[48] S. Tschierlei, M. Karnahl, M. Presselt, B. Dietzek, J. Guthmuller, L. González, M. Schmitt, S. Rau, J. Popp, Angew. Chem. Int. Ed. 49, 3981 (2010)
[49] U.S. Schubert, C. Eschbaumer, P.R. Andres, H. Hofmeier, C.H. Weidl, E. Herdtweck, E. Dulkeith, A. Morteani, N.E. Hecker, J. Feldmann, Synth. Metals 121, 1249 (2001)
[50] A. Winter, C. Friebe, M.D. Hager, U.S. Schubert, Eur. J. Org. Chem. 801 (2009)
[51] R. Hooft, COLLECT Data Collection Software (Nonius B.V., Delft, The Netheralnds, 1998)
[52] Z. Otwinowski, W. Minor, In: C.W. Carter, R.M. Sweet (Eds.), Processing of X-Ray Diffraction Data Collected in Oscillation Mode in Methods in Enzymology in Macromolecular Crystallography (Academic Press, San Diego, USA, 1997) Part A, Vol. 276, p.307

# Veröffentlichungen

## Veröffentlichungen in referierten Zeitschriften

1. R. Siebert, Y. Tian, R. Camacho, A. Winter, A. Wild, A. Krieg, U. S. Schubert, I. Scheblykin, B. Dietzek and J. Popp, Fluorescence Quenching in $Zm^{2+}$ *bis*-Terpyridine Coordination Polymers. A Single Molecule Study, *Manuskript in Vorbereitung*

2. R. Siebert, A. Winter, M. Schmitt, J. Popp, U. S. Schubert and B. Dietzek, Light-Induced Dynamics in Conjugated Bis(terpyridine) Ligands - A Case Study Toward Photoactive Coordination Polymers, *Macromolecular Rapid Communications*, **2012**, *33*, 481-497.

3. B. Schulze, D. Escudero, R. Siebert, C. Friebe, H. Görls, M. D. Hager, A. Winter, B. Dietzek, J. Popp, L. González, and U. S. Schubert, Ruthenium(II) Photosensitizers of Tridentate Click-Derived Cyclometalated Ligands, *Chemistry - A European Journal*, **2012**, *18*, 4010-4025

4. R. Siebert, F. Schlütter, A. Winter, M. Presselt, H. Görls, U. S. Schubert, B. Dietzek and J. Popp, Ruthenium(II)-*bis*(4‘-(4-ethinylphenyl)-2,2‘:6‘,2“-terpyridine) - A Versatile Synthon in Supramolecular Chemistry. Synthesis and Characterization, *Central European Journal of Chemistry*, **2011**, *9*, 990-999.

5. R. Siebert, C. Hunger, J. Guthmuller, F. Schlütter, A. Winter, U. S. Schubert, L. Gonzàlez, B. Dietzek and J. Popp, Direct Observation of Temperature Dependent Excited-State Equilibrium in Dinuclear Ruthenium Terpyridine Complexes Bearing Electron-Poor Bridging Ligands, *Journal of Physical Chemistry C*, **2011**, *115*, 12677-12688

6. B. Schulze, D. Escudero, C. Friebe, R. Siebert, H. Görls, U. Köhn, E. Altuntas, A. Baumgärtel, M. D. Hager, A. Winter, B. Dietzek, L. Gonzàlez, and U. S. Schubert, A Heteroleptic Bis(tridentate) Ruthenium(II) Complex of a Click-Derived Abnormal Carbene Pincer Ligand with Potential for Photosensitizer Applications, *Chemistry a European Journal*, **2011**, *17*, 5494-5498.

7. R. Siebert, A. Winter, U. S. Schubert, B. Dietzek and J. Popp, The Molecular Mechanism of Dual Emission in Terpyridine Transition Metal Complexes - Ultrafast Investigation of Photoinduced Dynamics, *Physical Chemistry Chemical Physics*, **2011**, *13*, 1606-1617.

8. R. Siebert, A. Winter, B. Dietzek, U. S. Schubert and J. Popp, Dual Emission from Highly Conjugated 2,2‘:6‘:2“-Terpyridine Complexes - A Potential Route to White Emitters, *Macromolecular Rapid Communications*, **2010**, *31*, 883-888.

9. R. Siebert, A. Winter, U. S. Schubert, B. Dietzek and J. Popp, Excited-State Planarization as Free Barrierless Motion in a $\pi$-Conjugated Terpyridine, *Journal of Physical Chemistry C*, **2010**, *114*, 6841-6848.

10. D. Cialla, R. Siebert, U. Hübner, R. Möller, H. Schneidewind, R. Mattheis, J. Petschulat, A. Tünnermann, T. Pertsch, B. Dietzek and J. Popp, Ultrafast Plasmon Dynamics and Evanescent Field Distribution of Reproducible Surface-Enhanced Raman-Scattering Substrates, *Analytical and Bioanalytical Chemistry*, **2009**, *394*, 1811-1818.

11. R. Siebert, D. Akimov, M. Schmitt, A. Winter, U. S. Schubert, B. Dietzek and J. Popp, Spectroscopic Investigation of the Ultrafsat Photoinduced Dynamics in $\pi$-Conjugated Terpyridines, *ChemPhysChem*, **2009**, *10*, 910-919.

## Veröffentlichungen in nicht-referierten Zeitschriften

1. R. Siebert, A. Winter, U. S. Schubert, M. Schmitt, B. Dietzek and J. Popp, *Proceedings of SPIE, 77221U*, **2010**

2. A. Winter, R. Siebert, D. Akimov, C. Friebe, M. Schmitt, B. Dietzek, J. Popp and U. S. Schubert, *Proceedings of the ACS National Meeting, POLY-344*, **2009**

3. A. Winter, F. Schlütter, R. Siebert, A. Wild, C. Friebe, M. D. Hager, B. Dietzek, M. Schmitt, J. Popp and U. S. Schubert, *Proceedings of the ACS National Meeting, ORGN-288*, **2009**

## Posterpräsentationen

1. *Investigation of the Change of the Molecular Geometrical Structure in Different Physical Environments*
   $6^{th}$ International Conference on Advanced Vibrational Spectroscopy (ICAVS), 2011, Sonoma County
   J. Meyer Ilse, R. Siebert, D. Akimov and B. Diezek

2. *Light Induced Relaxation Pathways in Building Blocks of Photoactive Coordination Polymers*
   110. Hauptversammlung der Deutschen Bunsen-Gesellschaft für Physikalische Chemie (Bunsentagung), 2011, Berlin
   R. Siebert, A. Winter, U. S. Schubert, B. Dietzek and J. Popp

3. *Untersuchung strahlender und strahlungsloser Zerfallskanäle in Eisen- Ruthenium- und Osmiumpolypyridylkomplexen*
   109. Hauptversammlung der Deutschen Bunsen-Gesellschaft für Physikalische Chemie (Bunsentagung), 2010, Bielefeld
   R. Siebert, M. Schmitt, A. Winter, U. S. Schubert, B. Dietzek and J. Popp

4. *Towards new Photovoltaic Materials: The Ultrafast Light Induced Processes in Rigid $\pi$-Conjugated Terpyridines and Their Metal Complexes*
   $24^{th}$ International Conference on Photochemistry (ICP), 2009, Toledo, Spanien
   R. Siebert, M. Schmitt, A. Winter, U. S. Schubert, B. Dietzek and J. Popp

5. *Towards New Photovoltaic Materials: Rigid $\pi$-Conjugated Terpyridines - Synthesis, Characterization and Ultrafast Photoinduced Dynamics*
   $16^{th}$ European Symposium on Organic Chemistry (ESOC), 2009, Prag, Czech Republic
   A. Winter, C. Friebe, M. D. Hager, U. S. Schubert, R. Siebert, D. Akimov, M. Schmitt, B. Dietzek and Popp,

6. *Ultrafast plasmon dynamics in reproducible SERS-substrates*
   Molecular Plasmonics, 2009, Jena
   R. Siebert, D. Cialla, R. Möller, U. Hübner, H. Schneidewind, R. Mattheis, J. Petschulat, A. Tünnermann, T. Pertsch, B. Dietzek and J. Popp

7. *Untersuchung ligandstabilisierter Ladungstransfer-Zustände mittels zeitaufgelöster Spektroskopie*
   108. Hauptversammlung der Deutschen Bunsen-Gesellschaft für Physikalische Chemie (Bunsentagung), 2009, Köln
   R.Siebert, A. Winter, U. S. Schubert, M. Schmitt, B. Dietzek und J. Popp

# Danksagung

An dieser Stelle möchte ich mich bei allen Bedanken, die zum Gelingen dieser Arbeit beigetragen haben.

An erster Stelle betrifft das Herr Prof. Dr. Jürgen Popp, der mir die Möglichkeit geschaffen hat, meine Dissertation in seiner Arbeitsgruppe anzufertigen. Besonders herauszukehren ist dabei der stets gewährte Freiraum, sowohl bei der Gestaltung des Themenbereichs als auch bei der Planung und Durchführung wissenschaftlicher Experimente.
Nicht weniger zu Dank verpflichtet bin ich Herrn Dr. habil. Benjamin Dietzek, der in vielen wissenschaftlichen Diskussionen wertvolle Impulse gab und durch die Lectur diverser Manuskripte wesentlich zum Gelingen der Dissertation beitrug.
Prof. Dr. Ulrich S. Schubert und seiner Arbeitsgruppe, insbesondere Dr. Andreas Winter und Florian Schlütter möchte ich ebenfalls aufrichtig danken. Sie haben durch die bereitwillige Synthese von Molekülen nach meinen Vostellungen die Möglichkeit geschaffen, so detaillierte und konsequente spektroskopische Experimente durchzuführen.
Ebenfalls nicht vergessen möchte ich Dr. Ivan G. Scheblykin und seine Arbeitsgruppe, insbesondere Dr. Yuxi Tian und Dr. Daniel Thomsson. Sie haben mir die Möglichkeit gegeben, erste Erfahrungen in der Einzelmolekülspektroskopie zu sammeln und darüber hinaus mit viel Geduld meine Arbeiten auf diesem Gebiet in in eine positive, produktive Richtung gelenkt.
Weiterhin möchte ich mich bei Christoph Hunger bedanken, der mich während seiner Diplomarbeit unterstützte. Die vielen wissenschaftlichen und nichtwissenschaftlichen Diskussionen haben uns beiden gut getan und auch diese Arbeit entscheidend voran gebracht.
Weiterhin dankend erwähnen möchte Herrn Dr. Birckner, Herrn Jacobi und Frau Kielmann, die mir in Belangen der stationären Emissions- und Absorptionsspektroskopie mit ihrem Erfahrungsschatz stets hilfreich zur Seite gestanden haben.
Die Schaffung einer angenehmen kollegialen Atmosphäre in den Laboren und Büros der Nachwuchsgruppe „Ultrakurzzeitspektroskopie“ innerhalb der AG Popp war das Verdienst meiner Kollegen. Diese Herausforderung haben wir stets gemeinsam mit sehr gutem Erfolg gemeistert. In vielen Debatten auf dem Weg zur Mensa wurden viele Fragen geklärt und so manche gute Idee geboren.
Letztendlich möchte ich noch meiner Familie, allen voran meinen Eltern und Melanie für das in mich gesetzte Vertrauen und die moralische Aufbauarbeit bedanken, wenn mal wieder alles nicht funktioniert hat.

# Lebenslauf

## Persönliche Daten

| | |
|---|---|
| Name | Ronald Siebert |
| Geburtstag | 29.09.1983 |
| Geburtsort | Gera |

## Schulausbildung

| | |
|---|---|
| 1990 - 1994 | 14. Grundschule Gera |
| 1994 - 2002 | Karl-Theodor-Liebe-Gymnasium Gera |

## Wehr-/Zivieldienst

| | |
|---|---|
| 08.2002 - 05.2003 | Zivieldinst (Waldklinikum Gera) |

## Hochschulausbildung

| | |
|---|---|
| 10.2003 - 06.2008 | Studium der Chemie (Diplom) an der Friedrich-Schiller-Universität Jena |
| 06.2008 - 12.2011 | Anfertigung der Dissertation am Institut für Physikalische Chemie der Friedrich-Schiller-Universität Jena und dem Institut für Photonische Technologien Jena |
| 08.2010 u. 09.2010 | Gastwissenschaftler in der Arbeitsgruppe von Dr. Ivan G. Scheblykin am Institute of Chemical Physics der Lund University (Schweden) |

Jena den Ronald Siebert

# Selbstständigkeitserklärung

Ich erkläre, dass ich die vorliegende Arbeit selbstständig und unter Verwendung der angegebenen Hilfsmittel, persönlichen Mitteilungen und Quellen angefertigt habe.

Jena den

Ronald Siebert